Preparation and characterisation of thin film CdS/CdTe solar cells produced by close space sublimation.

Alamri, Saleh Naeeman O.

Preparation and Characterisation of Thin Film CdS/CdTe Solar Cells Produced by Close Space Sublimation

by

Saleh Naeeman O. Alamri

Presented in Candidature for the Degree of

Doctor of Philosophy in the University of Durham

Physics Department

August 1999

To my family

(my parents, my wife, my children, my brothers and sisters)

Copyright

Declaration

I declare that the work reported in this thesis, unless otherwise stated, was carried out by the candidate, that is has not previously been submitted for any degree and that it is not currently being submitted for any other degree.

Dr. A. W. Brinkman
Supervisor

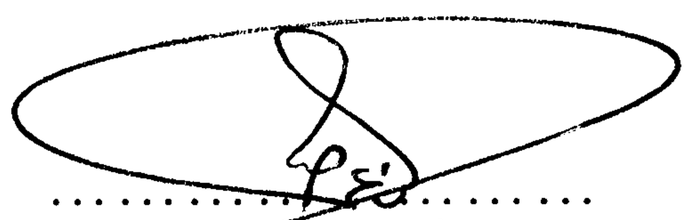

Saleh N. Alamri
Candidate

Abstract

This work concerns the preparation and characterisation of n-CdS/p-CdTe thin film solar cells using a close space sublimation system (CSS) to deposit the p-CdTe layer. The effects of preparation conditions of CdTe on growth rate and the texture of the film were investigated. The cells were characterised by measurements of *I-V*, *C-V*, spectral response, photocapacitance and electroluminescence.

The growth rate of CdTe increased as the source temperature increased with an activation energy ~ 1.9 eV, whereas it was constant and independent of the substrate temperature, up to some breakpoint temperature, above which the rate decreased rapidly to zero. Increasing the pressure during growth allows growth to take place at higher temperatures but at the expense of growth rate. The growth rate increased as the separation between the source and the substrate decreased. The CdTe films grown at 335 °C substrate temperature showed a highly preferred (111) orientation and small grain size, whereas the films deposited at higher temperature showed a progressive loss of (111) orientation and an increase in grain size.

The $CdCl_2$ treatment for the CdTe layer increased the efficiency of the solar cells from about 3% to around 10%. The *I-V* dark characteristics suggest that the $CdCl_2$ treatment changed the current transport mechanism across the junction from emission/recombination with activation energy around 0.07eV to a tunnelling mechanism. Solar cells fabricated with SnO_2 give higher efficiencies than cells fabricated with ITO due to the interface between the ITO and CdS layer, which becomes rectifying after heating at 400°C in air.

There are many preparation parameters which affect the interdiffusion between the CdTe and CdS layer, and so modify the spectral response. In the present study, the effects of the $CdCl_2$ treatment of CdTe and CdS layers, the thickness of $CdCl_2$ and the time of annealing, the thickness of the CdS layer and the substrate temperature were investigated in terms of the spectral response. These studies tended to confirm that interdiffusion had taken place, with significant effects on the spectral response.

The photocapacitance measurements indicated the existence of some levels below the conduction band at 0.4, 0.2 eV in p-CdTe and at 0.55eV in n-CdS, also some deep levels above the valance band at 0.24, 0.1 eV in p-CdTe and 0.71 eV in n-CdS.

Acknowledgements

It gives me a great pleasure to acknowledge those people who contribute to the preparation of this thesis. First of all, I would like to express my appreciation and gratitude to my supervisor Dr. A. W. Brinkman, for the valuable guidance and helpful encouragement.

I am grateful to Dr. Ken Durose, for his valuable discussions and all members of II-VI Semiconductors and Ceramics research group, Paul Edwards, Mike Cousins, Matt Hogan, Mark Potter and John Mullins. Thanks also due to Norman Thompson and Mr. David Pattinson for their friendship and technical support.

I wish to express my appreciation to the University of King Abdulaziz and Ministry of Higher Education in Saudi Arabia, for financial support.

Finally, I would like to express my gratitude to my Parents, for their patience and understanding, and to my wife and my children for their many sacrifices. My thanks go to my friends in Durham for their close friendship and kindness.

Contents

Chapter One:

Introduction.

1.1-Introduction

The supply of energy is obviously a very important issue for human prosperity. It would be hard to imagine in the modern world a house or a hospital without electricity, or cars or planes without petrol etc. The major energy sources at the present time are petroleum, coal, natural gas, hydropower (dams and tidal), and nuclear power. Unfortunately, these sources have many disadvantages. Conventional fuel resources are limited and expected to last only for a further 100-200 years. The nuclear power based on the fission of uranium is also a limited source. In addition these energy sources damage the global environmental system. Fossil fuel combustion emits CO_2 which contributes to pollution of the atmosphere and global warming (green house effect). The radioactive waste produced by nuclear power station has to be contained and buried in safe place possibly for hundreds of years which remains an unsolved problem. In addition, there are maintenance and safety questions with nuclear reactors which need substantial and very expensive effort.

For the conventional and nuclear sources there are, therefore, potential disadvantages in cost terms as well as environmental terms, and other alternative renewable energy sources, such as photovoltaic, wave, wind etc, must be developed. The development of these sources, which at the moment are expensive, seeks to reduce the cost of production and protect the environment, and thus Photovoltaics research has become one of the important renewable energy source studies. The major concerns in this field are to reduce the cost by improving the production methods, efficiency, lifetime etc.

The terrestrial photovoltaic solar cell device converts solar energy, "free" energy, to electrical energy (non-polluting energy). The performance of solar cells depends on the device structure and component materials, which are typically semiconductors such as Si, CdTe, CdS, GaAs etc.

1.2- Solar Energy and Solar Cells.

The sun gives the earth a huge amount of free radiant energy. Each hour the earth receives at its outer atmosphere around 173×10^{12} KWh [1] of energy, not all of this energy reaches the surface of the earth because some is reflected away by the clouds, some is absorbed in the atmosphere ..etc. The aim is to convert as much as possible of this energy to electrical power.

Unlike other renewable energy sources such as wind etc., photovoltaic (PV) power generation involves the direct conversion of solar radiation to electrical energy, (In wind, for example the conversion undergoes intermediate stages; solar ⟶ wind ⟶ mechanical ⟶ electrical). In PV, this conversion takes place when an incident photon of sufficient energy is absorbed in the semiconductor exciting an electron-hole pair. However, to generate useful power, the electron-hole pair must be separated by some sort of internal electric field to produce an electromotive force (e.m.f.) which can drive current around the load. Typically, this can be achieved by creating a p-n junction.

The main mismatch between the available solar radiation and the semiconductor is that the sunlight has a wide range of photons with different energy, whereas the semiconductor has a well defined bandgap energy. Since photons with a lower energy will not be absorbed, much of the solar spectrum may not be utilised. In addition although photons with an energy much greater than the bandgap will be absorbed, the excess energy is lost as heat, limiting efficiency in a fundamental way still further. This prevents the semiconductor from absorbing all the light, limiting the solar cell efficiency.

Many different types of solar cells are now available on the market, with different materials and structures, all seeking to get maximum power and minimum cost. Crystalline silicon cells hold the largest part of the market because they have a long lifetime ~20 years [2] and a high efficiency ~ 24% [3]. Other cells are based on compound semiconductors (for example gallium arsienide or indium phosphide) which although they have high efficiencies are expensive and because of their high cost are only used in specialised applications such as satellites or in systems operated under high intensity sunlight. An acceptable balance between cost and conversion efficiency can be

obtained from a variety of other kinds of solar cells, based on polycrystalline silicon or thin film compound semiconductors such as cadmium telluride or copper indium diselenide.

The basic construction unit of a commercial photovoltaic generator system is the module which consists of an array of encapsulated solar cells connected either in series to get high voltage or in parallel for high current, or in some combination, depending on the application. Most commercial modules have a standard configuration designed to work with 12 volt batteries, although they may have different areas depending on the material and the manufacturer. The output of a module is generally specified in terms of peak power and expressed in peak watts W_p (measured under standard conditions; 1KW/cm^2 and 25°C cell temperature). Silicon modules typically consist of between 33 and 36 crystalline silicon cells, each around 4-inch diameter or 10cm×10cm polycrystalline cells giving a power of between 40 and 60W_p. Currently planned commercial CdS/CdTe thin films modules will be 60 cm×120 cm produced by Solar Cells Inc.(SCI) [4] or 100 cm × 50 cm produced by ANTEC, each giving peak output power at around 50 W_p.[5].

The cost of a PV system has continued to decline over the recent past. They should soon be competitive with other forms of electrical generation, in addition to their environmental superiority. In order to achieve further significant cost reductions, there are a number of goals that should be achieved;[6]

- Improving the fundamental knowledge and understanding of PV materials, processes and devices.
- Increase communication and co-operation between laboratories word wide.
- Improving PV system reliability and durability.
- Develop and improve the technology of production.

These are the presently stated aims of those interested in improving PV industry and research such as the U.S. Department of Energy (DOS), the National Renewable Energy Laboratory (NREL) etc.

1.3-The History of Photovoltaic Solar Cells.

The development of photovoltaic cells began in 1839 when Becquerel discovered that the voltage between two electrodes, placed in an electrolyte solution, depends on the light directed onto the solution. In 1873, photoconductivity in selenium was discovered by Smith, and four years later Adams and Day observed a similar effect to that observed by Becquerel but in solid (Selenium). After that photovoltaic effects in Selenium and Copper Oxide were studied by Lange, Grandah and Schottky. In 1914, a solar conversion efficiency 1% was achieved with a Selenium solar cell. Half a century later in 1954, Chapin et al [7] at the Bell Telephone laboratories reported the achievement of 6% solar conversion efficiency for a crystalline silicon cell and then 11% 12 months later. The first silicon cells to be used on rockets and satellites in space was in 1959.

The cost of silicon cells was initially very high, and it was not until the cost had been reduced drastically from $1000/W to about $100/W that they could be used at all. They were still too expensive to use for terrestrial photovoltaic conversion, and therefore efforts were directed to discover optimum materials with high efficiency and low preparation cost. Theory indicated that the best material in terms of efficiency would be a semiconductor with a bandgap between 1.1 and 2 eV, with an optimum of around 1.5 eV. According to this classification, materials of interest included $CuInSe_2$ (1.1eV), InP (1.25eV), GaAs (1.4eV), CdTe (1.45), $CuInS_2$ (1.5eV), and CdSe (1.7eV). Jenny et al [8] in 1956 reported 4% efficiency in a gallium arsenide cell.

Photovoltaic research became more strongly directed towards terrestrial applications after the energy (oil) crises in the early 1970s, and after polycrystalline silicon was introduced. Polycrystalline silicon has a lower cost than crystal silicon but is also less efficient. Consequently greater efforts were made to find alternative materials, to provide lower cost and good efficiency. Initially interest focused on developing thin film solar cells based on polycrystalline Cu_2S/CdS and on amorphous silicon. The amorphous silicon cells proved to be more successful than the Cu_2S/CdS devices, but their use is limited to special applications because of their low conversion efficiency 6%. Then, the research and development effort was directed to efficient thin film solar cells based on copper indium diselenide ($CuInSe_2$) and cadmium telluride (CdTe) which

produced efficiencies in excess of 10%. The efficiency of $CuInSe_2$ has steadily improved from 6% to 17%, and from 8% to 16% for CdTe solar cells [9]. Although silicon crystal cells exceeded their theoretical maximum efficiency, due to several innovations in optical engineering, nevertheless they are still expensive for terrestrial application. Amorphous silicon cells, suffer from performance degradation when exposed to bright sunlight. GaAs has the highest efficiency around 30% [3] but is far too expensive for use in large-scale terrestrial application.

1.3.1- CdTe Based Solar Cells.

Cadmium telluride (CdTe) is one of the most promising thin film photovoltaic materials for use in solar cells, because it has a direct bandgap of 1.47eV, a steep optical absorption edge and a large absorption coefficient $>5\times10^{-4}$ cm^{-1}[10]. A thin film of only 2μm is enough to absorb all the solar radiation with energy above the bandgap energy. CdTe also has applications other than solar cells, for example, in single crystal form it is used as a nuclear radiation detector and as an optical material in the infrared.

The first CdTe based solar cells were reported in 1960 by Yu. Vodakov et al. [11] and G. Naumov [12] for 4 and 6% efficiency homojunction cells. The minority carrier lifetimes in CdTe were less than 10^{-8} sec, and therefore initially the use of cadmium telluride in solar cell applications was not thought to be feasible, even though, Berbe et al [13] reported 13% efficiency in a p-n-CdTe shallow homojunction cell. As CdTe has a short optical absorption length and it is difficult to form a thin film shallow junction with a high conductivity surface layer, it is preferable to form a heterojunction solar cell with a transparent conducting semiconductor as window layer partner. A number of different types of CdTe heterojunction cell have been fabricated in attempts to produce an efficient cell, but to date the best partner for CdTe has been found to be CdS in a n-CdS/p-CdTe structure.

1.3.2- CdS/CdTe Solar Cells.

The first CdS/CdTe heterojunction cells were made in the early 1960's when Muller and Zuleeg [14] in 1964 reported the fabrication of an Al/CdS/CdTe/Au structure produced by evaporating CdS onto vacuum evaporated CdTe. In 1968, Dutton and Muller [15] reported CdS/CdTe heterojunction diodes formed by the evaporation of around 100Å of CdTe onto CdS by standard vapour deposition procedures. The first layer structure using a transparent conducting oxide; n-SnO_2/n-CdS/p-CdTe/metal was reported in the early 1970's. Yamaguchi et al [16] in 1975 reported a single crystal CdTe/CdS cell with an efficiency of 4.5%, in which the CdS and CdTe were doped by In and P respectively. A year later, Yamaguchi et al [17] reported an efficiency of 12% under 68mW/cm^2 illumination with an In-Ga/CdS/CdTe/Ni cell fabricated by the epitaxial growth of CdS on the {111} face of p-doped CdTe single crystal substrates grown by the Bridgman technique. They calculated the theoretical efficiency of this cell to be 19.7% [18]. In 1982, Tyan and Fahrenbruch et al [19] reported 10.5% efficient thin film solar cells fabricated by close space sublimation. Since then many papers have been published on the structure of CdS/CdTe solar cells in attempts to understand the effects that limit the cell efficiency. The highest efficiency reported for a thin film CdS/CdTe was by Aramoto et al [20] in 1997, who achieved a conversion efficiency of 16%.

Cadmium Sulfide (CdS) has been successfully used as the window material in other solar cell systems such as CdS/Cu_2S, $CuInSe_2$ and InP/CdS. It has a direct wide bandgap (2.4 eV) and therefore, most of the incident solar spectrum is transmitted to the absorber layer. It also has an electron affinity of ~ 4.5 eV which is similar to CdTe and enables the conduction bands of CdS and CdTe to join smoothly at the interface.

CdS thin films have been prepared by a variety of techniques such as screen printing, close space sublimation, chemical bath deposition, physical vapour deposition, sputtering and electrodeposition [21]...etc. CdS generally crystallises in the hexagonal wurtize structure whereas CdTe is cubic, and therefore, there is a relatively large lattice mismatch (9.7%) [22] between CdS and CdTe. The electrical properties of CdS films vary over a wide range, depending on the method and conditions of growth. The CdS films are always n-type, with carrier concentrations in deposited films usually 10^{16}-10^{18}

cm^{-3} due to the presence of sulphur vacancies or Cd excess [23]. In a CdS/CdTe heterojunction, the CdS is normally heavily doped so that most of the depletion region lies in the p-CdTe layer.

The thickness of CdS has a crucial effect on the CdS/CdTe solar cell efficiency. A thin layer allows a high transmission to the absorber layer, giving an increase in short circuit current, J_{sc} but with a reduction in open circuit voltage V_{oc}. However the thickness should be sufficient and uniform to avoid short circuits. The effect of CdS thickness on the CdS/CdTe performance in for example *I-V* characterisation and spectral response will be investigated in chapters 5 and 6.

Many methods have been used to fabricate CdS/CdTe solar cells; RF sputtering [24], screen printing/sintering [25], close space sublimation [26], electrodeposition [27], spray deposition [28], stacked elemental layer processing [29], pulsed laser driven physical vapour deposition [30], organometallic vapour phase epitaxy [31], and writing method [32].

1.4- Thin Film CdS/CdTe Solar Cells.

Thin film CdS/CdTe photovoltaic (PV) modules are promising for large–scale economic generation (terrestrial application) because of the potentially low-cost deposition processes. The variety of thin film fabrication processes provide a high production capacity, reducing material consumption and the cost of manufacture. For example, the thickness of CdTe in CdS/CdTe thin film solar cells is around 2-5 μm, conversely, silicon cells require up to 20μm to absorb most of the photons with energy above its bandgap [33]. Furthermore, the fabrication of thin film modules is low cost compared to crystal cell module because it does not need to be cut in wafers and is easily integrated onto the substrate to form series and parallel contact modules.

There are three competitors for thin film solar cells; amorphous devices based on α-Si (or α-Si alloys) and polycrystalline structures based on the compound semiconductors CdTe and copper indium diselenide (CIS) and related alloys.

The first commercially available thin film cells were based on α-Si, mainly for use in consumer electronics such as portable calculators....etc. rather than for large-

scale power generation. The main problem with the α-Si cell is the stability, which is strongly dependent on the defect density in α-Si:H and its alloys. When α-Si cells are exposed to bright light, the performance degrades rapidly due to creation of metastable defects during illumination and refereed to as the Staebler-Wronski effect [34]. This defect impedes the diffusion of electrons and holes through the intrinsic layer causing the performance degradation. Amorphous silicon technology has made good progress in developing sophisticated, multi junction α-Si modules to minimise the Staebler-Wronski effect. The focus of research in α-Si cells is on improving laboratory cell efficiency (8% -12%), whether by incremental improvement of the multi-junction structures or by developing new α-Si technologies that avoid the Staebler-Wronski effect [35]. The production of α-Si module solar cells presently amounts to 21% of the global PV module production, that is around $62MW_p$/year. The principal manufacturers: are Nest Advanced Power System-NAPS (France), SANYO (Japan), Advanced Photovoltaic Systems-APS and United Solar Systems Corporation USSC (USA), Phototronics Solartechink-PST and Siemens Solar (Germany).

$CuInSe_2$-based PV devices are obtained by forming p-n heterojunction with a thin film of CdS. The use of related ternary or multinary compounds $Cu(In,Ga)(Se,S)_2$ allows the bandgap to be modified continuously over a wide rang (less than 1.1eV to around 1.7eV) by substituting Ga for In or by substituting S for Se. The highest efficiency of 17.1% was achieved by NREL in 1995 [36]. The CIS cell is an efficient cell, compared with other thin film cells, and has good stability. But the cost / manufacturability is affected by its complexity, so that CIS is still not commercially available.

CdTe is the easiest of the thin film cells to fabricate with different methods and potential manufacturers all have their favoured methods; Close-Space-Sublimation (ANTEC), High rate evaporation (Solar Cells Inc.), spray pyrolysis (Golden Photon Inc.) screen printing/sintering (Matsushita), and electrodeposition (BP).

There are three main problems encountered in the manufacture of CdS/CdTe thin film modules;

-The CdTe modules are much less efficient than the CdTe cell. High CdS/CdTe thin film cells efficiencies of around 16% have been reported in the laboratory,

but commercial module efficiencies remain relatively low at around 10%. The ability to achieve high current and high voltage with modules using thin CdS is a principal research problem in CdTe technology [35].

-Module reliability and long term stability is one of the most critical issues to establishing the commercial success of CdTe thin film PV. The stability of CdTe cells and modules is not always reproducible, some display excellent stability, which others do not. The reasons are not clear but are thought to be due to unstable contacts, eg. oxidation at the contact or copper diffusion from the contact to the junction with the CdS.

-The CdTe based PV modules obviously have cadmium which is highly toxic. It is still unknown if commercial CdTe modules will be classified as hazardous waste or not.

CdTe thin film technology can lead the PV industry especially if it can overcome these problems. Production cost of less than 1ECU/W_p at an annual production capacity of 10MW_p have been predicted for it [5].

1.5- Present Work

As demonstrated in section (1.4) cadmium telluride thin film solar cell industry is probably leading the other three thin film cells in the race to produce efficient low cost large scale terrestrial generation. It has therefore a strong position in solar cell manufacturing. Nevertheless, more research is needed in many aspects of material and associated device technology to enhance cell and module efficiency. Clearly there is a need to reduce the gap between the theoretical (~28%)[9] and the best current experimental (16%) efficiency.

This work aims to investigate the deposition of CdTe films by close space sublimation and to characterise the resulting CdS/CdTe thin film solar cells. Chapter 2 introduces the relevant scientific background for the solar cells. Chapter 3 presents the details of the experimental and characterisation techniques employed.

Chapter 4 is concerned with the deposition of CdTe by close space sublimation. The effects of the source and substrate temperature, pressure and the separation between the source and the substrate on the growth rate of CdTe films are studied. The

effects of substrate temperature on the texture of the CdTe films is investigated by scanning electron microscopy and X-ray diffraction.

Chapter 5 contains the photovoltaic output characteristics of CdS/CdTe cells as a function of CdTe and CdS layer thickness and for treated and untreated solar cells. Dark *I-V* characteristics are recorded at different temperatures in an attempt to study the current transport mechanisms across the junction. Space charge limited current analysis has been carried out before and after the $CdCl_2$ treatment. Dark *I-V* characteristics of TCO/CdS interface are also included.

Chapter 6 is concerned with the effects of the $CdCl_2$ procedure (the treatment of both CdS and CdTe, the thickness of $CdCl_2$, and the annealing time of $CdCl_2$) on the spectral response of solar cells. The spectral response characteristics of solar cells prepared at different substrate temperature of CdTe deposition, and at different CdS thickness are also studied.

The capacitance-voltage characteristics of untreated, treated CdTe, and treated CdS solar cells are presented in chapter 7. Photocapacitance and electroluminescence measurements of treated cells are also reported. The final conclusions of the study are discussed in chapter 8.

1.6-References:

(1)- Richard C. Neville. "Solar Energy Conversion: The Solar Cell". Elsevier Scientific Publishing Company, New York, 1978.

(2)- T. Markvart, "Solar Electricity". John Wiley & Sons, 1994.

(3)- M. A. Green, K. Emery, K. Bücher, D. L. King and S. Igari. "Solar Cell Efficiency Tables (Version 11) ". Prog. in Photovoltaics: Res. and Appl., 6 (1998) 35.

(4)- J. F. Nolan. "Development of 60cm ×120cm Thin Film CdTe PV modules". 23rd IEEE Photovoltaic Specialist Conf., Louisville, U.S.A., (1993) 34.

(5)- D. Bonnet, H. Richter, K. Jager, "The CTS Thin Film Solar Module Closer to Production". 13th European Photovoltaic Solar Energy Conf., Nice, France, 23-27 October (1995), 1456.

(6)- L. O. Herwing, and R. D. McConnell. "The Latest U. S. National PV Program Plan (1996-2000)". 13th European Photovoltaic Solar Energy Conf., Nice, France, 23-27 October (1995) 1190.

(7)- D. M. Chapin, C. S. Filler, and G. L. Peason. "A New Silicon p-n Junction Photocell for Converting Solar Radiation into Electrical Power". J. Appl. Phys. 25 (1954) 676.

(8)- D. A. Jenny, J. J. Loferski and P. Rappaport. "Photovoltaic Effect GaAs p-n Junction and Solar Energy Conversion". Phys. Rev., 101 (1956) 1208.

(9)- R. W. Birkmire and E. Eser. " Polycrystalline Thin Film Solar Cells: Present Status and Future Potential". Ann. Rev. Mater. Sci. 27 (1997) 625.

(10)- K. Zanio, "Semiconductors and Semimetals", Vol. 13 Cadmium Telluride, Academic Press, London 1978.

(11)- Yu. A. Vodakov, G. A. Lomakina, G. P. Naumov and Yu. P. Maslakovets. "A p-n Junction Photocell Made of Cadmium Telluride" Sov. Phys. Solid State, 2 (1960) 1.

(12)- G. P. Naumov and O. V. Nikolaeva. "The Efficiency of Transformation of Direct Solar Radiation Energy into Electric Energy using A CdTe Photocell". Sov. Phys. Solid State, 3. (1962) 2718.

(13)- M. Barbe, F. Bailly, D. Lincot and G. Cohen-Solal, 16th IEEE Photovoltaic Specialists Conf, San Diego, U.S.A., 1133 (1982). As quoted in (M. Bayhan. "Preparation and Characterisation of n-CdS/p-CdTe Thin Film Solar Cells". Ph.D. Thesis, University of Durham, U.K., 1994.

(14)- R. S. Muller and R. Zuleeg. "Vapour-Deposited, Thin-Film Heterojunction Diodes ". J. Appl. Phys. 35 (5) (1964) 1550

(15)- R. W. Dutton and R. S. Muller. "Thin Film CdS-CdTe Heterojunction Diodes" Solid –State Electron, 11 (1968) 749.

(16)- K. Yamaguchi, N. Nakayama, H. Matsumoto, Y. Hioki and S. Ikegami. "Photovoltaic Effect in CdS-CdTe Junction" Japan. J. Appl. Phys., 14 (1975) 1397.

(17)- K. Yamaguchi, H. Matsumoto, N. Nakayama and S. Ikegami. "Photovoltaic Effect in CdTe-CdS Junction Prepared by Vapour Phase Epitaxy". Japan. J. Appl. Phys. 15 (1976) 1575.

(18)- K. Yamaguch, N. Nakayama, H. Mastumoto and S. Ikagami. "CdS-CdTe Solar Cell Prepared by Vapor Phase Epitaxy". Japan. J. Appl. Phys., 16., (1977) 1203.

(19)- Y. S. Tyan and E.A. Perez-Aibuerne, Proc. 16th IEEE Photovoltaic Specialists Conf., San Diego, U.S.A., 794 (1982)

(20)- T. Aramoto, S. Kumazawa, H. Higughi. "16.0% Efficient Thin-Film CdS/CdTe Solar Cell". Japan. J. Appl. Phys., 36 (1997) 6304.

(21)- T. L. Chu and S. S. Chu. "Thin Film II-VI Photovoltaics". J. Solid State Electronics, 38 (1995) 533.

(22)- R. Dhere, D. Rose, D. Albin, S. Asher, M. Al-Jassim, H. Cheong, A. Swartzlander, H. Muotinho, T. Coitts and P. Sheldon. " Influence of CdS/CdTe Interface Properties on the Device Properties". 26th IEEE Photovoltaic Specialists Conf., Anaheim, California (1997).

(23)- K. Chopra and S. Das. "Thin Film Solar Cells" Plenum Press New York and London. 1983.

(24)- A. D. Compaan, C. N. Tabory, Y. Li, Z. Feng, and A. Fischer. " CdS/CdTe Solar Cells by RF Sputtering and Laser Physical Vapour Deposition". 23rd IEEE Photovoltaic Specialist Conf., Louisville, U.S.A. (1993) 394.

(25)- S. Ikegami. "CdS/CdTe Solar Cells by the Screen – Printing - Sintering Technique: Fabrication, Photovoltaic Properties and Application" Solar Cells 23 (1988) 89.

(26)- G. Gordillo, J. M. Florez and L. C. Hernandez. "Preparation and Characterisation of CdTe Thin Films Deposited by CSS". Solar Energy Mater. and Solar Cells, 37 (1995) 273.

(27)- G. C. Morris and S. K. Das. "Some Fabrication Procedures for Electrodeposited CdTe Solar Cell". Int. J. Solar Energy, 12 (1992) 95.

(28)- D. L. Schulz, M. Pehnt, C. J. Curtis, D. S. Ginley. "CdTe Thin Films: Spray Deposition Using A Nanoparticle Ink Precursor". Mater. Res. Soc. Symp. Proc. .426 (1996) 349.

(29)- R. W. Miles, M. T. Bhatti, K. M. Hynes, A. E. Baumann and R. Hill. "Thin Film of CdT Produced using Stacked Elemental Layer Processing for use in CdTe/CdS Solar Cells". Mater. Sci. and Eng., B16 (1993) 250.

(30)- A. Compaan, A. Bhat, C. Tabory, S. Liu, Y. Li, M. E. Savage, M. Shao, L. Tsien and R. G. Bohen. " Polycrystalline CdTe Solar Cell by Pulsed Laser Deposition". 22nd IEEE Photovoltaic Specialist Conf., Las Vegas, Nevada, (1991) 957.

(31)- H. G. Bhimnathwala, N. R. Taskar, W. I. Lee, I. Bhat, S. K. Ghanadhi and J. M. Borrogo. "Photovoltaic Properties of CdTe Layers Grown by OMVPE". 19th IEEE Photovoltaic Specialists Conf., New Orleans, Louisana, (1987) 1476.

(32)- T. Arita, A. Hanafusa, S. Kitamura, H. Takakura, and M. Murozono. "Large Area CdS/CdTe Solar Cells" 22nd IEEE Photovoltaic Specialists Conf., Las Vegas, Nevada, (1991) 946.

(33)- Anon, "Solar Cells: Outlook for Improved Efficiency", National Academy of Sciences, Washington, D. C. (1972). As quoted in {Kim W. Mitchell. "Evaluation of the CdS/CdTe Heterojunction Solar Cell". Academic Press, New York & London (1979).}

(34)- W. H. Bloss, F. Pfisterer, M. Schubert, T. Walter. "Thin-Film Solar Cells". Prog in Photovoltaics: Res. and Appl. 3 (1995) 3.

(35)- K. Zweibel, "Thin Film: Past, Present, Future". Prog in Photovoltaics: Res. and Appl. 3 (1995) 279.

(36)- J. Tuttle, M. Contreras, T. Gillespie, K. Ramanathan, A. Tennant, J. Keane, A. Gabor and R. Noufi. " 17.1% Efficiency Cu(In,Ga)Se_2-Based Thin Film Solar Cell". Prog in Photovoltaics: Res. and Appl., 3 (1995) 235.

Chapter Two:

Scientific Background.

2.1-Introduction.

In this chapter the background theory of solar cells and related mechanisms will be described. A brief review of solar irradiation relevant to solar cells will be included. The efficiency equation for the CdS/CdTe cell will be discussed and the equations of capacitance-voltage and spectral response are then deduced. Finally the environmental and the health issues will be presented.

2.2-Solar Radiation.

The solar spectrum extends over a wide range of wavelengths from the ultraviolet through the visible to the far infrared and can be approximated by a blackbody at 5800 K [1]. The intensity and the spectral distribution of the radiation arriving at the surface of the Earth depends on the optical path length between the Earth and the Sun, the angle of incident radiation (which is a function of the time of the day, season, the latitude and the longitude) and the atmosphere conditions (turbidity, water and ozone content, cloudiness and ground reflection).

The amount of solar power received per unit of time on unit area of collector surface perpendicular to the sun's direction is called the solar constant. This quantity is difficult to measure from the surface of the earth because of uncertainties in correcting the observed flux for losses in the Earth's atmosphere. The value of solar constant in free space at the Earth's mean distance from the Sun is 1.353KW/m^2 and differs from this value by up to 3.35% because of changes in the Earth - Sun distance through the year [2].

The optical path length between the Sun and the Earth depends on the Sun's declination angle. This angle is described by specifying a zenith angle of the Sun, z, the angle between the Earth-Sun radius and the normal of a plane containing the horizon circle as illustrated in figure (2-1) [2]. The path length through the atmosphere is described in terms of an equivalent relative air mass mr which is defined as sec (z), thus the various solar spectra are labelled AMmr (air mass mr). AM0 corresponds to the solar spectrum in outer space and is important for the satellite application of solar cells. At sea level on a clear day at noon at a latitude when the Sun is directly overhead (e.g. on the equator at the equinox) the radiation from the Sun at zenith (the angle z = 0) corresponds to air mass1 (AM1), whereas, AM1.5 is a typical solar spectrum on the

Earth's surface at angle z = 48.19° on clear day with total intensity 1KW/m^2, and is often used to calibrate the solar cells modules. Figure (2.2) shows the solar flux density spectrum of AM0 and AM1.5.

The air mass number approaches unity only under perfect conditions and z = 0 which is difficult to achieve. Therefore, AM1.5 or AM2 are used as an approximate estimate of the air mass during daylight hours for the purposes of calculating cell efficiencies. For the measurement of solar cell performance long-term stability and reproducibility a solar simulator is required. This should approximate the solar spectrum with total intensity 1kW/m^2. Suitable filtering (water filter) should be used to adjust the source spectrum to that of the sun. The sample temperature in the simulator should be 25 °C under standard measurement conditions.

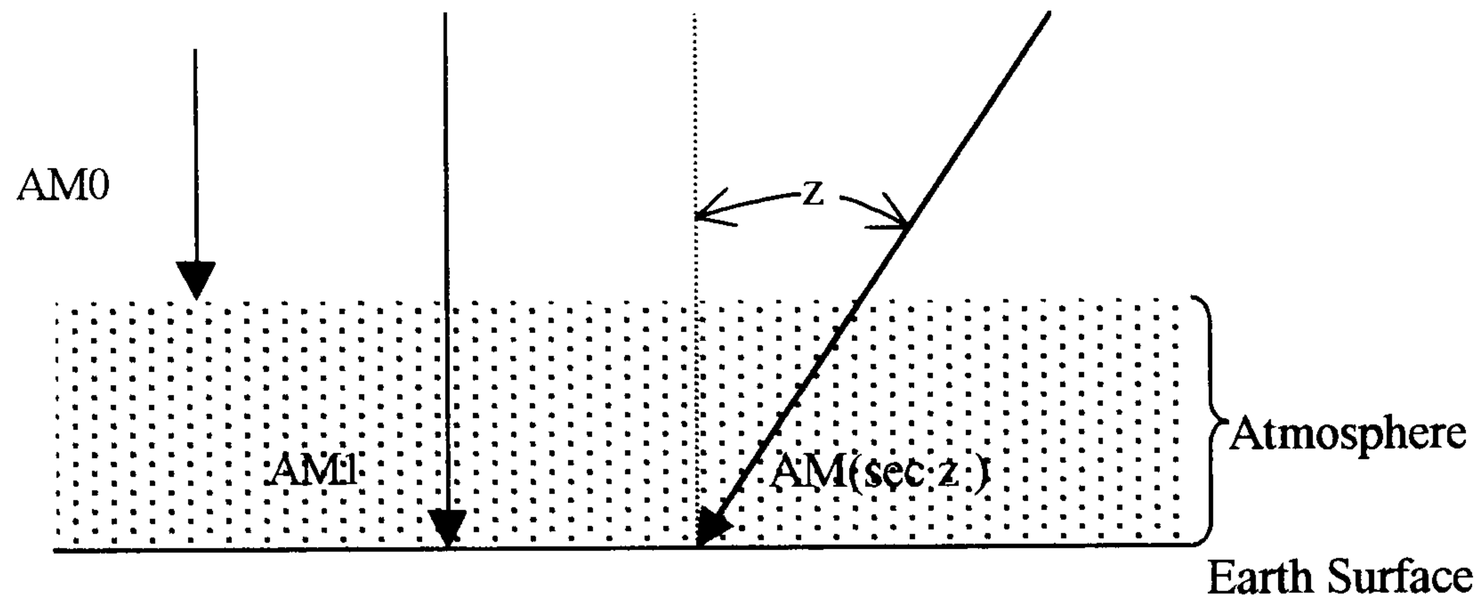

Figure (2.1)- Definition of air mass numbers: AM0 in space; AM1 at the Earth's surface at zenith; AM (sec z) at the Earth's surface at, z, deviation.

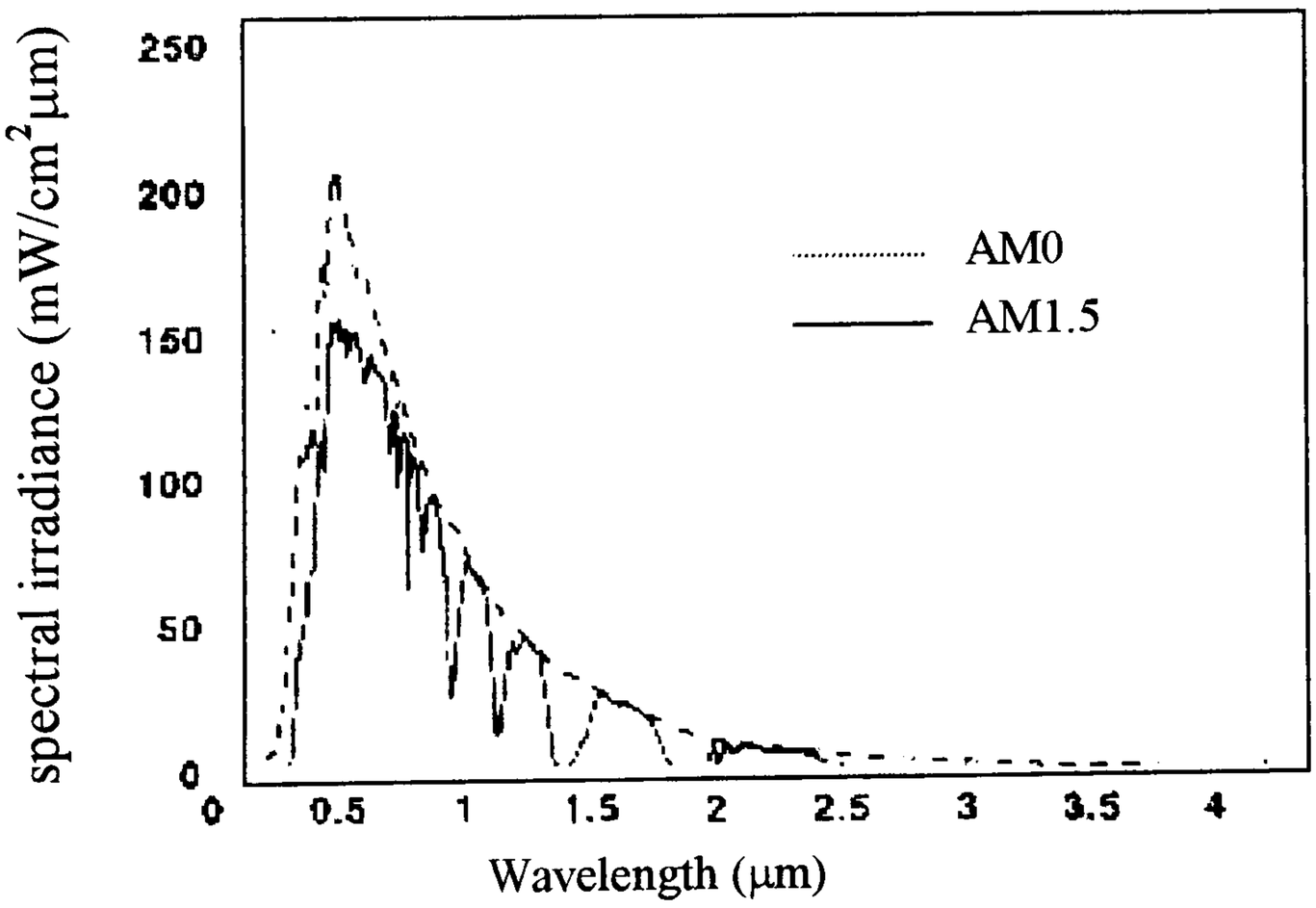

Figure (2.2)- Solar density spectrum for AM0 and AM1.5 [3].

2.3-The Heterojunction Solar Cell Structure.

The CdS/CdTe thin film solar cell is classified as a heterojunction solar cell because it is simply a junction between two dissimilar semiconductors (CdS and CdTe). If the two semiconductors are of similar conductivity type, then the junction is called an isotype heterojunction, otherwise it is termed an anisotype or (p-n) heterojunction.

The typical configuration of a heterojunction solar cell (CdS/CdTe) is given in figure (2-3). Such solar cells generally consist of a top window layer (collector – converter) composed of a semiconductor (CdS) with a large bandgap through which the light (with energy less than the bandgap of window layer) can pass to the junction and the absorber layer. The absorber layer composed of a semiconductor (CdTe) with a high absorption coefficient and smaller bandgap, is intended to absorb most of the light and generate the minority carriers which diffuse to the junction. It is normally preferable for the absorber layer to be p-type material because of the larger diffusion lengths for minority carriers (electron) in p-type semiconductors. The window layer collects the minority carriers which are swept across the junction to become majority carriers. Therefore the window layer should be of opposite conductivity type (i.e. n-type) compared to the absorber layer The front contact is a transparent conducting oxide TCO. The back contact is gold or graphite in our cells. Both front contact and back contact should be ohmic to their respective semiconductors. The metallurgical junction between the window and absorber layers creates a space charge region, across which charge separation takes place to generate an electromotive force (e.m.f.).

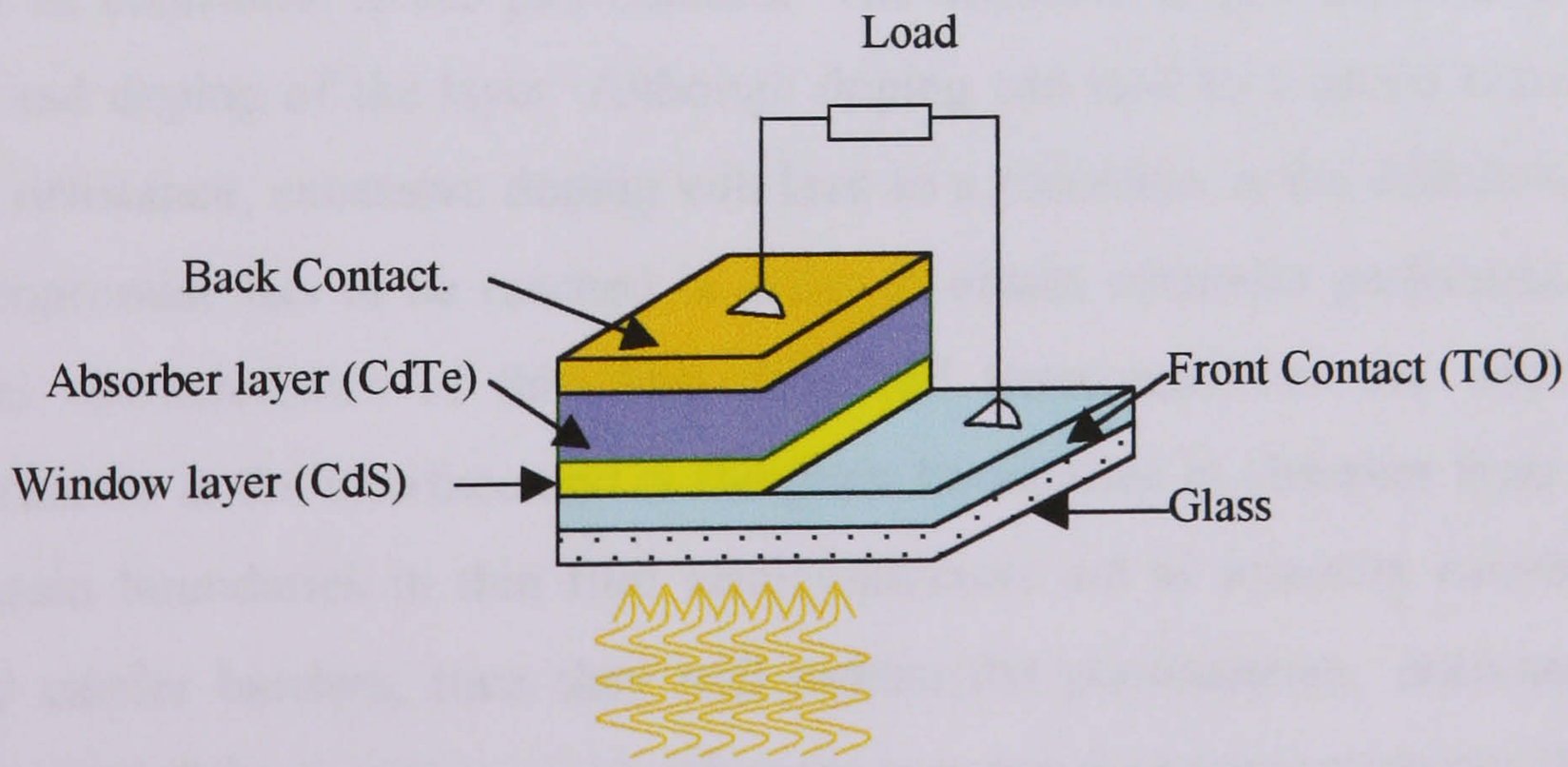

Figure (2-3)- A solar cell (CdS/CdTe) configuration.

2.4- Solar Cell Mechanisms.

Solar cells depend on the photovoltaic effect. When incident photons have an energy greater than the bandgap of the absorber layer, they are absorbed and electron – hole (EH) pairs are generated, with the electrons raised in energy from the valance band to the conduction band. In principle the excess minority carriers diffuse to the space charge region and are immediately separated by the built-in-field. However, not all of the photogenerated carriers are collected and swept out, because not all of the photogenerated electrons created in the absorber layer will diffuse to the junction. Some are attracted by the back surface ohmic contact and lost through interface recombination at the contact and some will be lost through bulk recombination. In addition, some of photogenerated carriers will be lost by interface recombination in the junction between the semiconductors, bulk recombination in the window layer and interface recombination between the window layer and the front contact [4]

The performance of solar cells depends on the absorber layer parameters which affect its ability to absorb the light and transport carriers. The most important of these parameters are the optical bandgap, absorption coefficient, diffusion length, lattice parameters and purity/doping. The absorber semiconductor bandgap has to be matched to the solar spectrum and optimum bandgaps lie in the range 1.1 to 1.5eV [5]. The minority and majority carrier diffusion lengths have important effects on the collection efficiency, because any minority carriers that recombine before they reach the junction will not be contribute to the photocurrent. The diffusion length depends on the defect density and doping of the layer. Although doping can lead to a useful reduction in the internal resistance, excessive doping will lead to a reduction in the diffusion length and so a compromise has to be reached in order to obtain optimum performance [6]. The electrical characteristics of thin film solar cell heterojunctions are affected by the microstructure at the interface and at the grain boundaries in absorber layer (CdTe)[7]. If the grain boundaries in thin film semiconductors act as minority carrier sinks and majority carrier barriers, then they will reduce the photocurrent, decrease the shunt resistance and if the structure is not columnar increase the series resistance [8].

2.5-Formation of Energy Band Diagram.

The heterojunction model was first developed by Anderson [9] as an extension of the homojunction model. The energy band diagram for the n-CdS/p-CdTe heterojunction before and after n-p junction formation is shown in figure (2-4). (The effect of dipoles at the interface are neglected). The semiconductors are characterised by their electron affinity χ, energy bandgap E_g and work function ϕ. As the materials are contacted together, the Fermi level must be constant throughout the device and consequently there is an exchange of electrons and holes between the two semiconductors. As a result band bending will occur in the conduction and valance bands at the interface as the charge displacement between the semiconductors forms a depletion region. In the ideal junction, the barrier height is given by:

$$qV_b = E_{gp} + \Delta E_c - \delta_n - \delta_p \qquad (2.1)$$

Where ΔE_c is the conduction band discontinuity at the interface, E_{gp} is the bandgap of the p-type material, δ_n and δ_p are the displacement of the Fermi level from the conduction and valance band edges in the n- and p-type semiconductors respectively. The band discontinuities arise because of the requirement that the vacuum levels in the two semiconductors must coincide at the junction, and are given by:

$$\Delta E_c = \chi_p - \chi_n \qquad (2.2)$$

$$\Delta E_V = (E_{gn} - E_{gp}) - \Delta E_c \qquad (2.3)$$

Where E_{gn} is the band gap of n-type material, and χ_p , χ_n are the electron affinity of the p- and n-type materials respectively. The conduction band discontinuity ΔE_c may be a "spike" or a "notch" (Anderson model [9]), that would tend to impede the photogenerated carrier transport and allow recombination at the interface to dominate the current transport.

2.6-Photovoltaic Characteristics of Heterojunction Solar Cells.

The current –voltage characteristics in a heterojunction takes the form [10]:

$$\mathrm{J} = J_{oo} \exp(-qV_{bp}/kT)[\exp(\frac{qV_p}{kT}) - \exp(\frac{-qV_n}{kT})] \qquad (2.4)$$

$$J_{oo} = XqN_D D_n / L_n \qquad (2.5)$$

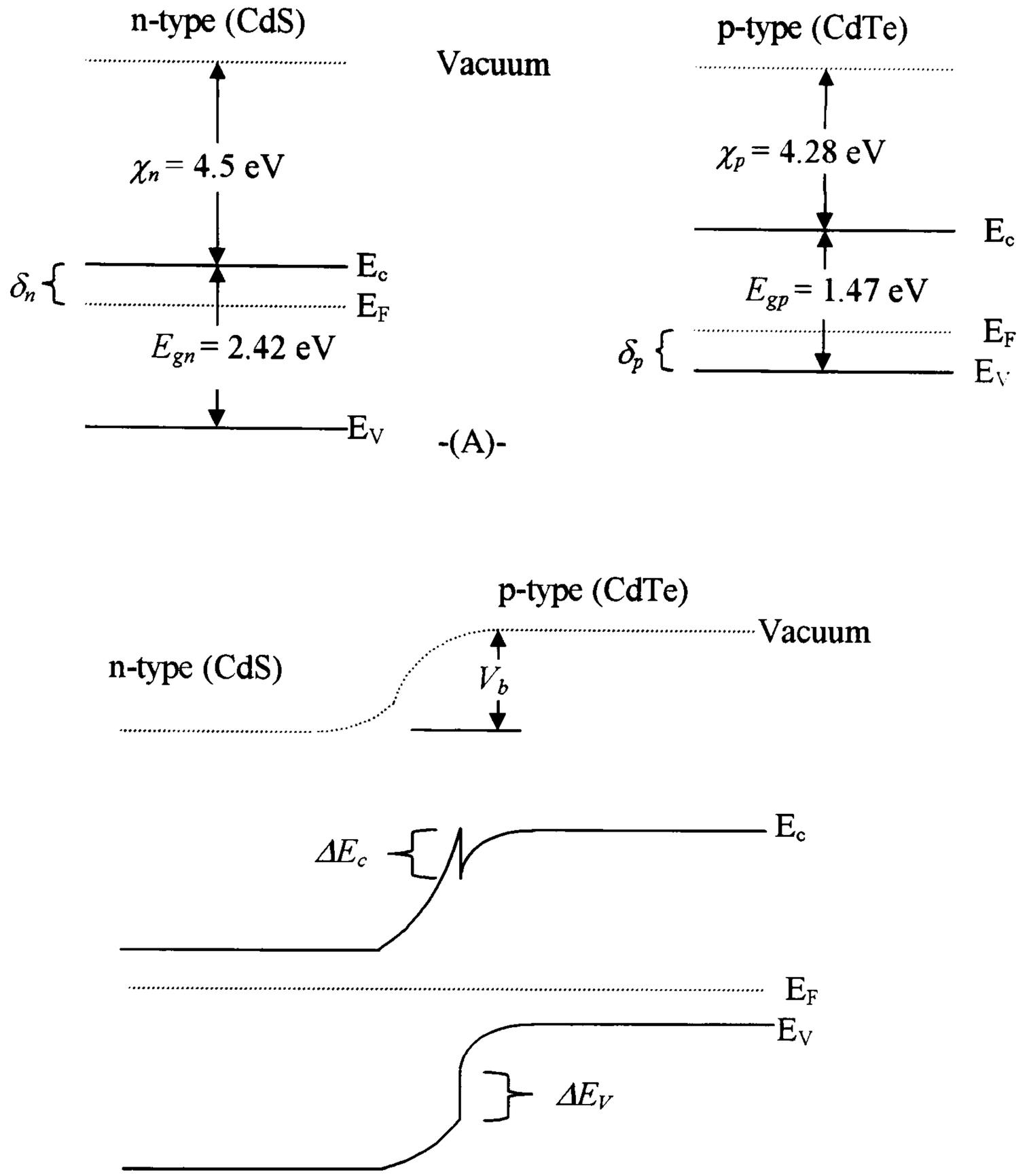

Figure (2-4)- Energy bands diagram for CdS/CdTe before (A) and after (B) the forming p-n heterojunction.

$$V_{bp} = K_P V_b \tag{2.6}$$

where
$$K_P = (1 + N_A \varepsilon_p / N_D \varepsilon_n)^{-1} \tag{2.7}$$

$$V_P = K_P V \tag{2.8}$$

$$V_n = K_n V \tag{2.9}$$

Where V_{bP} is the portion of the built-in voltage on the p-side of the junction, V_P and V_n are the portions of the applied voltage appearing as defined by K_p and K_n on the p and n-side of the junction, X is the transmission coefficient for electrons to pass the interface, D_n and L_n are the diffusion constant and diffusion length respectively for

electrons in the p-type semiconductor. N_A and N_D are the concentration of acceptor and donors respectively.

If the n-type is highly doped with respect to the p-type semiconductor, (i.e. $N_D >> N_A$) the current – voltage equation simplifies to give the ideal diode equation:

$$J = J_o[\exp(\frac{qV}{kT}) - 1] \tag{2.10}$$

$$J_o = (\frac{XqN_D D_n}{L_n})\exp(\frac{-qV_b}{kT}) \tag{2.11}$$

In practice the ideal diode equation is normally modified to take the following form:

$$J = J_o[\exp(\frac{qV}{nkT}) - 1] \tag{2.12}$$

where n is an ideality factor which varies between 1and 2 depending on the imperfection density in the two semiconductors. When the diode is exposed to light, excess electrons and holes are generated and diffuse to the junction where they are separated, the total current through the illuminated diode is then given by the following equation:

$$J = J_o[\exp(\frac{qV}{nkT}) - 1] - J_L \tag{2.13}$$

Where J_L is the light generated current density, which in practice is the total photocurrent density J_{ph}, generated in the depletion region and within one minority diffusion length of the depletion region edge, reduced by the recombination current J_r associated with the interface states.

$$J_L = J_{ph} - J_r \tag{2.14}$$

The photogenerated current and the recombination current will be discussed in more detail in section (2.9).

2.7- Solar Cell Parameters.

Solar cell performance is described in term of the short – circuit current density J_{sc}, the open - circuit voltage V_{oc}, the fill factor FF, and the conversion efficiency η. These parameters are derived from the photovoltaic output characteristics of the solar cell. Dark and illuminated current-voltage characteristics for the ideal case are illustrated in figure (2-5).

Short Circuit Current Density (J_{sc}): This is the photocurrent flowing through a cell junction at zero applied bias, or it could be defined as the photocurrent output of a solar cell when the load impedance is much smaller than the device impedance. In the ideal case, when the recombination current and the series and shunt resistances are unimportant, it will be equal to the total light generated current density J_L. Then it is proportional to the incident photon flux with energy greater than or equal to the absorber bandgap. The short circuit current density depends on the spectrum of the light source and the spectral response of the device.

Open Circuit Voltage (V_{oc}): The open circuit voltage is the output voltage of the device under illumination when the current flowing through the junction is zero and the load impedance is much greater than the device impedance. In the ideal case, i.e. very small series resistance and very large shunt resistance, the open circuit voltage can be obtained from equation (2.13) when $J = 0$ as [2]:

$$V_{oc} = \frac{nkT}{q} \ln \left[\frac{J_L}{J_o} + 1\right] \qquad (2.15)$$

Increasing the ideality factor n, leads to a corresponding increase in the saturation current density J_o and consequently the open circuit voltage is actually reduced, so the ideal value of n is unity. As the bandgap of the absorber layer is increased, J_o is decreased strongly, which in turn increases the V_{oc} however the photogenerated current decreases. Thus there is a trade-off between a high V_{oc} with a large bandgap absorber and a high photogenerated current from a low bandgap absorber layer.

Fill Factor (FF): The fill factor is the ratio of the maximum electrical power output ($P_m = I_m \times V_m$) to the product of V_{oc} and I_{sc} . It is affected by the value of the ideality factor n, series resistance R_s and the shunt resistance R_{sh} of the cell. Low values of n and R_s and a large value of R_{sh} are required for a high fill factor.

Efficiency (η): The efficiency of a solar cell is the parameter which describes the overall performance and is expressed in term of J_{sc} ,V_{oc} , P_{in} and FF as[11]:

$$\eta = \frac{J_{sc} V_{oc}}{P_{in}} FF \tag{2.16}$$

Where P_{in} is the incident radiation power density and expressed in mW/cm^2. In general there are many parameters which affect the efficiency of a cell through their effect on J_{sc}, V_{oc} and FF as shown in figure (2-6).

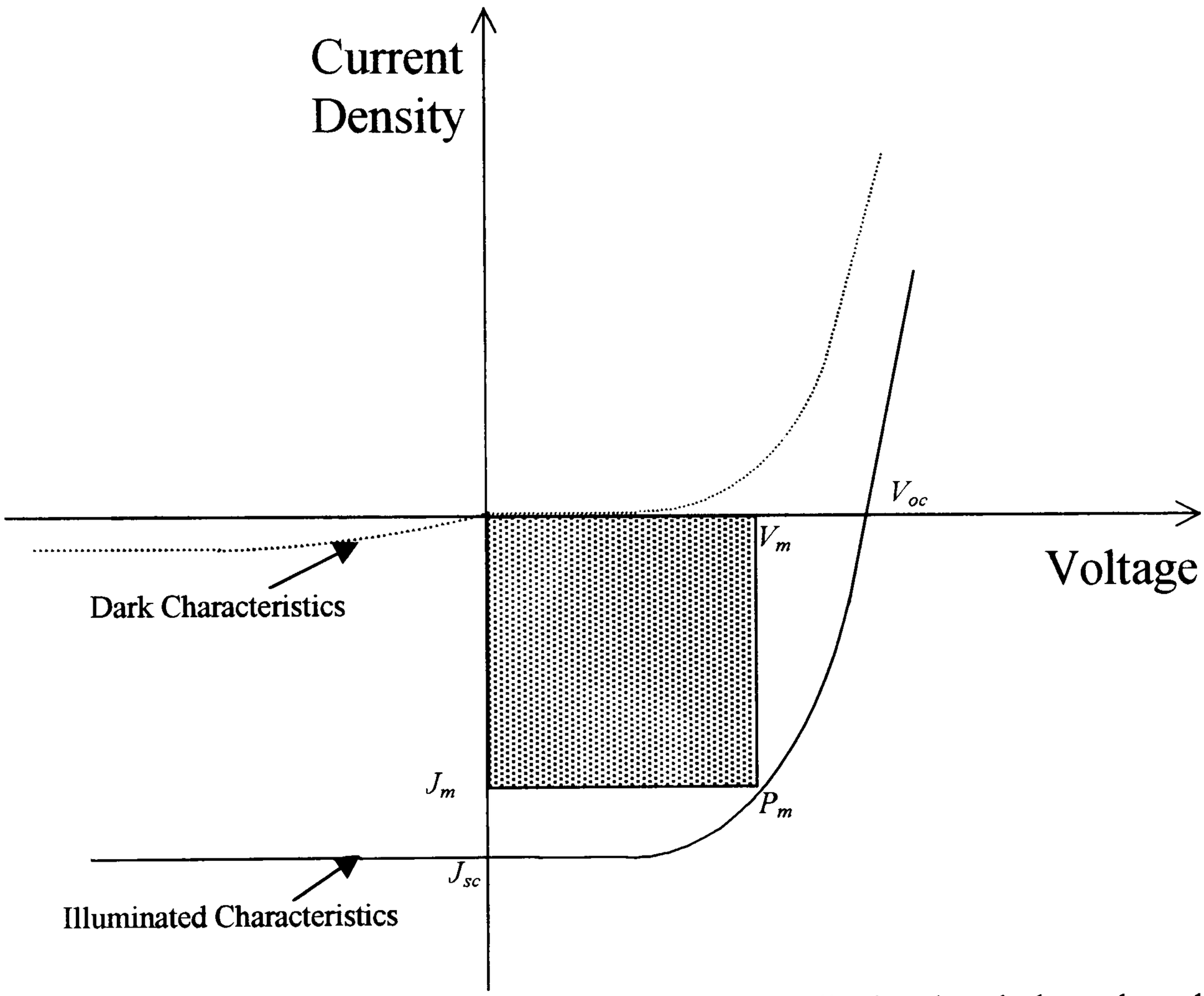

Figure (2-5)- Current-voltage characteristics of solar cells in the dark and under illumination.

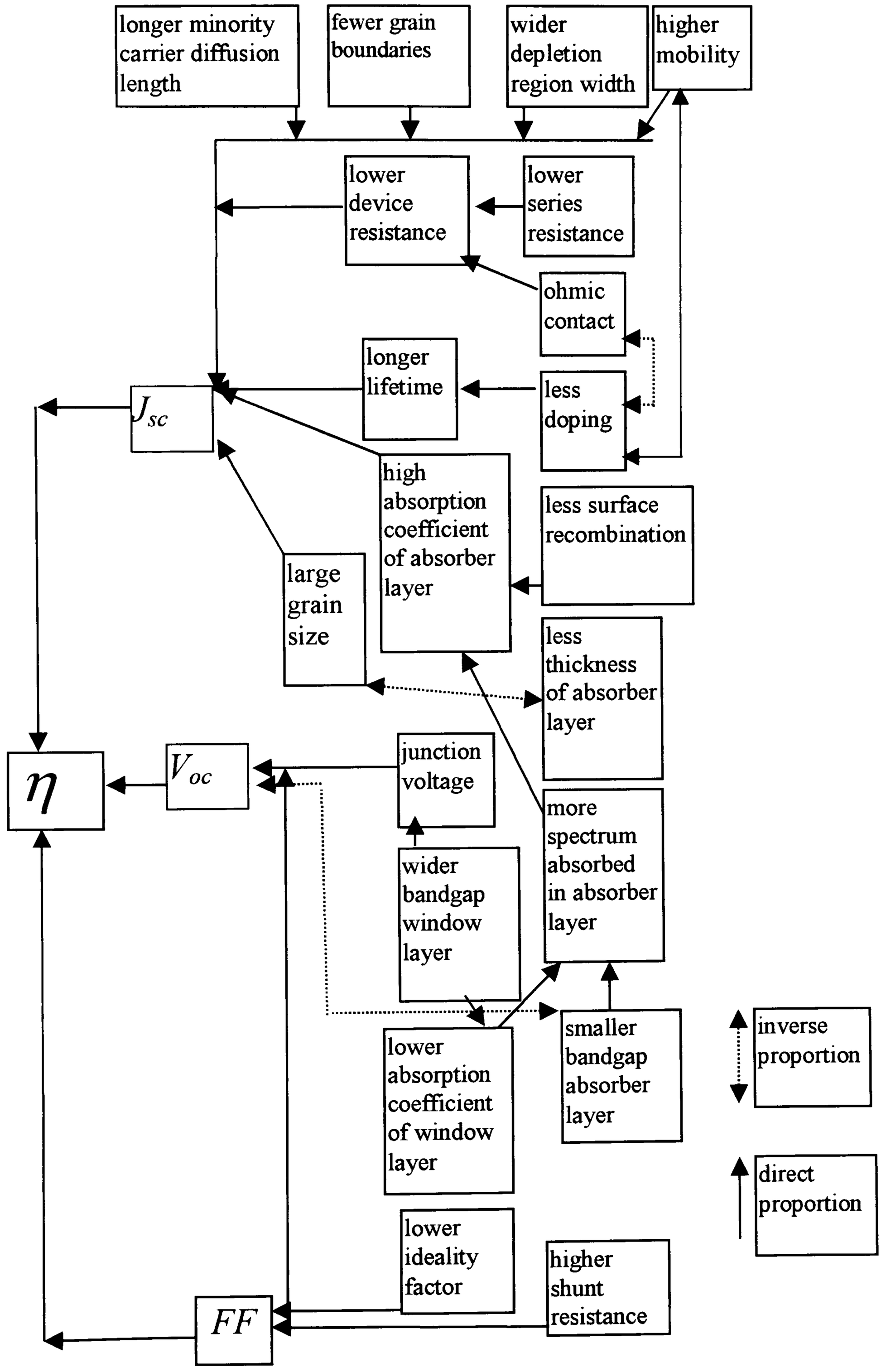

Figure (2-6) -The relationships between the various parameters and the efficiency of a solar cell.

2.8-Capacitance –Voltage Characteristics of p-n Junctions.

In the space charge region it may be assumed that all the donors and acceptors are ionised and for space charge computation, the free carrier density can be neglected (i.e. the depletion region approximation). Since the dipole about the junction must have an equal number of charges on either side ($Q_+ = |Q_-|$):

$$qA\,x_p N_A = qA\,x_n N_D \tag{2.17}$$

Where A is the cross-section area, N_A and N_D are the acceptor and donor concentrations respectively, x_p is the penetration of the space charge region into the p material, and x_n is the penetration into the n-type region. The transition region may extend into the p and n regions unequally, e.g. if the p-type side is more lightly doped than the n side ($N_A < N_D$) the space charge region will extend further into the p-type material.

The electric field $\zeta(x)$ distribution within the transition region may be calculated using Gauss law, which relates the gradient of the electric field to the local space charge at any point x: [12]

$$\frac{d\zeta(x)}{dx} = \frac{q}{\varepsilon\varepsilon_o}[(p(x) - n(x)) + N_D - N_A] \tag{2.18}$$

this equation is simplified in the transition region since the contribution of the carriers $(p(x) - n(x))$ may be neglected. So with this approximation we have two regions for constant space charge:

$$\frac{d\zeta(x)}{dx} = \frac{q}{\varepsilon_n\varepsilon_o} N_D \qquad \text{for } 0 < x < x_n \tag{2.19a}$$

$$\frac{d\zeta(x)}{dx} = -\frac{q}{\varepsilon_p\varepsilon_o} N_A \qquad \text{for } -x_p < x < 0 \tag{2.19b}$$

There will be a maximum ζ_0 at the junction, as this point is between the charge Q_+ and Q_- on either side of the transition region (i.e. $x = 0$). The value of ζ_0 can be found by integrating both parts of equation (2.19) with appropriate limits:

$$\int_{\zeta_0}^{0} d\zeta = \frac{q}{\varepsilon_n\varepsilon} N_D \int_0^{x_n} dx \qquad 0 < x < x_n \tag{2.20a}$$

$$\int_0^{\zeta_0} d\zeta = -\frac{q}{\varepsilon_n \varepsilon} N_A \int_{-x_p}^{0} dx \qquad -x_p < x < 0 \qquad (2.20b)$$

Since the electric field at any x is the negative of the potential gradient at that point, the contact potential V_{bn} in the n-type side and V_{bp} in p-type side will be:

$$V_{bn} = \frac{q}{2\varepsilon_n \varepsilon_o} N_D x_n^2 \qquad (2.21a)$$

$$V_{bp} = \frac{q}{2\varepsilon_p \varepsilon_o} N_A x_p^2 \qquad (2.21b)$$

Then the total potential V_b will be:

$$V_b = V_{bn} + V_{bp} = \frac{q}{2\varepsilon_n \varepsilon_o} N_D x_n^2 + \frac{q}{2\varepsilon_p \varepsilon_o} N_A x_p^2 \qquad (2.22)$$

The total electrostatic potential across the junction is (V_b + V) in reverse bias (positive voltage connected to n – region) and (V_b - V) in forward bias. From equations (2.17) and (2.22) the width of each space charge region as a function of applied voltage can be written:

$$x_n = \left(\frac{2N_A \varepsilon_n \varepsilon_p \varepsilon_o (V_b \pm V)}{qN_D (\varepsilon_p N_A + \varepsilon_n N_D)} \right)^{1/2} \qquad (2.23a)$$

$$x_p = \left(\frac{2N_D \varepsilon_n \varepsilon_p \varepsilon_o (V_b \pm V)}{qN_A (\varepsilon_p N_A + \varepsilon_n N_D)} \right)^{1/2} \qquad (2.23b)$$

The total width ,W, of the depletion region therefore is given by:

$$W = x_n + x_p = \left(\frac{2\varepsilon_n \varepsilon_p \varepsilon_o (N_D^2 + N_A^2)\ (V_b \pm V)}{qN_D N_A (\varepsilon_n N_D + \varepsilon_P N_A)} \right)^{1/2} \qquad (2.24)$$

The depletion region capacitance per unit area is by definition:

$$C = \left| \frac{dQ}{d(V_b \pm V)} \right| \qquad (2.25)$$

Then the capacitance per unit area of an abrupt heterojunction (neglecting dipole and interface states effects) from equations (2.17), (2.23) and (2.25) is given by

$$C = \left[\frac{qN_D N_A \varepsilon_n \varepsilon_p \varepsilon_o}{2(\varepsilon_n N_D + \varepsilon_p N_A)(V_b \pm V)} \right]^{1/2} \quad (2.26)$$

When $N_D >> N_A$, ie the depletion region is entirely in the p-side of the junction, the latter equation simplifies to:

$$C \cong \left[\frac{qN_A \varepsilon_p \varepsilon_o}{2(V_b \pm V)} \right]^{1/2} \quad (2.27)$$

Thus then acceptor density N_A can be obtained from the slope of a plot of C^{-2} vs. V and the built-in voltage V_b from the intercept on the voltage axis.

2.9-The Collection of Photogenerated Carriers and Spectral Response:

The collection of photogenerated minority carriers in CdS/CdTe cells may be calculated by considering the contributions from two main regions;

(a) The depletion region where the junction electric field promotes carrier collection by sweeping out all carriers generated in it or arriving at its boundaries, assuming that there are no other electric fields.

(b) One minority diffusion length from the depletion edge in the absorber layer, assuming that the window layer (CdS) does not contribute to the photocurrent and that the absorber layer (CdTe) is wide enough compared to the absorption length so the effect of the back surface may be neglected.

The absorption of light in general is described by deBeer's law:

$$\phi(x,\lambda) = \phi_0(\lambda)\exp[-\alpha(\lambda)x] \quad (2.28)$$

Where $\phi(x,\lambda)$ is the photon flux available at a distance x from the surface, $\phi_0(\lambda)$ is the photon flux entering the semiconductor in unit of photons /cm^2 sec, $\alpha(\lambda)$ is the optical absorption coefficient of the semiconductor. If the window layer (CdS) has width (d), the photon flux transmitted to the junction is

$$\phi(d,\lambda) = \phi_0(\lambda)\exp[-\alpha_2(\lambda)d] \quad (2.29)$$

Where $\alpha_2(\lambda)$ is the absorption coefficient of the window layer (CdS). If this is the photon flux entering to the depletion region, which has width w, then the flux absorbed in the depletion region will be:

$$= \phi_0(\lambda)\exp(-\alpha_2(\lambda)d)[1-\exp(-\alpha_1 w)] \quad (2.30)$$

Where $\alpha_1(\lambda)$ is the absorption coefficient of absorber layer (CdTe) and it is assumed that all the depletion region lies in the absorber layer. The total generation in the depletion layer, G_w, is:

$$G_w = a_0\phi_0(\lambda)\exp(-\alpha_2(\lambda)d)[1-\exp(-\alpha_1 w)] \tag{2.31}$$

Where a_0 is the quantum efficiency in the absorber layer. The photocurrent due to generation in the depletion region is given by [13]:

$$J_w(\lambda) = qG_w(\lambda) = qa_0\phi_0(\lambda)\exp(-\alpha_2(\lambda)d)[1-\exp(-\alpha_1(\lambda)w)] \tag{2.32}$$

The net flux entering the absorption layer after crossing the junction will be:

$$= \phi_0(\lambda)\exp(-\alpha_2(\lambda)d)\exp(-\alpha_1(\lambda)w) \tag{2.33}$$

Then the total flux absorbed in one minority carrier diffusion length (L) in the absorber layer will be:

$$= \phi_0(\lambda)\exp(-\alpha_2(\lambda)d)\exp(-\alpha_1(\lambda)w)[1-\exp(-\alpha_1(\lambda)L)] \tag{2.34}$$

The total generation in this region will be:

$$G_b = a_0\phi_0(\lambda)\exp(-\alpha_2(\lambda)d)\exp(-\alpha_1(\lambda)w)[1-\exp(-\alpha_1(\lambda)L)] \tag{2.35}$$

and the photocurrent:

$$J_B(\lambda) = qa_0\phi_0(\lambda)\exp(-\alpha_2(\lambda)d)\exp(-\alpha_1(\lambda)w)[1-\exp(-\alpha_1(\lambda)L)] \tag{2.36}$$

The total photocurrent density $J_{ph}(\lambda)$ is the sum of the photocurrents generated in the depletion region $J_W(\lambda)$ and within one minority carrier diffusion length in the absorber layer from the edge of the depletion region $J_B(\lambda)$:

$$J_{ph}(\lambda) = J_W(\lambda) + J_B(\lambda) \tag{2.37}$$

$$J_{ph}(\lambda) = qa_0\phi_0\exp(-\alpha_2(\lambda)d)[1+\exp(-\alpha_1(\lambda)w)\exp(-\alpha_1(\lambda)L)] \tag{2.38}$$

The recombination current J_r can be written as [14]:

$$J_r = qSn_I \tag{2.39}$$

Where S is the interface recombination velocity and n_I is the excess minority carrier density at the junction interface. The photon current can be expressed as:

$$J_{ph} = J_r + J_L = J_L(1+J_r/J_L) \tag{2.14}$$

$$J_L = qn_I\mu_e\zeta \tag{2.40}$$

Where μ_e is the electron mobility in the junction region, ζ is the electric field at the junction interface. From equation (2.14), (2.39) and (2.40), and solving for n_I, the light current can be expressed as:

$$J_L = J_{ph}/(1+\frac{S}{\mu_e \zeta}) \tag{2.41}$$

From equation (2.38) and (2.41) the photogenerated minority carrier current reaching the CdS is:

$$J_L(\lambda) = qa_0\phi_0(1+\frac{S}{\mu_e \varepsilon})^{-1}\exp(-\alpha_2(\lambda)d)[1+\exp(-\alpha_1(\lambda)w)\exp(-\alpha_1(\lambda)L)] \tag{2.42}$$

The equation may be written:

$$J_L = qa_0\phi_0 H(V) \tag{2.43}$$

where $H(V)$ is called the collection function.

The spectral response is the photocurrent collected at each wavelength relative to the number of photons incident on the surface of the device [8]. The spectral response is sometimes known as the quantum efficiency or collection efficiency at each wavelength. The internal spectral response SR_{int} of the device is defined as the number of carriers relative to the number of photons entering the material. Then the external response SR_{ext} is just the internal response modified by reflection of light from the front surface of the device:

$$SR_{ext}(\lambda) = SR_{\text{int}}(\lambda)[1-R(\lambda)] \tag{2.44}$$

Where $R(\lambda)$ is the overall reflection loss.

The quantum efficiency from the definition will be;

$$Q(\lambda) = \frac{J_L}{q\phi_0} = \frac{N_e}{N_{ph}} \tag{2.45}$$

Where N_e and N_{ph} are the number of electrons and photons respectively.

If we assume that the recombination current J_r is much smaller than the photocurrent J_{ph}, then the equation (2.14) will be:

$$J_{ph} \approx J_L \tag{2.46}$$

Then the quantum efficiency can be expressed as:

$$Q(\lambda) = a_0\exp(-\alpha_2(\lambda)d)[1-\exp(-\alpha_1(\lambda)w)\exp(-\alpha_1(\lambda)L)] \tag{2.47}$$

Where a_0 is equal to unity [15].

Figure (2.7) shows the theoretical quantum efficiency of a CdS/CdTe heterojunction according to equation (2.47) (values of the absorption coefficient of CdS and CdTe were taken from [16] [17]). The calculation was done for two cases where the space charge region and the minority diffusion length were set to 2.5μm and 2.5 μm respectively, and 0.5μm and 0.3μm. The figure shows that the quantum efficiency increases as the depletion region width and the minority carrier diffusion length increases.

Figure (2-7)- Simulated quantum efficiency of CdS/CdTe cell.

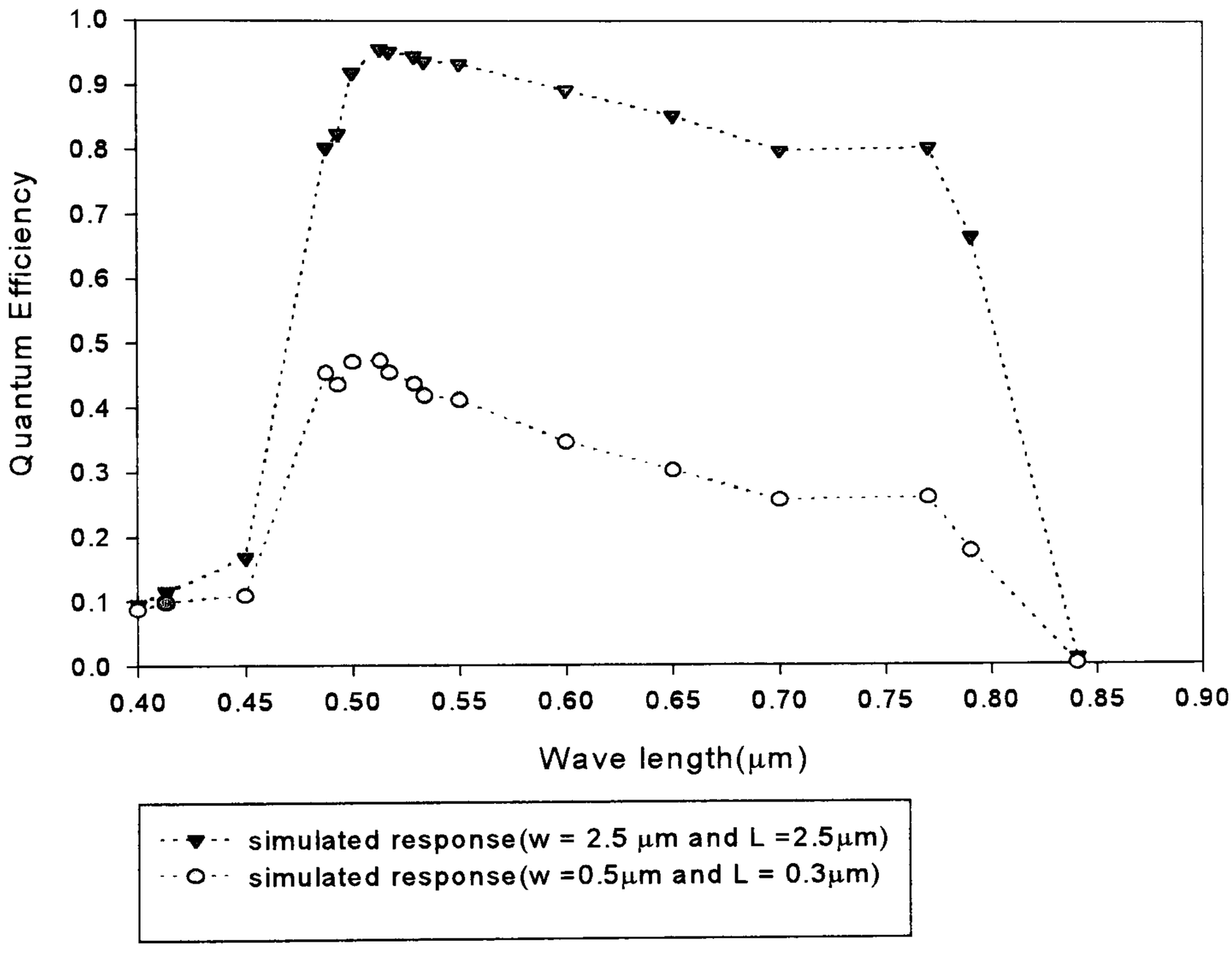

2.10-Metal-Semiconductor Contacts.

The metal – semiconductor contact has a significant effect on the performance and behaviour of electrical devices. In some devices, it is essential to form a contact that gives raise to an electrical barrier, a Schottky barrier, at the interface with the semiconductor which allows the current to flow in only one direction. In other devices (e.g. solar cells), it is important that there is no barrier between the metal and the semiconductor, i.e. an Ohmic contact, to ensure low series resistance.

A Schottky barrier can take place between a metal and an n-type semiconductor when $\phi_m > \phi_s$ and between a metal and p-type semiconductor when $\phi_m < \phi_s$, where ϕ_m and ϕ_s are the work functions of the metal and the semiconductor respectively. Figure (2-8) shows the idealised band profiles for a Schottky contact between a metal and semiconductor.

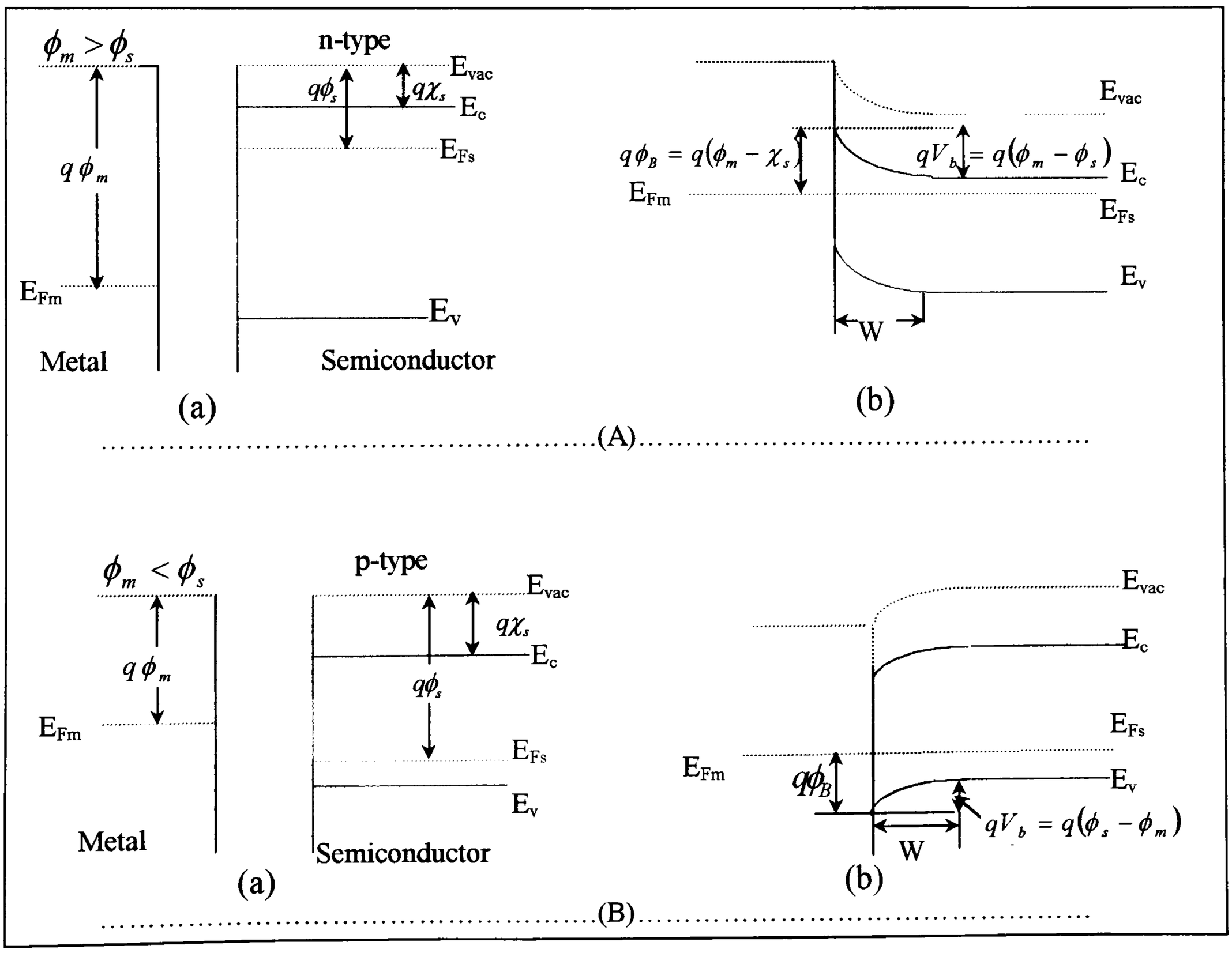

Figure (2-8)-Band diagrams for the metal and n-type (A) and p-type (B) semiconductor before (a) and after (b) forming the Schottky contact.

When a metal and an n-type semiconductor are brought into intimate contact, figure (2-8-A-b), electrons from the conduction band of the semiconductor flow into the metal, leaving positively charged ionised donors behind, till the Fermi levels on the two sides are brought into coincidence. Consequently an electric field is established between the semiconductor and the metal. The potential barrier V_b which prevents further net electron diffusion from the semiconductor conduction band into the metal is given by:

$$V_b = \phi_m - \phi_s \tag{2.48}$$

And the barrier looking from the metal towards the semiconductor is known as a Schottky barrier and is given by:

$$\phi_B = (\phi_m - \chi_s) \tag{2.49}$$

Figure (2-7-B-b) illustrates a Schottky barrier on a p-type semiconductor. In this case the potential barrier V_b which opposes hole flow from the semiconductor to the metal is given by:

$$V_b = (\phi_s - \phi_m) \tag{2.50}$$

and the barrier to holes travelling in the other direction (i.e. from the metal to the semiconductor) is given by:

$$\phi_B = \chi_s + E_{gs} - \phi_m \tag{2.51}$$

where E_{gs} is the bandgap of the semiconductor.

The metal – semiconductor contact will be Ohmic if the current can pass equally in either direction, in other words, has a liner *I-V* characteristic. An Ohmic contact can take place between a metal and a n-type semiconductor when $\phi_m < \phi_s$ and between a metal and a p-type semiconductor when $\phi_m > \phi_s$. Ideal Ohmic metal-semiconductor contacts are formed when the charge induced in the semiconductor in aligning the Fermi levels is provided by majority carriers and results in an accumulation layer of majority carriers in the semiconductor [12]. Figure (2-9) shows the idealised band profile for an Ohmic contact between a metal and a semiconductor.

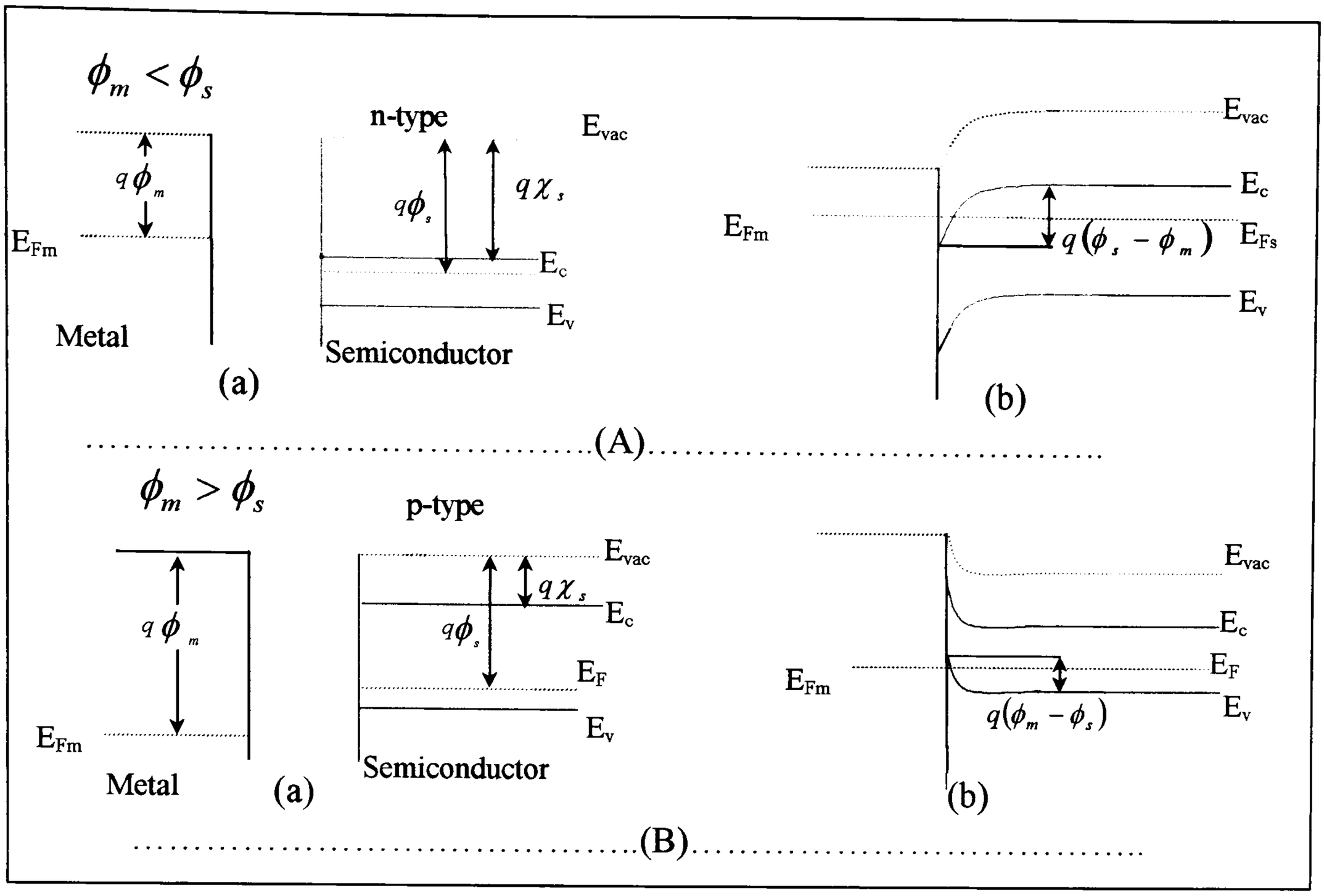

Figure (2-9)-Band diagrams for the metal and n-type (A) and p-type (B) semiconductor before joining (a) and after (b) forming an ohmic contact.

2.10.1- Ohmic Contact to p-CdTe.

The contact between the p-CdTe and a metal should be ohmic in CdTe/CdS solar cells to achieve good performance. According to equation (2.51) to make an Ohmic contact between the metal and a p-type semiconductor (CdTe), the metal work function should be greater than the sum of the electron affinity and the bandgap of the semiconductor (approximately equal to the work function $\phi_s \approx \chi_s + E_{gs}$). The work function of p-CdTe is around 5.97eV at room temperature, and thus the metal should have this value as a minimum for the work function to make an ohmic contact with p-CdTe. Unfortunately, no such metal exists, and alternative methods have to be used: [18]

(i)-by heavily doping the surface to produce a p^+-layer at the surface of the semiconductor, which narrows the width of the metal/semiconductor barrier and allows to the holes tunnel throw the barrier. Such contacts have been realised using Au-P, Au-Li, Au-Ni and Au-Cu combinations. For example, the surface could be doped with phosphorus using H_3PO_4 followed by an evaporated Au contact [15].

(ii)-by surface treatment using a varity of etches to adjust the surface stoichiometry. The p-CdTe surface could be etched with $K_2Cr_2O_7$:H_2SO_4 or Br/MeOH to leave a Cd-

depleted surface. The excess Te may then react with Cu to form Cu_2Te enhancing the diffusion into the surface. The Cu may be evaporated using a Au-Cu alloy onto the CdTe surface or by using an aqueous graphite pastes loaded with Cu or Hg-salts. The diffusion of Cu or Hg into the CdTe surface has often been achieved by heating the sample at 280°C in an inert ambient for around 5 minutes.

(iii)-using some compounds with greater work function than p-CdTe such as HgTe and p-ZnTe. The use of HgTe as buffer layer to p-CdTe was first reported by Janik and Triboult [19]. The mercury telluride work function matches very well with that of p-CdTe and an interdiffusion zone is formed with a graded band and non-rectifying junction between mercury telluride and p-CdTe. The HgTe was deposited by a vapor phase epitaxy technique onto CdTe surface etched by Br/MeOH. A solar cell of efficiency around 12.1% using ZnTe:Cu as back contact of the cell was reported by Gessert et. al.[20].

2.11-Environmental and Health Issues.

The handling of Cd and Te in the production of CdS/CdTe thin film photovoltaic modules presents hazards to health, safety and the environment, since both Cd and Te have been classified as toxic and as probable carcinogens. Prior recognition of this hazard does allow the module manufacturer to implement appropriate hazard management strategies. It does not matter how efficient, cheap and reliable CdTe thin film PV modules become, the commercial future of this module depends on how well the environmental concerns surrounding cadmium have been satisfactorily addressed.

The most likely health effects would be those associated with long term exposure to low levels of Cd, particularly for workers in manufacturing facilities. Therefore, there should be fail-safe administrative controls in manufacturing and research establishments to ensure worker safety. These must address the following points [21]:

- Ensure that all reasonable measures are taken to protect the health and safety of both employees and the public.
- Ensure that no work proceeds without the health and safety ramifications of that work being considered.

- Develop and establish training programs to ensure that workers understand the hazards, engineering controls and responsibilities associated with the handling of human carcinogens.
- Establish workplace air monitoring programs to ensure that employee exposure to Cd is below established thresholds.
- Make regular medical checks of employees to ensure their health.

For public health, many active hazard control strategies will be required. In general, public health will best be protected by the establishment and implementation of necessary precautionary procedures to mange the release of waste products to the environment from manufacturing and waste disposal operations. Before CdTe modules can be installed in public areas, users must be educated and notified about the risk and how they should deal with modules in the case of an emergency. The recycling of spent or broken CdTe modules is one possible way of eliminating expensive disposal costs and protecting public health and the environment.

2.12- References:

(1)- Richard C. Neville. "Solar Energy Conversion: The Solar Cell". Elsevier Scientific Pub. Co., New York, 1978.

(2)- Alan L. Fahrenbruch and Richard H. Bube. "Fundamentals of Solar Cells" Academic Press, Inc (London) LTD. 1983.

(3)- T. Markvart, "Solar Electricity". John Wiley & Sons, 1994.

(4)- T. J. Coutts and J. D. Meakin. "Current Topics in Photovoltaic". Academic Press (Harcourt Brace Jovanovich, Publishers) London, 1985.

(5)- Kasturi Lal Chopra and Suhit Ranjan Das. "Thin Film Solar Cells" Academic Press. (Plenum Press New York and London). 1983.

(6)- Murat Bayhan. "Preparation and Characterisation of n-CdS/p-CdTe Thin Film Solar Cells". Ph.D. Thesis, University of Durham, U.K., 1994.

(7)- T. L. Chu and S. S. Chu. "Thin Film II-VI Photovoltaics". J. Solid State Electronics, 38 (1995) 533.

(8)- Harold J. Hovel. "Semiconductors and Semimetals". Vol.11 Solar cells. Academic Press Inc. London (1975).

(9)- R. L. Anderson. "Experiments on Ge-GaAs Heterojunctions". Solid State Electronics, 5, 341 (1962)

(10)- Kim W. Mitchell. "Evaluation of the CdS/CdTe Heterojunction Solar Cell". Academic Press, New York & London (1979).

(11)- S. M. Sze, "Semiconductor Devices Physics and Technology". Academic Press, (John Wiley & Sons) New York, (1985).

(12)- Ben G. Streetman. "Solid State Electronic Devices". Prentice-Hall Inc. Academic Press, (1990).

(13)- J. P. Donnelly and A. G. Milnes. "The Photovoltaic Characteristics of p-n Ge-Si and Ge-GaAs Heterojunction" Int. J. Electronics, 20 (1966) 295.

(14)- K. W. Boer et al. "Direct Solar Energy for Large Scale Terrestrial Use". Report No. NSF/RANN/AER72-03478 A03/FR/75 (1975). As quoted in (-Kim W. Mitchell. "Evaluation of the CdS/CdTe Heterojunction Solar Cell". Academic Press, New York & London (1979).

(15)- Abdalla A. A. Alnajjar. "Single Crystal CdS/CdTe: P Solar Cells" Ph.D. Thesis, University of Durham, UK (1992).

(16)- Lawrence E. Murr. "Solar Materials Science". Academic Press, London, (1980).

(17)- A. M. Branett, A. Rothwarf. "Thin-Film Solar Cells: A Unified Analysis of their Potential". IEEE Transactions on Electron Devices, Vol.ED- 27,No. 4, (1980) 615.

(18)- A. W. Brinkman, "Contacts to Cd/Zn/Te/Se Compounds". In "Properties of Narrow Gap Cadmium-Based Compound". Ed. P. Capper. EMIS Data Review Series 10, INSPEC (IEE), London. P. 575 (1994).

(19)- E. Janik and R. Triboulet. "Ohmic Contacts to p-type Cadmium Telluride and Cadmium Mercury Telluride". Phys. D: Appl. Phys., 16 (1983) 2333.

(20)- T. A. Gessert, P. Sheldon, X. Li, D. Dunlavy, D. Niles, R. Sasala, and S. Albright. "Studies of ZnTe Back Contacts to CdS/CdTe Solar Cells". 26th IEEE Photovoltaic Specialists Conf., California (1997) 1250.

(21)- Paul D. Moskowitz. "Environmental, Health and Safety Issues Related to the Production and use of CdTe Photovoltaic Modules". Int. J. Solar Energy, 12 (1992) 259.

Chapter Three :

Sample Preparation and Characterisation Techniques.

3.1 -Introduction

This chapter describes the techniques employed in devices fabrication and the experimental techniques used to characterise both the materials and the devices. The main techniques used to fabricate the device are Physical Vapour Deposition (PVD) to deposit the CdS and $CdCl_2$ layers, and Close Space Sublimation (CSS) to deposit the CdTe layer.

The characterisation techniques are classified according to those used in the analysis of device performance such as; Current–Voltage (*I-V*), Capacitance Voltage (*C-V*), Spectral Response (SR), Photocapacitance (PHCAP) and Electroluminescence (EL), and those techniques employed to investigate the structure of the materials such as; Scanning Electron Microscopy (SEM) and X-Ray Diffraction (XRD).

3.2-Fabrication of n-CdS/p-CdTe Thin Film Solar Cell.

The following procedure was used in the production of CdS/CdTe thin film solar cell:

1- Clean transparent conducting oxide (TCO) – coated glass substrate.

2- Deposit CdS layer by physical vapour deposition onto the TCO-coated glass substrate.

3- Deposit CdTe layer by close space sublimation (CSS) onto the glass/TCO/CdS.

4- Evaporate $CdCl_2$ onto the CdTe layer, then heat treat in air at 400°C for about 30 minutes. Remove excess $CdCl_2$ with de-ionised water.

5- Etch the CdTe surface with 0.03% Br-Methanol for about 10-15s.

6- Make the back contact to the solar cell using either graphite or gold.

Figure (3-1) shows a flow chart for the fabrication procedure.

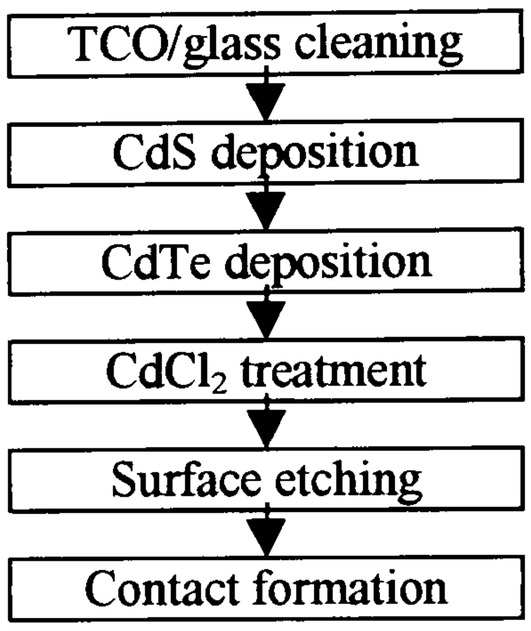

Figure (3-1)- Flow chart summering the CdS/CdTe solar cell fabrication process.

3.2.1-Cleaning of Glass Substrate Surface.

The TCO- coated glass was cleaved into samples approximately 50mm × 23mm and cleaned using the following procedure:

1-Wash in a solution of Decon 90 (cleaning agent) in de-ionised water in an ultrasonic bath at room temperature for approximately one hour.

2-Rinse thoroughly in de-ionised water for at least five minutes.

3-Reflux in iso-propyl-alcohol (IPA) for about one hour to remove grease and organic contamination.

4-The sample was left to dry naturally or in a stream of dry nitrogen gas if necessary.

3.2.2-Thermal Evaporation of CdS.

A schematic diagram of the evaporator used for the deposition of CdS is given in figure (3-2). The evaporator was an oil diffusion pumped system capable of achieving a base pressure of $\sim 10^{-6}$ mbar. The substrates were heated from the rear by a quartz - halogen lamp. The CdS powder was placed in a silica glass crucible, heated by a tungsten wire wrapped around it. The substrate and source temperatures were measured with thermocouples and controlled by Eurotherm programmable temperature controllers. CdS was deposited at source and substrate temperatures of 700°C and 190°C respectively at a pressure of around 10^{-5} torr. The evaporation cycle was as follows;

1-Two glass substrates were placed at a height of around 19 cm above the source, with the TCO face downward.

2-The system was evacuated to a pressure of less than 10^{-5} torr.

3-The substrates were heated to 190°C and the source temperature was gradually increased to 700°C with the shutter closed.

4-When steady state conditions had been attained, the mechanical shutter was opened for 4 minutes to deposit 0.2 μm of CdS .

5-The shutter was closed and the substrate and the source heating were switched off. The substrates were allowed to cool to room temperature before being removed from the vacuum system.

The position of the filament around the crucible has a considerable effect on the deposition rate and the quality of film. When the filament was near the bottom of the

crucible (figure (3-3)-a), there was no evaporation; whereas when it was in the middle of the crucible (figure (3-3)-b) there was a small rate of deposition, and particles of solid CdS were deposited on the layer. When it was at the top of the crucible (figure (3-3)-c) there was a high rate of deposition and no particles of solid CdS were formed. This was probably because it was only in the latter case that the evaporating surface was hot enough.

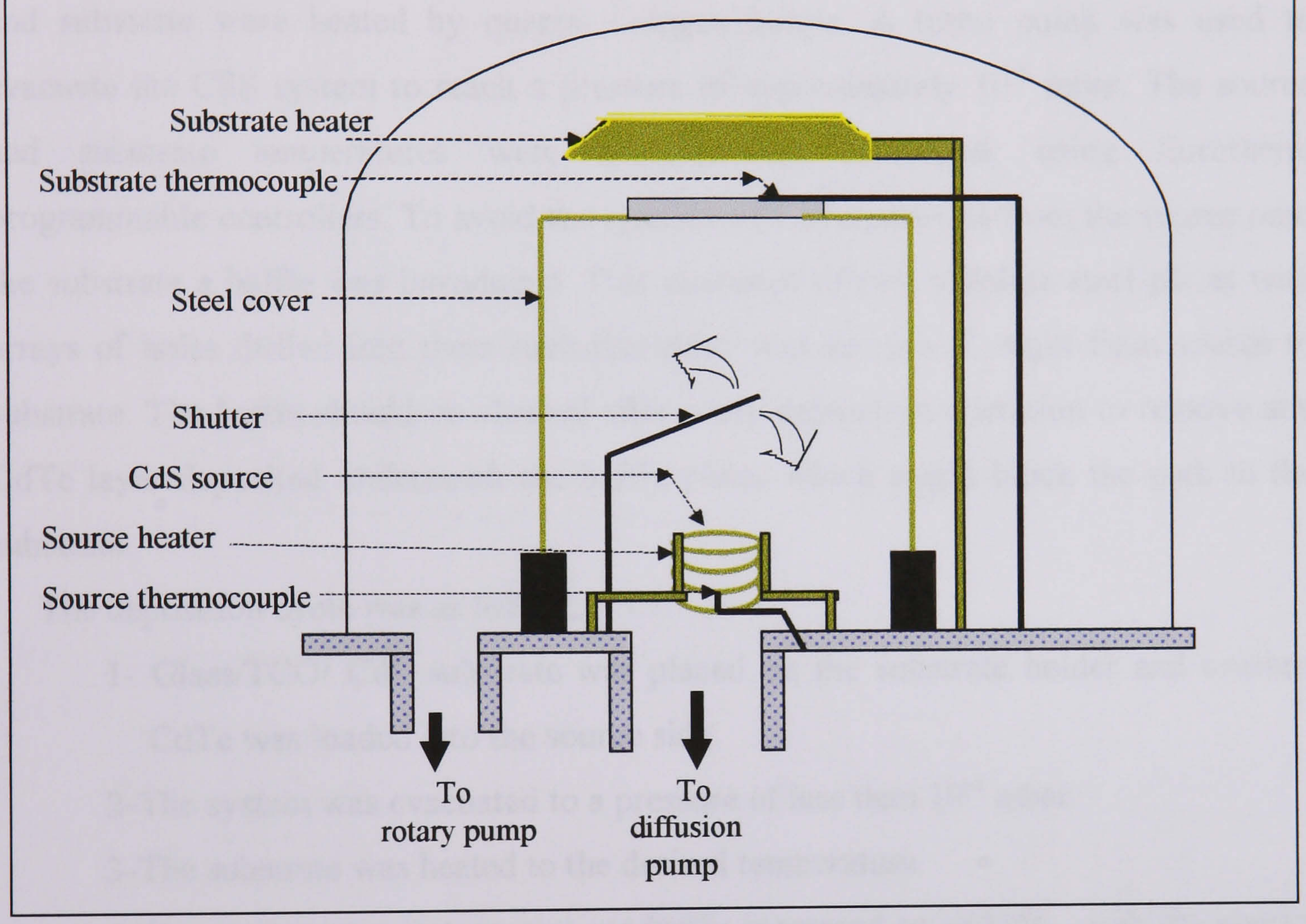

Figure (3-2)- Schematic diagram of the evaporation system used in the deposition of CdS .

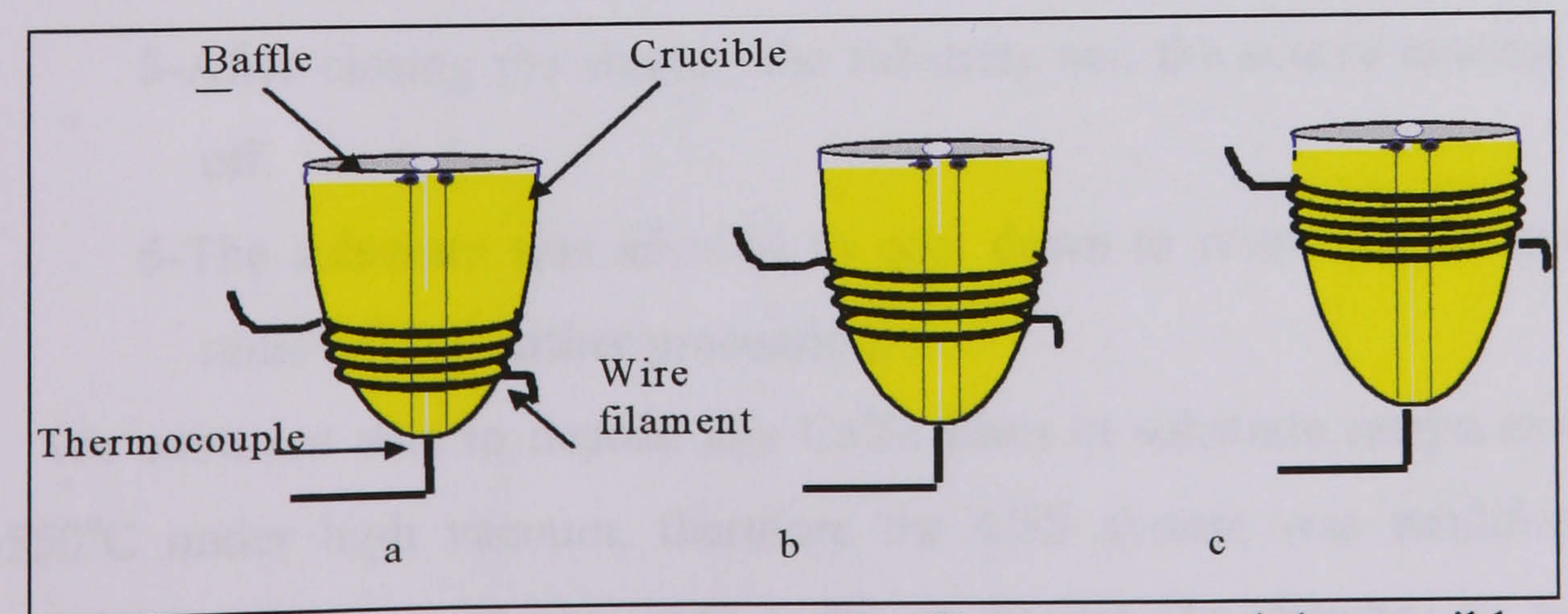

Figure (3-3)-The position of the filament around the crucible.

3.2.3-Deposition of CdTe Layer.

Close Space Sublimation (CSS) was used to deposit CdTe onto the ITO/CdS substrates. A schematic diagram of the first Close Space Sublimation kit, which used a lamp heating system, is shown in figure (3-4-A). The distance between the substrate and the source was <11mm. The CdTe was placed in a graphite block which had a thermocouple placed internally. The substrate holder was also made from graphite with an internal thermocouple and was designed to hold one glass slide at a time. The source and substrate were heated by quartz- halogen lamps. A turbo pump was used to evacuate the CSS system to reach a pressure of approximately 10^{-6} mbar. The source and substrate temperatures were automatically controlled, using Eurotherm programmable controllers. To avoid the ejection of CdTe particles from the source onto the substrate a baffle was introduced. This consisted of two stainless steel plates with arrays of holes drilled into them such that there was no line-of- sight from source to substrate. The baffle should be cleaned after every deposition operation to remove any CdTe layer deposited underneath the baffle plates which might block the path to the substrate.

The deposition cycle was as follow;

1- Glass/TCO/ CdS substrate was placed on the substrate holder and crushed CdTe was loaded into the source side.

2-The system was evacuated to a pressure of less than 10^{-5} mbar.

3-The substrate was heated to the desired temperature.

4-The source temperature was gradually increased to <650°C, with the shutter closed.When steady state conditions were attained, the mechanical shutter was opened for some minutes depending on the thickness required.

5-After closing the shutter, the substrate and the source heating were switched off.

6-The substrate was allowed to cool down to room temperature before being removed for further processing.

We were not able to deposit any CdTe films at substrate temperatures higher than ~550°C under high vacuum, therefore the CSS system was modified to allow the introduction of an inert gas, such as N_2 or Ar into the chamber so as to reduce the vacuum to a level that could be maintained with using just a rotary pump. However, at pressures of ~10mbar, arcing from the terminal of the lamps (240V) caused the fast

fuses to blow. To solve this problem, a low voltage filament heating system was filled to replace the lamp system, as shown in figure (3-4-B). The filament was made from Tungsten or Molybdenum, but since the latter was less brittle after heating it was preferred to Tungsten.

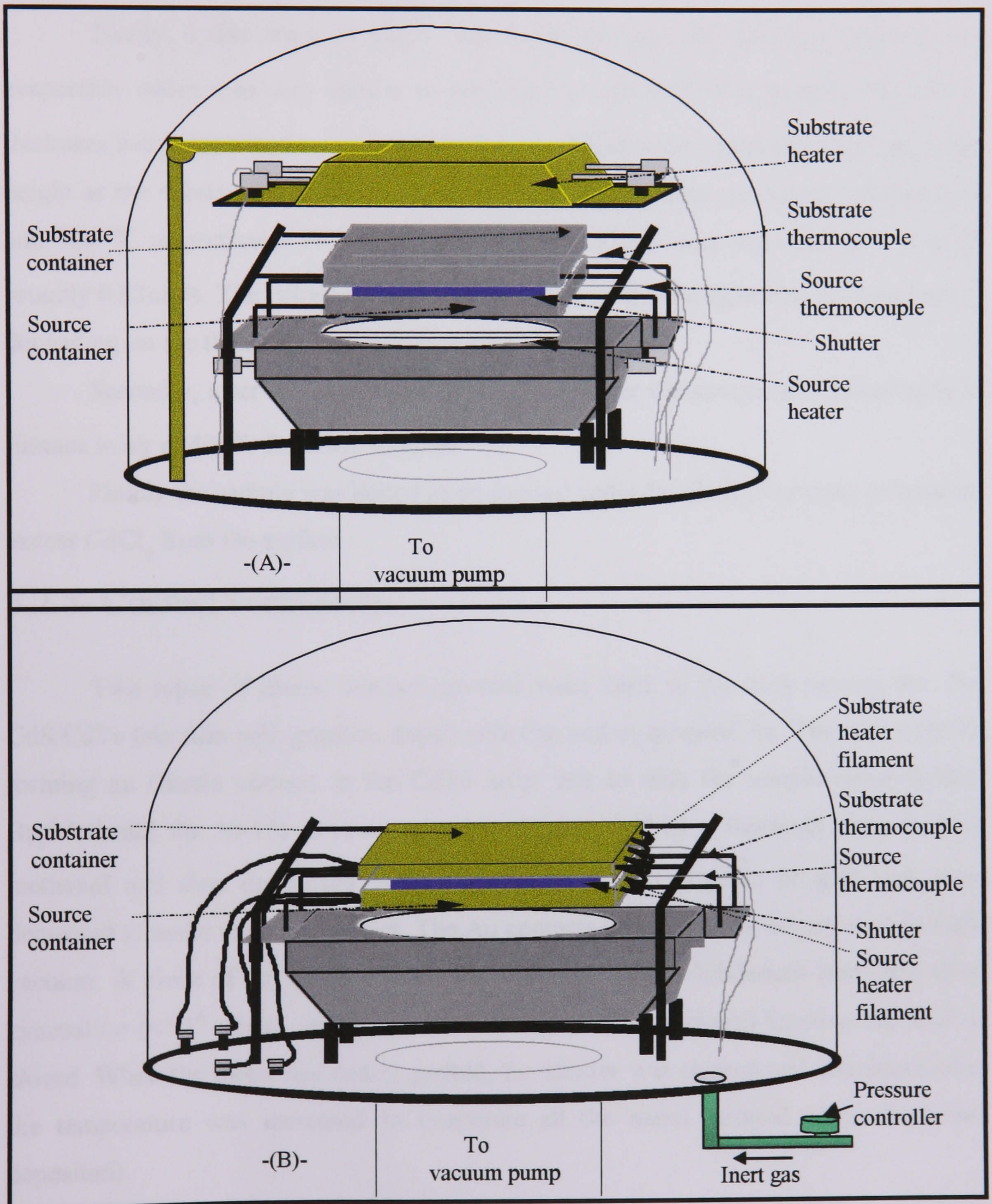

Figure (3-4)- A schematic diagram of the Close Space Sublimation system with lamps (A) and filament (B) heating system.

3.2.4- $CdCl_2$ Treatment.

Treatment of the CdTe layer with $CdCl_2$ improves the performance of the solar cell as we will see later in chapters 5 and 6. The $CdCl_2$ treatment consisted of two stages:

Firstly, a thin layer of $CdCl_2$ was deposited onto the sample surface by an evaporator which was very similar to that used for the CdS evaporation. The $CdCl_2$ thickness being deposited was monitored with a piezoelectric gauge placed at the same height as the substrate. The substrate and source temperatures were room temperature and 500 °C respectively. A $CdCl_2$ layer of about 200nm was deposited at a rate of roughly 0.83nm/s. The colour of the CdTe layer changed from light blue to dark brown depending on the thickness of $CdCl_2$ deposited.

Secondly, after the deposition of the $CdCl_2$ layer the sample was annealed in a furnace in air at 400°C for thirty minutes.

Finally the sample was boiled in de-ionised water for about 5 minutes to remove excess $CdCl_2$ from the surface.

3.2.5- Contact Formation.

Two types of ohmic contact material were used as the back contact for the CdS/CdTe thin film cell: graphite doped with Cu; and evaporated Au. The first stage in forming an Ohmic contact to the CdTe layer was to etch the sample using 0.03% Br_2/Methanol for 10-15s at room temperature, followed by a thorough rinse in first methanol and then de-ionised water. After etching, the graphite or gold was then deposited to make the back contact. The Au contacts were made by evaporation in high vacuum. A piece of Au (around 30mg) was placed in a molybdenum boat, and after evacuation ($<10^{-6}$ mbar), the temperature was gradually increased keeping the shutter closed. When the metal had nearly melted, the shutter was opened and simultaneously the temperature was increased to evaporate all the metal (around 60nm thickness deposited).

The Cu-doped graphite contacts were painted onto the sample, and then annealed under nitrogen at 280 °C for five minutes, to diffuse Cu^+ ions into the CdTe layer.

Some In contacts were made to the CdS, by evaporation in high vacuum, for studies of the TCO/CdS interface.

3.3- Characterisation Techniques.

3.3.1- Electrical Characterisation.

3.3.1.1- Dark and Illuminated *I-V* Characterisation:

I-V measurements were carried out using a Keithely 617 programmable electrometer, which comprises a high impedance voltmeter, a low impedance ammeter and dc calibrated power supply, controlled by a PC computer. The temperature dependent dark *I-V* measurements were performed while the sample was placed in an Oxford DN1704 cryostat, a schematic diagram of which is shown in figure (3-5). The liquid nitrogen cryostat has vacuum insulation and uses helium as a heat exchange gas to allow the sample to be held at temperatures in the range 77K to 400K. *I-V* measurements could then be taken at any desired fixed temperature in this range.

The photovoltaic output characteristics of the cells were measured under AM1.5 simulation. A general view of the Durham solar simulator is shown in figure (3-6). The illumination was provided by a 1.5KW quartz halogen strip lamp with a parabolic reflector, which was mounted in a levelled stainless steel frame fitted with a tray containing around 2cm deep flowing water intended to simulate the moisture absorption in the atmosphere. The inside wall of the simulator was painted mat black colour. The measurements were carried out at room temperature and fixed by circulating cooling water beneath of the sample. The distance between the sample and the light source could be adjusted to calibrate the intensity of the light using a silicon photodiode which was placed at the same level of the sample and calibrated to give 385±5mA at $100mW/cm^2$ (AM1.5).

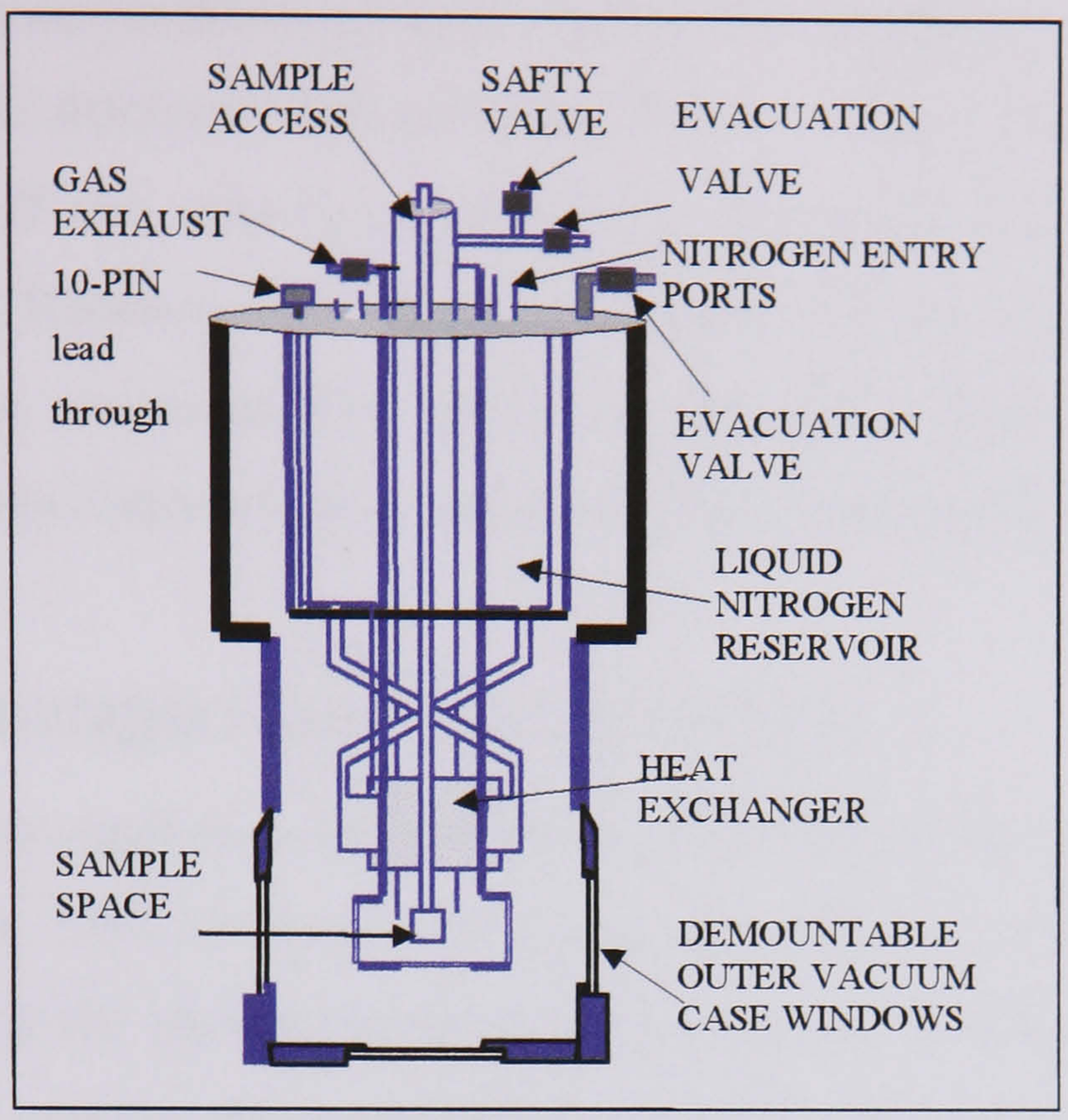

Figure (3-5)-DN1704 Liquid Nitrogen Cryostat.

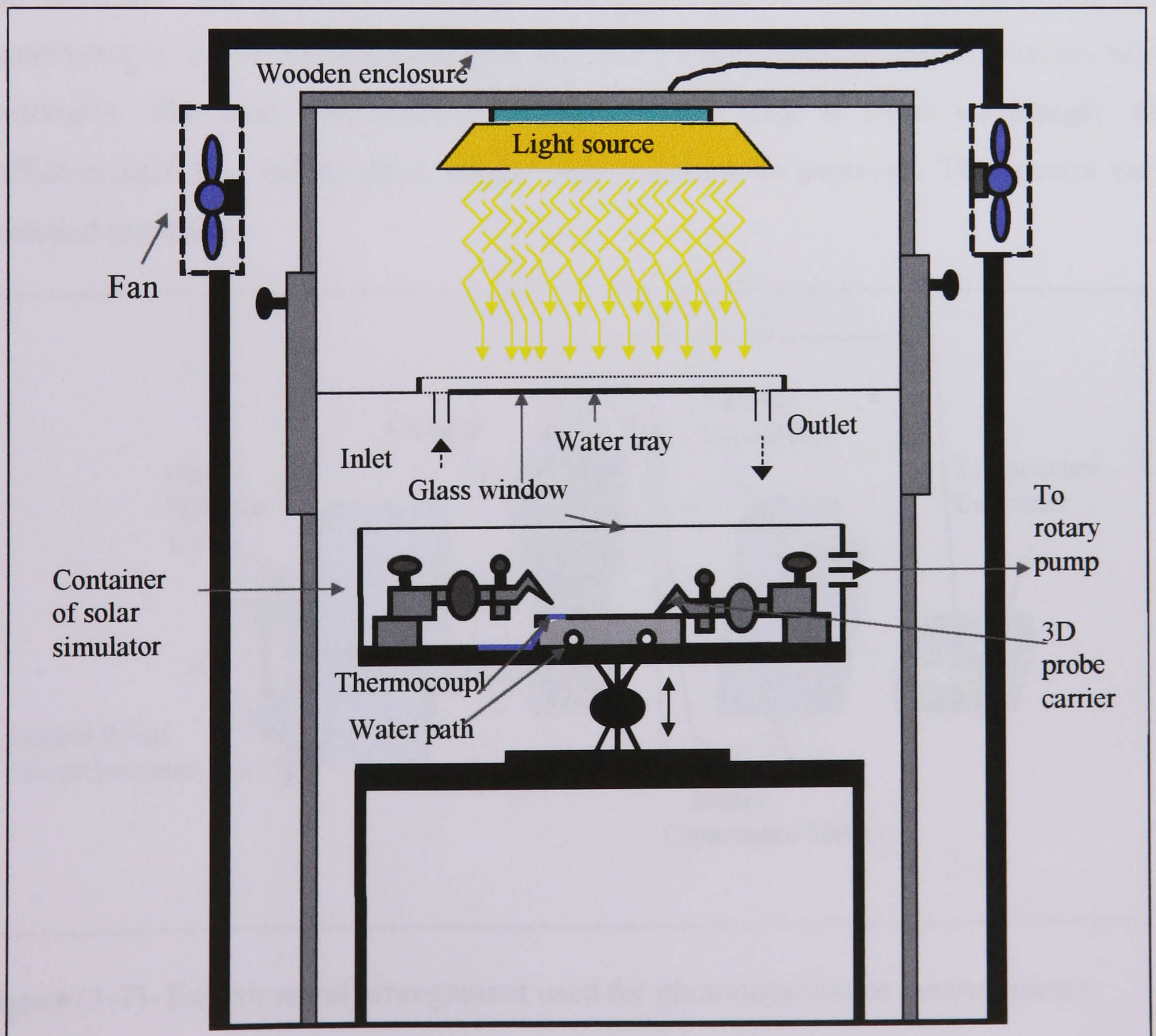

Figure (3-6)-Durham Solar Simulator.

3.3.1.2-Capacitance-Voltage Characteristics (*C-V*):

The capacitance-voltage measurements were carried out for the CdS/CdTe thin film solar cells to determine the acceptor density, and to estimate the built-in-voltage and the width of the junction. Capacitance-voltage measurements were measured manually with a Boonton 72B capacitance meter, which operates at 1MHz, together with a dc voltage source supply. The liquid nitrogen cryostat, shown in figure (3-5), was used to obtain temperature dependent capacitance voltage measurements between 77K and 400K.

3.3.1.3- Photocapacitance Measurements:

The photocapacitance measurements were carried out at room temperature and 200K using the DN1704 liquid nitrogen cryostat. A schematic diagram of the arrangement used for photocapacitance measurements is shown in figure (3-7). The monochromator, used in this experiment gave a broad spectral range between 400nm and 2000nm. The device capacitance was compensated with an external variable capacitance to allow the small changes induced by the monochromatic radiation to be noticeable. The scan was made very slowly from long to short wavelength and sufficient time was left to allow steady state condition to achieved. The spectra were recorded manually.

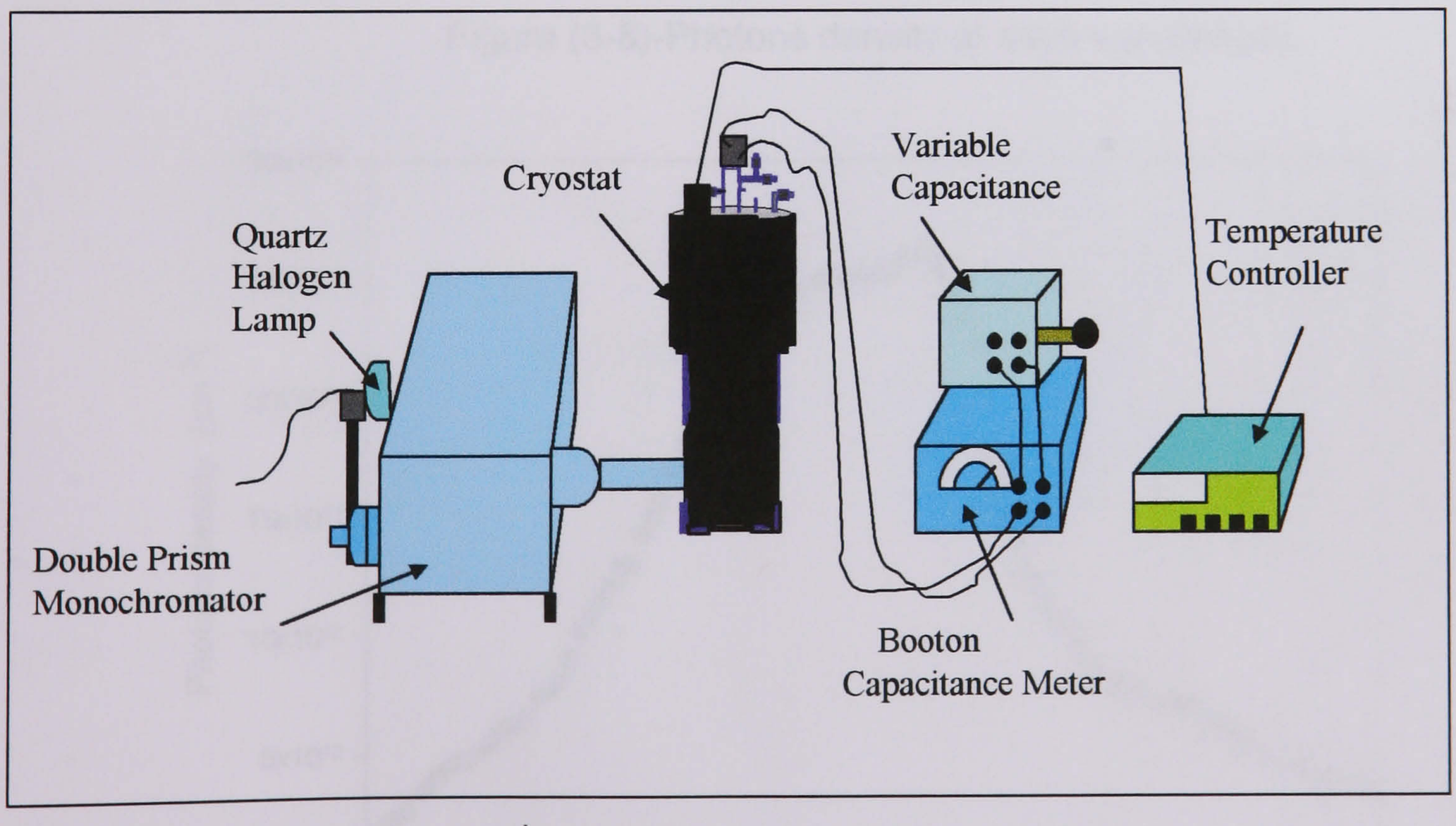

Figure (3-7)- Experimental arrangement used for photocapacitance measurements.

3.3.1.4-Spectral Response Measurements.

The quantum efficiency of the solar cell is the photocurrent collected at each wavelength relative to the number of photons incident on the surface of the device (as stated in chapter 2). From the definition, in order to calculate the quantum efficiency we have to know the photon flux (N_{ph}) and the photocurrent density (J_{ph}) collected at each wavelength.

The illumination power was measured at each wavelength by a calibrated photodiode and converted to the number of photons at each wavelength (the area of the diode was 1cm^2) using the following equation:

$$N_{ph} = E_m(\text{eV}) / E_{th}(\text{eV}) \qquad (3.1)$$

Where E_m(eV) is the energy measured at each wavelength and E_{th}(eV) is the photon energy at the wavelength given by the following equation:

$$E_{th}(\text{eV}) = 1.24 / \lambda(\mu\text{m}) \qquad (3.2)$$

Figure (3-8) shows the number of photons per cm^2. A filter (Bentham 0S700) was used at wavelengths greater than 700nm to remove second order diffraction in the monochromator output. The slight discontinuity in the graph at 700nm is as a result of this added filter.

Figure (3-8)-Photons density at each wavelength.

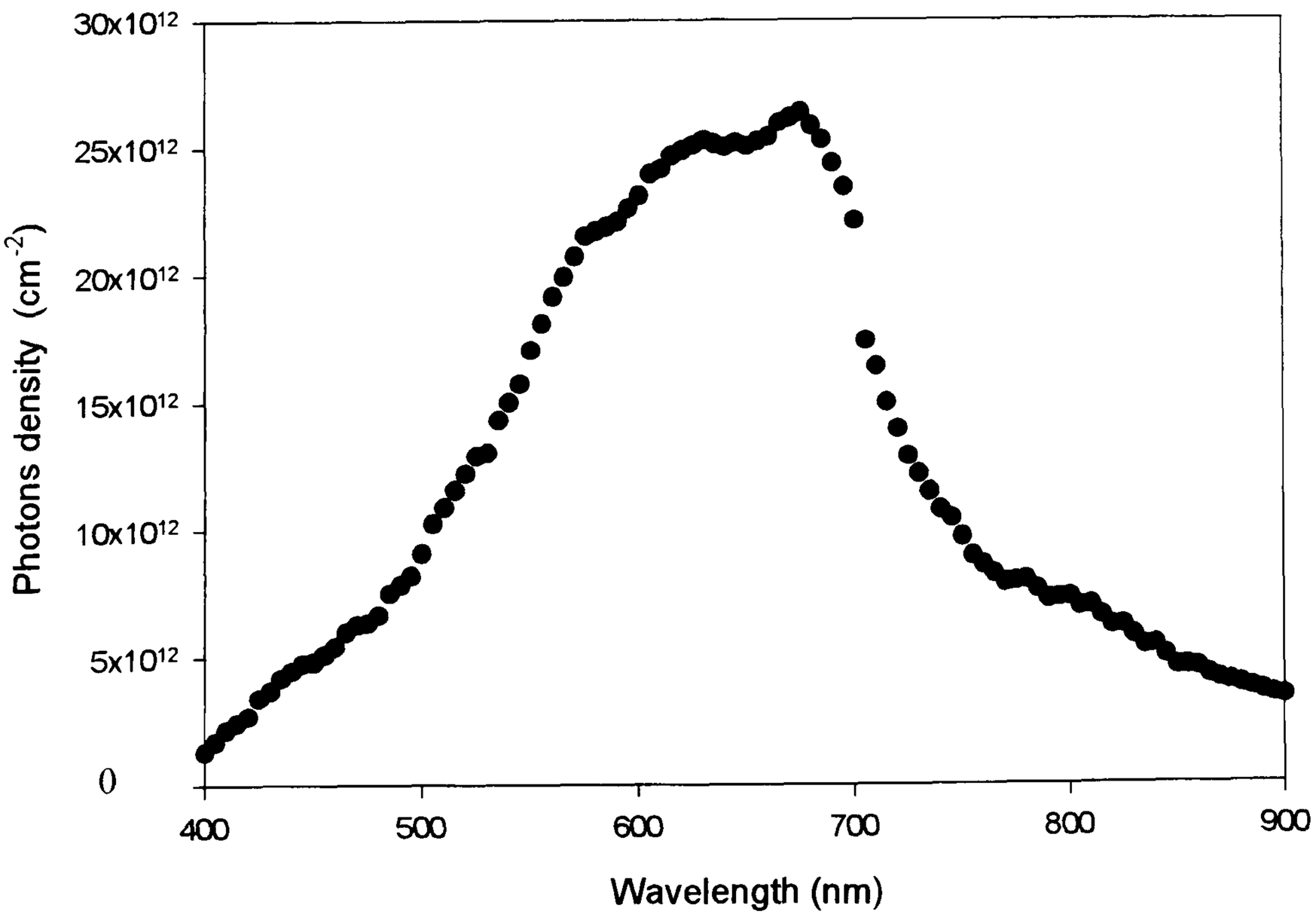

The sample was placed in the same postion as the photodiode and the photocurrent density (J_{ph}) measured using a Keithely 617 programmable electrometer. Then the quantum efficiency was calculated at each wavelength using equation (2.45).

3.3.1.5- Electroluminescence Measurements.

The electroluminescence measurements were carried out by Mark Potter. The sample was placed in a closed cycle helium cryostat capable of cooling the sample down to 10K under vacuum. Analysis of the light emitted by the sample, was peformed using a Bentham Monochromator coupled to an array of 1024 photodiodes. The monochromator contained diffraction gratings of several different line spacing which could be used to provide spectra of different resolution. A Keithley 2400 voltage supply was used for pulsing larger currents of up to 15mA through the device for periods of approximately 10ms to produce the electroluminescence spectrum. Figure (3-11) shows the experimental arrangement used for electroluminescence measurements.

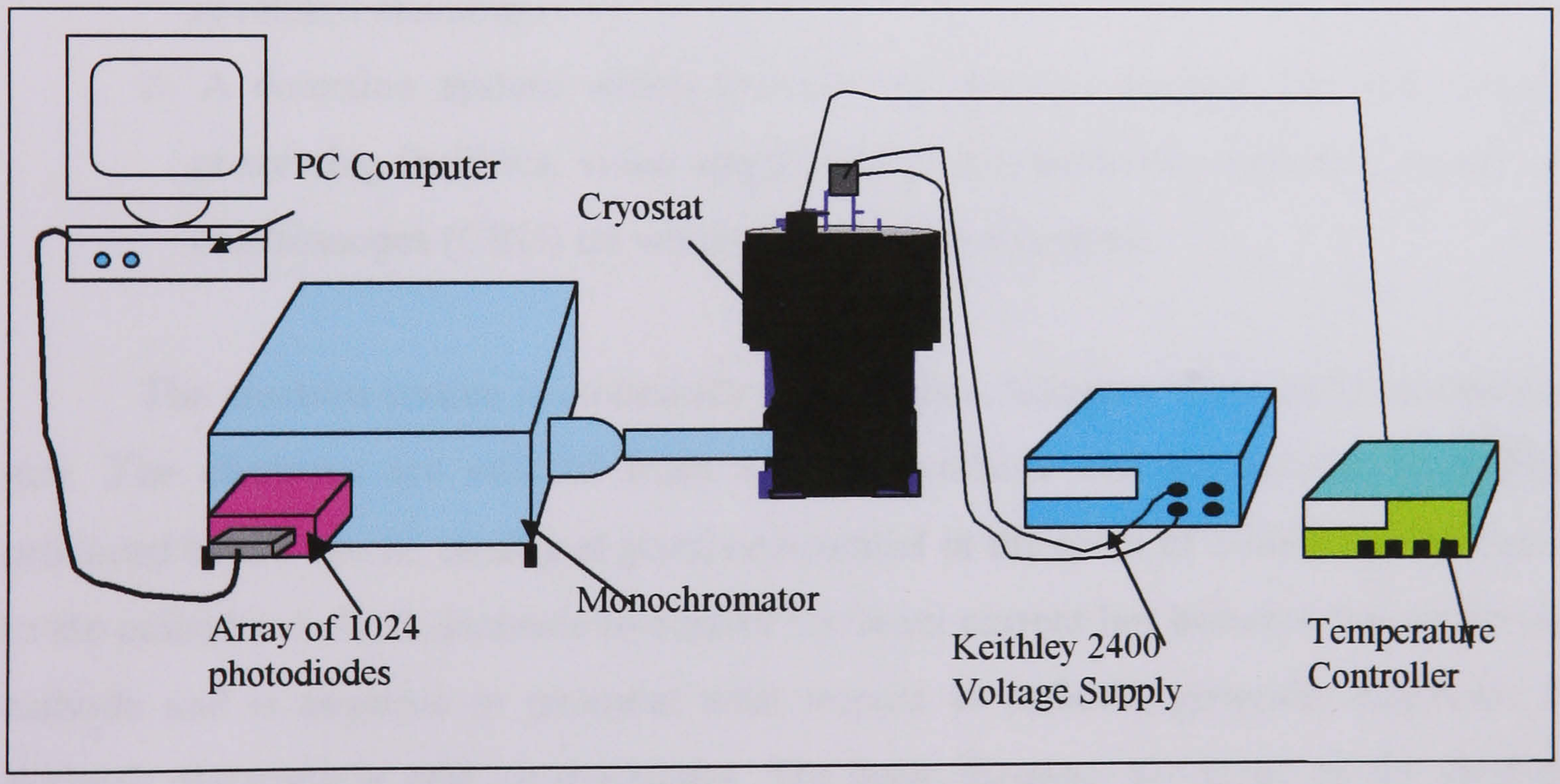

Figure (3-11)- The experimental arrangement used for electroluminescence measurements.

3.3.2- Structure Characterisation.

3.3.2.1-Scanning Electron Microscopy.

Scanning electron microscopy (SEM) is a very powerful tool for characterising the semiconductor surface morphology, since it provides high resolution and simultaneously a variety of modes and forms of contrast to allow a wide range of analyses to be completed [1]. Further details about the construction, modes of operation and uses of scanning electron microscopy may be obtained from textbooks [2][3].

In the present study, assessment of the surface morphology of CdTe thin films prepared at different substrate temperatures, was performed using a Jeol-JMS- IC848 Scanning Electron Microscope. The basic components of the SEM are shown schematically in figure (3-12). It consists of two subsystems;

1- An electron optical column that produces a finely focused electron probe which can be scanned over the specimen surface in a raster. The electron column includes the electron gun, the electromagnetic lenses and the specimen chamber.

2- A detection system which includes an electron detector and other signal processing facilities, video amplifier and synchronously scanned cathode ray oscilloscopes (CRO) on which the image is displayed.

The electron source is commonly a thermionic tungsten filament in an electron gun. The electrons are emitted from a heated cathode and accelerated by a field produced by the anode, usually at positive potential in the order of 1-40KV with respect to the cathode. A third electrode to control the beam current lies between the anode and cathode and is negative in potential with respect to cathode, generally described as Wehnelt electrode or grid, or modulator. The beam diameter produced by the electron gun is too large to generate a sharp image at high magnification, therefore, electron lenses are used to reduce the diameter of these source electrons and to direct a small focused electron beam onto the specimen. Two pairs of electromagnetic deflection coils (scan coils) are used to control the raster of the beam over the specimen, which is maintained at earth potential. The magnification (M) of the specimen image is the ratio of the linear size of viewing screen (CRO) to the linear size of raster on specimen.

The interaction of the electron beam with the specimen causes the generation of many signals (for more detail see [2][3]). The signals most often used to produce images are secondary electrons. These are collected by an Everhart-Thornley (E-T) detector which consists of a scintillator, a light pipe and a photomultiplier tube. The secondary electrons strike the scintillator and produce light that travels down the light pipe to the photomultiplier tube, where it is converted to an amplified electrical signal. Variations in the signal occurring as the beam moves over the specimen surface provide the intensity changes which are seen as an image on the viewing screen.

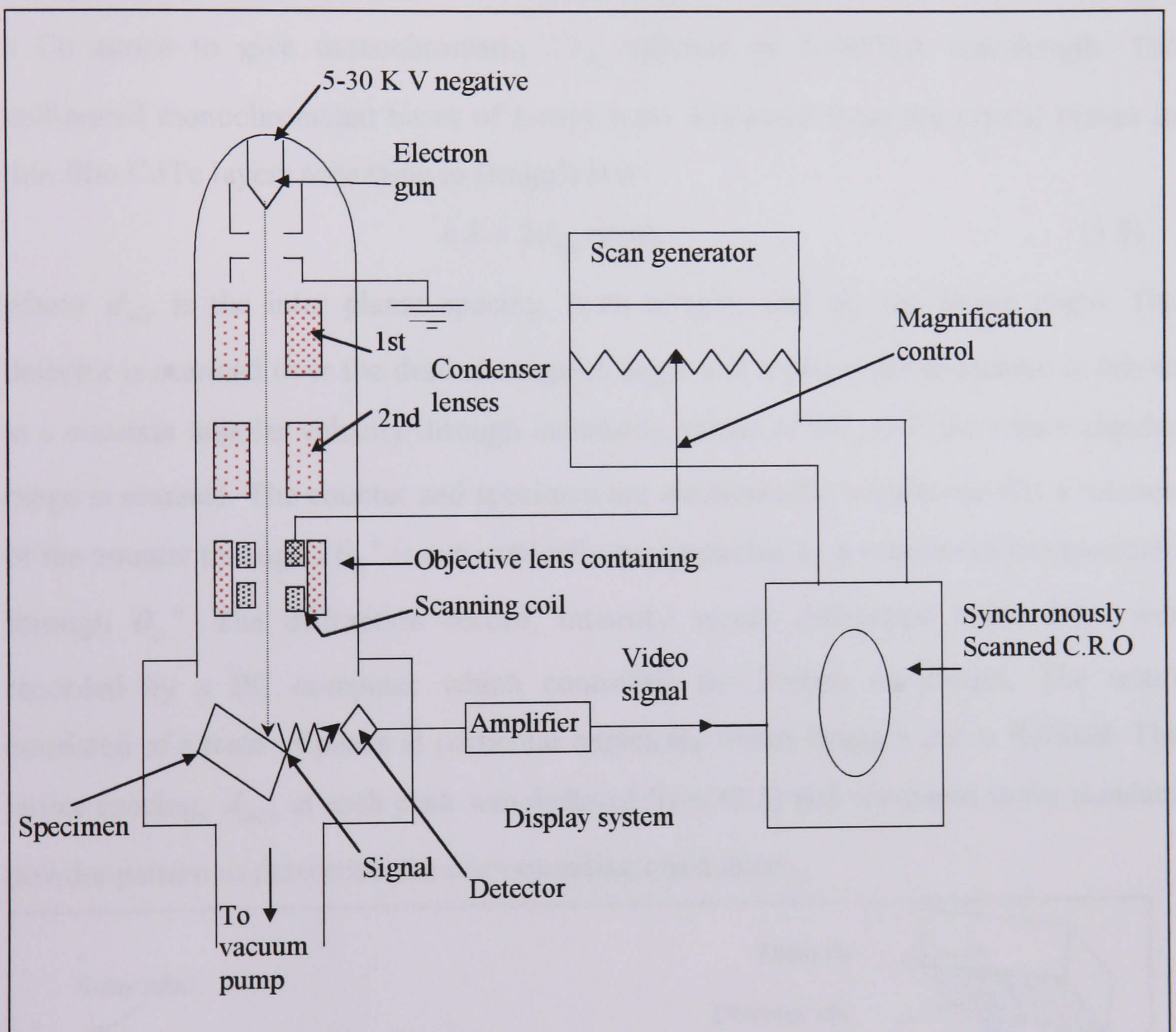

Figure (3-12) Schematic diagram of components of a simple scanning electron microscope.

3.3.2.2- X-Ray Diffractometry.

The diffraction of x-rays by matter forms the basis of a unique scientific tool that can yield fundamental and important data when applied to crystalline materials, liquids and amorphous solids. A very useful and comprehensive account of X-rays diffraction theory and related techniques can be found in Klug and Alexander [4]. The schematic diagram of a x-ray powder diffractrometer is shown in figure (3-13)

The x-ray diffraction measurements were carried out in the Bragg-Bretono configuration where the source, sample normal and detector all lie in the same plane. The instrument was a Philips PW1130 generator/diffractrometer assembly, which used a Cu anode to give monochromatic Cu_{k_α} radiation of 1.54056Å wavelength. The collimated monochromated beam of x-rays were diffracted from the crystal planes in thin film CdTe layers according to Bragg's law :

$$n\lambda = 2d_{hkl} \sin\theta_B \qquad (3.3)$$

where d_{hkl} is the inter planar spacing, n an integer, and θ_B the Bragg angle. The detector is scanned over the desired range of angle and a proportional counter is driven at a constant angular velocity through increasing values of $2\theta_B$ until the whole angular range is scanned. The counter and specimen are mechanically coupled so that a rotation of the counter through $2\theta_B{}^\circ$ is automatically accompanied by a rotation of the specimen through $\theta_B{}^\circ$. The diffraction record, intensity versus diffraction angle $2\theta_B$, was recorded by a PC computer which controlled the Philips equipment. The result consisted of a trace of peaks at particular angles for which Bragg's law is fulfilled. The lattice spacing, d_{hkl}, at each peak was deduced from (3.3) and compared to the standard powder pattern to determine the corresponding orientation.

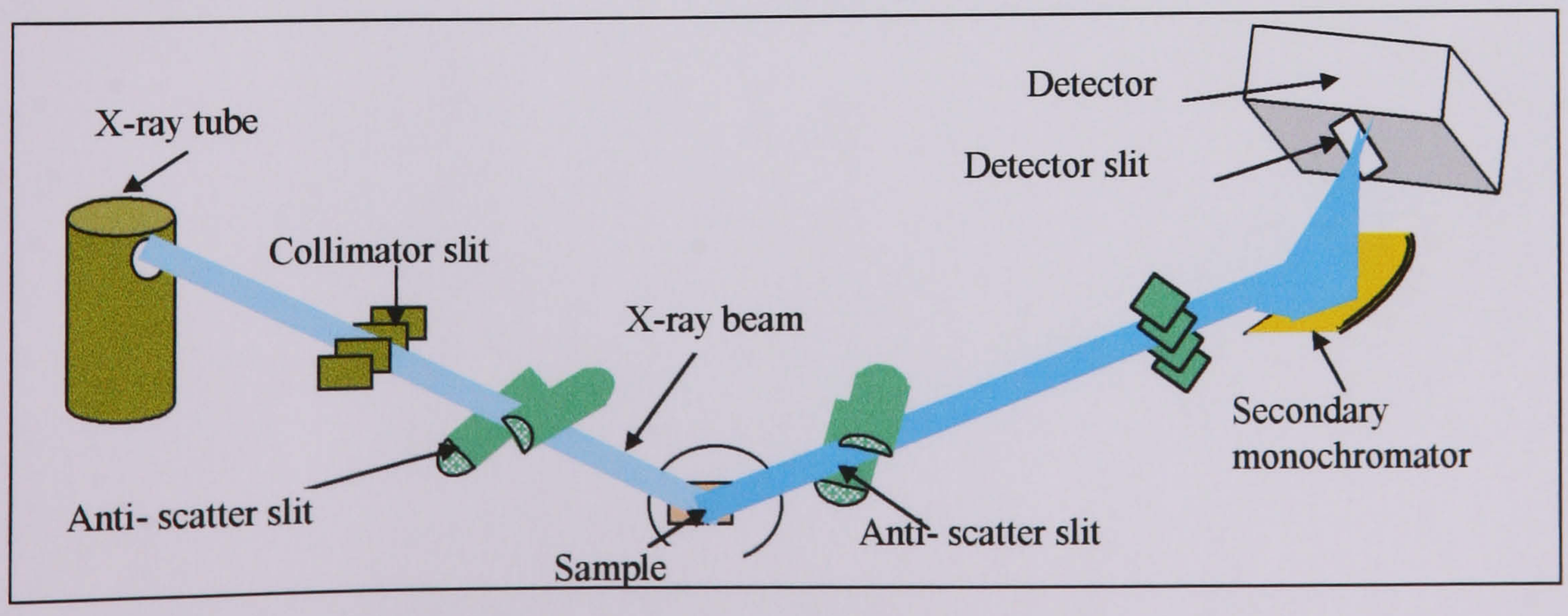

Figure (3-13)- Schematic diagram of a x-ray powder diffractrometer.

3.4-References:

(1)- D. B. Holt and D. C. Joy. " SEM Microcharacterization of Semiconductors". Academic Press, London (1989).

(2)- D. B. Holt, M. D. Mutr, P. R. Grant and I. M. Boswarva. " Quantitative Scanning Electron Microscopy". Academic Press, London. (1974).

(3)- Joseph I. Goldstein, A. D. Roming, Dale E. Newbry, Charles E. Lyman, Patrick Echline, Chales Fiori,. Davaid C. Yoy, Eric Lifshin. "Scanning Electron Microscopy and X-Ray Microanalysis". Plenum Press, London (1992).

(4)- Harold P. Klug and Leroy E. Alexander. "X-Ray Diffraction Procedures For Polycrystalline and Amorphous Materials". Wiley-Interscience Publication (London) 1974.

Chapter Four:

Close Space Sublimation of CdTe.

4.1- Introduction

A common feature of all the most efficient laboratory scale CdS/CdTe cells has been the use of close space sublimation (CSS)[1] [2] to deposit the CdTe layer. The technique was first suggested by Nicoll in 1963[3] for the heteroepitaxal growth of GaAs on Ge and is characterised by placing the source very close to the substrate. The deposition of CdTe films by CSS is based on the reversible dissociation of CdTe at high temperature:

$$2CdTe(s) \rightleftharpoons 2Cd(g) + Te_2(g)[4] \qquad (4.1)$$

According to the above equation the CdTe source dissociates into its elements Cd and Te_2 which recombine on the substrate surface to form the film. The growth rate depends on several interrelated parameters: the temperatures of the source T_{so} and the substrate T_{sub}, the separation between the source and the substrate, and the pressure, temperature and composition of gases in the deposition chamber.

Depending on the pressure, the deposition of CdTe by CSS may be described by either diffusion limited transport or by Langmuir's expression for free sublimation. In the diffusion limited transport model the Cd atoms and Te_2 molecules migrating to the substrate diffuse through the ambient gas, colliding several times with gas molecules before they condense on the substrate. According to this model, the deposition rate is an inverse function of gas pressure and is directly proportional to the exponential factor $\exp(-E_a/kT_{so})$ i.e. thermally activated with activation energy E_a . In the Langmuir theory, the Cd atoms and Te_2 molecules move directly to the substrate without any gas phase collisions. The sublimation rate according to this theory is independent of the gas pressure, but is still proportional to $\exp(-E_a/kT_{so})$.

In this chapter we shall investigate the effects of source and substrate temperature, ambient gas pressure and the separation between source and substrate on the growth rate of CdTe using the CSS system described in chapter 3. The deposition of CdTe films was carried out onto layers of CdS (~100-150nm) previously deposited on TCO coated glass substrate using PVD. The presence of the baffle, above the source and the open space between the baffle and substrate, will reduce the growth rate compared to other systems [5] [6].

The microstructure of CSS CdTe films is strongly affected by the substrate temperature [7], and the effects of substrate temperature on the orientation and grain size of CdTe films are investigated by X-ray diffraction and scanning electron microscopy.

4.2- Effect of Source Temperature on Growth Rate.

Several layers of CdTe were deposited by CSS at different source temperatures between 873K and 958K. The substrate temperature was maintained at 773K and the chamber vacuum was maintained at around 7.5×10^{-5} mbar of air. Layer thickness was measured by a Tencor α-step 200 surface profiler at the centre of the film. Figure (4-1) shows the variation in growth rate versus source temperature. The growth rate increased from 1.1 μm/minute at 915 K to 3.3 μm/minute at 958 K indicating that the growth rate (R) depends strongly on source temperature. Replotting the data as log(R) vs. $1/T$, as shown in figure (4-2), gives a straight line and suggests that the deposition rate may be expressed in terms of an Arrhenuis equation: [8]

$$R\ (\mu m/minute) = R_o \exp(-\Delta E / kT_{so}) \qquad (4.2)$$

Where R_o is constant, ΔE is the activation energy and T_{so} is the source temperature. The value of activation energy is 1.9 eV calculated from the slope of the line in figure (4-2). Mitchell et al [6] reported a similar result 1.83 eV at 1 atm of H_2. Sosa et al [9] also reported a value of $(1.9 \pm .1)$ at 4×10^{-4}Torr. Fahrenbruch et al [10] and Saraie et al [11] reported the similar values of 1.8 eV.

As the density of CdTe at room temperature is 5.845g/cm^3 [12], then a volume growth rate of 1μm^3/min corresponds to the deposition to 1.52×10^{10} molecules/minutes. In the present case, a growth rate of 1 μm/min corresponds to a molecular flux of 1.52×10^{18} molecules/minutes/cm^2. This represents a lower limit, because the sticking coefficient will be less than unity.

Figure (4 -1)-Growth Rate of CdTe vs. source temperature at 500 ^{o}C substrate temperature.

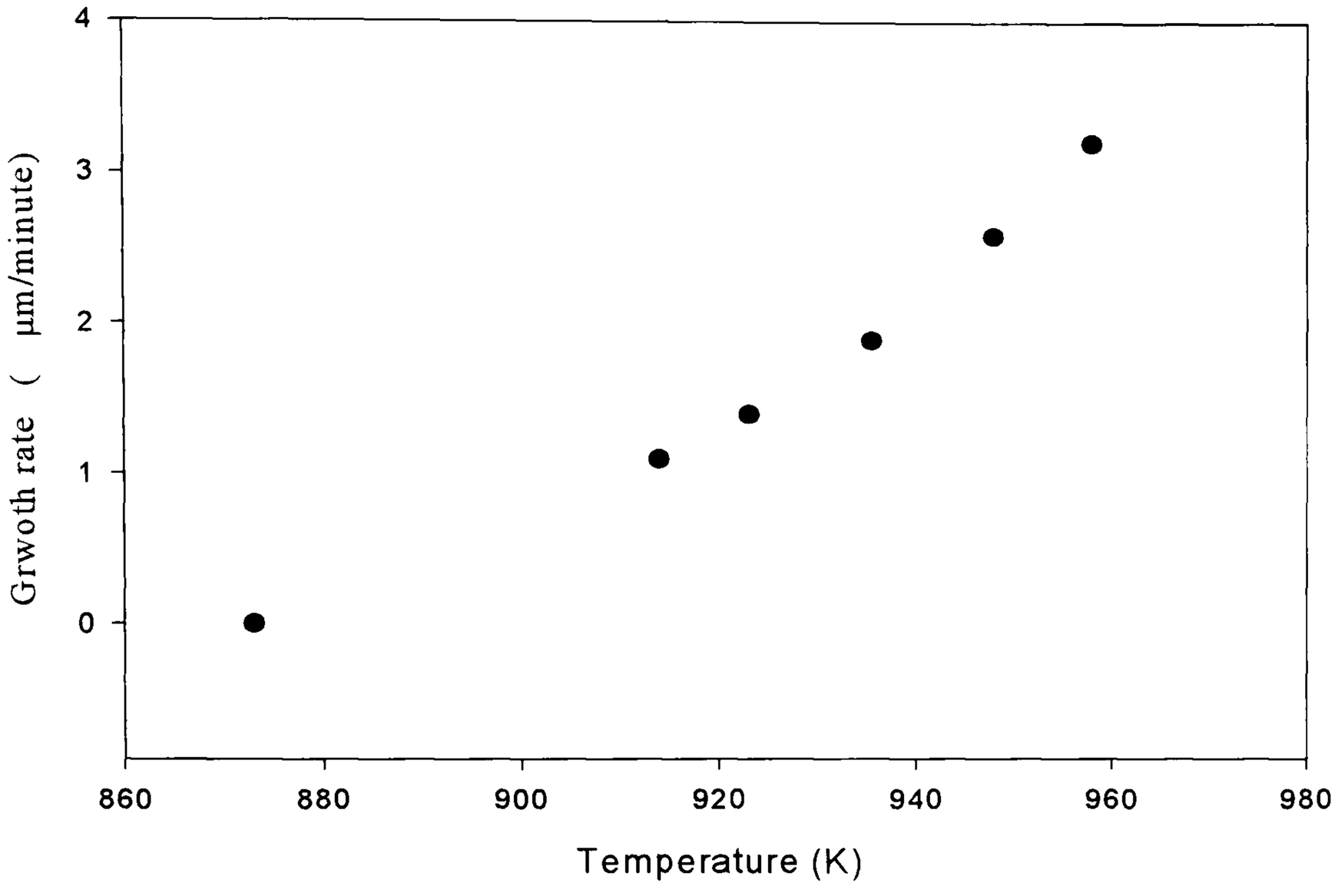

Figure (4-2)-Log R vs. 1/source temperature at 500 ^{o}C substrate temperature.

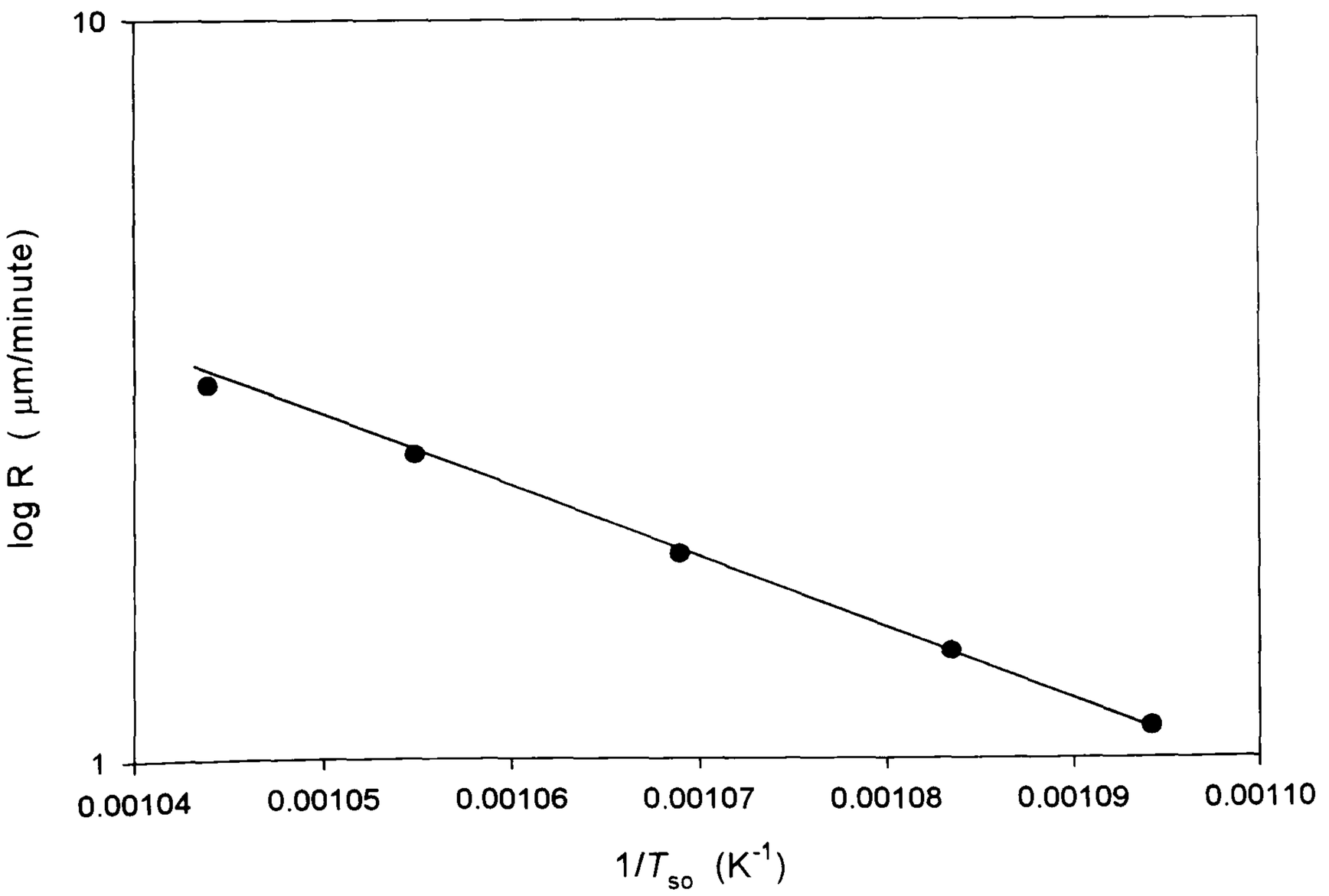

4.3- Effect of Substrate Temperature on Growth Rate.

Several layers of CdTe were deposited at different substrate temperatures between 687K and 823K. The source temperature was maintained at 923K and the chamber was at a pressure of 7.5×10^{-5}mbar of air. Figure (4-3) shows the dependence of the growth rate on the substrate temperature. The results show that for a given ambient, the growth rate was constant (i.e. independent of temperature) up to some characteristic break point temperature, above which the rate decreased rapidly to zero. Below this breakpoint temperature, where the growth rate was temperature independent, growth was limited by the supply of Cd and Te_2 vapours. Above the breakpoint temperature the growth is limited by surface kinetic processes of adsorption, compound formation and evaporation. As the temperature is increased beyond this point, then evaporation losses become increasingly dominant, until virtually no growth can occur at all.

Figure(4-3) Growth rate vs. substrate teperature
at 650 ^{o}C source temperature and 7.5x10^{-5} mbar.

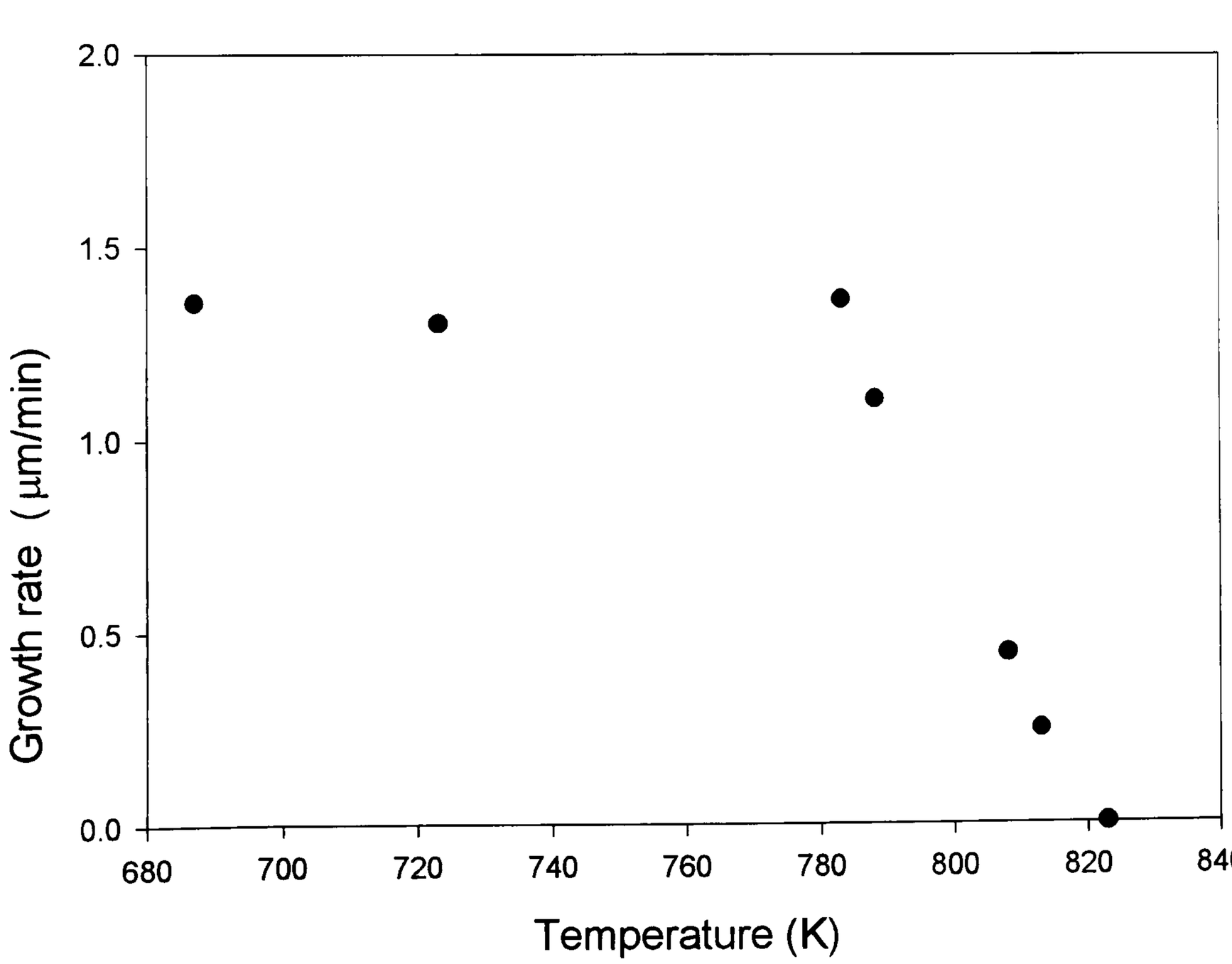

4.4- Effect of The Pressure on Growth Rate.

To investigate the effects of pressure on growth rate, several CdTe thin films were deposited at different pressures of ambient gas. Two different systems of heating were used to heat the source and substrate. Optical heating was used to deposit the films at ~7.5×10^{-5} mbar of air and at 10 mbar of N_2 at source temperature of 650°C. Tungsten wire filaments were used to heat the system during deposition of the films at 6 mbar and 2 mbar of N_2 at source temperature of 700°C . Figure (4-4) and figure (4-5) show the results using lamp and filament heating respectively. In all cases the growth follows the same general behaviour as shown in figure (4-3), i.e. temperature independent growth at temperatures below some threshold, and a rapid decrease in growth rate at higher temperatures. However, the growth rate values and threshold temperatures differ quite substantially. The growth rate at 7.5×10^{-5} mbar was ~ 1.35μ/min between 686K and 783K, and above 783K it reduced rapidly to zero at 822K. The growth rate at 10 mbar was about half this (0.73μ/min) but the threshold temperature had increased to 893K. In figure (4-5) the growth rate reduced from 1.1μ/min to 0.47μ/min between 773K and 863K as the pressure increased from 2 mbar to 6 mbar, and in the temperature independent part of characteristics although the threshold temperature was only slightly increased from ~863K to 877K.

Figure (4-4)-Growth rate vs. subtrate temperature at 7.5×10^{-5} mbar of air and 10 mbar of N_2.

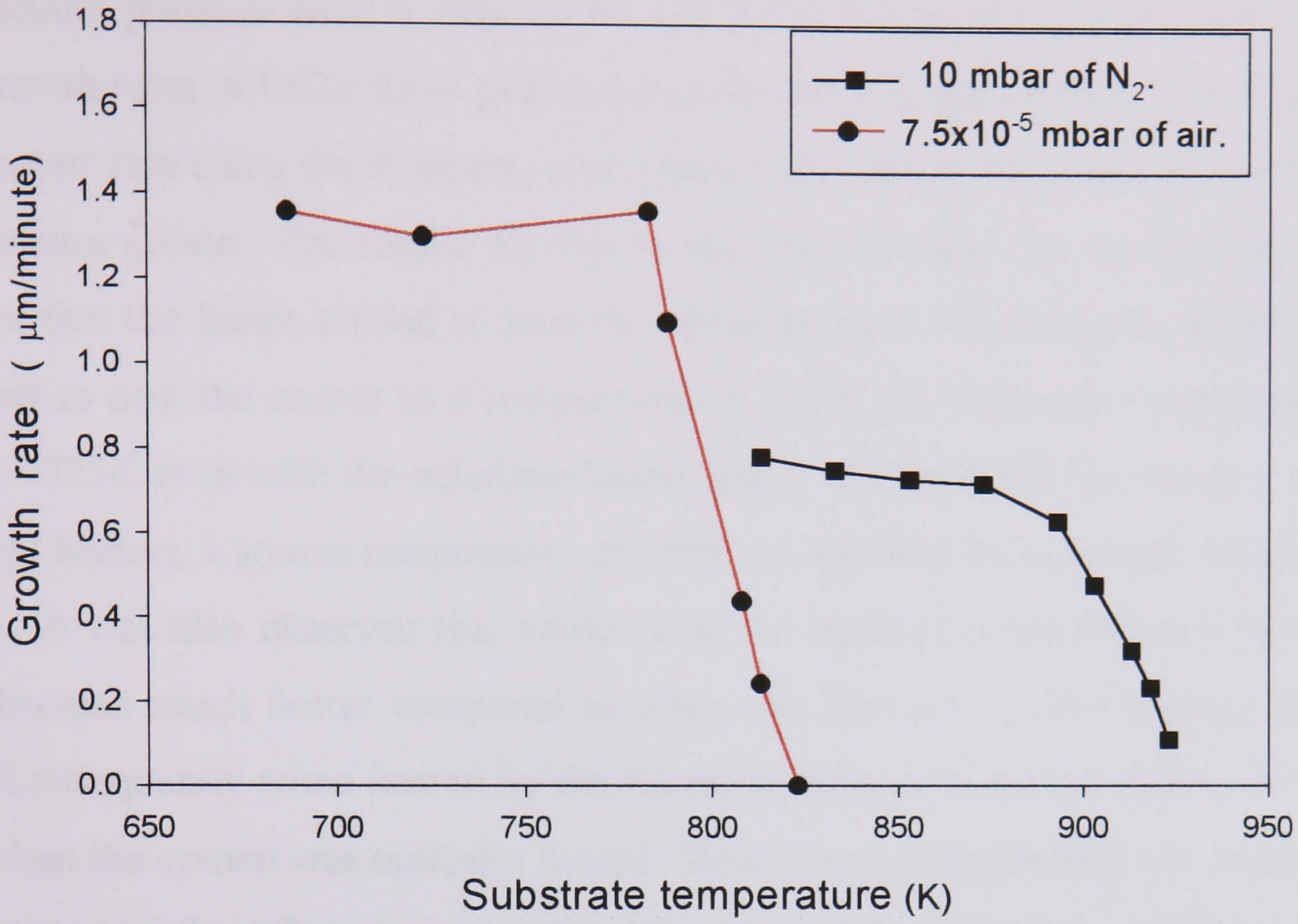

Figure (4-5) Growth rate vs. substrate temperature at 2 mbar and 6 mbar of N_2.

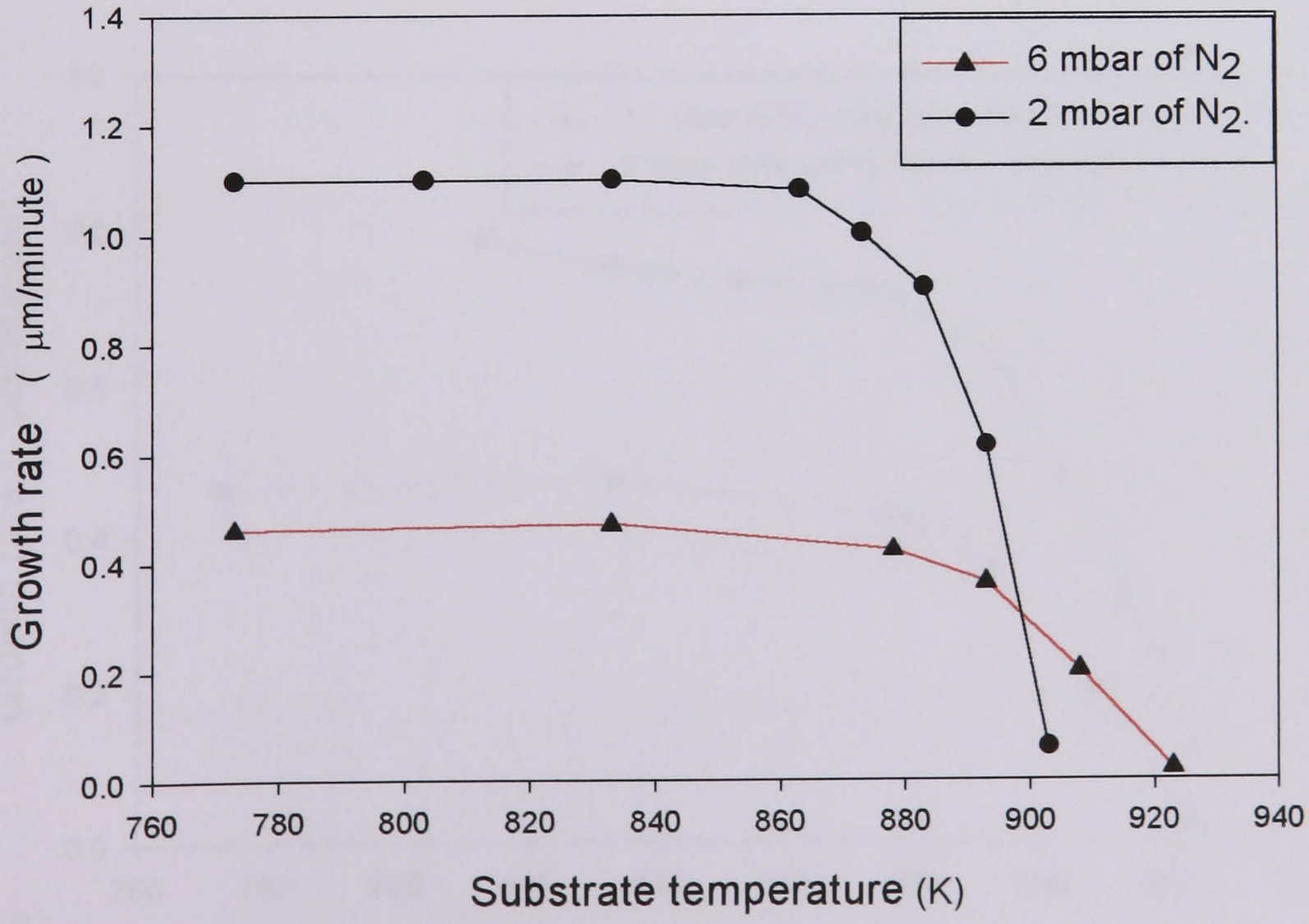

Figure (4-6) shows the growth rate of CdTe films deposited by the two different heating systems. The source temperature was 923K and the pressure of vacuum was 10 mbar of N_2 during the deposition by the lamp heating system. The source temperature and vacuum pressure were 6 mbar of N_2 and 973K during the deposition by filament. The growth rates of CdTe films grown using the lamp heating system were higher than the greatest rate using the filament, even though the source temperature was lower and the pressure greater. The reason for this is not entirely clear, but was probably due to the fact that the lamps tended to heat the entire system. For example, with the source lamp set to heat the source to a temperature of 923K, the substrate temperature would rise to ~723K even with the substrate heater lamps switched off. Conversely, using the filament heaters, a source temperature of 953K would raise the substrate temperature to ~623K. It was also observed that when using the optical heaters the bell jar and base plate became much hotter compared to when the filament system heating was being used. Consequently when heated by the filament the system cooled down more rapidly than when the system was optically heated. Thus it was probable that the space between the source and the substrate was hotter when optical heating was used than when the filament heating system was used. This would be expected to affect growth rate. In addition the layer cool down period may, in effect, have increased the growth time.

Figure (4-6)Growth rate of CdTe films depositied by using different heating systems.

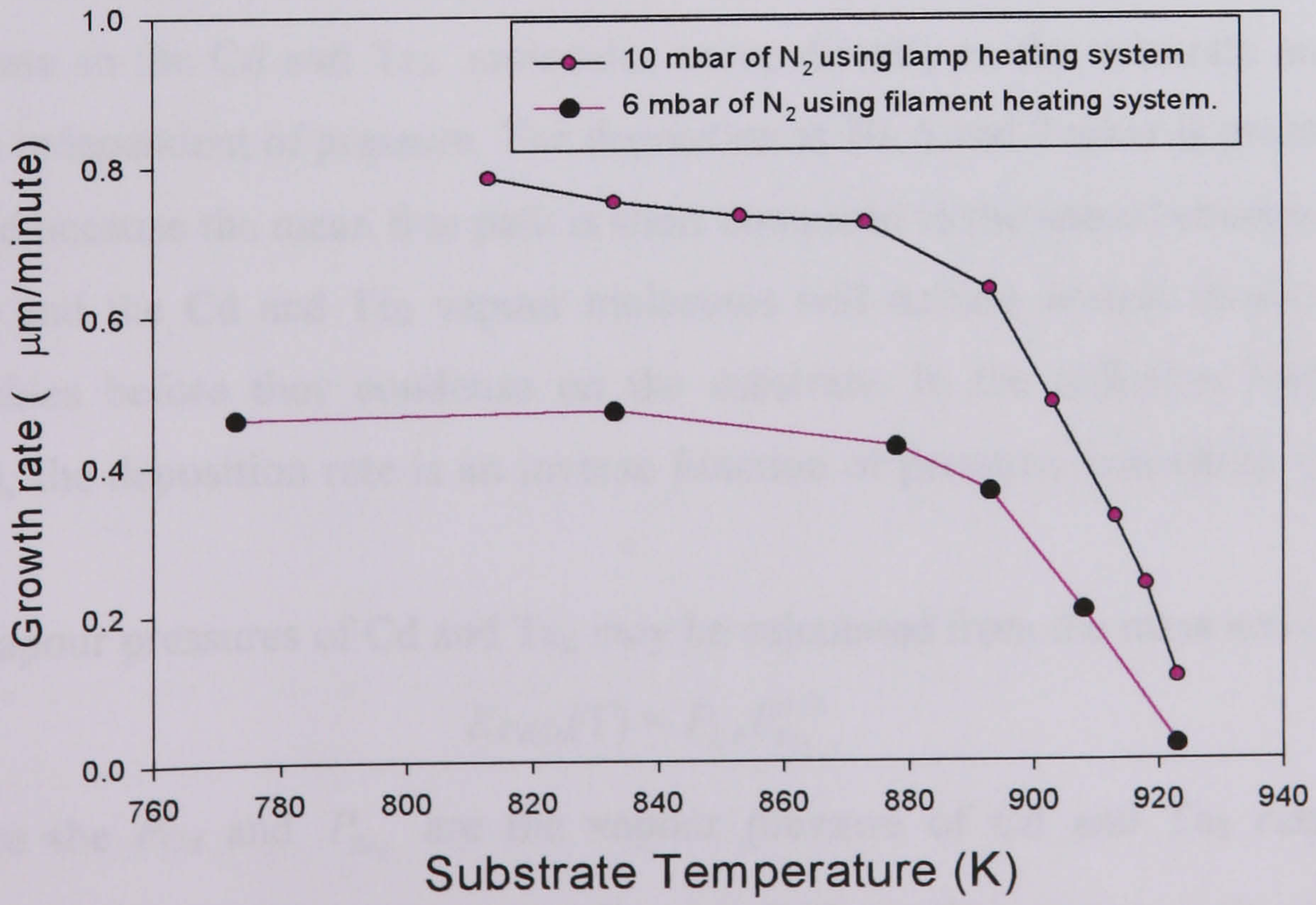

The mean free path of Cd atoms and Te_2 molecules evaporated from a CdTe source, depends on the source temperature and the pressure according to the following equation [13]:

$$h = \frac{kT}{2^{1/2}\pi d^2 P} \tag{4.3}$$

Where k is the Boltzman's constant, P is the pressure of ambient gas (Pa), T is the source temperature (K) and d is the molecular diameter. The molecular diameter of Cd and Te_2 is 2.606 and 3.966Å [14] respectively. Table (4-1) shows values of the mean free paths of Cd and Te_2 at different pressures and source temperatures.

Table (4-1) Mean free paths of Cd and Te_2 at different pressures and source temperatures.

Pressure (mbar) source tem.(K)	$7.5x10^{-5}$ 923	10 923	2 973	6 973
h of Cd (cm)	563	$4.22x10^{-3}$	0.022	$7.42x10^{-3}$
h of Te_2 (cm)	343	$1.82x10^{-3}$	$9.61x10^{-3}$	$3.2x10^{-3}$

These results suggest that the deposition at 7.5×10^{-5}mbar is by free molecular transport because the mean free path is longer than the space between the baffle and the substrate so the Cd and Te_2 molecules move directly to the substrate and the growth rate is independent of pressure. The deposition at 10, 6 and 2 mbar is probably diffusion limited because the mean free path is short compared to the space between substrate and baffle and the Cd and Te_2 vapour molecules will collide several times with nitrogen molecules before they condense on the substrate. In the diffusion limited transport model, the deposition rate is an inverse function of pressure, consistent with figure (4-5).

The vapour pressures of Cd and Te_2 may be calculated from the mass action law [15]:

$$K_{CdTe}(T) = P_{Cd}P_{Te_2}^{1/2} \tag{4.4}$$

Where the P_{Cd} and P_{Te_2} are the vapour pressure of Cd and Te_2 respectively and $K_{CdTe}(T)$ is the equilibrium constant. For a stoichiemetric source equation (4-1) gives:

$$P_{Cd} = 2P_{Te_2} \tag{4.5}$$

And therefore:

$$P_{Cd} = 2^{1/3} K_{CdTe}^{2/3}(T) \tag{4.6}$$

The equilibrium constant may be calculated from the expression given by deLargy et al [16] for 912K<T<1324K:

$$\ln K(T) = -(69446 \pm 786)/RT + (45.842 \pm 1.532)/R \tag{4.7}$$

Where R is the universal gas constant. Substituting in (4.6)

$$P_{Cd} = 2^{1/3}(\exp(-69446+45.842T/RT))^{2/3} \tag{4.8}$$

The vapour pressures of Cd at 923 and 973 K (source temperatures) are 0.067 and 0.243 mbar respectively and the corresponding vapour pressures of Te_2 are 0.033 and 0.12 mbar respectively. Similar values have been reported by Chu et al [17] at 973K. The mean free paths in the vapour would be 6.5 and 1.8 mm respectively. The value of mean free path at 6.5 mm is comparable to the distance between the baffle and the substrate, suggesting that at a vacuum pressure of 7.5×10^{-5} mbar, deposition at 923K was by free sublimation and transport of CdTe.

The molecular flux from the source depends on the source temperature and the vapour pressure, and is given by: [13]

$$f_m = \frac{PN_{Av}}{(2\pi MRT)^{1/2}} \tag{4.9}$$

Where M is the molecular weight and N_{Av} is Avogadro's Number. The flux of Cd at 923K (0.067 mbar) is 0.061 g $cm^{-2}min^{-1}$ and the flux of Te_2 (0.033 mbar) is 0.045g cm^{-2} min^{-1}. According to the equation (4-1), the CdTe flux would be 0.084g $cm^{-2}min^{-1}$, whereas 0.043g $cm^{-2}min^{-1}$ was measured experimentally. The difference between the experimental and calculated values could refer to the fraction of CdTe that is deposited on the underside of the baffle. This means the baffle temperature was lower than the source temperature.

4.5- Effect of Source - Substrate Separation on Growth Rate.

The effects of the separation between the substrate and the source was apparent when the pattern of baffle holes was reproduced on the CdTe film. Parts of the film, located directly above a baffle hole were darker in colour indicting that this area was thicker than other parts of layer (i.e. not located above holes in the baffle). Figure (4-7-a) shows the thickness of the peak is around 72.7μm at when the substrate placed

directly on the baffle. The reduction of peak height is shown in figure (4-7-b, c, d, and f) at separation distances of 1.3, 2.7, 3.8, 8.3 and 11 mm respectively.

The figure (4-8) shows the height between the peak and the valley reduces as the separation between the baffle and the substrate increases, whereas the width at half-maximum increases, figure (4-9), as the growth become more uniform. The peak growth rate (i.e. above the hole) reduces as the separation between the substrate and holes of baffle (source) increases [18] as shown in figure (4-10). The behaviour of the curves in figures (4-8), (4-9) and (4-10) changed after ~ 4mm, this probably due to change of deposition mechanism, e.g. from mean free path to diffusion limited transport.

The grain size of CdTe films increase with the layer thickness [17][19] as determined by the source – substrate separation. We found the grain size increased from around 2.8μm at a thickness of ~ 3 μm to 19μm at a thickness of ~ 72.7μm. The variation of grain size with the thickness of film is clear in figure (4-11) which shows the secondary emission micrographs of different thickness of CdTe films 72.7, 15, 10, 5 and 3 μm for films which had be deposited under nominally the same conditions of temperature and pressure.

Figure (4-7)- Film thickness as function of separation between the baffle and substrate.

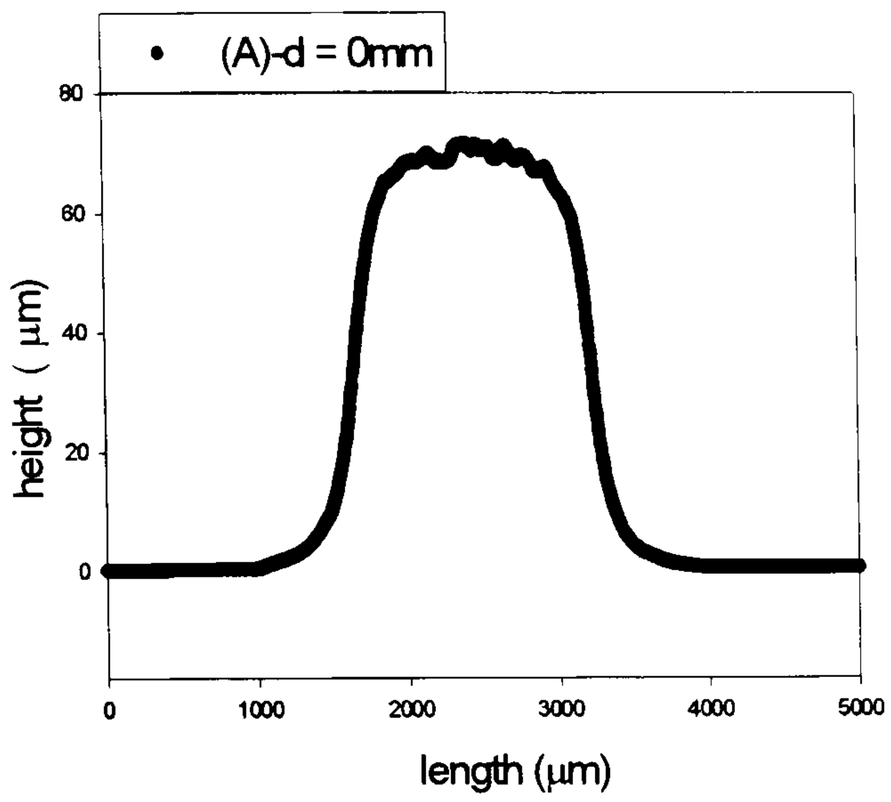

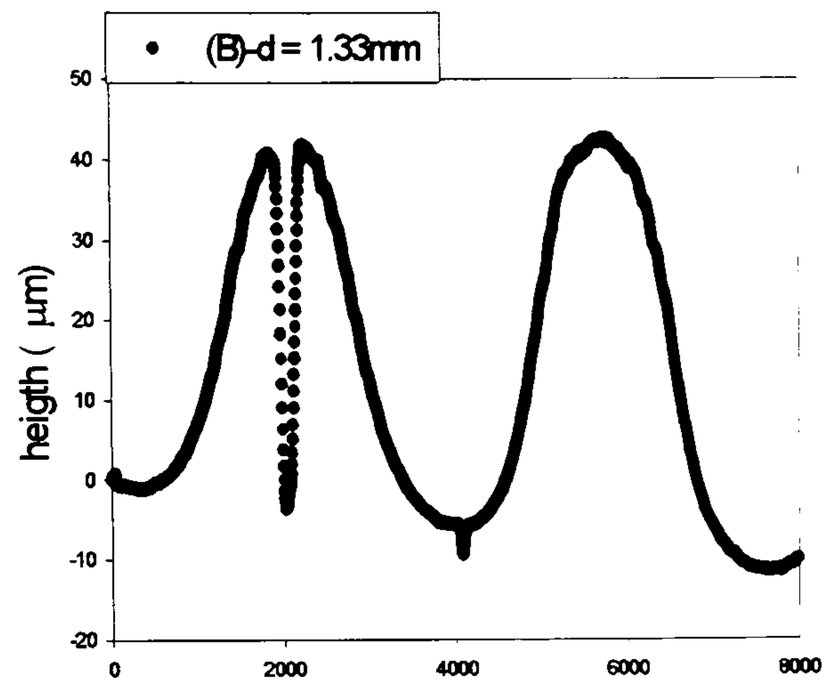

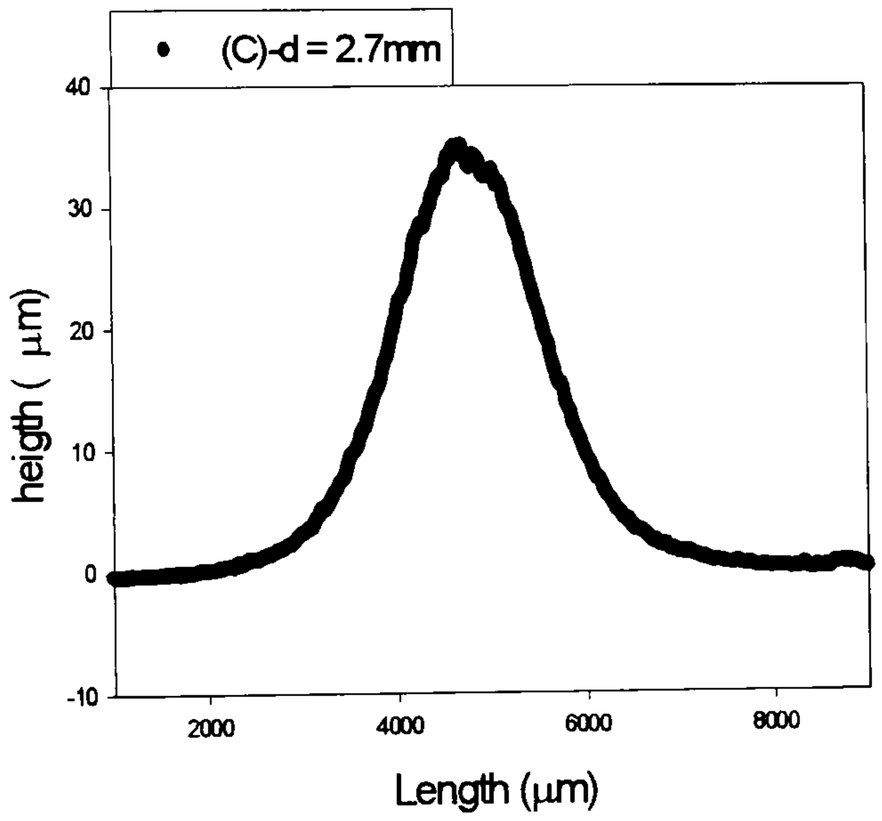

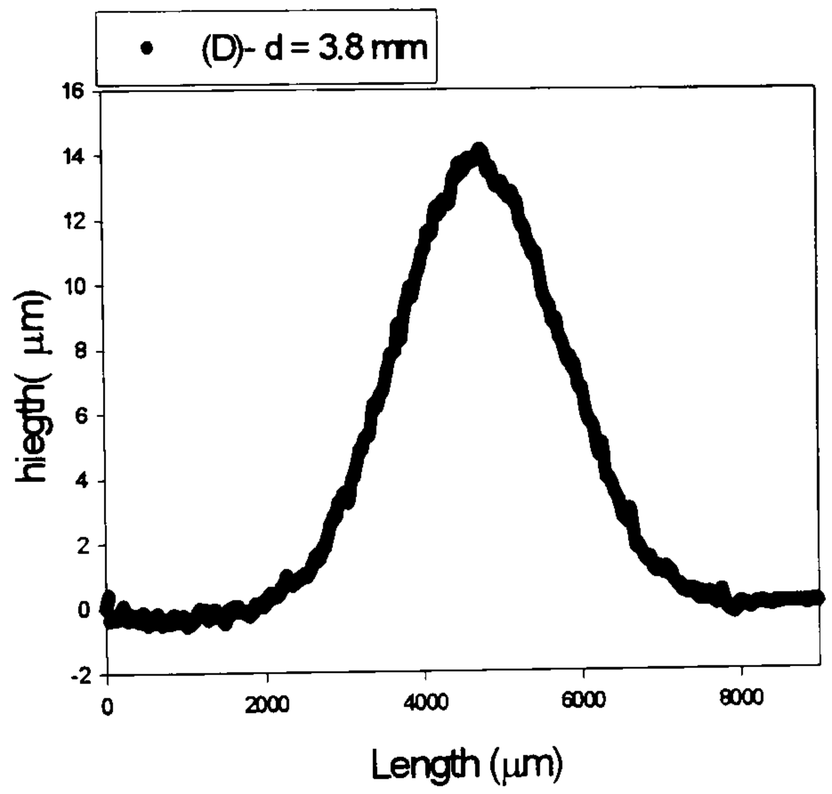

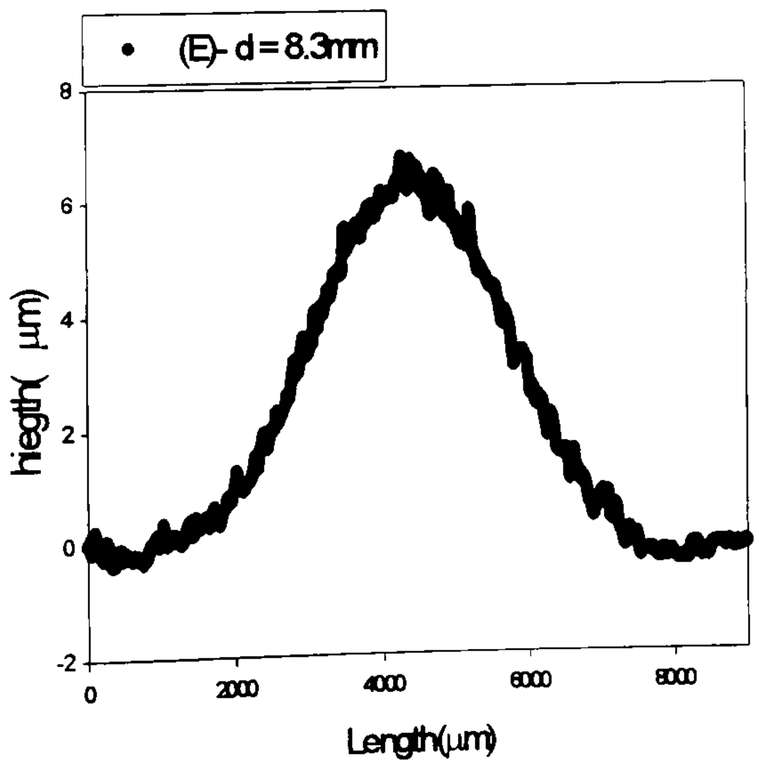

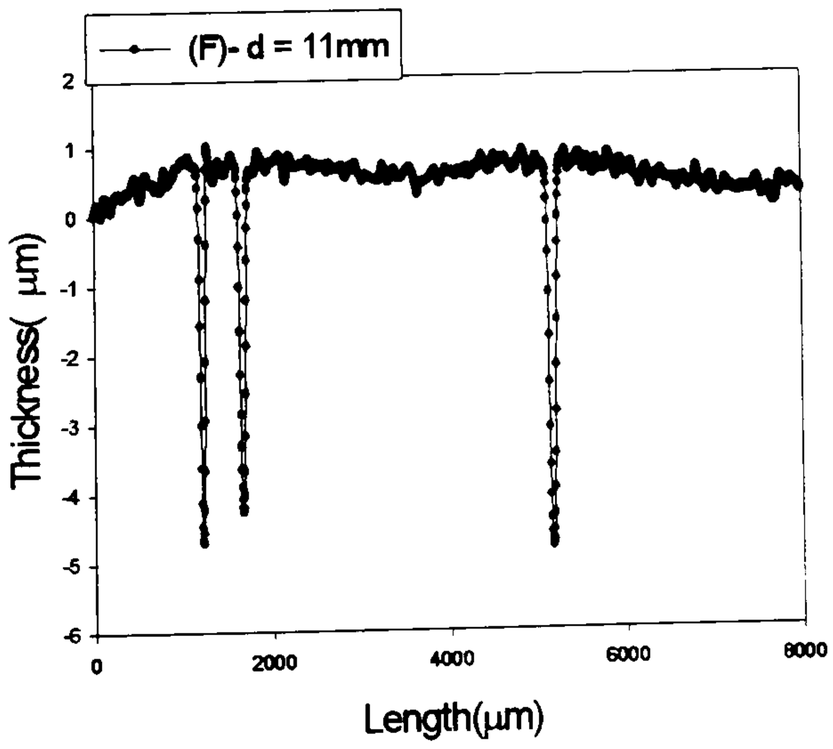

Figure (4-8)-Peak height vs. the separation between the substrate and baffle.

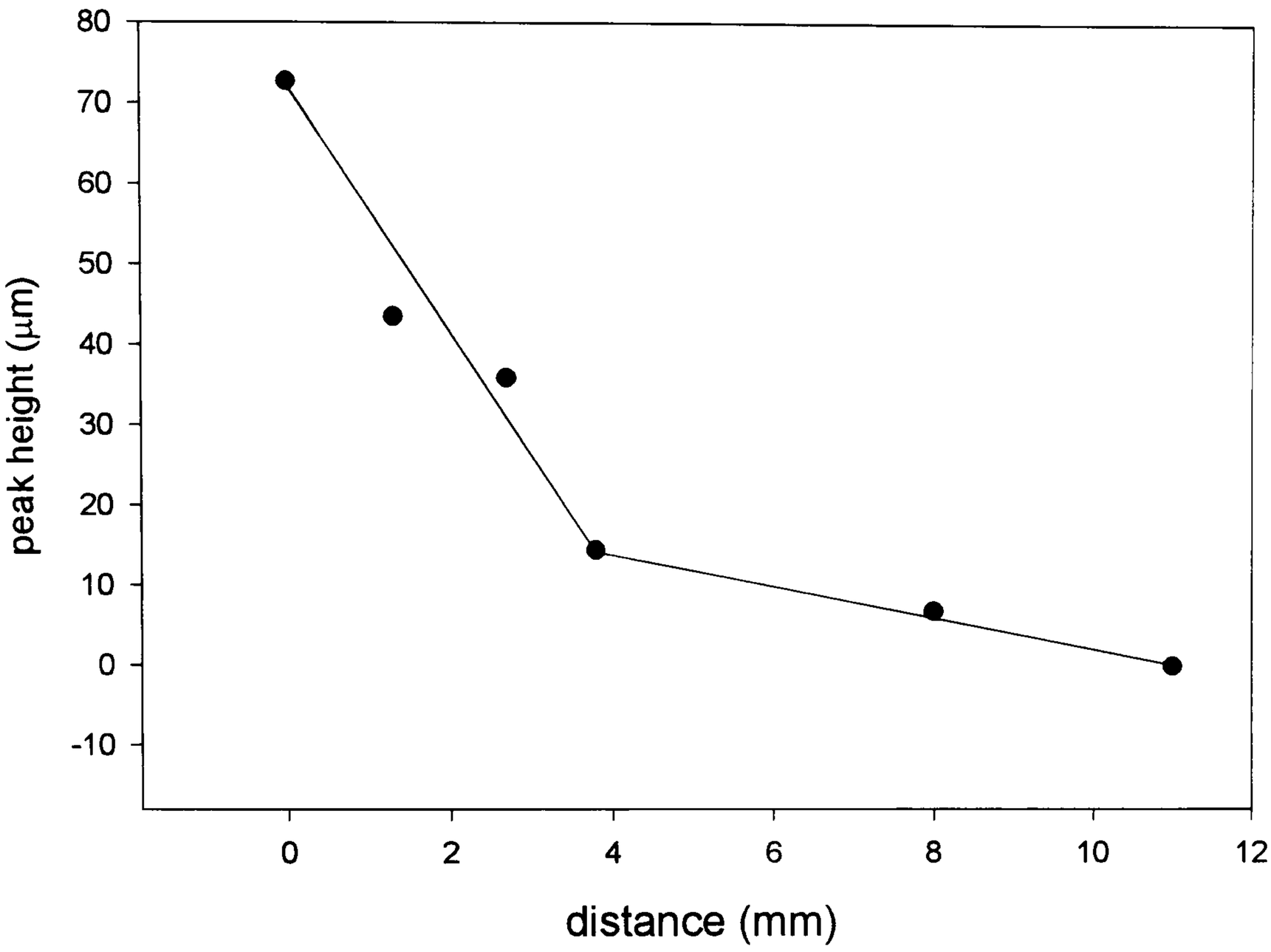

Figure(4-9)- FWHM of peak vs. the distance from the baffle.

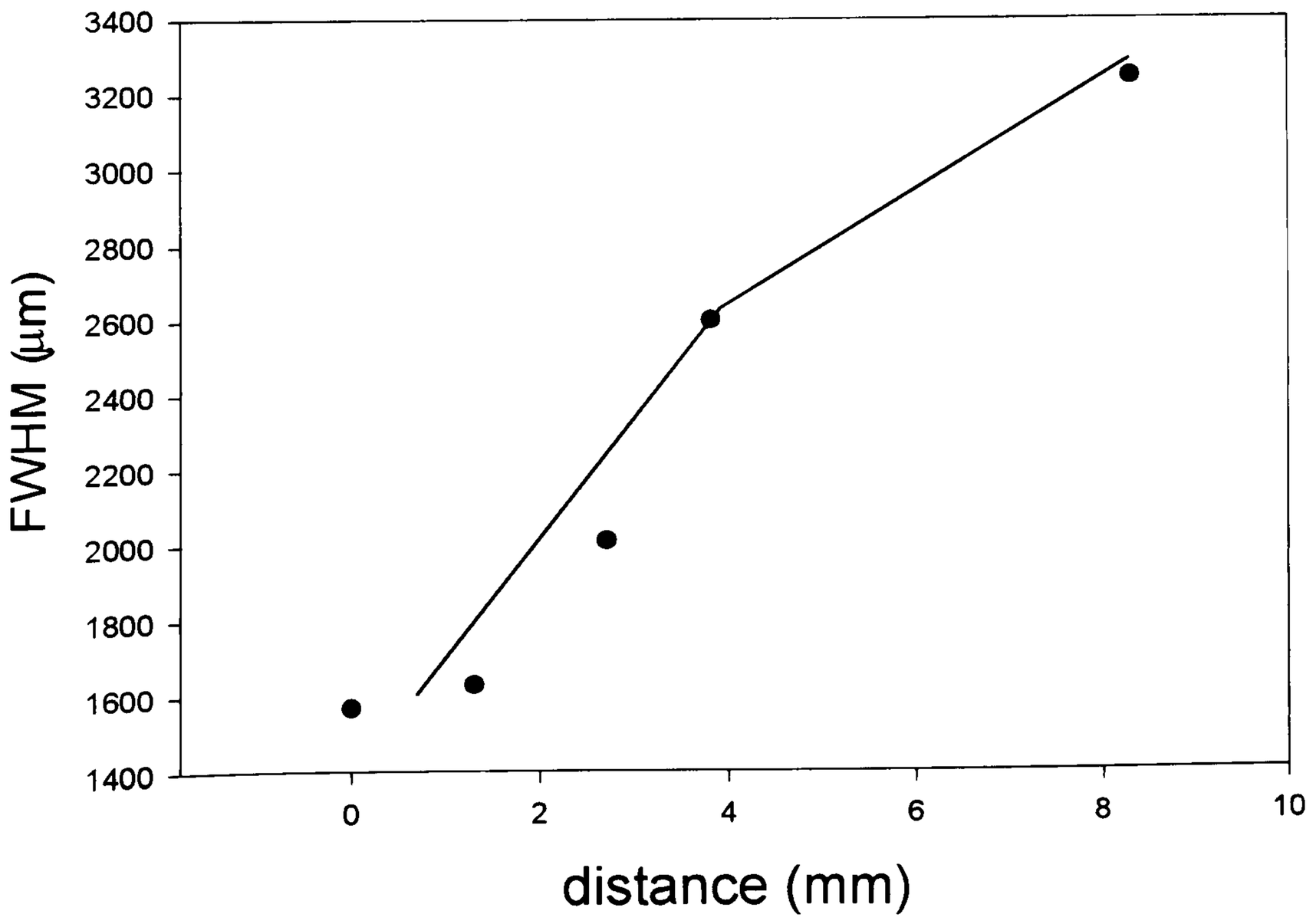

Figure (4-10)- Growth rate of CdTe vs. the distance between the baffle and the substrate.

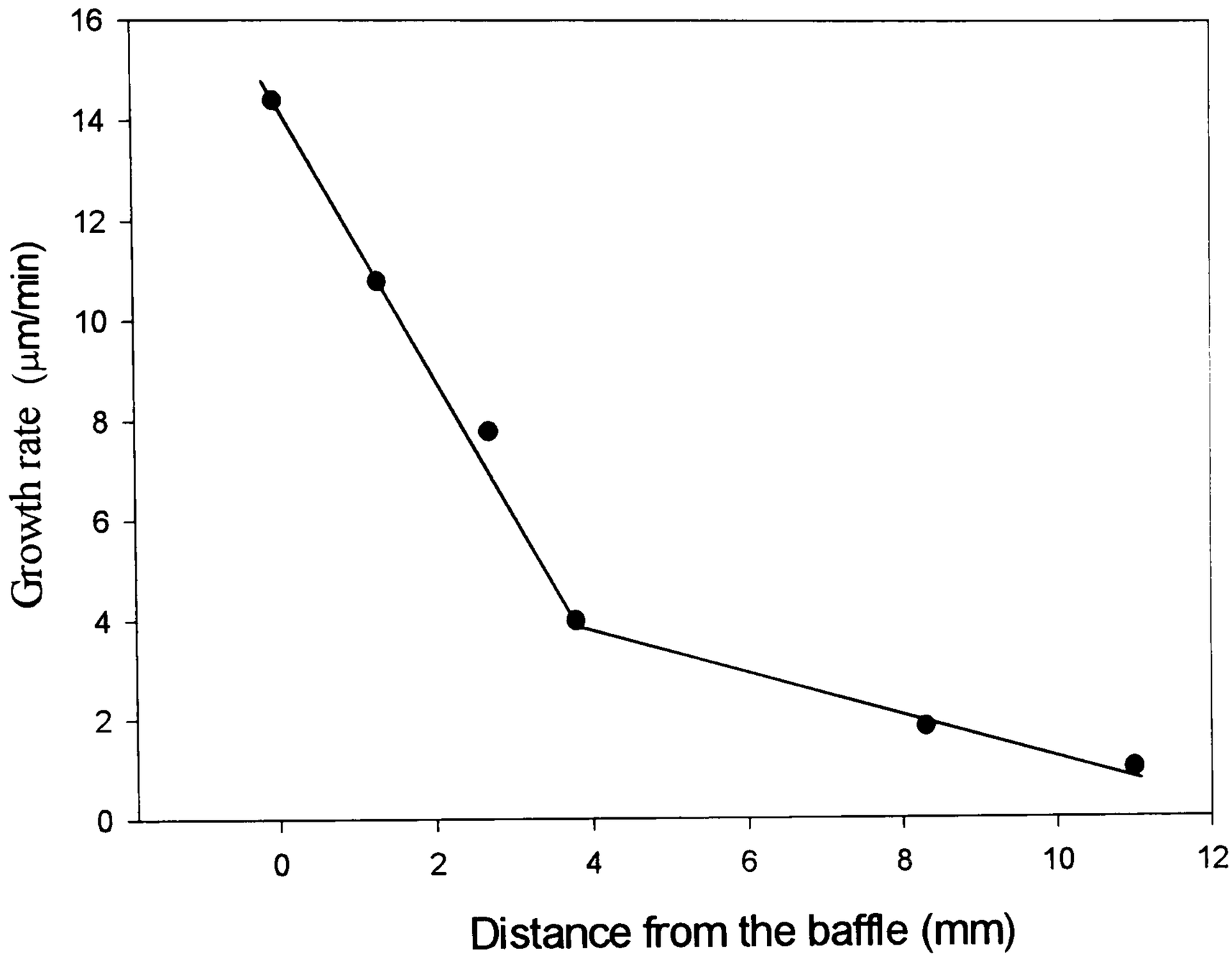

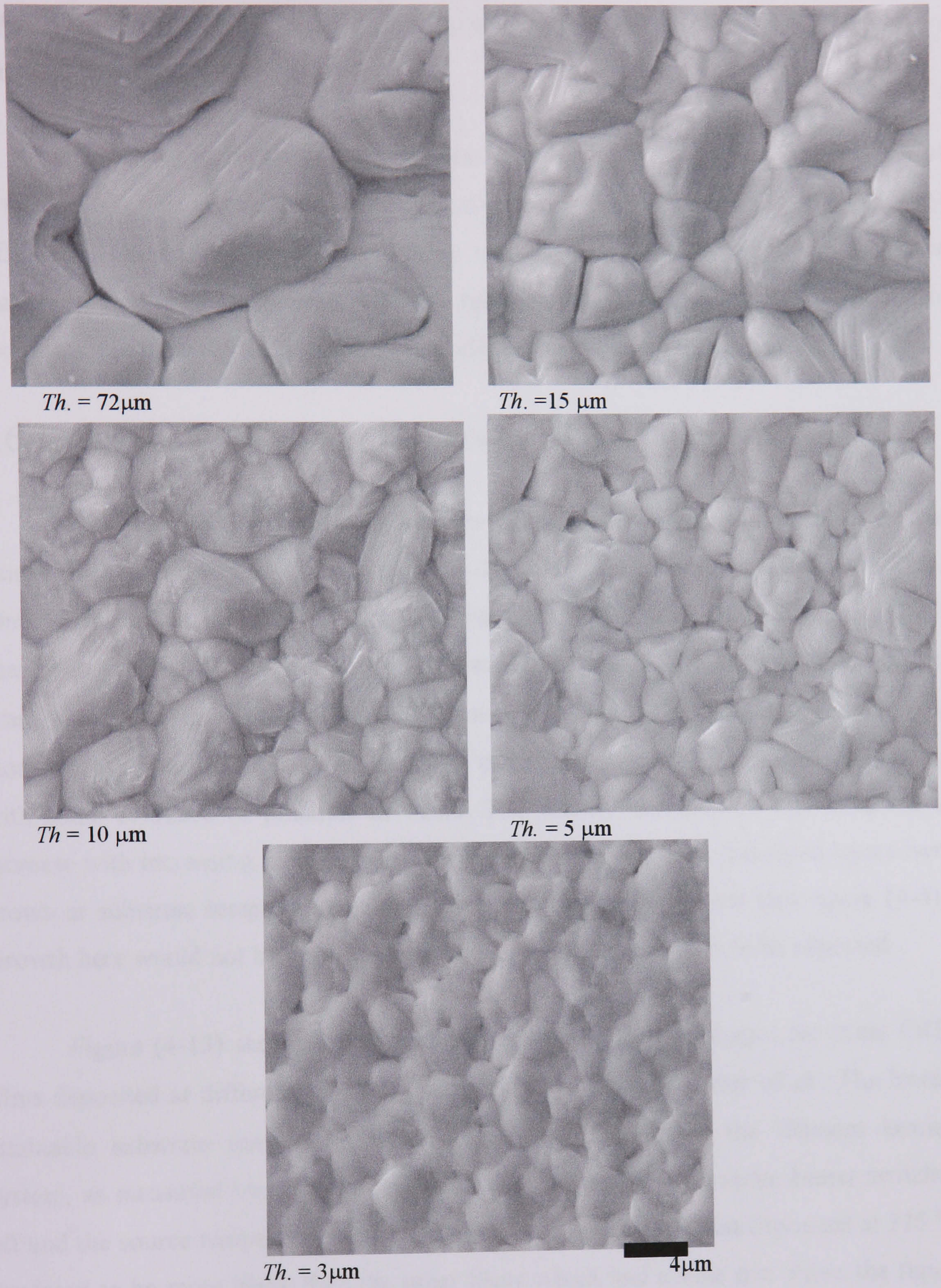

Figure (4-11)- Secondary emission micrographs of different thickness of CdTe film.

4.6- The Effects of Substrate Temperature on The Morphology and Structure of CdTe Films.

The effects of the substrate temperature on the morphology and microstructure of CdTe films was investigated using Scanning Electron Microscopy (SEM) and X-ray diffraction. Scanning electron microscopy was used to record changes in the grain shape and size with changes in substrate temperature. X-ray diffraction was used to determine variations in the preferred orientation with substrate temperature.

4.6.1- Scanning Electron Microscopy (SEM) Studies.

The secondary electron (SE) mode of the SEM was used to examine the morphology of CdTe thin films. Figure (4-12) shows SEM images taken from CdTe films deposited at different substrate temperature in 10 mbar of N_2. There is little change in grain size with increasing substrate temperature. The films have a range of grain sizes between 2.5 and 4 μm. However, there is a pronounced change in morphology. The films deposited at 630°C and 650°C have a more granulated surface with some evidence of pinholes or voids. The density of pinholes was observed to increase with increasing temperature [20]. It is interesting to note that these layers were grown at substrate temperatures above the break point temperature (see figure (4-4)). Growth here would not be very stable and so a poor morphology is to be expected.

Figure (4-13) shows the scanning electron microscope images for some CdTe films deposited at different substrates temperature in 7.5×10^{-5} mbar of air. The lowest attainable substrate temperature was 335 ^{0}C, obtained using the filament heating system, as measured by the substrate thermocouple with the substrate heater switched off and the source temperature set to 680 °C. The colour of the film deposited at 335 °C appeared to be more black than the other films which had a blue tint. From the figure (4-12) it is clear that the grain sizes of the layer deposited at 335 °C was very much smaller (<1μm) than for the other layers (>2.5μm). The morphology of the layer grown at 520°C while still appearing to be composed of smooth grain, is arguably beginning to display the same rough structure observed for the layer grown at higher temperatures in 10mbar N_2 (figure (4-12,630°C & 650°C). The break point temperature for layers grown at 7.5×10^{-5} mbar is ~520°C.

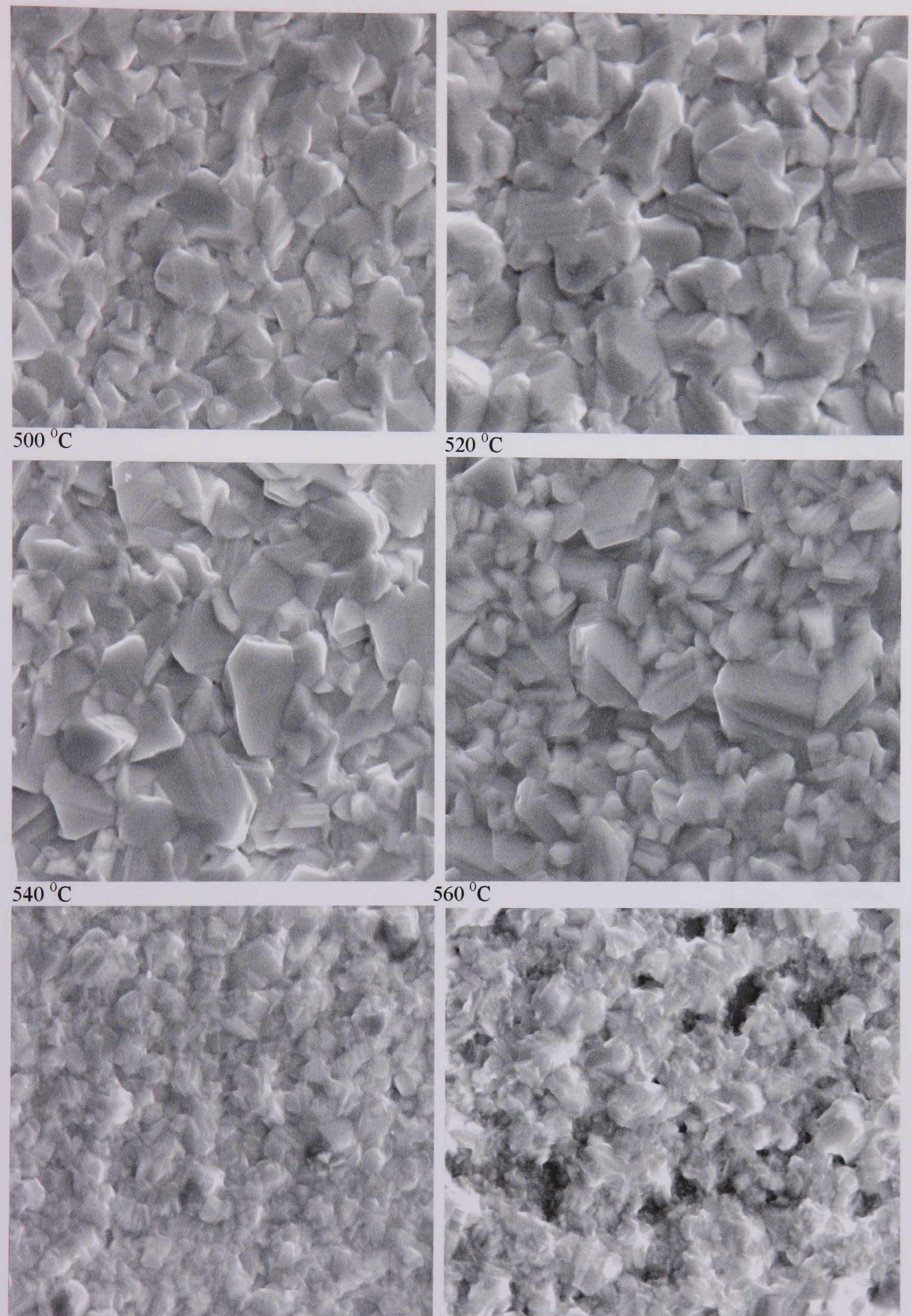

Figure (4-12) Scanning electron microscope images of CdTe films deposited at different substrate temperature in 10 mbar of N_2.

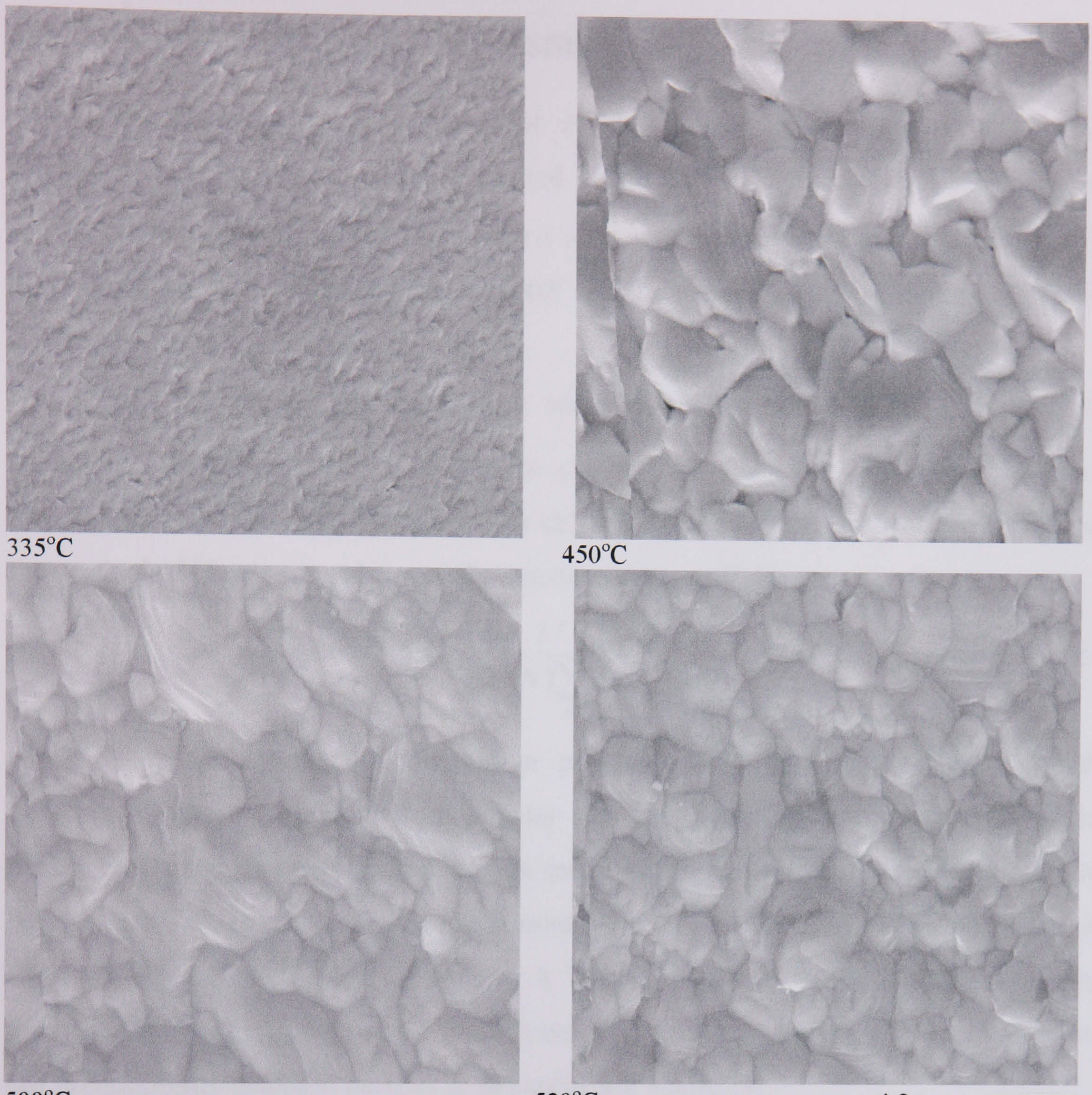

Figure (4-13) Scanning electron microscopy images of CdTe films deposited at different substrate temperatures and ~7.5×10^{-5} mbar of air.

4.6.2- X-ray Diffraction Assessment.

The X-ray diffraction traces for several CdTe films deposited at different substrate temperatures, were recorded with a computer controlled Philips diffractometer, using $Cu_{k\alpha}$ radiation with a wavelength of $\lambda = 1.54056$Å. Wide-angle 2θ scans from 10 to 90 degrees taken in 0.02^{o} steps were used to determine the preferred orientation.

The interplanar spacing (d_{hkl}) were calculated and used to confirm the orientation of the peak by reference to the JCPDS files. The degree of preferred orientation in the film was determined by calculating the texture coefficient (T.C.) using the method of Harris for polycrystalline texture analysis [21]:

$$\text{T.C.} = \frac{I / I_o(hkl)}{(1/N)\sum_N I / I_o(hkl)} \qquad (4.10)$$

where N is the number of diffraction peaks (reflections) expected in the XRD diffraction pattern from a random powder sample, I_o (hkl) is the intensity of the hkl peak from a random powder, I(hkl) is the measured intensity of the same peak from the layer. If the T.C. (hkl) is equal to the number of peaks expected (N) all the grains of the films are oriented in the (hkl) direction. A T.C.(hkl) value of unity indicates a random grain orientation [22], whereas T.C.(hkl) larger than unity implies that the (hkl) planes are preferentially oriented parallel to the substrate plane[23].

The existence of a preferred orientation may be assessed from the standard deviation, σ, for all values of T.C. according to the following expression [22]:

$$\sigma = \left[\frac{\sum_N \{T.C.(hkl) - T.C._R(hkl)\}^2}{N} \right]^{1/2} \qquad (4.11)$$

where the T.C.(hkl) is the measured texture coefficient and $T.C._R$(hkl) is the value for a randomly oriented sample (i.e. unity).Clearly more random samples, where T.C.(hkl) $\cong$ $T.C._R$(hkl) will give low values of σ.

Figure (4-14) shows the X-ray diffraction patterns of CdTe films deposited at different temperature in 10 mbar of N_2. In this figure the background was not flat, and the peaks intensities were calculated from the top of the peak to the background level at the peak. X-ray diffraction traces showed peaks corresponding to the (111), (220), (311) [24] [25] and (331) [26] planes of cubic CdTe. The values of T.C. were calculated for all observed orientations for all films and these are listed in Table (4-2) together with

the standard deviation. It is clear that the (111) texture coefficient is reduced as the substrate temperature was increased while the (220) texture coefficient increased. The overall reduction in σ suggests that generally layers grown at higher temperature were less well ordered.

Figure (4-14) X-ray diffraction traces for CdTe films deposited at different substrate temperature in 10 mbar of N_2.

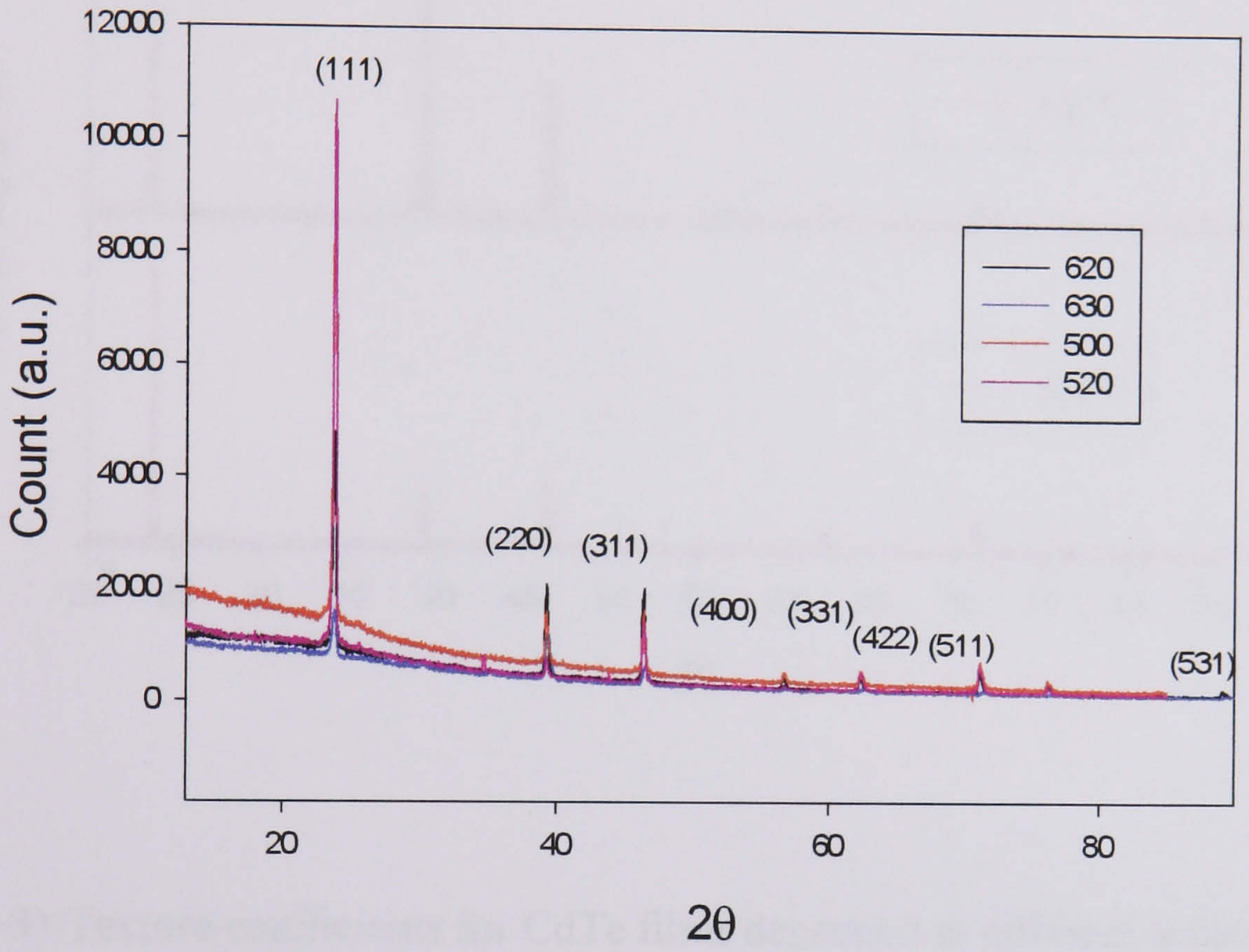

Table (4-2)-Texture coefficient for different orientations vs. substrate temperature of CdTe layers deposited in 10 mbar of N_2.

substrate temperature	1 1 1	2 2 0	3 1 1	4 0 0	3 3 1	4 2 2	5 1 1	4 4 0	5 3 1	σ
500 °C	2.94	0.49	1.2	0.86	0.78	1.4	1.3	-	-	0.9
520 °C	2.6	0.13	0.94	-	0.78	1.17	2.1	-	-	1
620 °C	1.075	0.75	1.53	1.15	0.71	1.08	1.23	0.67	0.78	0.3
630 °C	1.04	1.72	1.36	0.5	0.84	0.62	0.81	1.43	0.66	0.3

The X-ray diffraction traces of CdTe films deposited at different substrate temperatures in 6 mbar of N_2,is shown in figure (4-15). This shows that the intensity of the (111) peak tended to reduce as the substrate temperature increased, while the (111) T.C. also reduced from 2.6 at 500°C to 0.27 at 605 °C with random variations for other planes as illustrated in the table (4-3). However, the values of σ for the layer grown at 605°C is larger than for layers grown at lower temperatures.

Figure (4-15) X-ray diffraction traces for CdTe films deposited at different substrate temperature in 6 mbar of N_2.

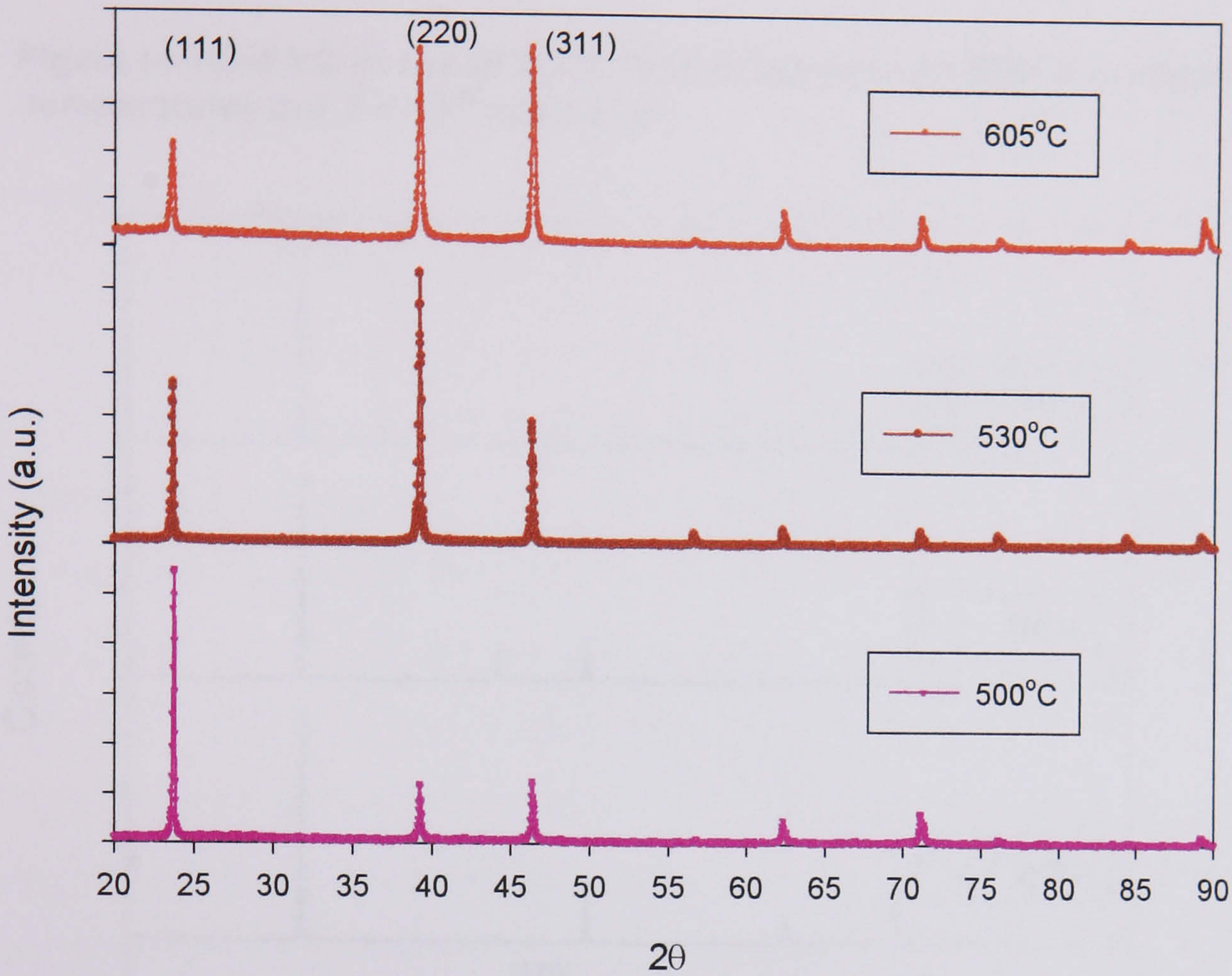

Table (4-3)-Texture coefficients for CdTe films deposited at different substrate temperature and in 6 mbar of N_2.

substrate temperature	1 1 1	2 2 0	3 1 1	3 3 1	400	4 2 2	4 4 0	511	5 3 1	σ
500 °C	2.62	0.96	2	2.35	-	1	-	-	-	1
530 °C	0.63	1.8	1.6	0.75	0.9	0.64	-	1.34	1.34	0.5
605 °C	0.27	0.9	1.7	1	-	0.9	1.8	-	2.4	0.8

X-ray diffraction traces for CdTe films deposited in 7.5×10^{-5} mbar are illustrated in figure (4-16). At 335 °C substrate temperature just a single sharp (111) peak was found, indicating that all the grains were oriented along the (111). In the case of CdTe, in general a maximum of nine diffraction peaks were observed in a random sample and for this analysis a value of N = 9 was chosen. The (111) texture coefficient reduced to zero as the substrate temperature was increased as illustrated in table (4-4). Values of σ confirm the loss of ordering with increasing substrate temperature. A reduction in the (111) peak intensity and increased intensities of the (220), (311) and (440) peaks

after annealing of electrodeposited CdTe films has also been reported by Morris and Das [27] [28] and by Bin Qi et al [29].

Figure (4-16)-XRD traces of CdTe films deposited at different substrate temperatures in 7.5 x 10^{-5} mbar of air.

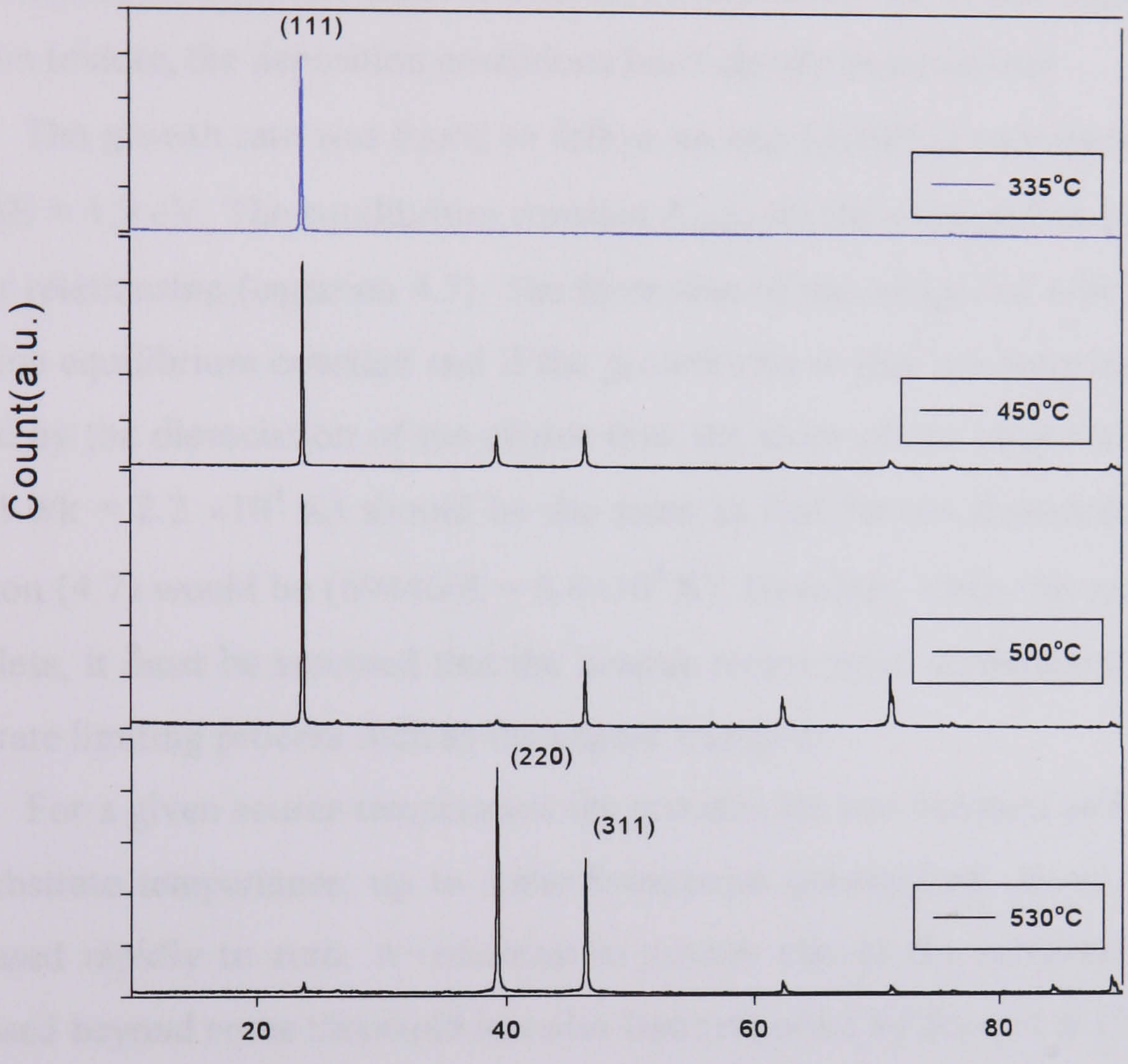

Table (4-4)- The texture coefficient of CdTe layers deposited in 7.5× 10^{-5}mbar of air.

substrate temperature	1 1 1	2 2 0	3 1 1	3 3 1	400	4 2 2	4 4 0	511	5 3 1	σ
335 °C	9	-	-	-	-	-	-	-	-	2.8
450 °C	4.8	1.3	2.9	-	-	-	-	-	-	1.64
500 °C	1.6	-	1.5	2.2	-	3.7	-	-	-	1.3
530 °C	-	2.6	3.17	-	-	-	-	-	3.17	1.3

4.7-. Conclusions:

The deposition of CdTe by Close Space Sublimation is affected by several interrelated parameters; substrate and source temperature, the ambient gas pressure and the separation and temperature difference between the source and the substrate. These parameters affect the growth rate and also the microstructure of the films, and thus could influence the performance of CdS/CdTe solar cells. To obtain a given growth rate and film texture, the deposition conditions must clearly be optimised.

The growth rate was found to follow an exp ($\Delta E/kT_{so}$) relationship (figure 4-2) with $\Delta E = 1.9$ eV. The equilibrium constant K_{CdTe} for the dissociation of CdTe obeys a similar relationship (equation 4.7). The formation of the compound will be governed by the same equilibrium constant and if the growth rate at that substrate temperatures was limited by the dissociation of the source then the slope of the ln(growth rate)/vs. $1/T_{so}$ plot ($1.9/k = 2.2 \times 10^4$ K) should be the same as that for the dissociation which from equation (4.7) would be ($69446/R = 8.4 \times 10^3$ K). However, since this nearly a factor of three less, it must be assumed that the inverse temperature dependence is due to some other rate limiting process such as the vapour transport.

For a given source temperature the growth rate was constant and independent of the substrate temperature, up to some breakpoint temperature, above which the rate decreased rapidly to zero. A reduction in growth rate as the substrate temperature is increased beyond some threshold has also been reported by Sosa et al [9]. Their system was similar to that used here, although the separation between the source and substrate was around 6 mm approximately half that in the present study. Uda et al [30] also have reported that the growth rate decreased as both the substrate temperature and the separation between the source and the substrate were increased. However, Chu et al [31] reported that the growth rate increased as the substrate temperature increased, which is in conflict with our result. The difference may result for the following reasons:

-They maintained a constant temperature difference of 100°C between the source and the substrate, so that the source temperature always tracked the substrate temperatures.

-The space between the source and substrate in their system was very small, a millimetre or less, so there was no shutter to control the deposition rate. Film thickness, from which growth rate would be calculated, would be controlled by

the heating and cooling times rather than by the substrate temperature. Heating/cooling times would depend on the substrate temperature.

The pressure of ambient gas defines the mechanism for the deposition involved in the CSS system. Free sublimation and transport is involved at low pressures such as 7.5×10^{-5} mbar because the mean free path is longer or equal to the space between the source and substrate. There were no pinholes in the films deposited at this pressure. Diffusion limited transport was involved at pressures of 2, 6, and 10 mbar of N_2, because the mean free path is short compared to the space between substrate and the source. There were pinholes in these films, possibly as a result of collisions between the Cd, Te_2 and N_2 molecules during the deposition.

The growth rate increased as the separation between the source and the substrate decreased. This is as would be expected, due to vapour beam divergence.

The use of the baffle between the source and the substrate had a significant effect on the uniformity of the film. When the substrate was too close to the baffle (less than 11mm) at high vacuum (7.5×10^{-5} mbar), then those parts of the film which were directly above the holes, were considerably thicker than the rest of the layer. The baffle was necessary to prevent spitting of CdTe particles onto the layer. Fortunately the increased separation did not restrict growth rate too severely.

The microstructure and morphology of the CdTe films were strongly affected by the substrate temperature, as observed in the Scanning Electron Microscopy (SEM) and with X-ray diffraction. The grain size increased from <1μm at 335°C to more than 2.5μm at above 445°C. The CdTe films grown at 335 °C showed a highly preferred (111) orientation. The intensity and the (111) texture coefficient reduced when the substrate temperature increased. Analysis of the XRD traces indicated that there was a general reduction in the degree of ordering as the substrate temperature was increased.

4.8- References:

(1)- T. Aramoto, S. Kumazawa, H. Higughi. "16.0% Efficient Thin-Film CdS/CdTe Solar Cell". Japan. J. Appl. Phys., 36 (1997) 6304.

(2)- J. Britt and C. Ferekides. "Thin-Film CdS/CdTe Solar Cell with 15.8% Efficiency". Appl. Phys. Lett., 62 (1933) 2851.

(3)- F. N. Nicoll. "The Use of Close Spacing in Chemical – Transport Systems for Growing Epitaxial Layers of Semiconductors". J. Electrochem. Soc., 11 (1963) 1165.

(4)- D. Albin, D. Rose, A. Swartlzander, H. Moutinho, F. Hasoon, S. Asher, R. Matson and P. Sheldon. "The Effect of Source Microstructure on the Close-Space Sublimation of CdTe Thin Films for Solar Cell Application". Mat. Res. Soc. Symp., 410 (1996) 45.

(5)- G. Gordillo, J. M. Florez and L. C. Hernandez. "Preparation and Characterization of CdTe Thin Films Deposited by CSS". Solar Energy Mater. and Solar Cells, 57 (1995) 273.

(6)- K. W. Mitchell, C. Eberspacher, F. Cohen, J. avery, G. Guran and W. Bottenbrg. "Progress Toward High Efficiency Thin Film CdTe Solar Cells" Solar Cells, 23 (1988) 49.

(7)- T. L. Chu. "Thin Film Cadmium Telluride Solar Cell by Two Chemical Vapour Deposition Techniques". J. Solar Cell, 23 (1988) 31.

(8)- Samuel Glasstone and David Lewis. "Elements of Physical Chemistry" Published by Macmillan and Co. Ltd, London (1970).

(9)- V. Sosa, R. Castro and J. L. Pena. "Pressure and Temperature Influence on CdTe Thin -Film Deposit by Close-Space Vapour Transport Technique ". J. Vac. Sci. Technol. A, 8 (1990) 979.

(10)- A. L. Fahrenbruch, V. Vasilchenko, F. Buch, K. Mitchell and R. H. Bube. "II-VI Photovoltaic Heterojunction for Solar Energy Conversion" Apple. Phys. Lett., 25 (1974) 605.

(11)- J. Sarie, M. Akiyama and T. Tankana. "Epitaxial Growth of CdTe by a Close-Space Technique." Japan. J. Appl. Phys., 11 (1972) 1758.

(12)- D. J. Williams. "Densities and Lattice Parameters of CdTe, CdZnTe and CdTeSe". Properties of Narrow gap Cadmium based Compounds. Ed. by P. Capper. Emis, Datareviews series No.10, (1994) 399.

(13)- Robert A. Alberty and Robert J. Silbey. "Physical Chemistry". Published by John Wiley & Sons. New York (1992).

(14)- W. Palos and H. Wiedemeier. "Physical Vapour Transport of Cadmium Telluride in Closed Ampoules". J. Crystal Growth, 129 (1993) 653.

(15)- J.C. Alabert. "Optical Vapour Pressure Monitoring and Mass Transport Control During Bulk CdTe Crystal Growth in a Novel Multi-Tube PVT System". Ph. D. Thesis, University of Durham, UK (1998).

(16)- B. deLargy, A. Finch and P. J. Grander. "Thermodynamic Function for the Congruent Sublimation of Cadmium Telluride". J. Crystal Growth, 61 (1983) 194.

(17)- T. L. Chu and S. S. Chu. "Thin Film II-VI Photovoltaics". J. Solid State Electronics, 38 (1995) 533.

(18)- T. C. Anthony, A. L. Fahrenbruch and R. H. Bule. "Growth of CdTe Films by Close -Space Vapour Transport". J. Vac. Sci. Technol. A, 2 (1984) 1296.

(19)- R. J. Matson, F. S. Hasoon, K. M. Jones, M. M. Al-jassim and R. D. Tomlison. "Microcharacterisation of CdTe Films Deposited by Close-Spaced Sublimation". Progress in Photovoltaics: Research and Application, 2 (1994) 203.

(20)- X. Li, D. Albin, S. Asher, H. Moutinho, B. Keyes, R. Matson, F. Hasoon, and P. Sheldon. "The Effect of Substrate Temperature on Material Properties and Device Performance of Close-Space Sublimation Deposited CdTe/CdS Devices". AIP Conference Proceedings 353, 1 (1996) 376.

(21)-G. B. Harris "Quantitative Measurement of Preferred Orientation in Rolled Uranium Bars". Phil. Mag. 43, (1952) 113.

(22)- K. H. Kim and J. S. Chun. "X-Ray Studies of SnO_2 Prepared by Chemical Vapour Deposition". Thin Solid Film, 41 (1986) 287.

(23)- K. Li, A. T. Wee, J. Lin, K. L. Tan, L. Zhou, S.F.Li, Z. Feng, H. Chou, S.Kamara, A. Rohatgi. "A Microstructural Study on the Surface and Interface of CdTe/CdS Solar Cells". J. Mater. Sci.: Mater. Electron., 8 (1997) 125.

(24)- S. Naseem, Naseer-ud-Din, K. Hussain. "Preparation of Thermally CdTe Thin Film". Chinese Phys. Lett ., 7 (1990) 510.

(25)- T. H. Myers, S. W. Edward and J. F. Schetzina. "Optical Properties of Polycrystalline CdTe Films". J. Appl. Phys., 52 (1981) 4231.

(26)- G. C. Morris, S. K. Das and P. G. Tanner. "Some Factors Affecting Efficiencies of n-CdS/p-CdTe Thin Film Solar Cells". J. Crystal Growth, 117 (1992) 929.

(27)- G. C. Morris and S. K. Das. "Some Fabrication Procedures for Electrodeposited CdTe Solar Cell". Int. J. Solar Energy, 12 (1992) 95.

(28)- S. K. Das and G. C. Morris. "Influence of Growth and Microstructure of Electrodeposited Cadmium Telluride Films on the Properties of n-CdS/CdTe Thin-Film Solar Cells". J. Appl. Phys., 72(1992) 4940.

(29)- Bin Qi, D. Kim, D. L. Williamson, and J. Trefny. "Effect of Postdeposition Heat-Treatment on Morphology and Microstructure of CdTe Grown by Electrodeposition". J. Electrochem. Soc., 143 (1996) 517.

(30)- H. Uda, S. Ikegami, and H. Sonomura. " Effect of Substrate Temperature on the Photovoltaic Properties of a CdS/CdTe Solar Cell". Japan. J. Appl. Phys., 29 (1990) 2003.

(31)- T. L. Chu, S. S. Chu, S. T. Ang, K. D. Han and Y. Z. Liu. "High Efficiency Thin Film Cadmium Telluride Solar Cells". 19th IEEE Photovoltaic Specialists Conference, New Orleans, Louisiana, (1987) 1466.

Chapter Five:

Current Transport Measurements in CdS/CdTe Cells.

5.1- Introduction:

The measurement and analysis of *I-V* characteristics are a commonly used and powerful tool to investigate the performance of CdS/CdTe solar cells. *I-V* characteristics measured under illumination of around AM 1.5 and at room temperature, has been used to determine the optimum thickness of CdTe and CdS for CdS/CdTe thin film cells prepared by Close Space Sublimation. The performance of the cells has been investigated in term of the parameters, which may be calculated from the *I-V* curves recorded under illumination, such as the efficiency (η), short circuit current (I_{sc}), open circuit voltage (V_{oc}), fill factor (FF), series resistance (R_s) and shunt resistance (R_{sh}).

Significant improvements in CdS/CdTe solar cell efficiencies are commonly observed as a result of $CdCl_2$ treatment of the CdTe layer. *I-V* measurements under illumination and in the dark at different temperatures were carried out to investigate the effects of $CdCl_2$ treatment on the performance of the cell, trap density and current transport mechanisms.

Transparent conducting oxides (TCOs) such as indium tin oxide (ITO) and tin oxide SnO_2 are used as transparent conducting electrodes for CdS/CdTe solar cell. The TCO/CdS interface must be thermally stable during the preparation processes of the cells. The effects of heating at 400°C, the temperature used in the $CdCl_2$ treatment, for various times on the *I-V* characteristics for TCO/CdS interface were also examined.

5.2- Photovoltaic Output Characteristics.

The series resistance and the shunt resistance of the CdS/CdTe cell may be determined approximately from their *I-V* characteristics. The influence of the series resistance and the shunt resistance on the device current is illustrated in the equivalent circuit diagram for a solar cell, figure (5-1). The current under illumination is given by:

$$I = - I_d - I_{sh} + I_L \tag{5.1}$$

where I_d is the current through the diode and is given from the diode equation [1]:

$$I_d = I_0\left[\exp(\frac{q(V + IR_s)}{nkT}) - 1\right] \tag{5.2}$$

I_{sh} is current flowing through (R_{sh}) and I_L is the phototgenerated current.

$$I_{sh} = (V + IR_s)/R_{sh} \tag{5.3}$$

Then, the output current under illumination would be:

$$I = -\ I_0\left[\exp(\frac{q(V+IR_s)}{nkT}) - 1\right] - \frac{V+IR_s}{R_{sh}} + I_L \tag{5.4}$$

Under open circuit conditions, $V=V_{oc}$, $I = 0$;

$$V_{oc} = \frac{nkT}{q}\ \ln\ \{\frac{I_L}{I_o} + 1 - \frac{V_{oc}}{I_o R_{sh}}\} \tag{5.5}$$

Equation (5.5) shows that V_{oc} depends logarithmically on I_L but that a low value of shunt resistance can reduce V_{oc} significantly. In the limit of $R_{sh} \longrightarrow \infty$, then equation (5.5) tends to the ideal case, equation (2.15). Under short circuit conditions where $V= 0$ and $I=I_{sc}$, equation (5.4) becomes;

$$I_{sc} = -I_0\left[\exp(\frac{qI_{sc}R_s)}{nkT}) - 1\right] - \frac{I_{sc}R_s}{R_{sh}} + I_L \tag{5.6}$$

Equation (5.6) indicates that the short circuit current is dependent on the series resistance, and will be significantly reduced if R_s is too large. In the limit $R_s \longrightarrow 0$, I_{sc} $= I_L$ the theoretical maximum for a given level of illumination.

In principle R_{sh} and R_s may be obtained from equation (5.5) and (5.6) providing I_L is known. In practice it is generally easier to estimate R_s and R_{sh} from the PV output characteristics. R_s may be determined from the slope at forward bias voltage above V_{oc} where the forward current does not vary exponentially with the voltage (R_s and not the junction is limiting) [2], i.e. $\left.\frac{dI}{dV}\right|_{V \geq V_{oc}} \approx 1/R_{s,}$

R_{sh} may be determined approximately from the slope at low reverse bias voltage where reverse current changes linearly with reverse bias voltage, i.e. $\left.\frac{dI}{dV}\right|_{V \leq 0} \approx 1/R_{sh}$

The series resistance is not only due to the bulk resistance (i.e. thickness) of the CdTe layer. It is the sum of several components; back contact resistance R_b, absorber layer resistance R_{CdTe}, window resistance R_{CdS}, and front contact resistance R_{TCO} as illustrated in figure (5-2).

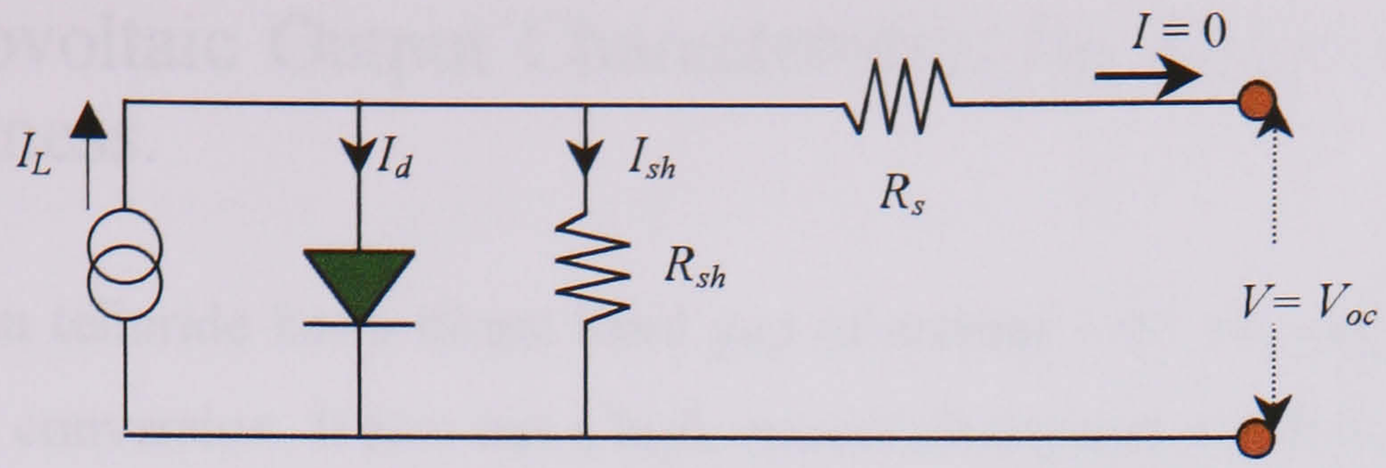

(a)

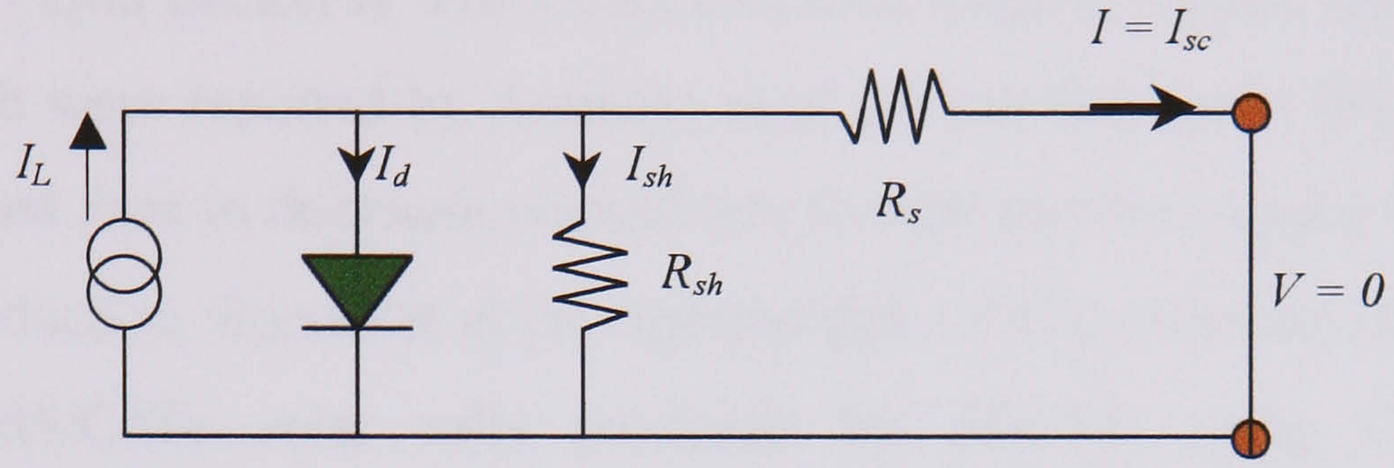

(b)

Figure (5-1) Solar cell equivalent circuits under illumination (a) open circuit voltage, (b) short circuit current.

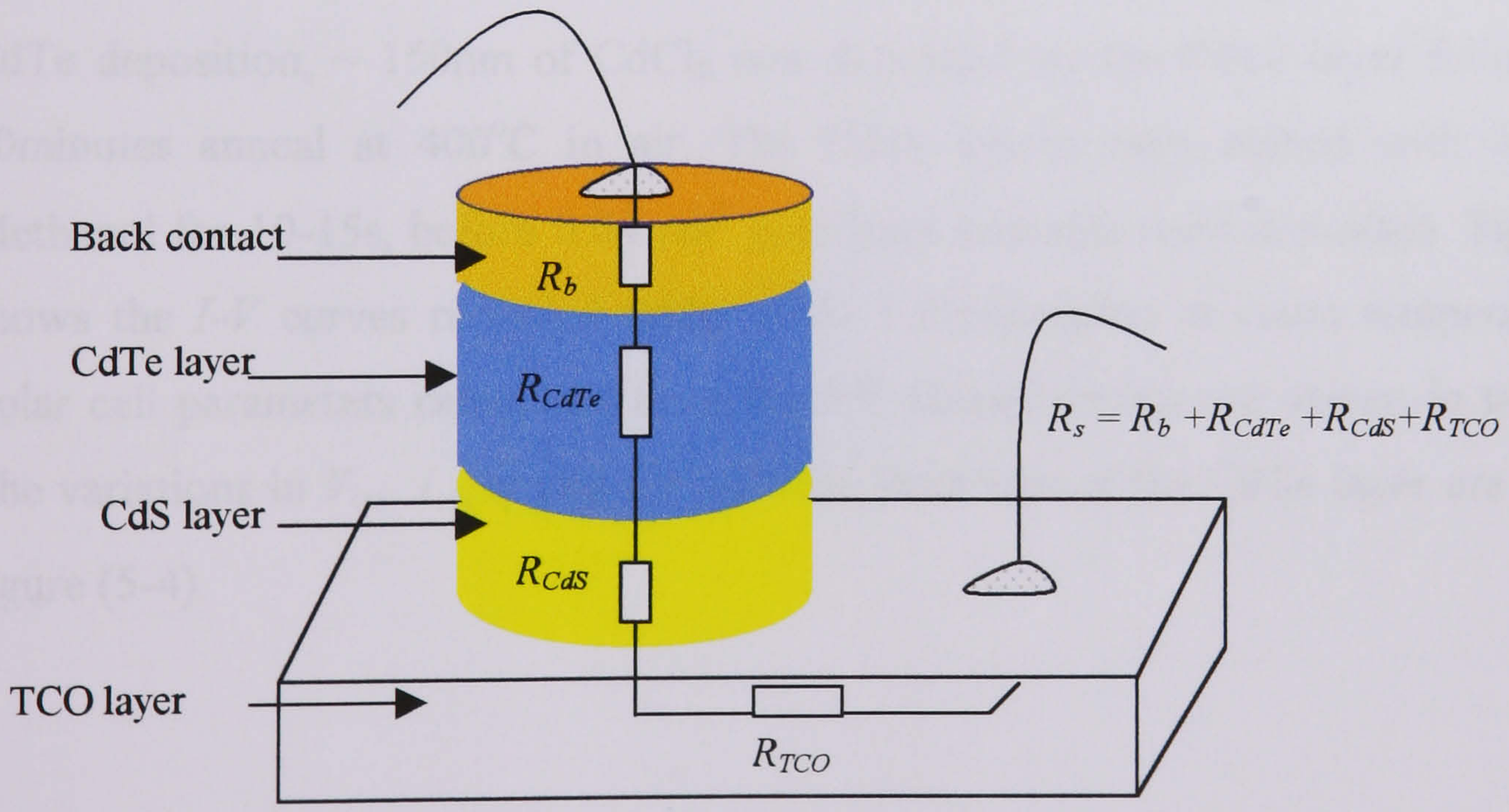

Figure (5-2)- Series resistance components of CdS / CdTe solar cell.

5.2.1- Photovoltaic Output Characteristics for Cells of Different CdTe Thickness.

Cadmium telluride has a direct band gap of around 1.47 eV, near the optimum for solar energy conversion. It also has a high optical absorption coefficient (>10^4 cm^{-1}) which means that solar radiation with energy in excess of the band gap of CdTe is absorbed within ~ 2μm thickness. The CdS/CdTe solar cells of highest efficiency 16% and 15.8%, which were reported by Aramoto et al [3] and Britt et al [4], have CdTe layers of 3.5μm and 5μm in thickness respectively formed by Close Space Sublimation. For industrial production, Bonnet et al [5] reported that a CdTe thickness of 3-5μm was optimum for CdS/CdTe solar cells produced by ANTEC using Close Space Sublimation. Conversely, Barker et al [6] reported that the preferred thickness of CdTe layers in CdS/CdTe solar cells produced by BP using Electrodeposition to deposit the CdTe layer was around 1.6 μm.

To determine the optimum thickness of CdTe layers deposited using the Durham Close Space Sublimation system, as described in Chapter 3, several cells were fabricated with a range of CdTe thickness. All cells had nominally the same preparation conditions; the CdS thickness was around 150nm, substrate temperature of 500°C for CdTe deposition, ~ 150nm of $CdCl_2$ was deposited on the CdTe layer followed by a 30minutes anneal at 400°C in air. The CdTe layers were etched with 0.03% Br-Methanol for 10-15s, before 0.04 cm^2 gold back contacts were deposited. Figure (5-3) shows the *I-V* curves recorded under AM1.5 illumination at room temperature. The Solar cell parameters calculated from the PV characteristics are shown in table (5-1). The variations in V_{oc}, J_{sc}, η and *FF* with the thickness of the CdTe layer are plotted in figure (5-4).

Figure (5-3)-PV Output characteristics of the cells having different thicknesses of CdTe.

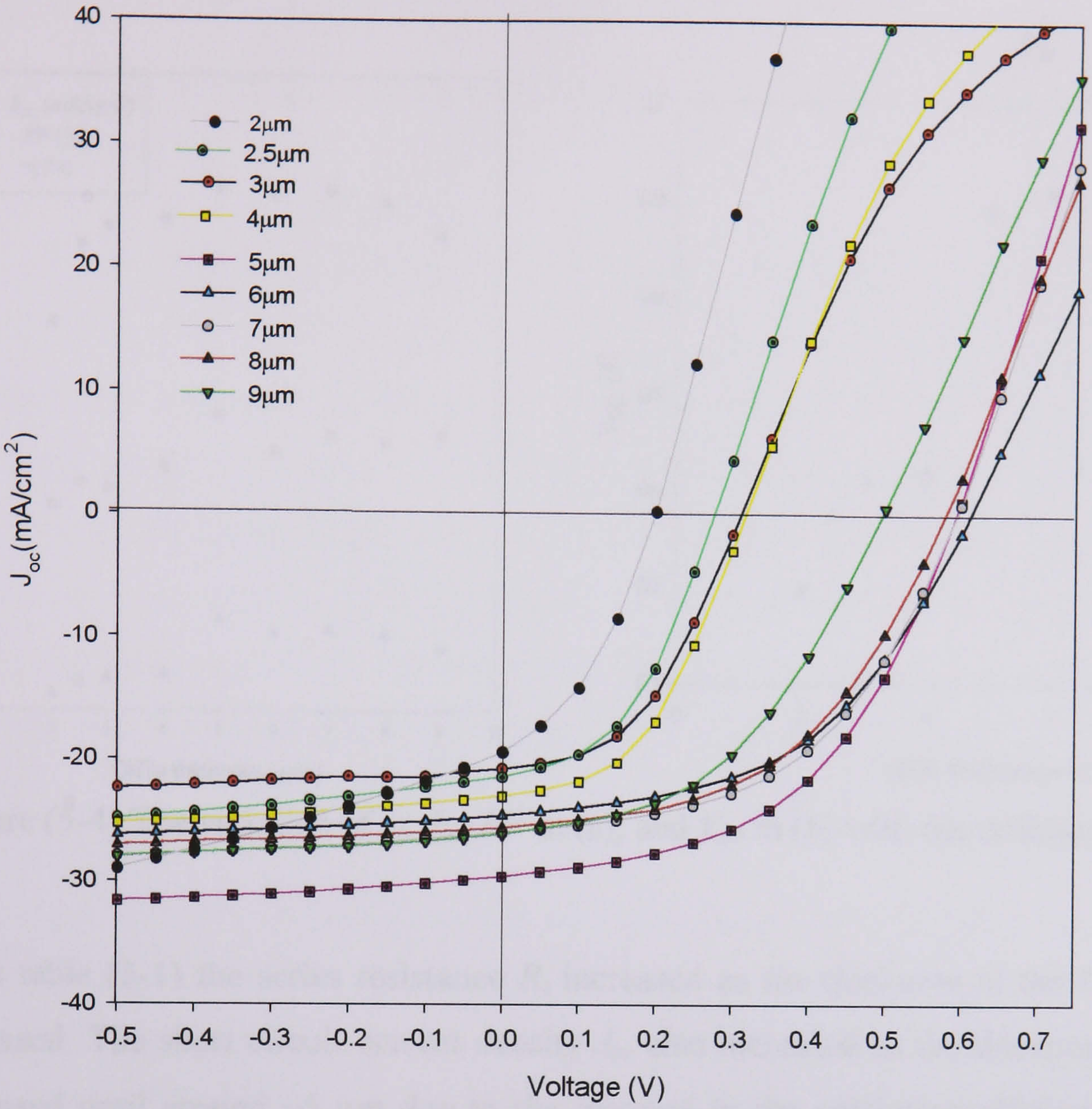

Table (5-1)- The Parameters of the solar cells as a function of the thickness of CdTe.

CdTe (μ m)	V_{oc}(V)	J_{sc}(mA/cm^2)	η %	FF %	R_s. (Ω . cm^2)	R_{sh}. (Ω . cm^2)
2	0.2	19.38	1.41	36.6	4.9	23.9
2.5	0.275	21.4	2.49	43.9	5.9	87.1
3	0.31	21	2.94	45.7	6	125.7
4	0.317	23	3.4	46.3	6.	120.5
5	0.6	28.5	8.63	49.2	6.1	200
6	0.61	24.6	7.304	48.7	6.1	190
7	0.594	26	7.6	49	7	185.6
8	0.578	25.5	7.1	48	7.6	147.5
9	0.495	26.1	5.9	45	7.9	107.7

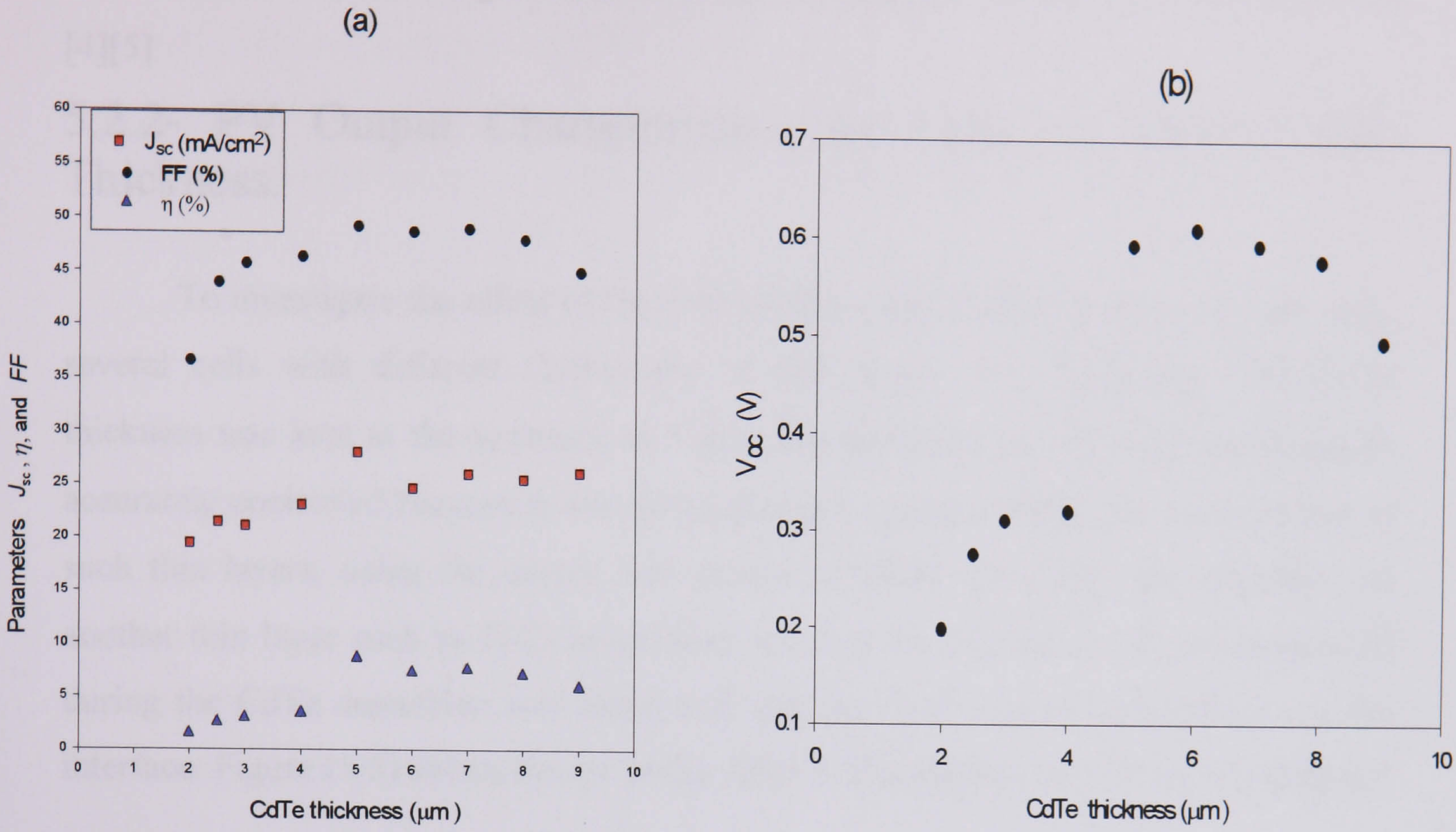

Figure (5-4) The variation of η, J_{sc}, FF in (a), and V_{oc} in (b) with the thickness of CdTe

From table (5-1) the series resistance R_s increased as the thickness of the CdTe layer increased. The short circuit current density J_{sc} also increased as the thickness of CdTe increased until around ~5 μm due to the increase in the collection efficiency, then it reduced as the series resistance effects began to dominate. The shunt resistance, represents the leakage of current along for example; the edges of the cell, diffusion spikes associated with dislocations, grain boundaries, or to crystal defects such as stacking faults [7]. The shunt resistance increased with the CdTe thickness reaching a maximum value at around ~ 5μm, after which it reduced as the thickness increased further. When the CdTe layer is thin there is a much greater chance of pinhole formation, resulting in short circuits between the back and front contacts. The pinhole density reduces as the CdTe thickness increases, with a corresponding increase in R_{sh}. For CdTe thickness greater than 5μm the progressive reduction in shunt resistance may be due to an increase in grain boundaries, which act as minority carrier sinks and majority carriers barriers [8]. The fill factor and the open circuit voltage are reduced as the shunt resistance decreased [7]. So the thickness of the CdTe film has to be a compromise between the requirements for complete absorption of the incident radiation

and the need to keep a low series resistance and high shunt resistance. It seems that the optimum thickness of CdTe deposited by Close Space Sublimation in CdS/CdTe solar cells is around 5μm, in agreement with values reported for the most efficient cells [4][5].

5.2.2- PV Output Characteristics for Cells of Varying CdS Thickness.

To investigate the effect of the CdS thickness on the performance of solar cells, several cells with different thicknesses of CdS layer were fabricated. The CdTe thickness was kept at the optimum of 5 μm. The thickness of CdS layer could not be accurately controlled because it was difficult to get a precise thickness measurement of such thin layers, using the α-step 200 surface profiler, when they are deposited on another thin layer such as ITO. In addition some of the CdS layer will be evaporated during the CdTe deposition and some CdS will be "lost" due to interdiffusion at the interface. Figure (5-5) shows the *I-V* under AM1.5 illumination of cells having different

Figure (5-5)- PV characteristics for solar cells having different thickness of CdS.

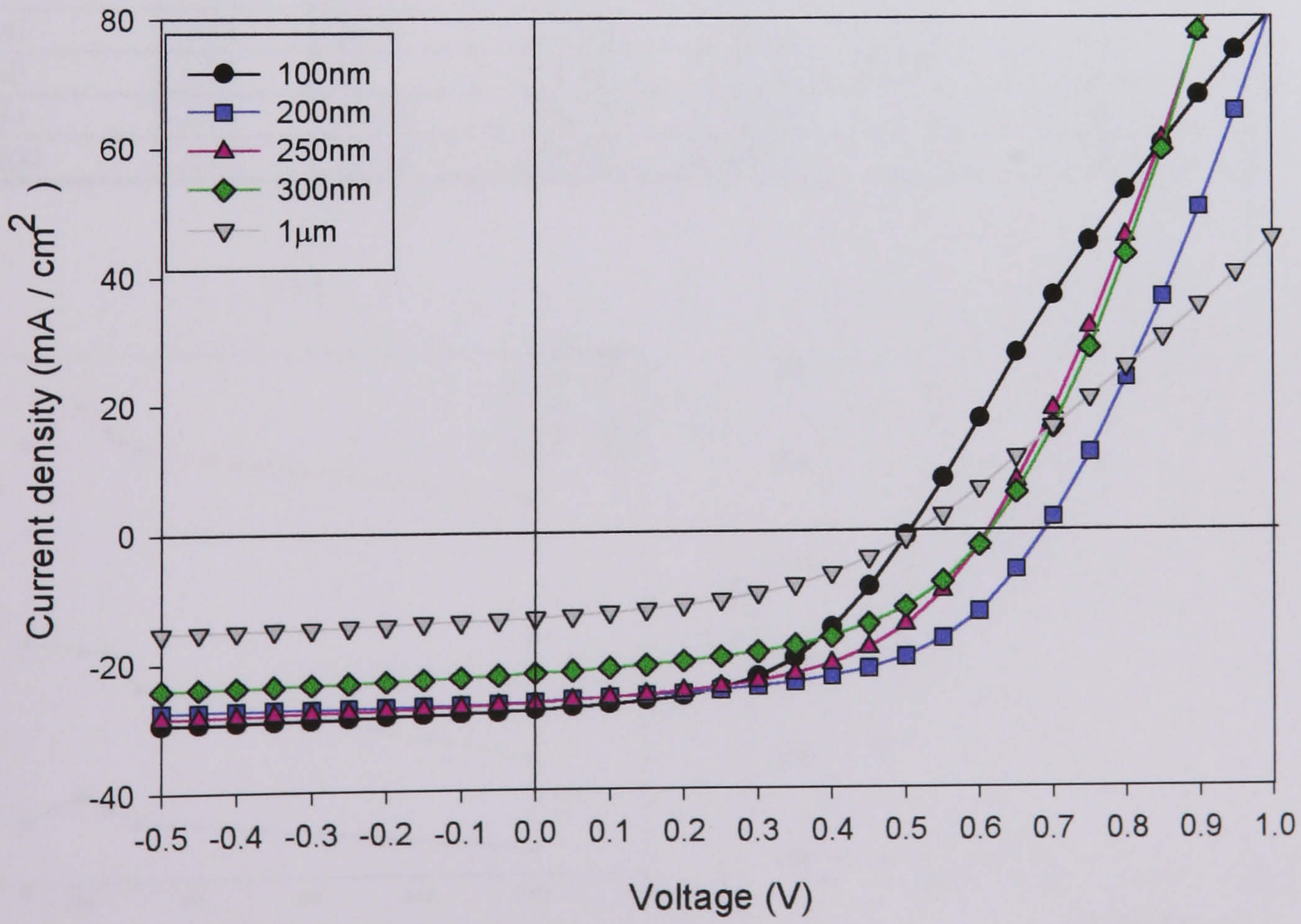

thickness of CdS at room temperature. The parameters of these cells calculated from the illuminated *I-V* curves in table (5-2). The photovoltaic parameters of the cells are illustrated in figure (5-6). These results indicate that the CdS thickness is a critical factor affecting cell performance. The current density decreases as the thickness of CdS increases [9] for two reasons. Firstly, as the thickness of CdS decreases the blue response of the cells increase [10]. (see the spectral response measurements in chapter 6). Secondly, as the CdS thickness increases the internal series resistance of cells increase as shown in table (5-2). The open circuit voltage (V_{oc}) and the Fill Factor (FF) increased as the CdS thickness increased [11] until around 200nm, after which they were affected by the reduction in the shunt resistance R_{sh}. Even though the cell prepared with thin CdS films typically exhibit higher short current density J_{sc} as the blue response of the cell is greater, this comes at the expense of a lower fill factor FF and open circuit voltage V_{oc} [12]. There is therefore a compromise between the increased J_{sc} and the reduction in R_{sh}. The best thickness of CdS for our CdTe/CdS cells appears to be between 200 and 250 nm before the deposition of CdTe layer.

Table (5-2) the Parameters of the solar cell with different thickness of CdS.

CdS (nm)	V_{oc}(V)	J_{sc}(mA/cm^2)	η %	FF %	series res. (Ω . cm^2)	shunt res. (Ω . cm^2)
100	0.505	27.52	6.9	49.7	5.8	152.43
200	.688	26.3	9.81	54.1	5.46	190
250	.612	26	8.29	51.144	5.5	174
300	.614	21.89	6.581	48.94	6.1	147
1000	.517	13.31	2.94	42.72	13.7	128

(a) (b)

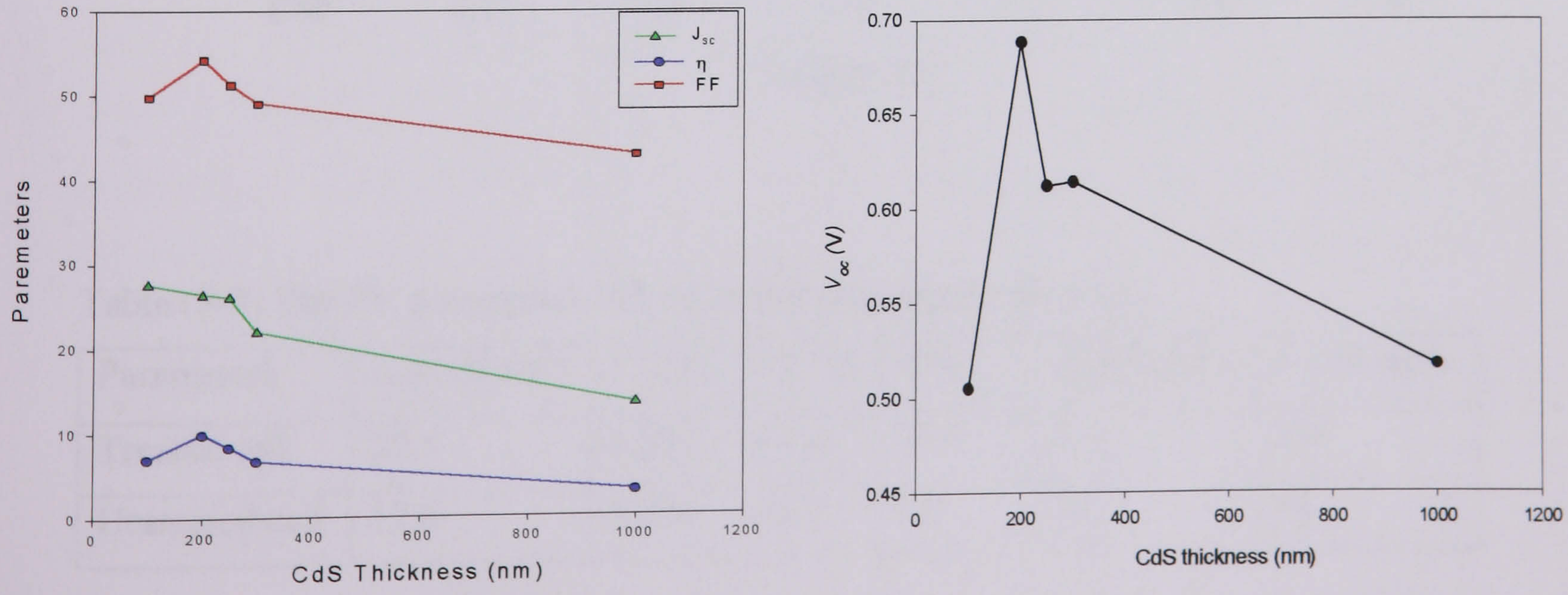

Figure (5-6) The variation of η, J_{sc}, FF in (a), and V_{oc} in (b) with the thickness of CdS

5.2.3- PV Characteristics of Treated and Untreated Solar Cells.

Two solar cells were fabricated with the same thickness of CdS and CdTe, and the same back contact procedure. One of these was prepared in the usual way; ~ 150 nm of $CdCl_2$ was deposited on the CdTe layer followed by heating at 400°C in air for 30minutes the other was not. Figure (5-7) shows the PV characteristics of treated and untreated solar cells at room temperature and around AM1.5. Table (5-3) shows the corresponding photovoltaic parameters, and the series and shunt resistances.

Figure (5-7)- PV characteristics of treated and unteated solar cells.

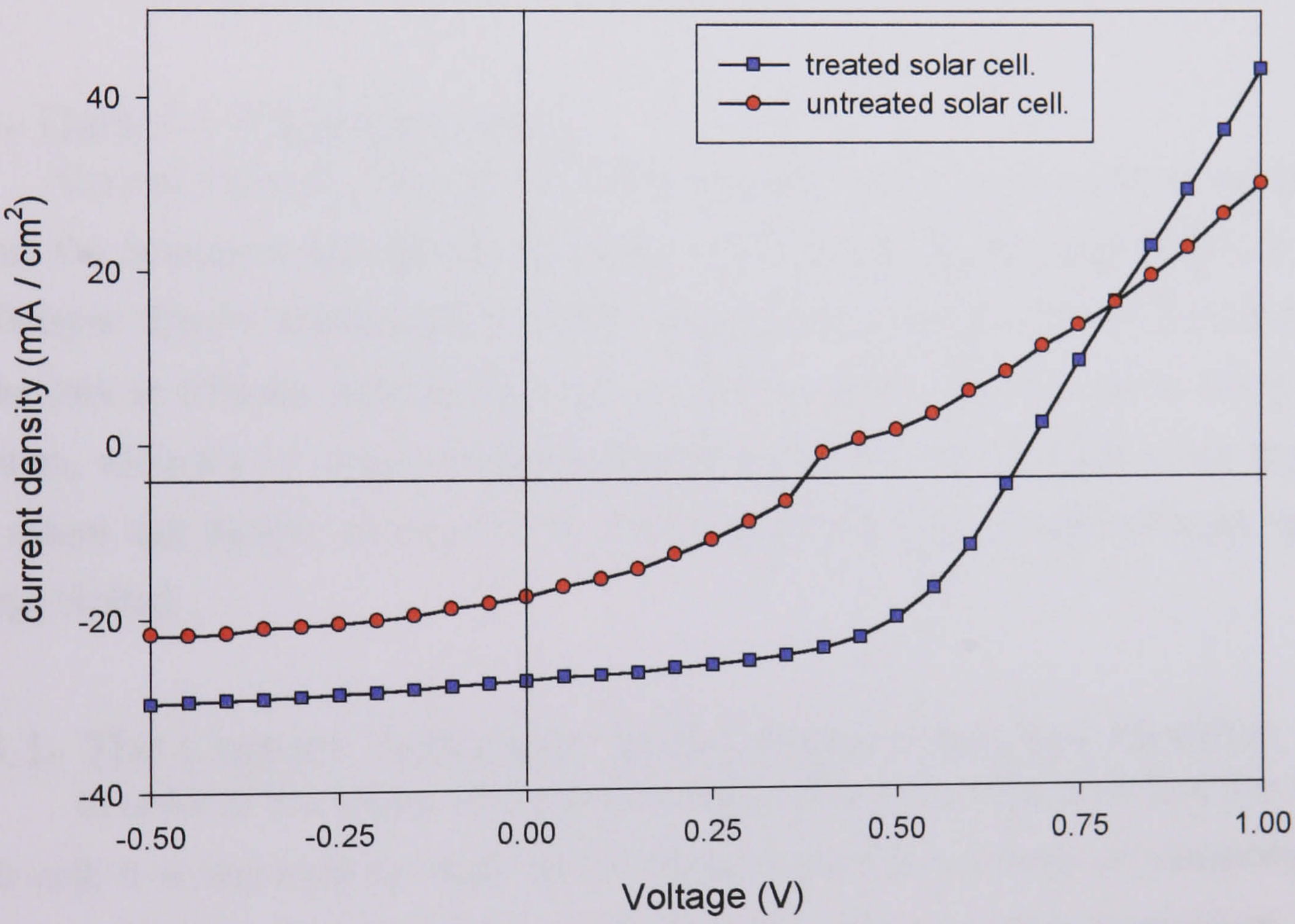

Table (5-3) The PV parameters of treated and untreated solar cells.

Parameters	J_{sc}(mA/cm^2)	V_{oc}(V)	FF %	η %	R_s (Ω.cm^2)	R_{sh}(Ω.cm^2)
Treated cell	27.3	0.684	54.4	10.1	6	196
Untreated cell	17.6	0.438	36.3	2.8	34	48

The $CdCl_2$ treatment of the CdTe layer increased the efficiency of the solar cells from 2.8% to around 10% [13] due to an improvement in all the photovoltaic parameters of the cells. It resulted in a drastic improvement in the series and shunt resistance, reducing the series resistance from 34 to 6 $\Omega.cm^2$ and increasing the shunt resistance from 48 to 196 $\Omega.cm^2$[14]. The reduction in the series resistance and the increase in the shunt resistance resulted in an increase in the fill factor from 36.3 to 54.4%, the open circuit voltage from 438mV to 684mV and short circuit current density from 17.6 to 27.3 mA/cm^2. Many explanations have been suggested for the effects of the $CdCl_2$ treatment; promotion of recrystallization and grain growth of CdTe [15][16], filling of minority carrier traps at the interface changing the depletion region width [17], passivation of grain boundaries and inducing a reaction between CdS and CdTe at the interface producing a thin layer of CdS_xTe_{1-x} [13].

5.3- Dark *I-V* Characteristics.

Current transport through the CdS/CdTe solar cell is controlled by transport across the heterojunction between the CdS and CdTe and by the trap density in the CdTe layer. The *I-V* characteristics of the cells at low forward bias (0<V<0.5) measured in the dark at different temperatures may be used to study current transport across the junction, while the *I-V* characteristics at higher bias voltage may be used to investigate the nature and density of traps in the CdTe layer when the current becomes space charge limited.

5.3.1- The Current Transport Mechanisms Across the Junction.

In order to investigate the current-voltage mechanisms across the junction of a solar cell, it is important to study its *I-V* characteristics at a variety of temperatures. Many models have been suggested to describe the charge transport mechanisms and more details may be obtained from [18]. The relevant current transport mechanisms in the p-CdTe/n-CdS heterojunction are; thermal emission of carriers over the junction with high recombination at interface states, tunnelling mechanisms and multi-step tunnelling/ recombination.

The thermal emission /recombination mechanism is described by the following expression [19]:

$$J = J_o[\exp(\frac{qV}{nkT}) - 1] \qquad (5.7)$$

$$J_o = J_{oo} \exp(\frac{-\Delta E}{kT}) \quad (5.8)$$

Where V is the applied voltage, the diode factor (n) usually lies between 1 and 2 and is a function of the junction and material perfection. J_o is the reverse saturation current density, ΔE is the thermal activation energy, J_{oo} is a weak function of temperature.

In the tunnelling mechanisms, the electron or holes tunnel through the junction potential barrier. This model is described by the following expression [20]:

$$J = J_o \exp(AV) = J_{oo} \exp(BT) \exp(AV) \quad (5.9)$$

Where A gives the field dependence and B the temperature dependence of the available carrier density. According to the above expressions J_o is related exponentially to T in tunnelling mechanisms, but exponentially with $1/T$ in emission/recombination processes.

The forward current in a multi-step tunnelling/recombination model can be expressed as [21]:

$$J_f(V,T) = X N_T \exp[-\alpha R^{-0.5}(V_b - KV)] \quad (5.10)$$

Where X is the transmission coefficient of electron across the junction and α is given by:

$$\alpha = (\pi/4h)(m_e^* \varepsilon_n / N_D)^{1/2} \quad (5.11)$$

$$K = 1 + (\varepsilon_p N_A / \varepsilon_n N_D) \quad (5.12)$$

Where R is the number of tunnelling steps, N_T is the density of tunnelling/recombination centres, ε_p, ε_n, N_A and N_D, are the dielectric constants and net ionised acceptor and donor densities in the p-CdTe and the n-CdS respectively, m_e^* is the electron effective mass and h is Planck's constant.

In an attempt to investigate the effect of $CdCl_2$ on the current transport mechanisms throughout the junction, I-V characteristics at different temperature were taken for treated and untreated solar cells. The reverse saturation current (I_o) and the ideality factor were calculated for each temperature. Then the model mechanisms were defined according to the relation between the reverse saturation current and the temperature or the reverse temperature.

5.3.1.1- Current Transport Across the Junction in Untreated Solar Cells.

Figure (5-8) shows the forward (I_f) current voltage of an untreated solar cell for a range of temperatures from 200 K to 331 K. The current varied exponentially with voltage until around 0.4 volt, then it began to deviate from the exponential behaviour due to the series resistance of the CdTe thin film. Hence the current was limited by the junction at low voltage and by the CdTe film at high voltage. The ideality factor, n, and the reverse saturation current were estimated from the figure (5-8) and are listed in table (5-4). The ideality factor varied between 1.7 and 2.2. The temperature behaviour of saturation current, I_o, is given in figure (5-9) which presents plots of log (I_o) versus T and log (I_o) versus T^{-1}. These plots suggest that I_o appeared to vary exponentially with T^{-1} rather than exponentially with T. This indicates that the current transport mechanism across the junction in untreated cells was by a thermal/emission recombination mechanism. The activation energy was estimated from the slope in figure (5-9-a) to be 0.66 eV, close to the values of (0.6 eV) published by Kim W. Mitchell [22] and to 0.56 eV reported by Ringel [23] for annealed samples without $CdCl_2$ treatment.

Figure (5-8)-log (I_f) vs. V characteristics of untreated cell.

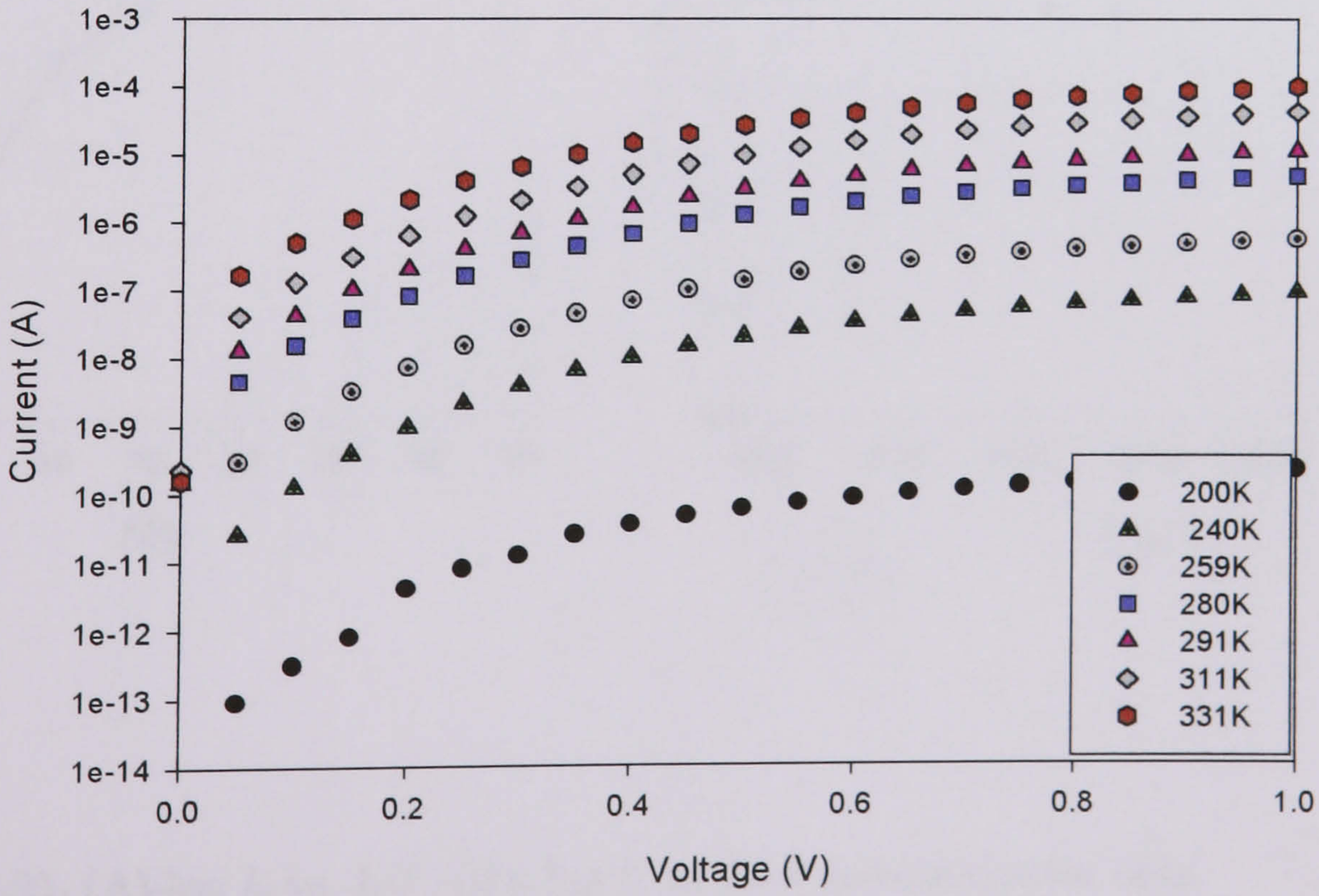

T (K)	I_o (A)	n
200	2.04×10^{-14}	2.2
240	2×10^{-11}	1.93
259	6.78×10^{-11}	1.7
280	1.21×10^{-9}	1.75
295	6.74×10^{-9}	1.91
311	1.36×10^{-8}	1.73
331	5.98×10^{-8}	1.75

Table (5-4)- I_o and ideality factor (n) of untreated solar cells.

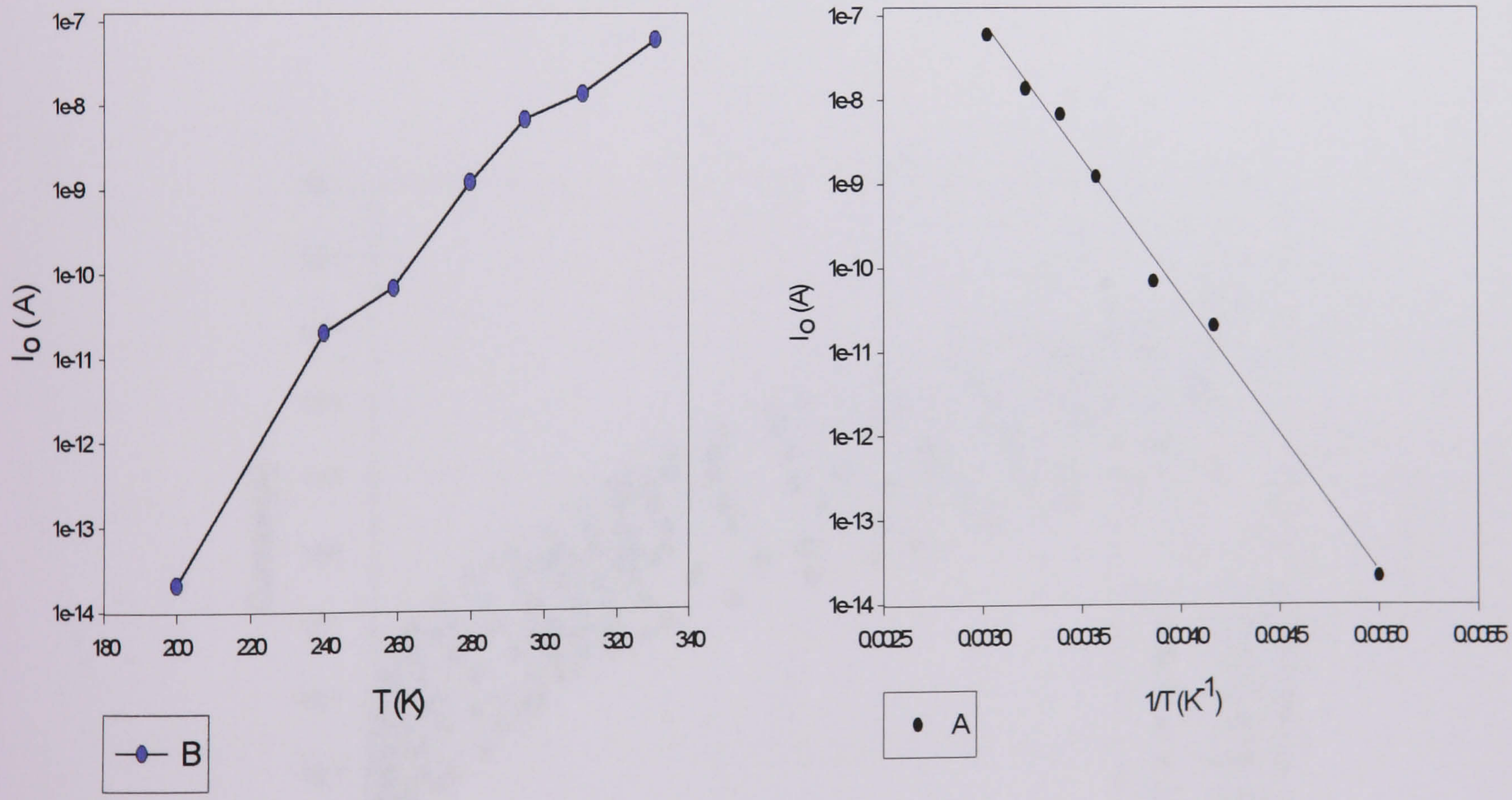

Figure (5-9)- (A)-log I_0 vs. $1/T$, (B)- log I_o vs. T for untreated solar cells .

5.3.1.2- Current Transport Across the Junction in Treated Solar Cells.

Dark *I-V* characteristics of the treated solar cell were measured for a range of temperature from 200 K to 320 K. The log (I_f) versus V characteristics are given in figure (5-10). The current also varied exponentially with voltage at low voltage, and then deviated from the exponential behaviour at higher bias voltages due to the series resistance of the CdTe thin film. The calculated values of the ideality factor (n) and the reverse saturation current I_o are given in table (5-5) The temperature behaviour of the reverse saturation current I_o is given in figure (5-11) which presents plots of log (I_o) versus T and log (I_o) versus T^{-1}. In this case, I_o appeared to vary exponentially with T, rather than with T^{-1}. This suggests that the current transport was by a tunnelling mechanism across the junction. The value of B in equation (5.9) was calculated from the slope in figure (5-11-A) to be 0.051 K^{-1}, between the values found by Murat, 0.06 K^{-1} for treated cell [2], and the value found by Ercelebi et al. (0.041 K^{-1}) for CdS deposited onto phosphours doped single crystal CdTe [24].

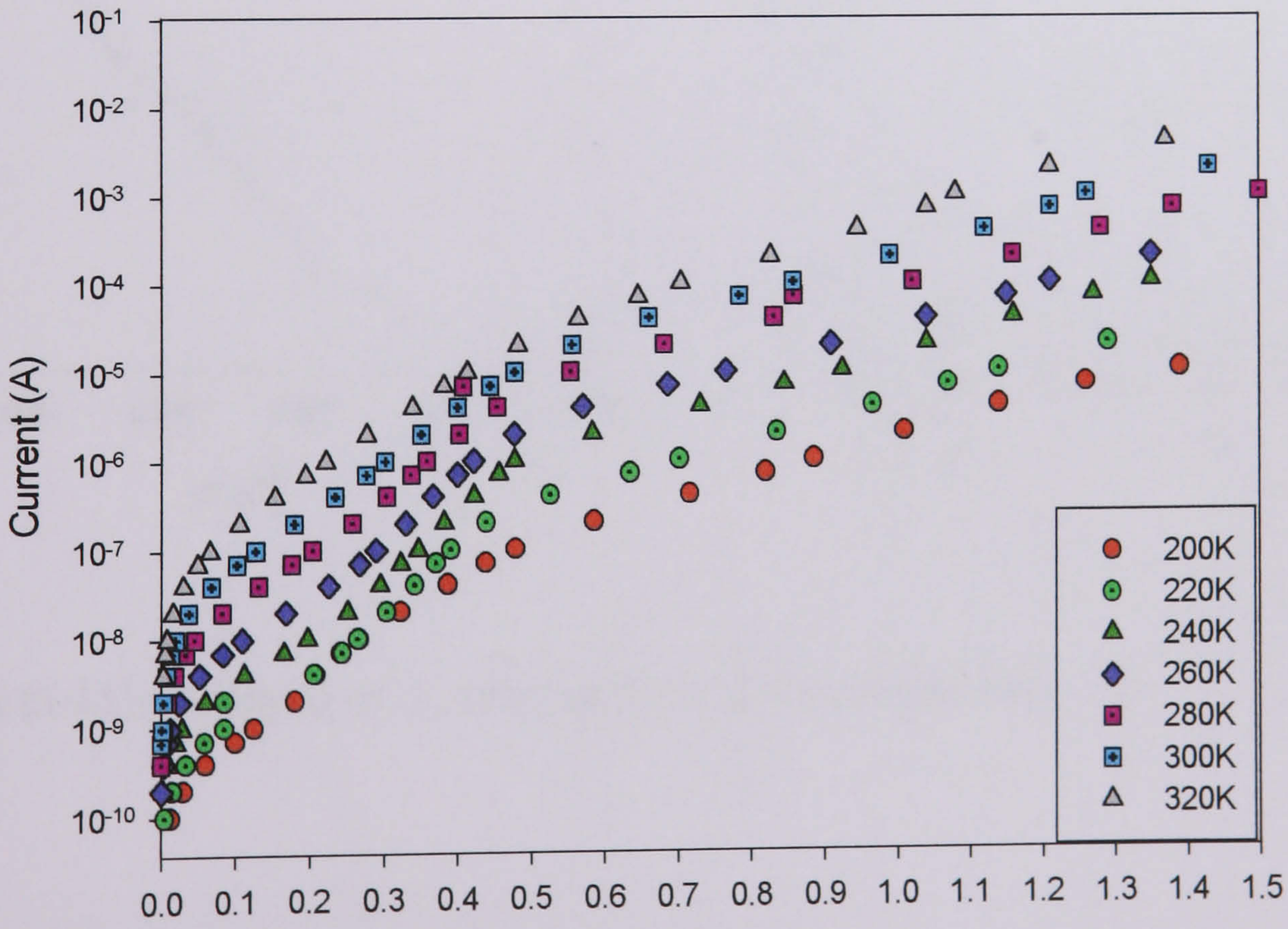

Figure (5-10)- Log (I_f) vs. V characteristics of treated solar cell.

T (K)	I_o (A)	n
200	6.5×10^{-11}	1.78
220	1.34×10^{-10}	1.77
240	4.86×10^{-10}	1.8
260	1×10^{-9}	1.81
280	3.63×10^{-9}	1.8
300	8.76×10^{-9}	1.93
320	2.8×10^{-8}	1.91

Table (5-5)- I_o and ideality factor (n) of treated solar cells.

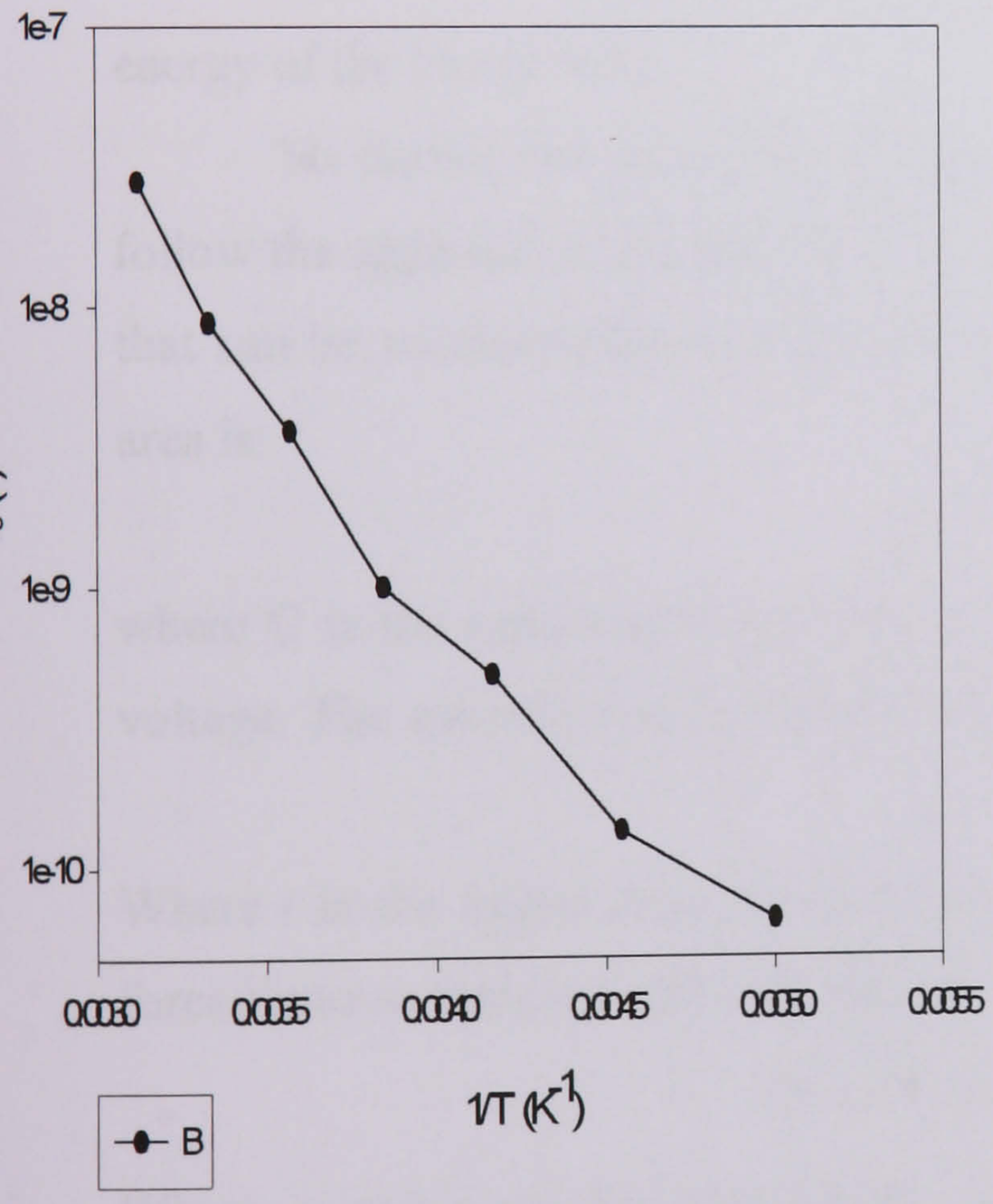

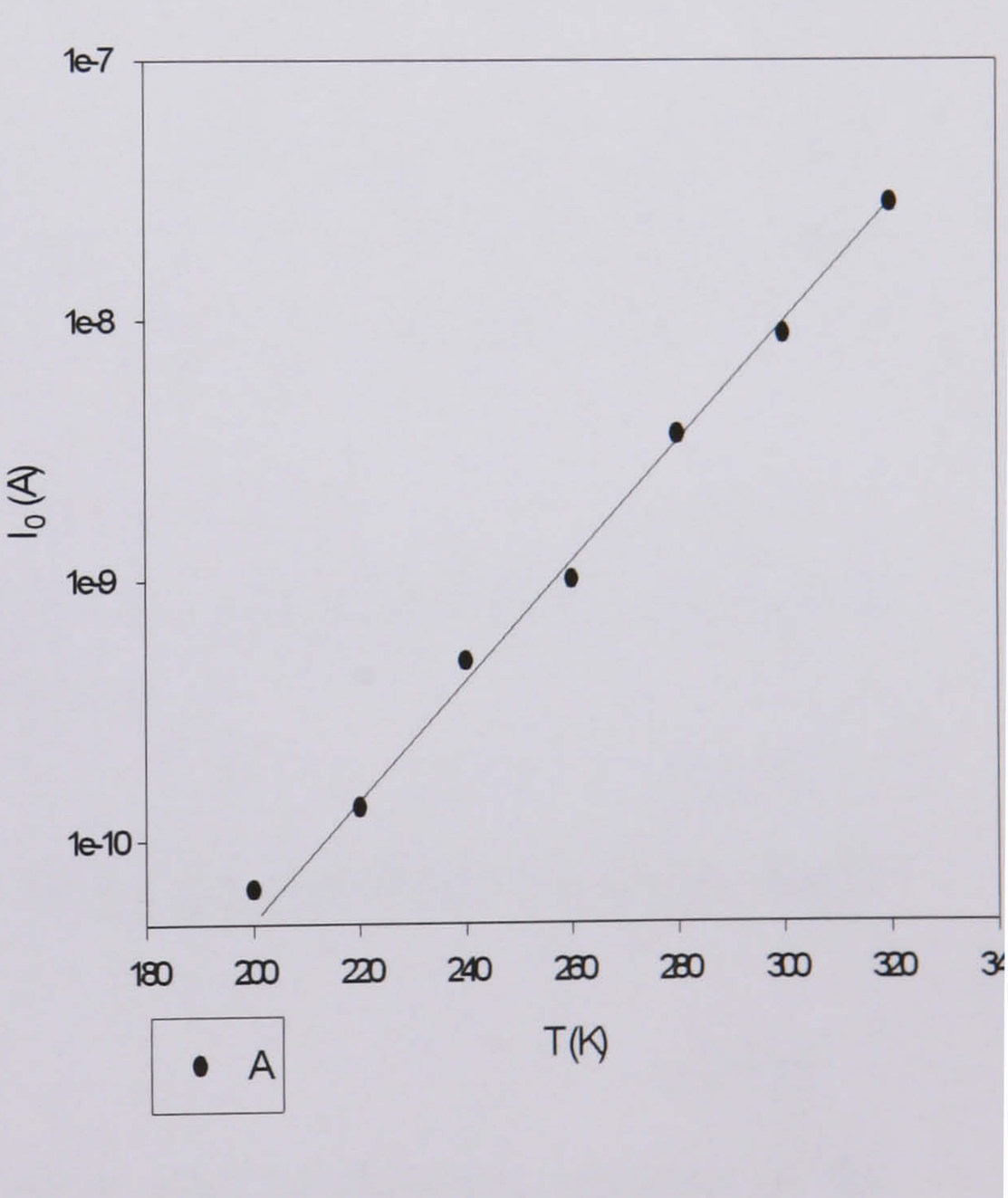

Figure (5-11)-(A)-log I_0 vs. T, (B)- log I_o vs. $1/T$ for treated solar cell.

5.3.2- Space Charge Limited Current Measurement.

Although the CdS/CdTe heterostructure is in principle a diode, the forward current-voltage characteristics are often dominated by the high resistance of the CdTe layer. This is partly due to defects in the layer, and therefore, it is necessary to study these. The forward-bias current-voltage characteristics are often limited by space-charge and trapping effects and useful information can be obtained from analysis of the space charge limited current. (SCLC). Space charge limited currents in solids have previously been discussed in general by Mott and Gurney [25] and analysed in detail by Rose [26]. In general, at least one of the two contacts should be ohmic in character in order to inject currents of significant magnitude. The $\log(I)$ – $\log(V)$ characteristic at sufficiently high bias of a CdS/CdTe heterojunction may be used to characterise traps and in particular analysis of SCLC effects allows discrimination between shallow traps and distributions of deeper traps and may be used to calculate the initial position in energy of the Fermi level.

To derive the equations of space charge limited current for p-CdTe we will follow the approach developed by Rose in 1955 for an n-type insulator [26]. The charge that can be accommodated in the interior space between to parallel electrodes of unit area is:

$$Q = C\,V \tag{5.13}$$

where C is the capacitance per unit area between the electrodes, and V is the applied voltage. The space charge limited current is given by:

$$I = Q/t \tag{5.14}$$

Where t is the transit time of the charge Q between the electrodes. The space charge forced into an insulator per unit area is:

$$Q = (V \varepsilon_o \varepsilon / d) \tag{5.15}$$

Where ε_o and ε are the permittivity of free space and the dielectric constant of the insulator respectively, and d is separation between the electrodes. The transit time between the electrodes is:

$$t = d/\,E\mu = d^2/V\mu \tag{5.16}$$

Where E is the electric field in the insulator and μ is the drift mobility. For a trap free insulator the space charge limited current density is given by the Mott-Gurney law for

steady current [27], which can be deduced from equations (5.14), (5.15) and (5.16) to be : [28]

$$J = (9V^2 \mu\ \varepsilon_o \varepsilon\ /8\ d^3) \tag{5.17}$$

If the insulator has only shallow traps lying close to the valance band, Then the drift mobility in equation (5.17) must be replaced by the product of the drift mobility for free carriers μ_o and the fraction of the total space charge that is free θ. The space charge limited current density is then given by:

$$J = (9V^2 \mu_o\, \theta\, \varepsilon_o\ \varepsilon\ /8\ d^3) \tag{5.18}$$

The free carrier to total space charge ratio is given by the approximate relation:

$$\theta = (N_v/N_t) \exp(-E_A / kT) \tag{5.19}$$

Where N_v is the effective density of states in the valance band, N_t is the density of shallow traps whose distance from the valance band is E_A.

When the insulator has deep traps, then for a given applied voltage, the charge injected into the insulator, is distributed in three major parts; free charge in the valance band, trapped charge condensed in states above the original Fermi level and giving rise to a higher quasi-Fermi level, and trapped charge above the newly determined quasi-Fermi level. Since the condensed charge is likely to be very nearly the total injected charge, the new location of the quasi-Fermi level is given very closely by considering all of the injected charge Q to be condensed. With this approximation the free carrier density is:

$$p_v = N_v\ \exp(-E_f / kT) \exp(\Delta E / kT) \tag{5.20}$$

where E_f is the original distance of the Fermi level from the valance band and ΔE is the shift in position of the quasi-Fermi level owing to the condensed charge Q. If the deep traps are distributed uniformly in energy then ΔE is given by:

$$\Delta E = Q/\ q\ n_t d\ = VC/\ q\ n_t\ d \tag{5.21}$$

where n_t is the number of traps per cm^3 per unit range in energy then:

$$p_v = N_v\ \exp(-E_f / kT) \exp(VC / n_t dqkT) \tag{5.22}$$

$$= p_o \exp(\alpha V) \tag{5.23}$$

Where p_o is the initial, thermal equilibrium concentration of free carriers. Since it has been assumed that the density of trapped carriers is very nearly equal to the total density of injected electrons, the density of trapped carriers = $Q\ d\ q = VC/\ d\ q$ and :

$$\theta = (q\, p_o\, d/VC)\ \exp(\alpha V) \qquad (5.24)$$

Substituting this in equation (5.18) for the space charge limited current density given by:

$$J = (9V\mu_o\, \varepsilon\, \varepsilon_o q\, p_o / 8\, C\, d^2)\ \exp(\alpha V)$$

$$J = (9V\mu_o\, q\, p_o/8d)\ \exp(CV\ /\ n_t dqkT) \qquad (5.25)$$

Assuming C to be given by an equivalent parallel plate capacitor then:

$$J = (9V\mu_o\, q\, p_o/8d)\ \exp(\varepsilon_o \varepsilon V\ /\ n_t d^2 qkT) \qquad (5.26)$$

Similar to the equation reported by Ou et al [29].

In equation (5.26) for a uniform distribution of deep traps the space charge limited current increases steeply with voltage and a graph of log (J/V) vs. V would give a straight line with a slope inversely proportional to n_t. Space charge limited current has the more usual square law dependence on voltage in equations (5.17) and (5.18) for the trap-free and shallow-trap cases respectively.

5.3.2.1- Space Charge Limited Current Analysis for The Treated Solar Cell.

Dark I-V measurements of treated solar cells were carried out at different temperatures and figure (5-12) shows the resulting log$I$-log$V$ characteristics. Each curve in the figure displays three limiting regimes:

- Junction limited as discussed in section (5.3.1).
- A trap-filled – limit (TFL) curve which has a voltage threshold and an enormously steep current rise and is a function of the trap distribution.
- After saturation of the traps any additional charge injected into the sample exists as free charge and follows the trap-free square law again [28].

To investigate the nature of the trap distribution, the dark log(I/V) versus V characteristics were plotted as shown in figure (5-13). This shows that in the TFL region, the characteristics are consistent with the case where there is a uniform distribution of traps. From the slope of the curves in figure (5-13) at around 1V, values of the n_t were estimated using equation (5.26) at different temperatures as shown in table (5-6).

Figure(5-12)-log(I_f) vs. log(V) of treated solar cell.

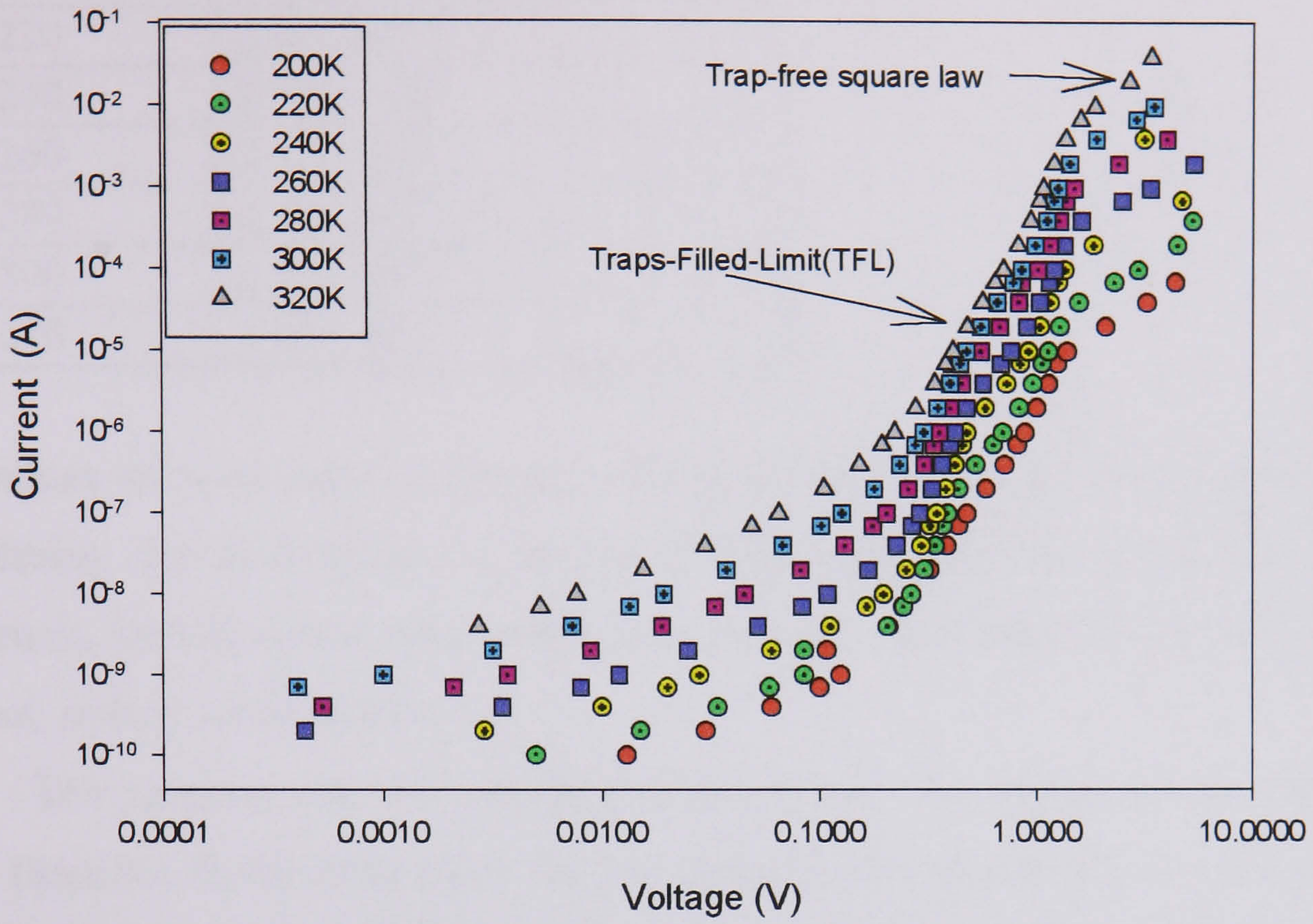

Figure(5-13)-log(I/V) versus V of treated solar cell.

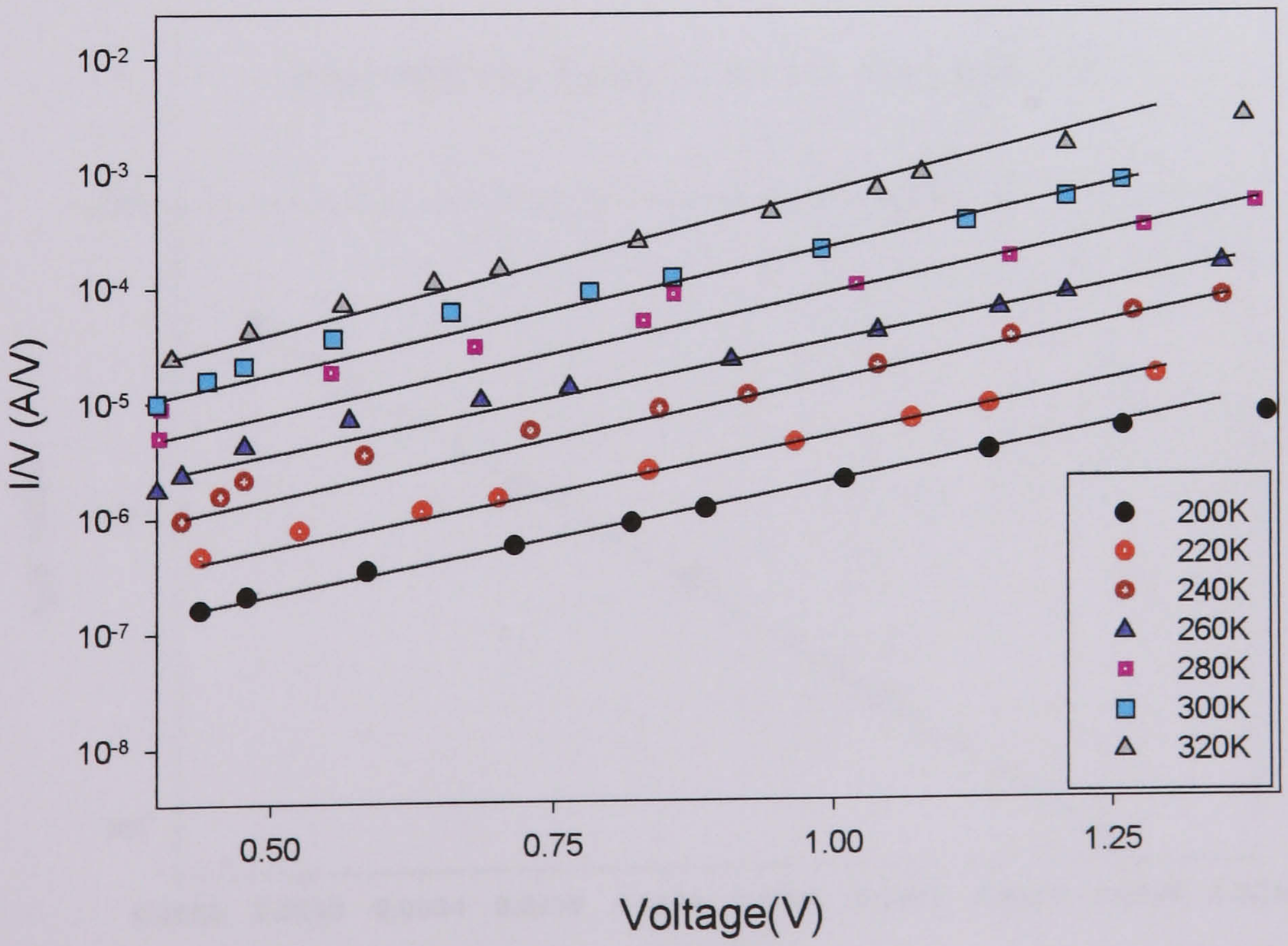

Table (5-6) –Trap density of treated p-type CdTe in solar cell

T(K)	n_t($cm^{-3}eV^{-1}$)
200	2.83×10^{14}
220	2.6×10^{14}
240	2.35×10^{14}
260	2.4×10^{14}
280	2.3×10^{14}
300	2.1×10^{14}
320	1.6×10^{14}

The values of n_t in table (5-6) vary comparatively little over the temperature range, considering the approximation nature of the analysis. The small, but apparently systematic, variation in n_t with temperature probably indicates that the trap distribution was not, in fact, quite uniform.

The analysis may be extended to determine an estimate for the initial Fermi level. Equation (5.26) shows that the extrapolated intercepts $(I/V)_o$ at $V = 0$ for the line in figure (5.13) are proportional to the free carrier density p_o. This in turn is given by equation (5.22) which shows that a plot of log $(I/V)_o$ vs. $1/T$ should gave a straight line with a slope proportional to the Fermi energy level. The initial position in energy of the Fermi level calculated from the slope of the line in figure (5-14) would be 0.23eV.

Figure(5-14)- $\log(I_o/V)$ vs. $1/T$ of treated cell.

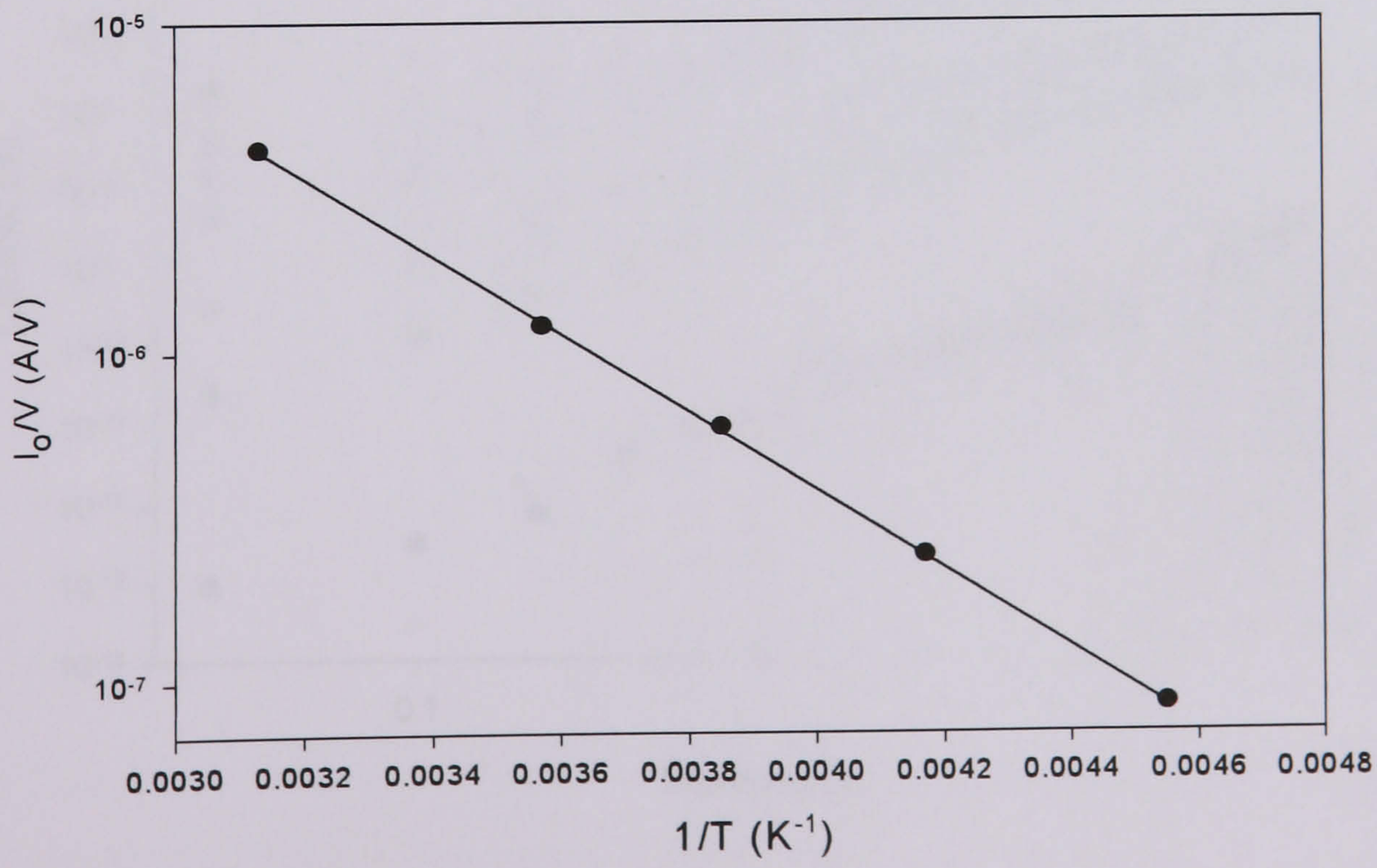

5.3.2.2- Space Charge Limited Current Analysis for The Untreated Solar Cell.

Log (I_f)-log (V) measurements of untreated solar cells at different temperatures are illustrated in figure (5-15). The space charge limited current increases steeply with voltage indicating that the untreated p-CdTe also had a distribution of traps. To determine the nature of the trap distribution, dark log (I/V) versus V characteristics were plotted as shown in figure (5-16) and as for the treated cells, gave straight lines. From the slopes of the curves in figure (5-16) at around 1V, values of n_t were estimated at different temperatures as shown in table (5-7). As for treated cells, fairly consistent values of n_t were observed, although the values were larger and did not vary quite so systematically with temperature.

Following the same procedure as before plots of log $(I/V)_o$ vs. $1/T$ were drawn in order to estimate the initial Fermi energy level. Figure (5.17) again shows a reasonable fit to a straight line, and the slope gives an estimate of 0.6 eV for the Fermi energy.

Figure (5-15)- log (I_f) vs. log (V) of untreated solar cell.

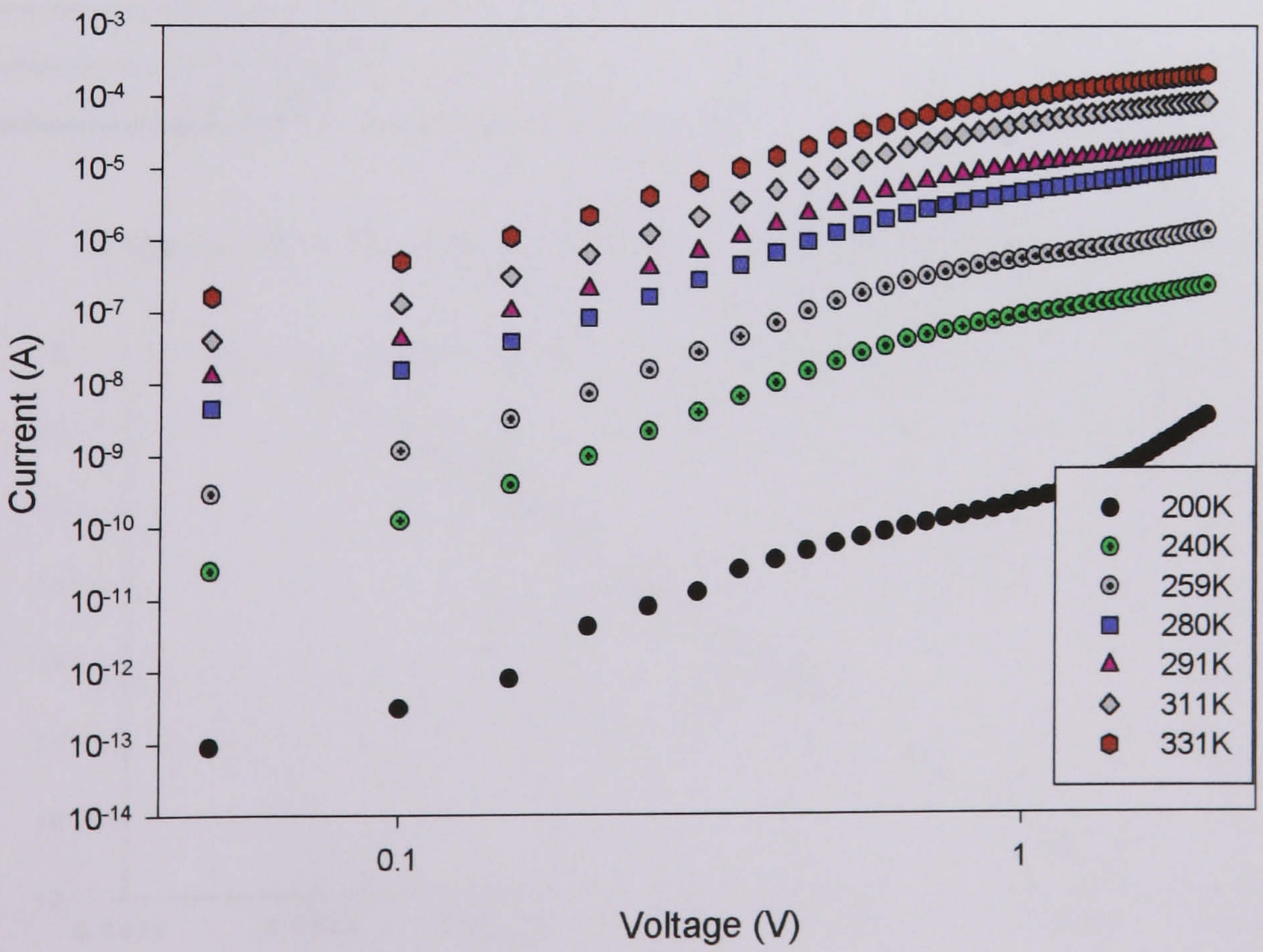

Figure (5-16) log (I/V) vs. V of untreated solar cell.

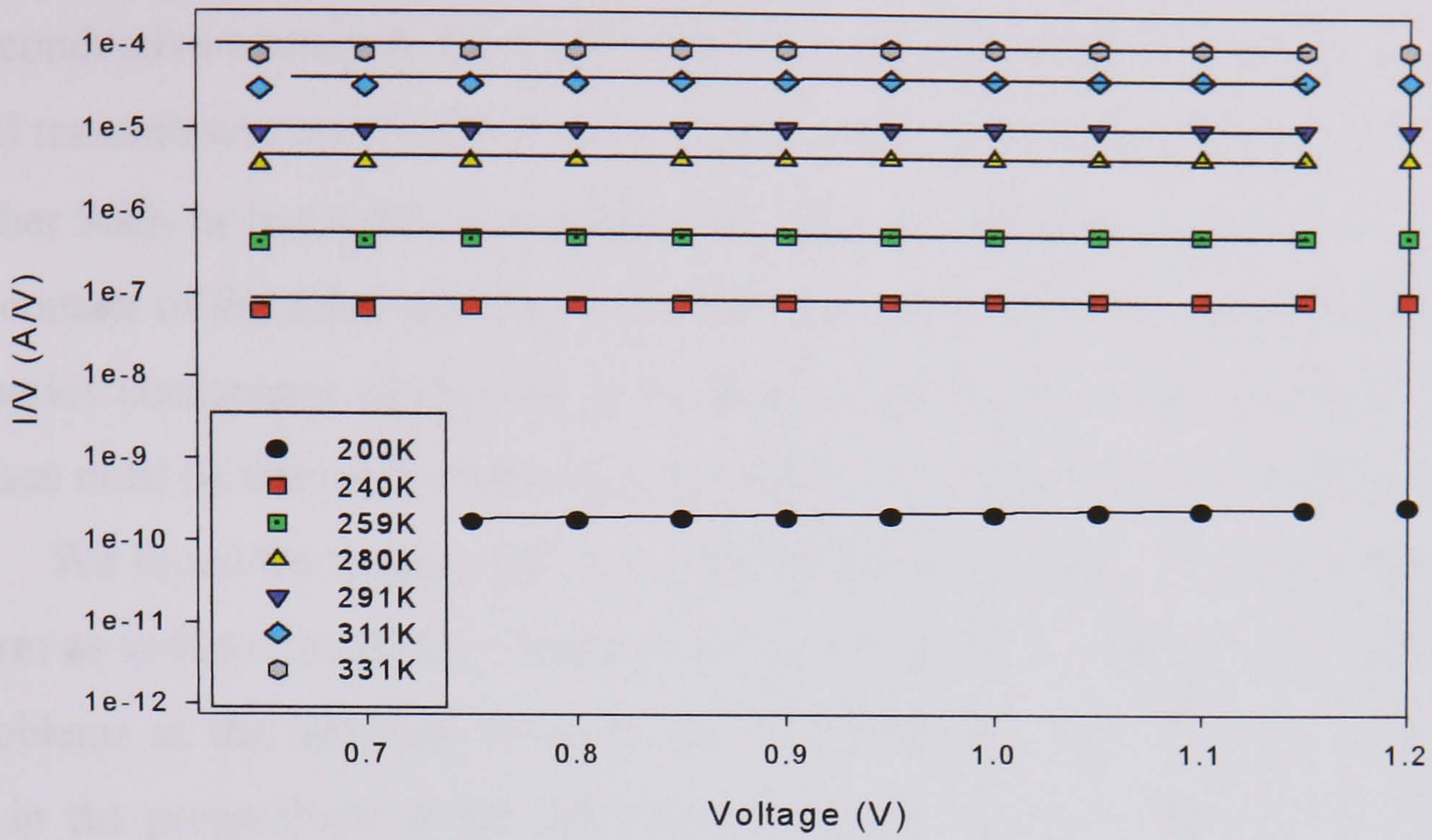

Table (5-7) The traps density of untreated p-CdTe of solar cell.

T (K)	n_t ($cm^{-3}eV^{-1}$)
200	4.9×10^{14}
240	4.7×10^{14}
259	3.7×10^{14}
280	4.4×10^{14}
311	5.7×10^{14}
331	6×10^{14}

Figure (5-17)- log (I_o/V) vs. 1/T of untreated solar cell.

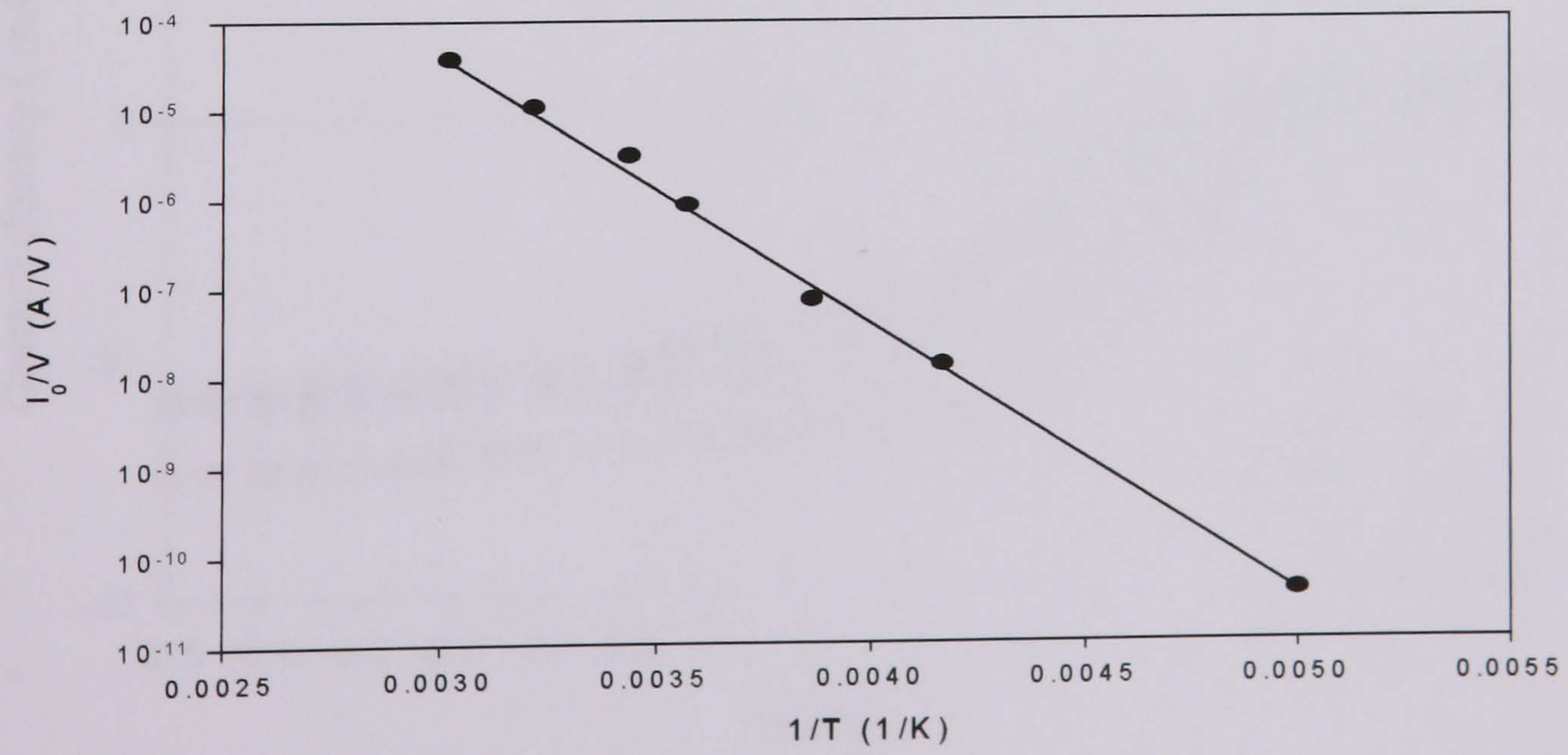

5.4- *I-V* Characteristics of TCO/CdS Interface.

The transparent conducting oxide (TCO) is used to provide a highly transparent front conductive contact to the CdS/CdTe solar cell. The desirable sheet resistance and optical transmission are $< 10\ \Omega/\square$ and $> 90\%$ respectively. Generally the TCO is based on either SnO_2 or In_2O_3 (ITO) sometimes doped or in combination (e.g. ITO-SnO_2). The front contact of the solar cell has received less attention than the back contact although as a series component of the cell, it is clearly significant. Importantly, the TCO/CdS interface must be thermally stable during the processing steps of solar cell preparation.

We found those solar cells with ITO as the front contact instead of SnO_2 did not perform as well as nominally identical cells using SnO_2. We thought this might be due to problems at the interface between the ITO and CdS occurring during the heating steps in the preparation of the cell. To investigate this, we prepared two samples of ITO/CdS/CdTe at different times of annealing during the $CdCl_2$ treatment. Figure (5-18) shows the PV output characteristics of a SnO_2/CdS/CdTe cell annealed for 30 minutes at 400 °C in air during $CdCl_2$ treatment (SnO_2), and two ITO/CdS/CdTe cells

Figure (5-18) PV characteristics of SnO_2,ITO15 and ITO30 samples.

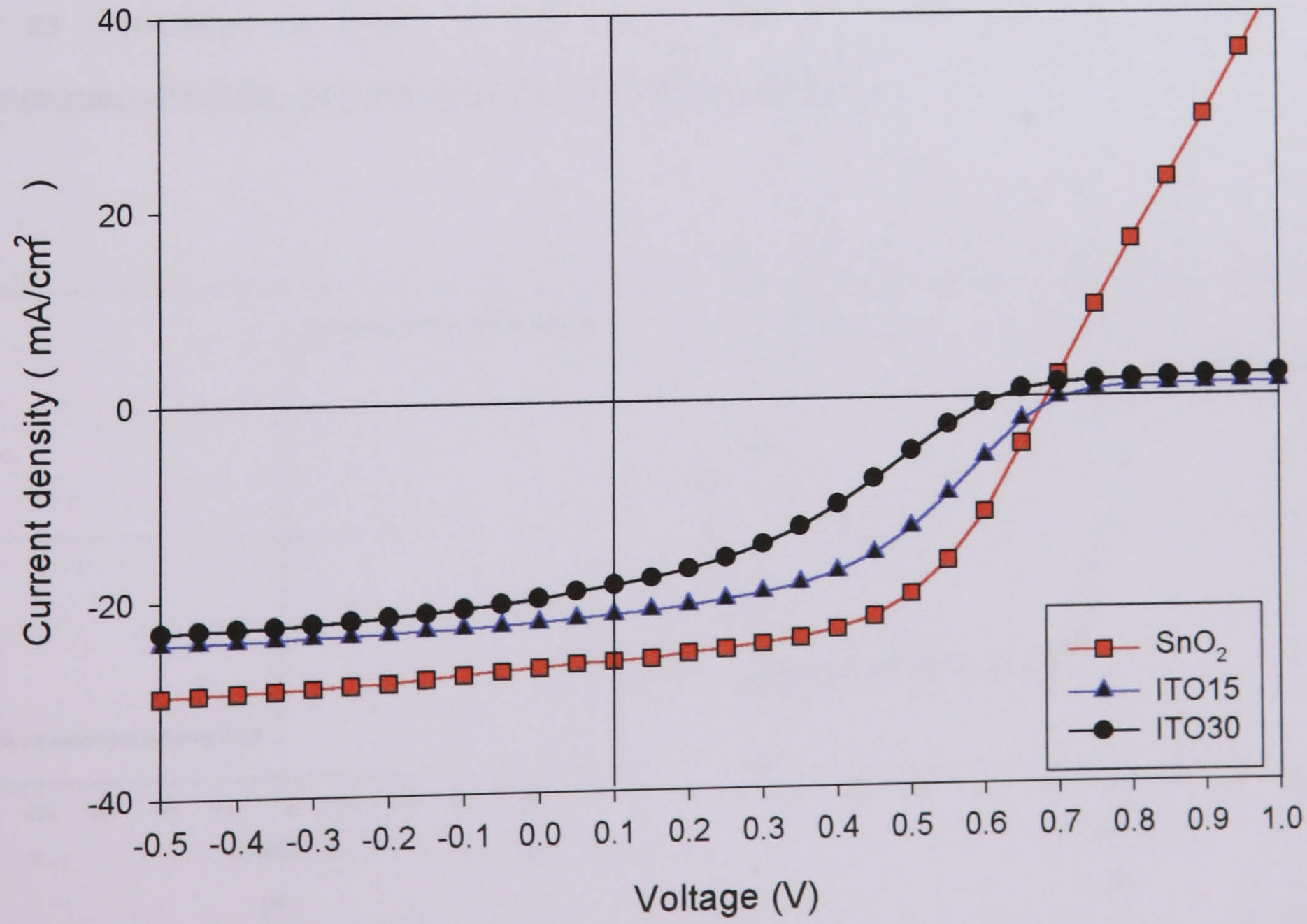

annealed for 15 (IT015) and 30 minutes (ITO30) at 400°C in air respectively. The photovoltaic parameters, series resistance, R_s , and shunt resistance R_{sh} of the solar cells are shown in table (5-8).

Parameters	J_{sc}(mA/cm^2)	V_{oc}(V)	FF %	η %	R_s (Ω.cm^2)	R_{sh}(Ω.cm^2)
SnO_2	27.3	0.684	54.4	10.1	6	196
ITO15	22.6	0.714	44.9	7.3	54.1	170.5
ITO30	20.15	0.623	36.7	4.6	34	81.99

Table (5-8)- The parameters of the cells of figure (5-18).

Table (5-8) which was calculated from the figure (5-18) shows that the performance of the SnO_2/CdS/CdTe cell is better than the performance of either of the ITO/CdS/CdTe cells because the SnO_2/CdS/CdTe cells has a lower R_s and a higher R_{sh}. The efficiency of ITO/CdS/CdTe reduced from around 7.3 to 4.6 when the time of annealing increased from 15 to 30 minutes. The reduction in the shunt resistance of ITO/CdS/CdTe cells with increased heating time indicates that the leaking current through the sample had increased.

To investigate the effect of heating time on the SnO_2/CdS interface and the ITO/CdS interface, four samples of SnO_2/CdS/In and ITO/CdS/In were made and dark *I-V* measurements were taken as deposited and after heating at 400°C for 30minutes in air as illustrated in figure (5-19) and (5-20). The saturation at ~±3.8mA was a consequence of the current limit on the instrumentation.

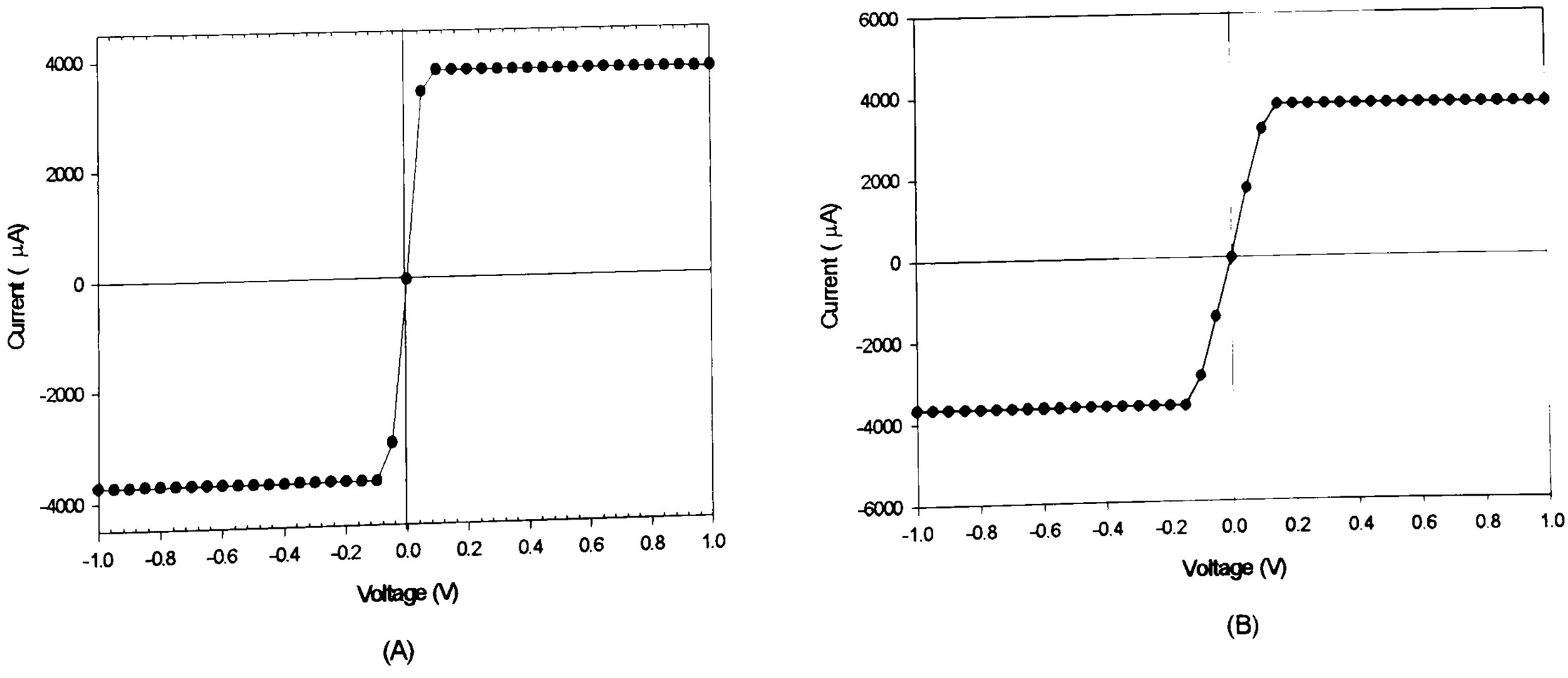

Figure (5-19)- Dark *I-V* characteristics of SnO_2/CdS/In before (A) and after (B) heating.

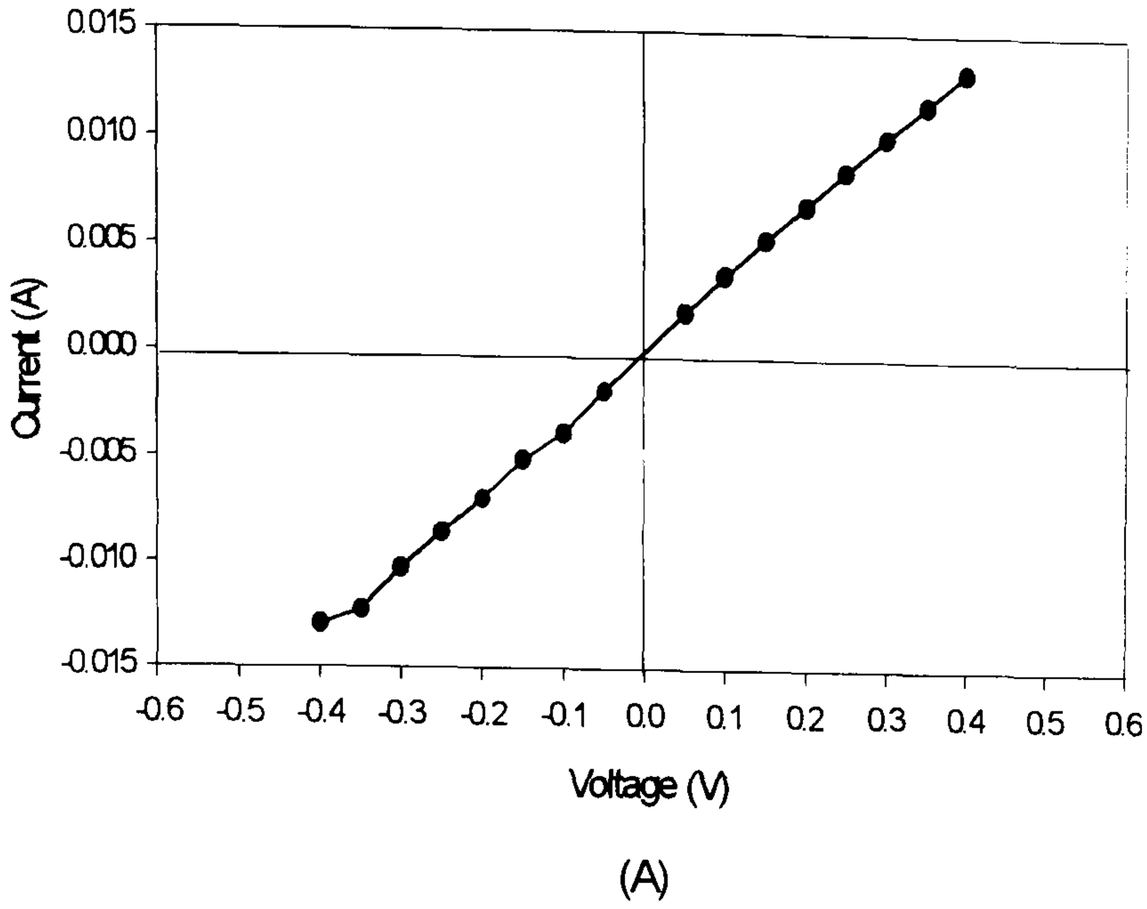

Figure (5-20)- Dark *I-V* characteristics of ITO/CdS/In before (A) and after heating (B).

Figure (5-19-A) shows that the dark *I-V* measurements in forward (TCO positive) and reverse bias for the SnO_2/CdS/In sample were similar and indicated that the contact between the CdS and SnO_2 was ohmic [30]. This behaviour remained after annealing as shown in figure (5-19-B), although the resistance appeared to have increased slightly (from 0.62 to 1.3 Ωcm^2). This suggest, that any chemical interaction between the CdS and SnO_2 [30] was probably of minimal significance for the performance of the cell.

Figure (5-20-A) shows that the dark *I-V* measurements in forward and reverse bias for the ITO/CdS/In devices were also similar which indicated that the contact between the CdS and ITO was also ohmic though more resistive ($1.2\Omega cm^2$). However after heating, figure (5-20-B) shows that the dark *I-V* characteristics became rectifying. Assuming that the contact between the In and CdS layer was ohmic since that was common to both the SnO_2/CdS/In and the ITO/CdS/In devices, then the rectifying effect which appeared after heating of the samples would seem to be due to the contact between the ITO and CdS. Hence annealing the CdS/ITO interface for 30minutes at 400°C in air, as used in $CdCl_2$ treatment, clearly resulted in some interaction, which impeded the flow of charge. Depuydt et al [31] have reported that an ITO/CdS interface contributes to an increase in the series resistance after CdTe deposition, i.e. after heating, whereas the ITO/CdS junction before deposition of CdTe behaves as an ohmic contact. This is in agreement with our result, which implies that the increased series

resistance and reduced shunt resistance of ITO/CdS/CdTe in figure (5-18) was mainly due to effects the ITO/CdS interface.

The behaviour of the ITO/CdS interface was studied in more detail by investigating the effect of annealing time on the dark *I-V* characteristics. Figure (5-21) shows the effect of time (10, 20 and 30 minutes) of heating at 400°C in air on the dark *I-V* characteristics of the ITO/CdS/In device.

It is clear from figure (5-21) that the ITO/CdS interface started to become rectifying within 10 minutes heating time at 400°C, and had become fully rectifying after ~ 20 minutes.

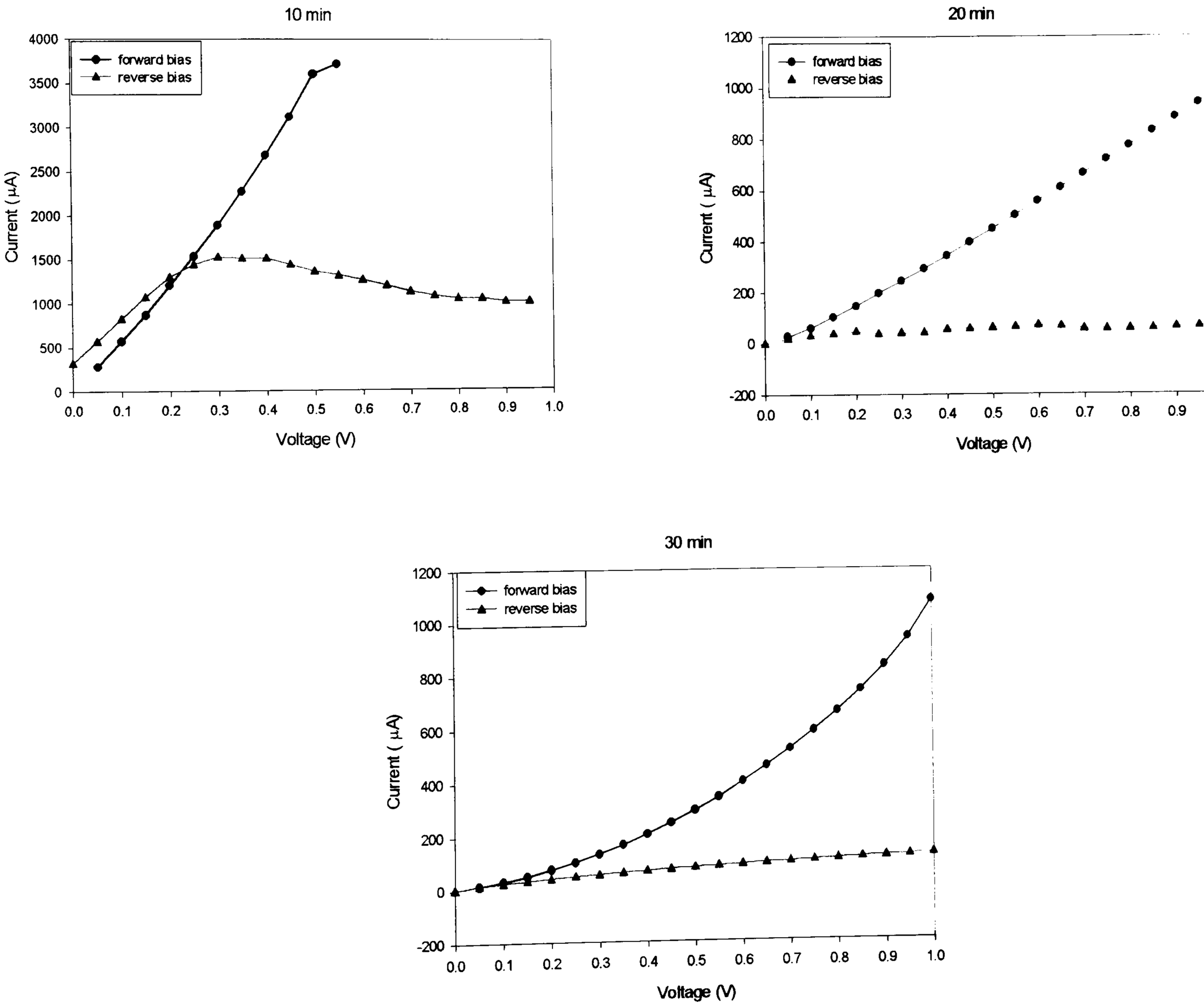

Figure (5-21)- Dark *I-V* characteristics of ITO/CdS/In after heating for different times.

5.5-Conclusion:

The thickness of the CdTe and CdS films should be a compromise between the requirements for complete absorption of the incident radiation and the need to keep the series resistance low and shunt resistance high. The optimum thickness of CdTe and CdS of CdS/CdTe solar cell deposited by Close Space Sublimation appear to be 5μm and 0.2μm respectively.

The $CdCl_2$ treatment for the CdTe layer increased the efficiency of the solar cells from 3% to around 10% due to an improvement in all of the photovoltaic parameters of the cells. The series resistance was reduced from ~ 34 to ~ 6 Ω. cm^2 and the shunt resistance increased from ~ 48 to ~ 196 $\Omega.cm^2$. The reduction in R_s and the increase in R_{sh} led to an increase the fill factor from 36.3 to 54.4%, the open circuit voltage from 438mV to 684mV and short circuit current density from 17.6 to 27.3 $mAcm^{-2}$.

The reverse saturation current of the untreated cell varied exponentially with inverse temperature, while after the $CdCl_2$ treatment the variation became exponential with temperature. This suggested that the $CdCl_2$ treatment changed the current transport mechanism across the junction from emission/recombination with an activation energy around 0.066eV to a tunnelling mechanism. This is in contrast to the Al-Allak et al [14] who found the reverse. The discrepancy is not fully understood but is probably a consequence of apparently minor difference in processing. This illustrates the sensitivity of these devices to detailed differences in the fabrication.

The Space Charge Limited Current measurements indicated that the CdTe layer in CdS/CdTe cells had a uniform distribution of traps with energy above the valance band with density around 3.7-6 $\times 10^{14}$ $cm^{-3}eV^{-1}$ before $CdCl_2$ treatment, which reduced to 1.6-2.8 $\times$ 10^{14} $cm^{-3}eV^{-1}$ after treatment. The initial position in energy of the Fermi level was calculated for untreated and treated CdTe to be 0.6 eV and 0.23eV respectively. These values of trap density of untreated CdTe in good agreement with the values of shallow traps found by Ou et al [20] for untreated cells.

Solar cells fabricated with SnO_2 give higher efficiencies than cells fabricated with ITO. This was due to the interface between the ITO and CdS layer, which became rectifying after heating at 400°C in air. The change in the ITO/CdS interface from ohmic to Schottky behaviour after heating, suggests that some chemical interaction had taken place between the ITO and the CdS. The nature of this interaction is not clear.

5.6-References.

(1)- B. G. Streetman. "Solid State Electronic Devices". Prentic-Hall, Inc.,(1990).

(2)- M. Bayhan. "Preparation and Characterisation of n-CdS/p-CdTe Thin Film Solar Cells". Ph. D. Thesis, University of Durham, U.K., 1994.

(3)- T. Aramoto, S. Kumazawa, H. Higughi. "16.0% Efficient Thin-Film CdS/CdTe Solar Cell". Japan. J. Appl. Phys., 36 (1997) 6304.

(4)- J. Britt and C. Ferekides. "Thin-Film CdS/CdTe Solar Cell with 15.8% Efficiency". Appl. Phys. Lett., 62 (1933) 2851.

(5)- D. Bonnet, H. Richter, K. Jager, "The CTS Thin Film Solar Module – Closer to Production". 13th European Photovoltaic Solar Energy Conference, 23-27 October, Nice France, (1995) 1456.

(6)- J. Barker, S. P. Binnes, D. R. Johnson, R. J. Marshhall, S. Oktik, M. E. Ozsan, M. H. Patterson, S. J. Ransome, S. Roberts, M. Sadeghi, J. Sherborne, A. K. Turner and J. M. Woodcock. "Electrodeposited CdTe for Thin Film Solar Cells". Int. J. Solar Energy, 12 (1992) 79.

(7)- Harold J. Hovel. "Semiconductors and Semimetals". Vol.11 Solar cells. Academic Press Inc. London (1975).

(8)- P. Rai-Choudhury and P. L. Hower. " Growth and Characterisation of Polycrystalline Silicon". 120 (1973) 1761.

(9)- J. E. Granata, J. R. Sites, G. Contreras-Puente, and A. D. Compaan. "Effect of CdS Thickness on CdS/CdTe Quantum Efficiency". 25th IEEE Photovoltaic Specialist Conf., Washington DC, (1996) 853.

(10)- R. W. Birkmire, B. E. McCandless and S. S. Hegedus. "Effects of Processing on CdTe/CdS Materials and Devices". Int. J. Solar Energy, 12 (1992) 145.

(11)- S. Kumazawa, S. Shibutani, T. Nishio, T. Aramoto, H. Higuchi, T. Arita, A. Hanafusa, K. Omura, M. Murozono and H. Takakura. "15.1% Highly Efficient Thin Film CdS/CdTe Solar Cell". Solar Energy Materials and Solar Cells, 49 (1997) 205.

(12)- C. S. Ferekides, B. Tetali, D. Marinskiy, S. Marinskaya, and D. Morel. "Effects of Processing Temperature on the Thickness of CdS and the Performance of CdTe Solar Cells". 14th Conf. NREl/SNL Photovoltaics Program Review, (1996) 631.

(13)- T. L. Chu and S. S. Chu. "Thin Film II-VI Photovoltaics". J. Solid State Electronics, 38 (1995) 533.

(14)- H. M. Al-Allak, A. W. Brinkman, H. Richter, D. Bonnet. "Dependence of CdS/CdTe Thin Film Solar Cell Characteristics on the Processing Conditions". J. Crystal Growth, 159 (1996) 910.

(15)- H. R. Moutinho, M. M. Al-Jassim, F. A. Abufoltuh, D. H. Levi, P. C. Dippo, R. G. Dhere, and L. L. Kazmerski. "Studies of Recrystallization of CdTe Thin Films after $CdCl_2$ Treatment". 26th IEEE Photovoltaic Specialists Conference, California, U.S.A, (1997).

(16)- A. Ayesh, J. Abu-shama, and R. N. Ahmad-Bitar, "Effect of Heat and $CdCl_2$ Treatment on the Structure and Photoluminescence of CdTe/CdS Thin Films". Arab Gulf J. Scientific. Res. 14(1996) 349.

(17)- S. A. Galloway, A. J. Holland, and K. Durose. "A Study of CdS/CdTe Thin Film Solar Cells Using Beam Injection Techniques". J. Crystal Growth, 159 (1996) 925.

(18)- B. L. Sharma and R. K. Purohit, "Semiconductor Heterojunctions" Academic Press, Oxford and New York 1974.

(19)- M. Arienzo and J. J. Loferski. "Single-Crystal Solar Cell Heterojunctions Involving/ V-Cadmium Sulfide". J. Appl. Phys. 51 (1980) 3393.

(20)- S. S. Ou, O. M. Stafsudd, B. M. Basol. " Current Transport Mechanisms of Elactrochemically Deposited CdS/CdTe Heterojunction". Solid–State Electronics, 27 (1984) 21.

(21)- A. R. Riben and D. L. Feucht, "Electrical Transport in n-Ge - p-GaAs Heterojunction". Int. J. Electronics, 20 (1966) 583.

(22)- Kim W. Mitchell. "Evaluation of the CdS/CdTe Heterojunction Solar Cell". Garland Publishing Inc. New York &London (1979).

(23)- S. A. Ringel, A.W. Smith, M. H. MacDougal and A. Rohatgi. "The Effects of $CdCl_2$ on the Electronic Properties of Molecular-Beam Epitaxally Grown CdTe/CdS Heterojunction Solar Cells". J. Appl. Phys. 70 (1991) 881.

(24)- C. Ercelebi, A.W. Brinkman, T. S. Furlong and J. Woods. "Current Transport Mechanisms in Epitaxial CdS/CdTe Heterojunctions". J. Crystal Growth 101 (1990) 162.

(25)- N. F. Mott and R. W. Gurney. "Electronic Processes in Ionic Crystals". Academic Press, New York 1940.

(26)- A. Rose. "Space- Charge- Limited Currents in Solids". Phys. Rev., 97 (1955) 1538.

(27)- A. Van Derziel. "Thermal Noise in Space-Charge –Limited Solid –State Diodes". Solid –State Electronic, 9 (1966) 1139.

(28)- J. G. Simmons. "DC Conduction in Thin Films". Academic Press, London, 1971.

(29)- S. S. Ou, O. M. Stafsudd, and B. M. Basol. "Space-Charge-Limited Current Measurement of Traps in p-type Electrochemically Deposited CdTe Thin Film". Thin Solid Film, 112 (1984) 301.

(30)- D. W. Niles, D. Rioux and Hartmut Hochst. "A Photoemission Investigation of the SnO_2/CdS Interface: A Front Contact Interface Study of CdS/CdTe Solar Cells". J. Appl. Phys. 73 (1993) 4586,

(31)- B. Depuydt, M. Burgelman, M. Casteleyn, A. Niemegeers, A. Vervaet. "The Effects of Diffusion of Impurities from Graphite Back Contacts on CdS/CdTe Cells". 13th European Photovoltaic Solar Energy Conference, Nice France, (1995) 593.

Chapter Six:

Spectral Response of CdS/CdTe Cells.

6.1- Introduction:

The quantum efficiency is defined as the ratio of the number of photocarriers collected at a given photon energy to the number of photons incident on the solar cell [1]. Hence, it is a very powerful tool in the analysis of the performance of solar cells in terms of the photocarriers produced at different wavelengths.

The diffusion of S into the CdTe and the diffusion of Te into the CdS take place during the deposition of CdTe on CdS and during $CdCl_2$ treatment of the CdTe layer. This interdiffusion forms a solid solution of S in CdTe on the CdTe side of the interface and a solid solution of Te in CdS on the CdS side of the interface. This gives a graded interface with varying band gap and lattice parameters [2] [3]. The modulation of the bandgap changes the absorption coefficients, which in turn influences the quantum efficiency, and as a result, the spectral response characteristic is changed according to the degree of interdiffusion between CdS and CdTe.

In this chapter, the spectral response of the treated solar cell ($CdCl_2$ treatment of CdTe and CdS layer) is compared with the untreated solar cell. The effects of some preparation conditions, such as the $CdCl_2$ thickness, time of heating treatment, substrate temperature of CdTe deposition and the thickness of CdS, on the shape of the spectral response are also investigated.

6.2- The Spectral Response of Solar Cells with Treated and Untreated CdTe Layers.

Figure (6-1) shows the spectral response of two solar cells with nominally the same parameters of preparation; CdS thickness, CdTe thickness, substrate temperature of CdTe deposition and the same back contact procedures, but where one had been $CdCl_2$ treated (by depositing $CdCl_2$ on the CdTe layer and annealing at 400°C in air for 30 minutes) and the other had not. The treated cell has a higher quantum efficiency than the untreated cell [4][5][6]. The quantum efficiency of the treated cell is roughly twice that observed in the untreated. There is also a shift to longer wavelengths of the absorption edge for the treated cell compared to the untreated cell. This may be due to the narrowing of the band gap resulting from the formation of the $CdTe_xS_{1-x}$ layer [7] [8]. Thus, it appears that the $CdCl_2$ treatment results in the formation of a $CdTe_{1-x}$ S_x layer with a corresponding decrease in the bandgap [9]. The improvement in the

Figure (6-1)- The spectral response of treated and untreated solar cell.

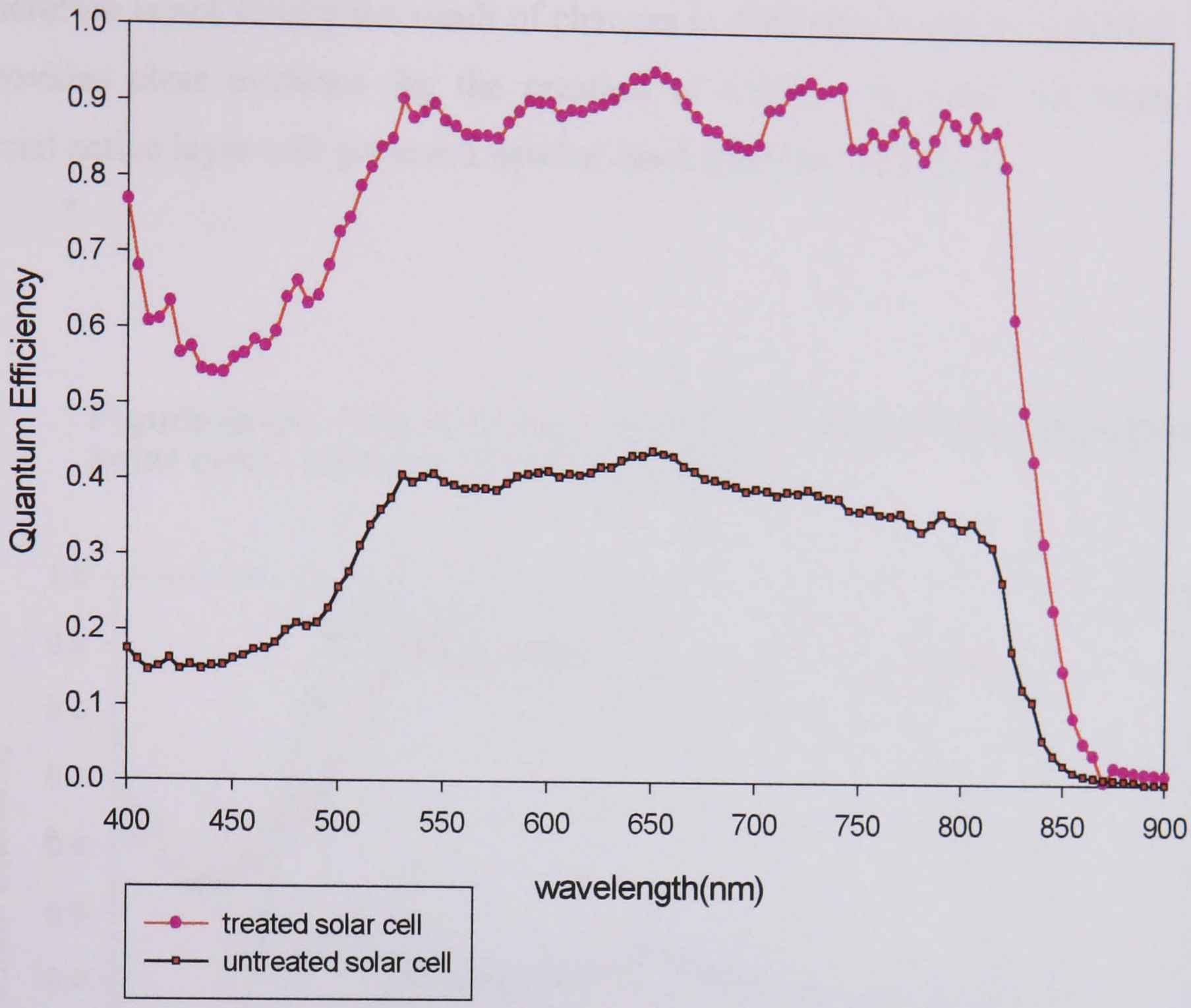

spectral response of treated solar cells indicates that the $CdCl_2$ improves carrier collection from the bulk as well as across the heterointerface [10]. The relatively high conversion efficiency of the treated cell appears to be at least partly related to the interface reaction between CdS and CdTe. It has been suggested [11] [12] that the CdS-CdTe interdiffusion shifts the electrical junction away from the metallurgical interface into the CdTe. While the results presented here do not conclusively demonstrate this, they are not inconsistent with this hypothesis.

The spectral response of treated and untreated solar cells are compared with the simulated response in figure (6-2). The simulated curves, which were calculated in chapter 2, depend on the absorption coefficients of CdS and CdTe without any possibility of interdiffusion between them, whereas the experimental curves would depend on any such interdiffusion. The simulated quantum efficiency coincides with the quantum efficiency of the untreated cell at long wavelengths although this depended on the device parameters of diffusion length and depletion width, which were not known.

Importantly the quantum efficiency of the treated cell is shifted to longer wavelengths when compared with the simulated curves, and this is not dependent on the choice of parameters, but only on the absorption coefficient of CdTe which are well known. This shift therefore is not simply the result of changes in diffusion length or depletion width, and provides clear evidence for the creation of $CdTe_{1-x}$ S_x, since for large x, the interfacial active layer will possess a smaller band gap than CdTe [13].

Figure (6-2)- The spectral response of treated and untreated solar cells, and simulated responses.

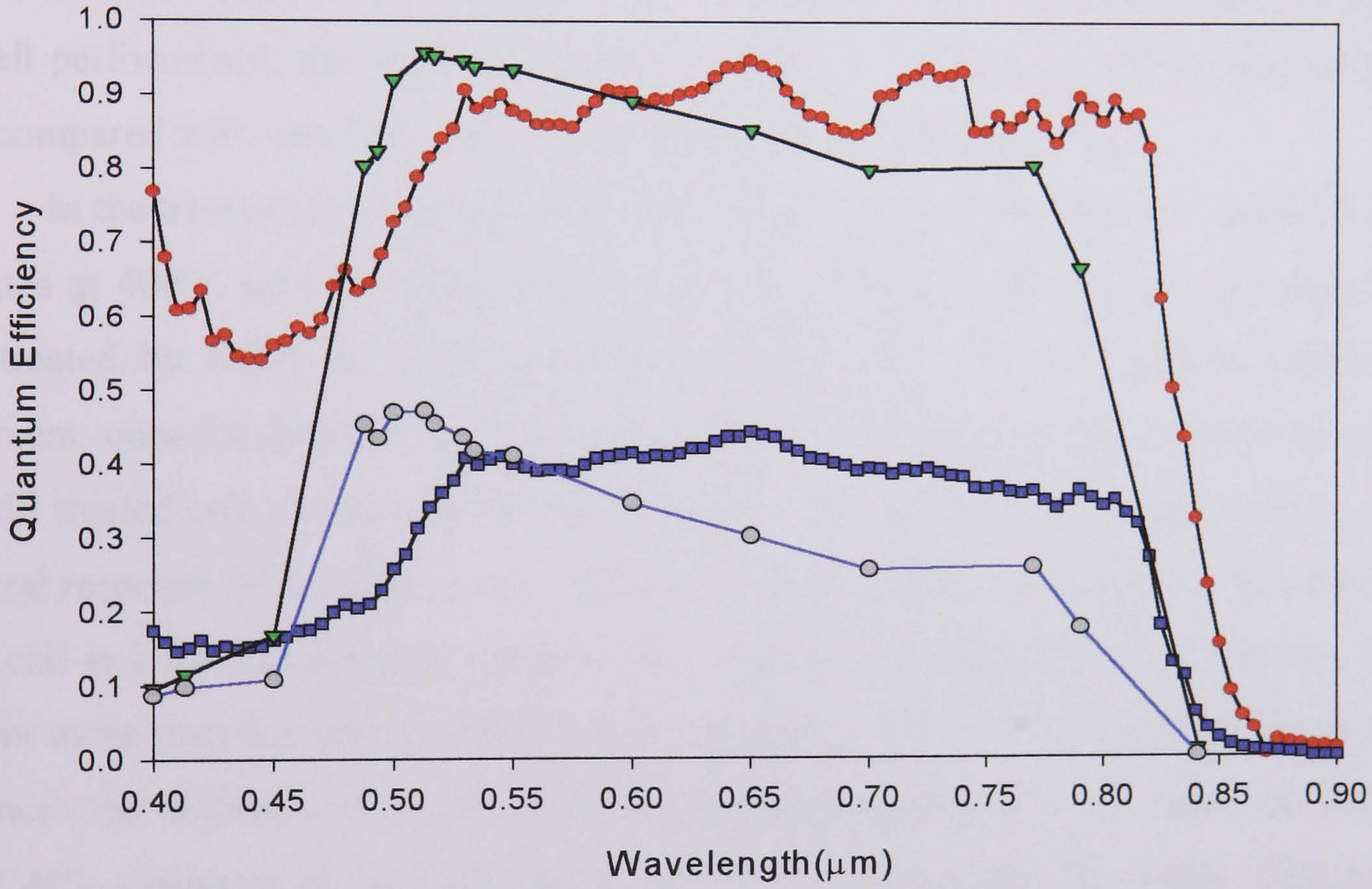

The quantum efficiency of the treated cells is higher than that of the simulated curves at up to ~ 550nm wavelength. This may also be due to the diffusion of S into the CdTe giving greater absorption of light than CdTe layer. The situation appears to be reversed at shorter wavelengths where the quantum efficiency of treated solar cells is less than that of the simulated curves, probably due to the diffusion of Te into the CdS to create S – rich $CdS_{1-x}Te_x$, giving increased absorption of light in the window layer.

This reduces transmission into the absorber layer with a corresponding reduction in the quantum efficiency.

These results strongly suggest that there is mutual diffusion between the CdS and CdTe during the $CdCl_2$ treatment [14]. Comparison of the simulated spectral response with the treated and untreated cells suggests that the depletion region and the diffusion length increased after $CdCl_2$ treatment (the same result was found from *C-V* measurements of depletion region see section (7.2.1)).

6.3- The Spectral Response of Solar Cells with Treated and Untreated CdS Layers.

In order to determine whether $CdCl_2$ treatment of the CdS layer had any effect on cell performance, the spectral response of cells in which the CdS had been treated was compared with untreated but other wise nominally identical cells.

In the treated cells the CdS layer was coated with a $CdCl_2$ film and heated for 30 minutes at 400°C prior to CdTe layer deposition. Then the CdTe layer was deposited and treated by $CdCl_2$ as usual (section 5.2.3). So this cell has received twice the treatment, once for the CdS layer and another for the CdTe layer. The spectral response of CdS treated cell compared with untreated CdS cell is illustrated in figure (6-3). The spectral response of the CdS treated cell has the same spectral response as the untreated CdS cell at long wavelengths, whereas the quantum efficiency declines between 700-500nm more than for the untreated cell. It is possible that $CdCl_2$ treatment of the CdS enhances the diffusion of Te into the CdS during deposition of CdTe layer (at 500°C) and $CdCl_2$ treatment of the CdTe layer, forming a S-rich $CdS_{1-x}Te_x$ layer. This has a bandgap narrower than CdS and absorbs photons with energy less than the bandgap of CdS [7]. Consequently, less photons in this wavelength range are transmitted into the CdTe layer.

Figure (6-3)- The spectral response for solar cells with treated CdS and untreated CdS layers.

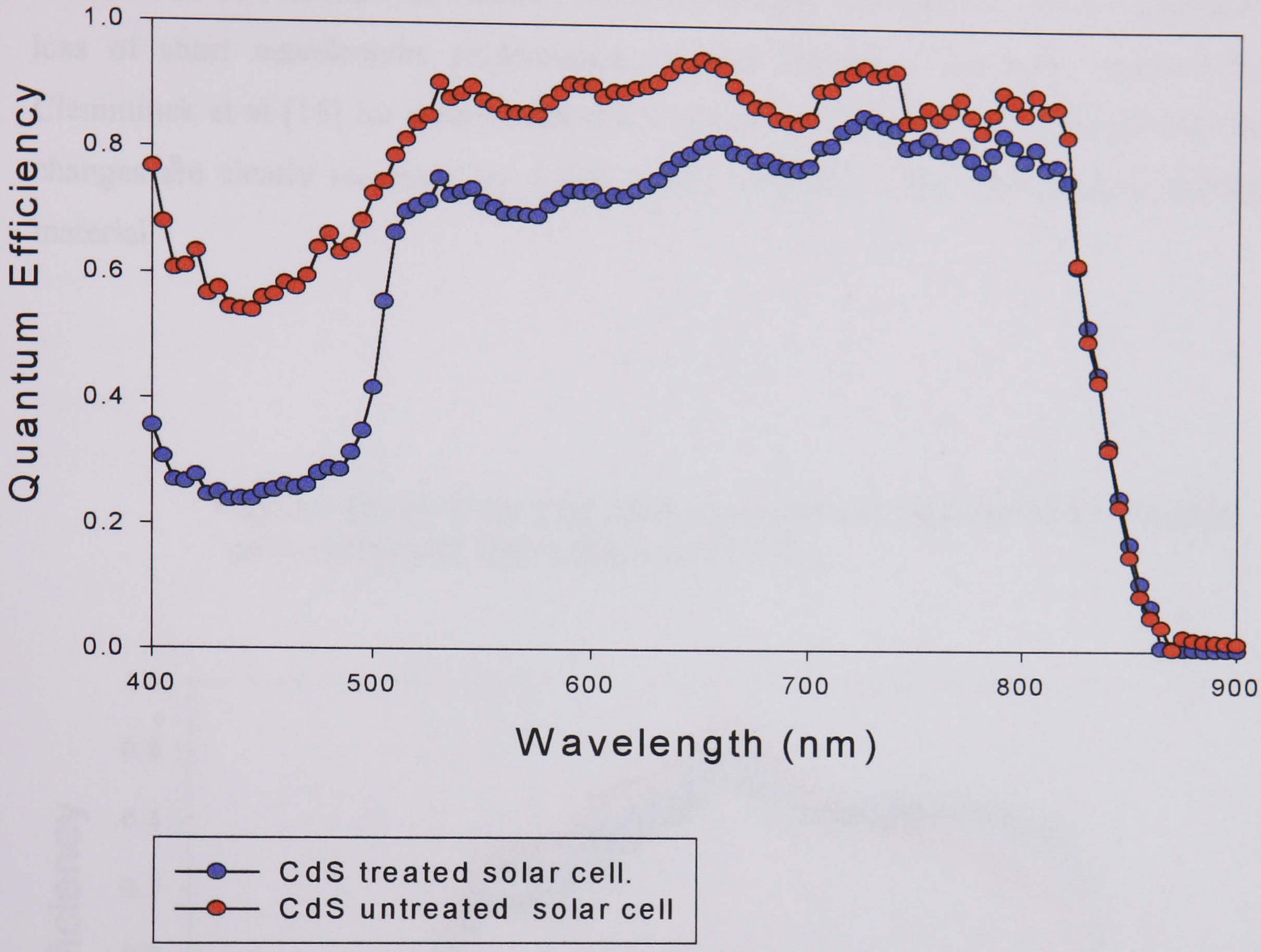

6.4- The Spectral Response of Solar Cells Treated with Different Thickness of $CdCl_2$.

Three solar cells were made with different thickness of $CdCl_2$ evaporated onto the CdTe layer. Figure (6-4) shows the spectral response of the cells, which had 70, 100 and 120nm of $CdCl_2$ deposited during the treatment with the same time of annealing. The $CdCl_2$ thickness is not very accurate because it was very difficult to measure such thin layers using the Tencor α-step 200 surface profiler.

They have similar spectral responses at long wavelengths beyond 825nm and at short wavelengths below 525nm, whereas, they have different quantum efficiency characteristics between 700-825nm and between 525-700nm wavelengths. Between 700 and 825nm the quantum efficiency increased as the thickness of $CdCl_2$ increased, whereas it was reduced for the thicker $CdCl_2$ between 525 and 700nm wavelengths.

This behaviour is consistent with the interdiffusion of S and Te, discussed above. Briefly increased diffusion of S into the CdTe resulted in a reduction of the bandgap and consequently improved collection at longer wavelengths. Conversely the increased diffusion of Te into the CdS reduced short wavelength transmission, and a consequent loss of short wavelengths performance. Similar behaviour has been reported by Clemminck et al [15] for screen printed and sintered cells. They also reported that the changes are clearly increased by a high $CdCl_2$ content in their Cd+Te paste starting material.

Figure (6-4)-The spectral response of solar cells treated with different thickness of $CdCl_2$.

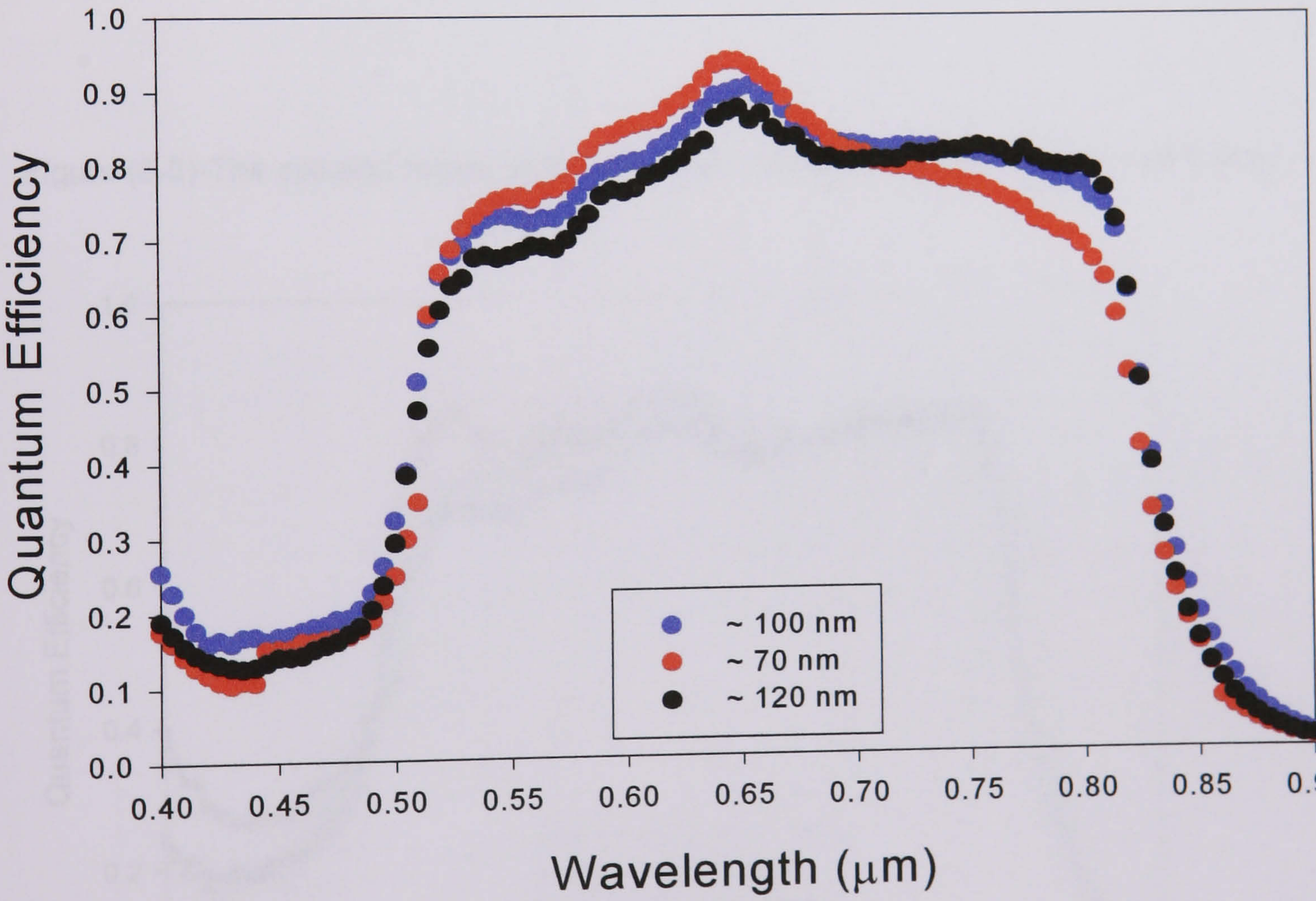

6.5- The Spectral Response of Solar Cells Treated for Different Times with $CdCl_2$.

Three cells were made using the same preparation conditions except for the time of $CdCl_2$ treatment heating. They were annealed at 400°C in air for 30, 60 and 90 minutes. The spectral responses of these cells are illustrated in figure (6-5). They all have the same quantum efficiency at the long wavelength absorption edge, although the quantum efficiency was increased slightly at around 800nm when the time of annealing was increased from 30 to 90 minutes. However, they have different spectral responses at wavelengths between 500 and 700nm. The quantum efficiency in this range decreased as the time of heating increased. The small disparity at around 810nm indicates some small increases in the diffusion of S into the CdTe layer with the time of annealing. On the other hand reduction in the quantum efficiency between 700-500nm implies that the diffusion of Te into the CdS was increased considerably as the time of heating increased from 30 to 90 minutes.

Figure (6-5)-The spectral response for solar cells treated for different times with $CdCl_2$.

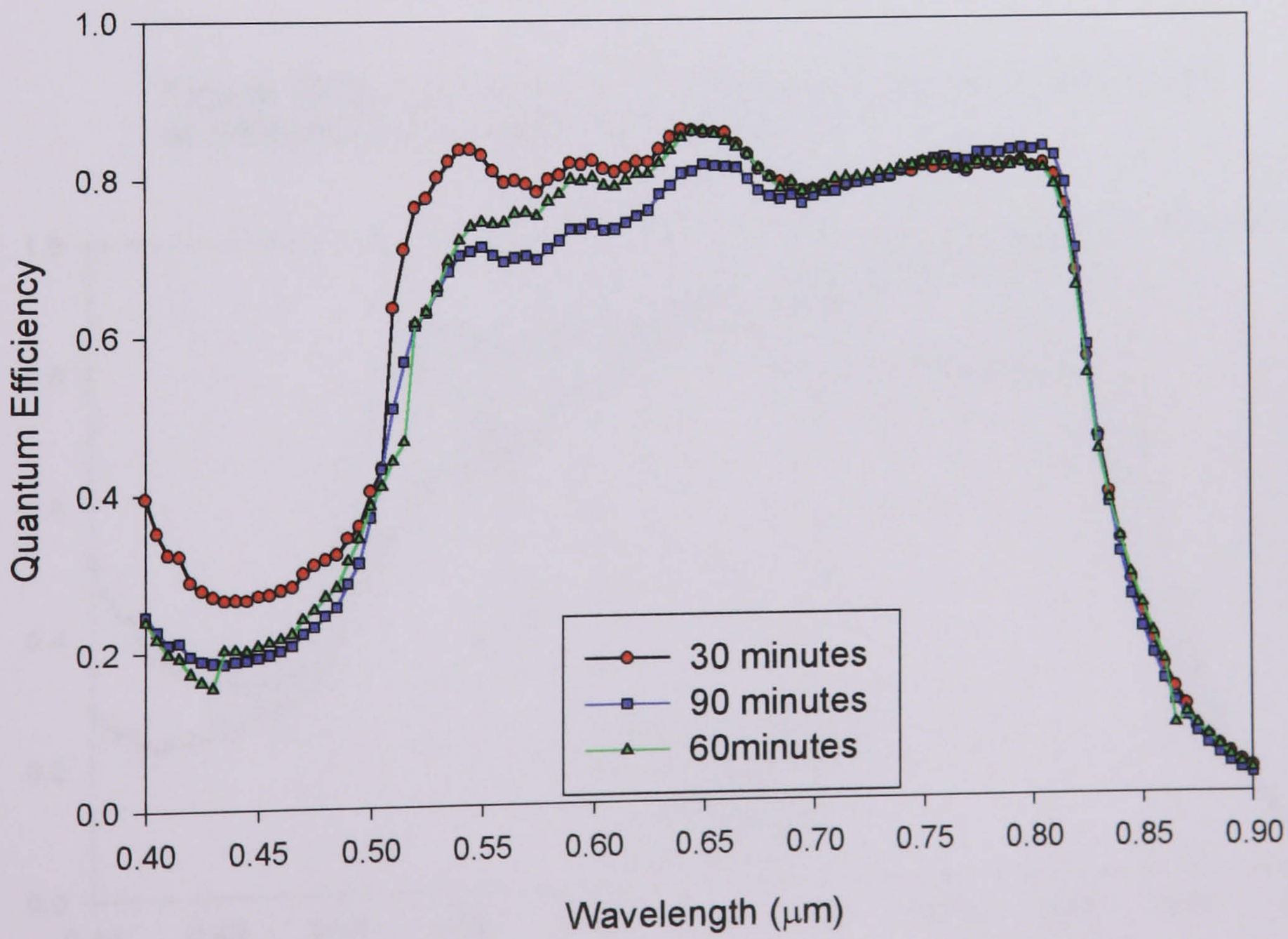

6.6- The Spectral Response of Solar Cells Prepared at Different CdTe Deposition Temperatures.

To investigate the effect of CdTe deposition temperature on the spectral response of solar cell, two cells were made at 500°C and 560°C substrate temperature during deposition of the CdTe layer. The rest of the preparation was in principle the same. The change in the spectral response with the CdTe deposition temperature is illustrated in figure (6-6). They have different quantum efficiencies at long and short wavelengths. The quantum efficiency increased between 875 and 650nm wavelength when the deposition temperature was increased from 500°C to 650°C, whereas it decreased between 650 and 400nm wavelength. The spectral response curve of the 650°C cell declined steadily from a peak at ~810nm, and fell below the response of the curve from the cell deposited at 500°C at a wavelength of ~650nm. Conversely the response of the cell grown at 500°C stayed more constant (increasing slightly) over the spectral range. The degree of interdiffusion between the CdS and CdTe would be expected to increase with increases in the substrate temperature of CdTe deposition [16] [17], leading to greater S incorporation in the CdTe and Te in the CdS. This is consistent with the observed change in the spectral response.

Figure (6-6)-The spectral response of solar cells fabricated at different CdTe depostion temperature.

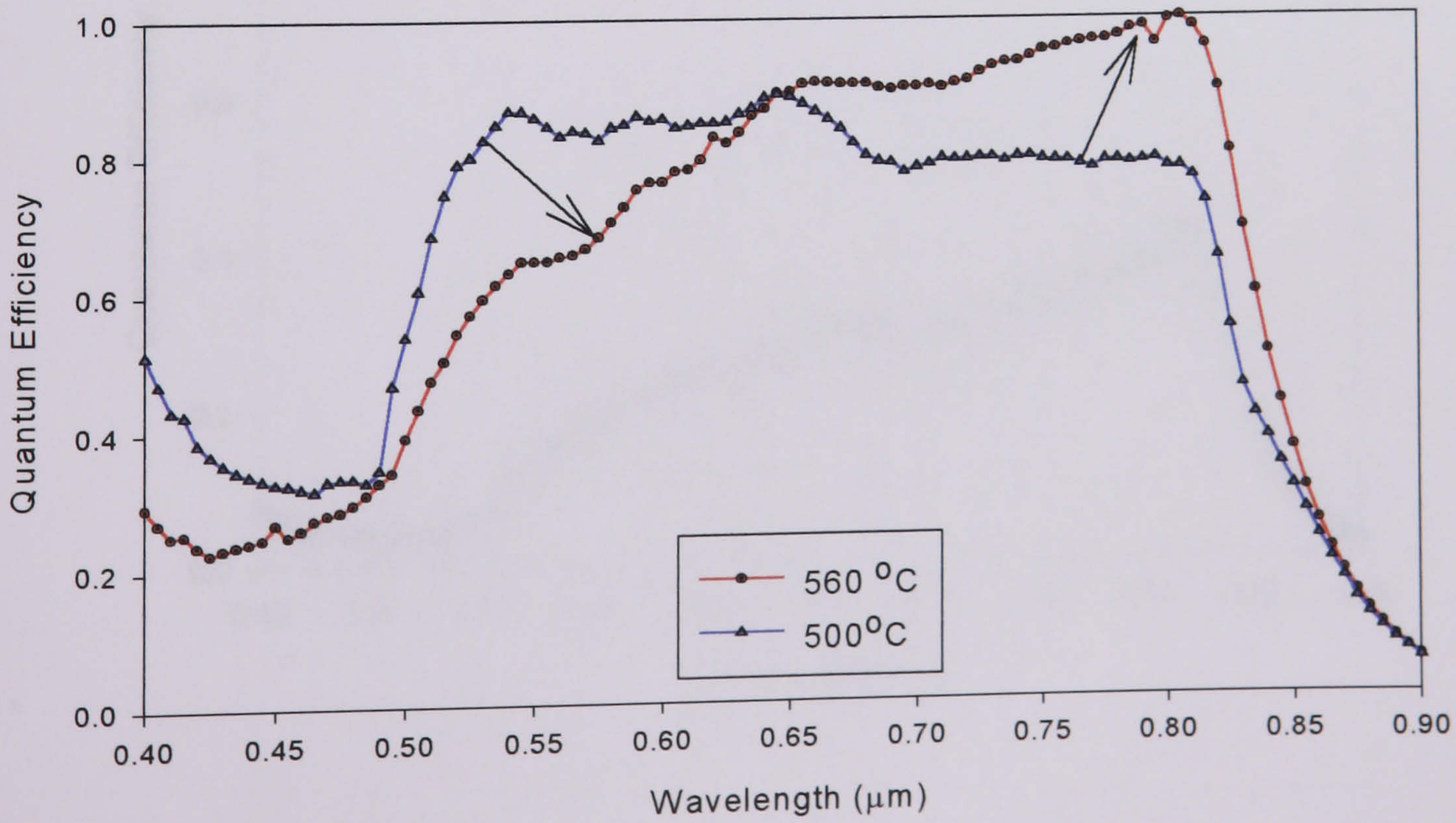

Figure (6-7) shows the spectral response of such a cell, where the CdTe layer had been deposited at a substrate temperature of 600°C. It has very a poor spectral response probably due to pinholes in the CdTe layer. In our system, as the substrate temperature increased above 600 °C, pinholes began to form in the CdTe layer. These provided shunt paths and reduced the effective area of the cell and thus reduced the efficiency and depressed the spectral response of the cell. The increased leakage currents due to the pinholes result in a reduction in the shunt resistance (see figure 5.1). This leads to an increase in the third term ($I_{sc}R_s/R_{sh}$) in equation (5.6) and in turn to a reduction in the short circuit current. Since the quantum efficiency is essentially a measurement of short circuit current as a function of wavelength, a decrease in R_{sh} will reduce the quantum efficiency.

Figures (6-6) and (6-7) indicate that the extent to which interdiffusion at the CdTe/CdS interface depends on the CdTe deposition temperature [18]. It is also possible that the higher substrate temperature led to some re- evaporation of the CdS prior to the CdTe deposition. This would also be expected to affect the performance.

Figure (6-7)-The spectral response of a cell,where the CdTe layer had been deposited at 600 °C.

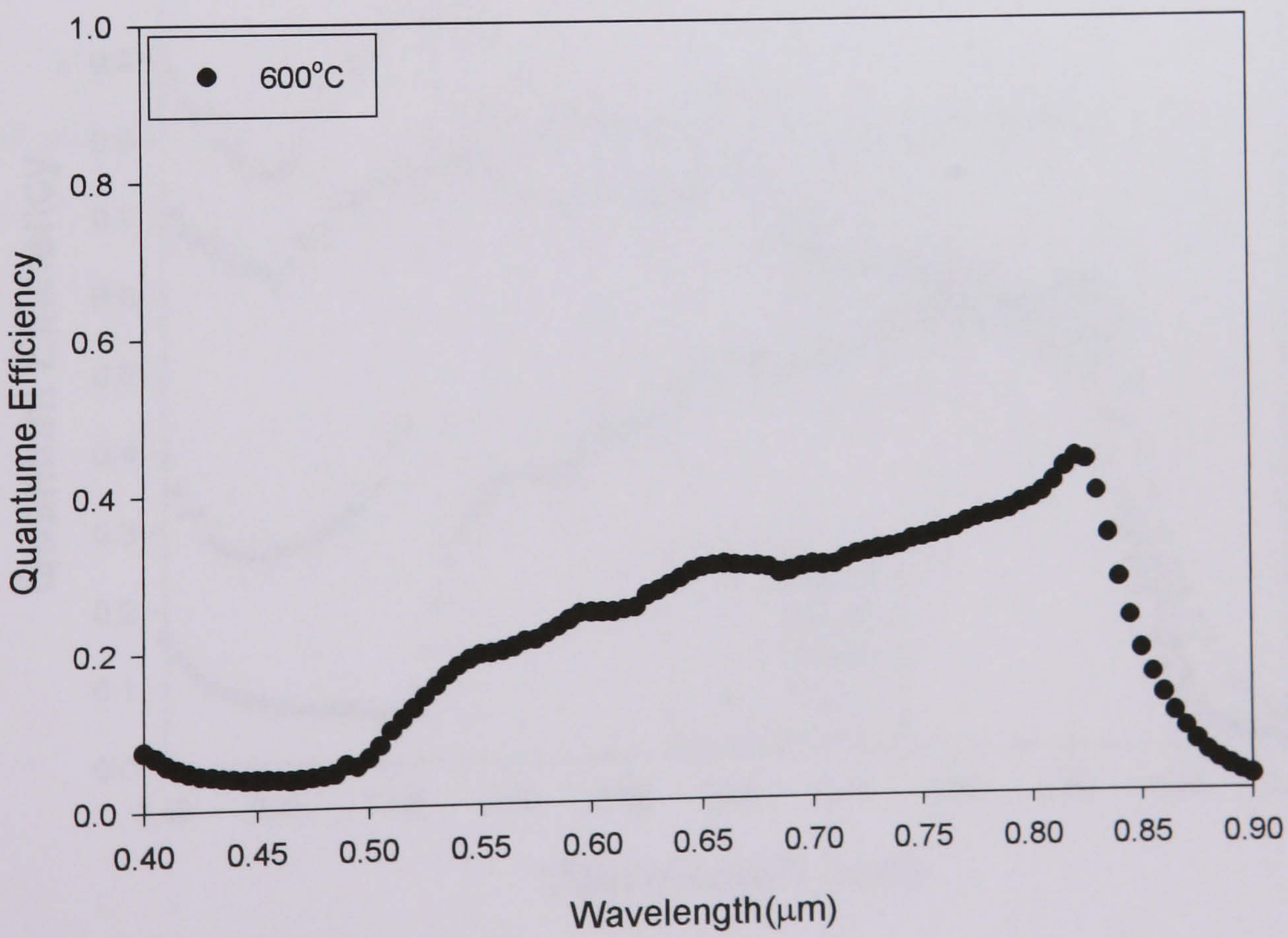

6.7- The Spectral Response of Solar Cells Fabricated with Different Thickness of CdS Layer.

To investigate the effect of the CdS thickness on the spectral response of CdS/CdTe cells, several cells were fabricated with different thickness of CdS layer: 100, 150, 250 and 1100 nm. As discussed in section 5.2.2, it was difficult to obtain a precise estimate for the thickness of the CdS layer, and the quoted layer thickness should be treated therefore as nominal.

Figure (6-8) shows the spectral responses of these solar cells. The quantum efficiency curves of the cells, with thinner CdS layer 100 and 150 nm, is very high at short wavelengths but declines progressively at longer wavelengths. The quantum efficiency of 250nm CdS cell is lower at short wavelength with a clear cut off at 510 nm corresponding to the CdS bandgap, but has the best performance at long wavelengths.

Figure (6-8)-The spectral response for solar cells with different thicknesses of CdS.

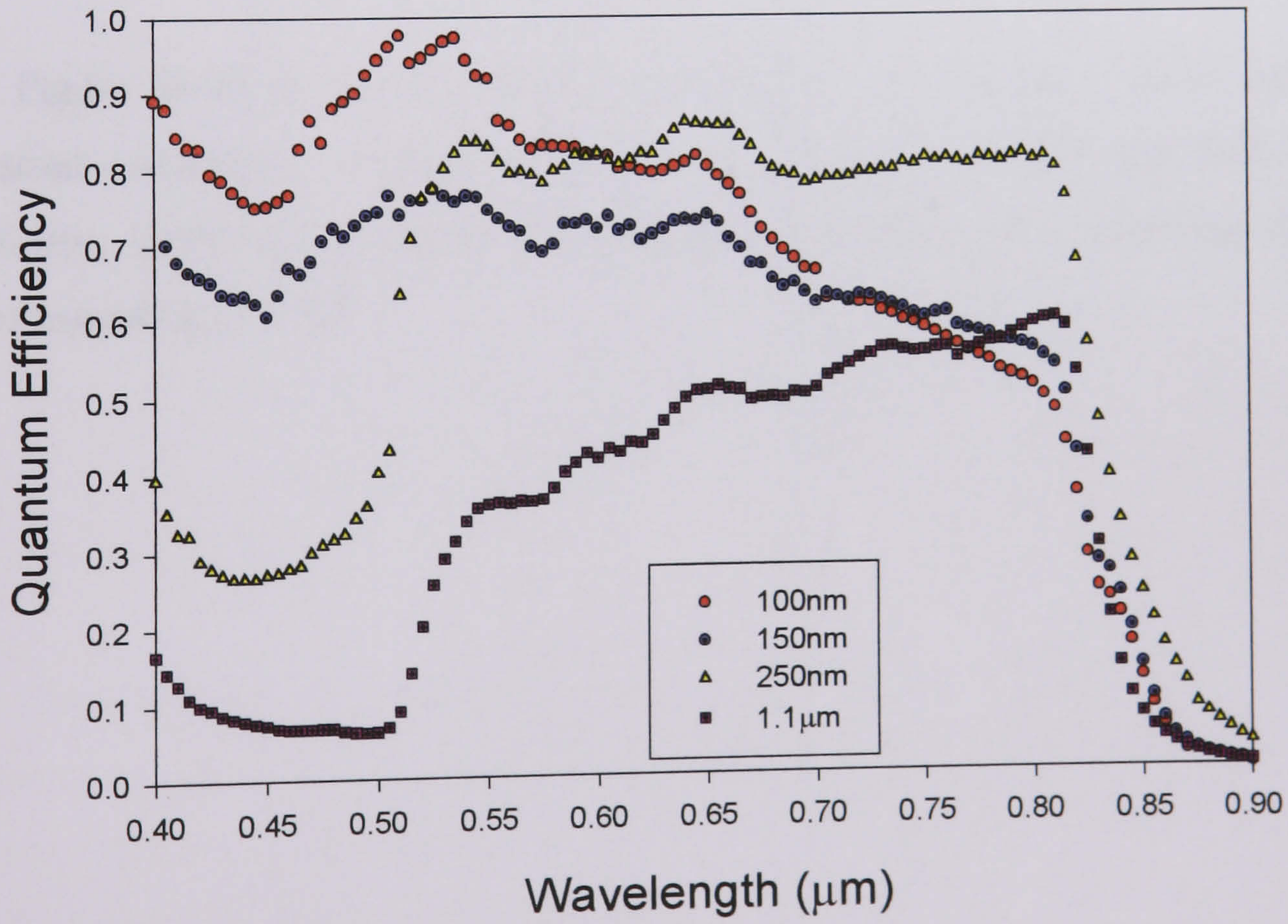

The quantum efficiency of the 1100nm CdS cell has the lowest values at short wavelengths but increases with increasing wavelengths, in contrast to the behaviour of cells with thinner CdS layers. Figure (5-8) indicates that the quantum efficiency decreases above the band gap of CdS as the thickness of the CdS increases [19][9][20][21][22] as would be expected since thinner layers would be less absorbing (equation 2.29). The short wavelength response is higher for the thinner CdS cells because more high energy photons are able to reach the CdTe film [23].

The thickness of the CdS is a very important parameter for good cell efficiency. In practice the choice of thickness will be a compromise because while a thin CdS layer may give a good value of short circuit current particularly at short wavelength as is clear from the spectral response, such cells tend to have low values of open circuit voltage and fill factor (see chapter 5), in contrast a thick film gives a low value of short circuit current but with good values of open circuit current and fill factor. The thick film gives very low value of short circuit current because it prevents photogeneration at wavelengths below the CdS band edge (~ 510nm) and reduces the photogeneration above it as is clear from the spectral response measurement. It would seem that a CdS layer thickness of around 250 nm is the optimum thickness for our cells.

Figure (6-9) shows the spectral response for a cell made under optimum preparation conditions; ~250nm and ~5μm the thickness of CdS and CdTe layer respectively, 500°C CdTe deposition temperature, ~100nm $CdCl_2$ thickness and 30 minutes annealing at 400°C.

Figure (6-9)- The spectral response for a cell prepared under optimum conditions.

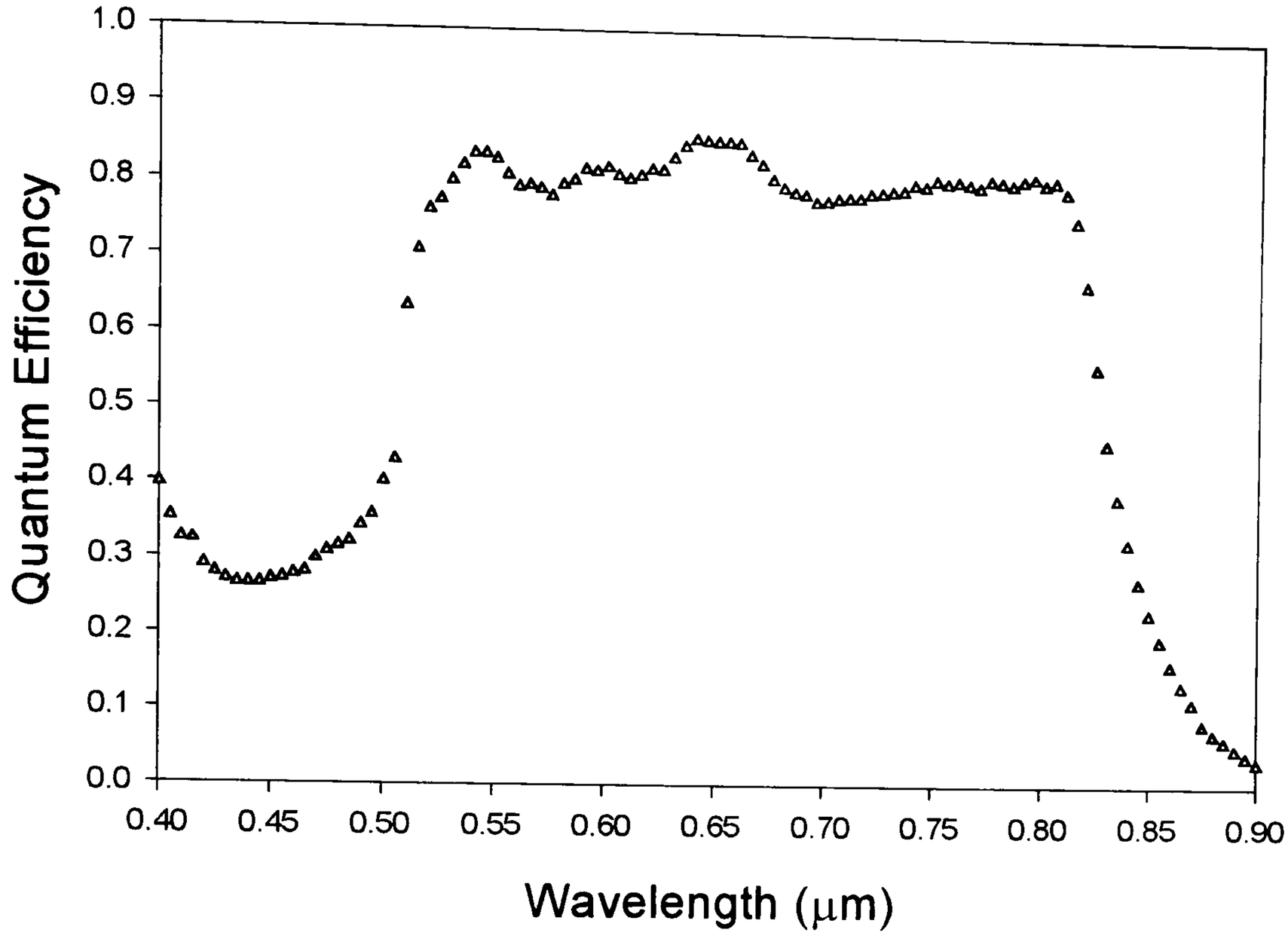

6.8- Conclusions:

The interdiffusion between the CdS and CdTe layers plays a crucial role in the performance of CdS/CdTe solar cells. It has a strong influence on the photogeneration of the cell at each wavelength, as shown in the spectral response measurements. The interdiffusion between the CdS and CdTe layers, which occurs during cell fabrication, results in a graded interface CdS_xTe_{1-x} layer, which is S-rich on the CdS side and Te-rich on the CdTe side. In effect this gives two different compositions at the interface between CdTe and CdS.

The existence of these layers in the interface between the CdS and CdTe may contribute to a reduction in the lattice mismatch between CdS and CdTe [24] [25]. More importantly the band gap of CdS_xTe_{1-x} has a quadratic variation with composition [2] [25] [26] [27] according to the following expression:

$$E(x) = E_2 + (E_1 - E_2 - b)\,x + bx^2 \qquad (6.1)$$

Where E_1 and E_2 are the band gap of CdS and CdTe films respectively and b is a bowing parameter, reported by Pal et al [27] to be 1.7eV,. Figure (6-11) shows the variation of the energy gap with the composition x as given by this equation.

Figure (6-11)-The bangap of CdS_xTe_{1-x} versus X.

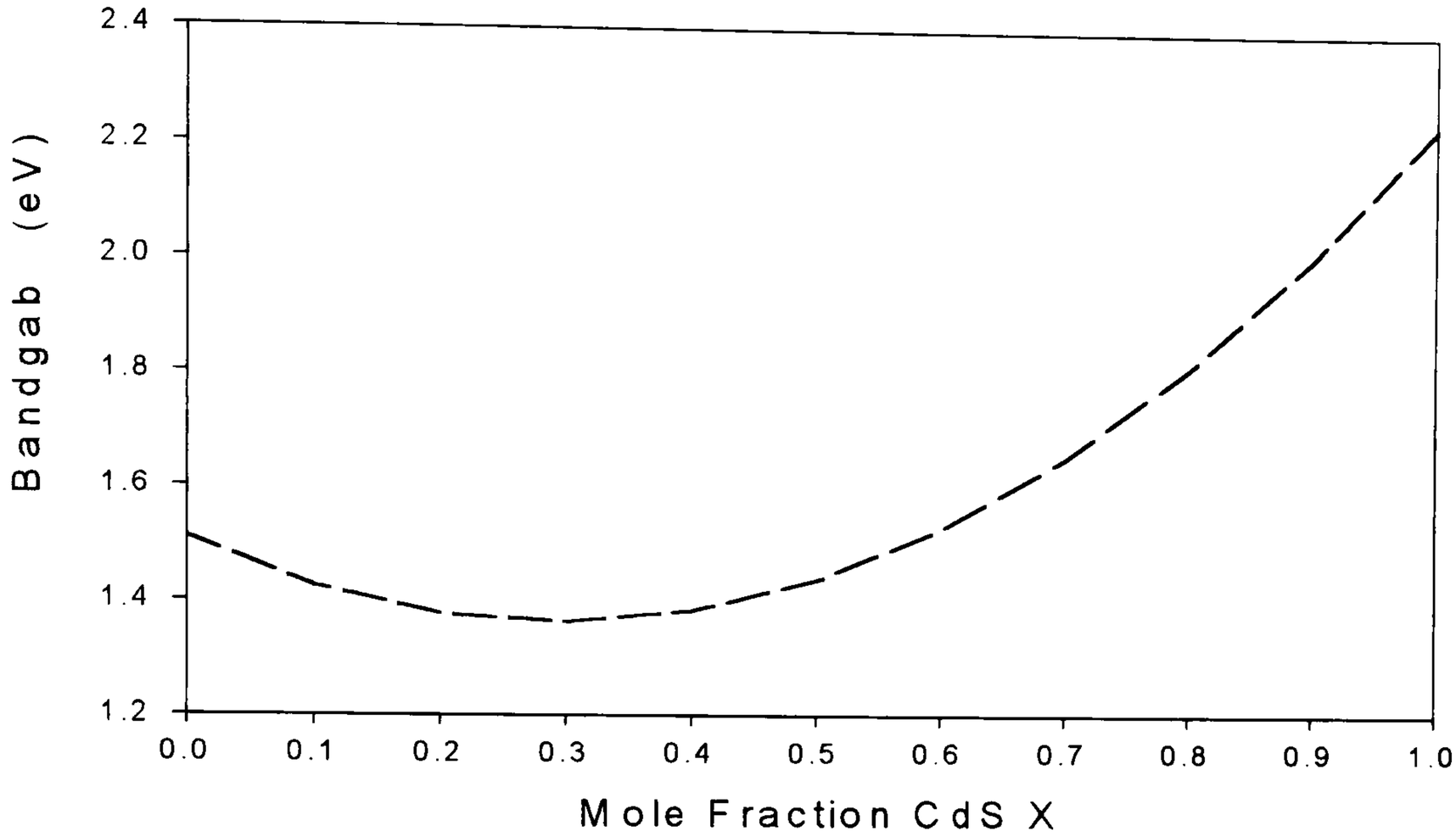

This shows that the bandgap of $CdTe_{1-x}$ S_x is reduced below the bandgap of CdTe for $0.3 \geq x > 0$, i.e. for Te-rich compositions, explaining the shift to longer wavelengths of the spectral response. So the diffusion of S to CdTe is desirable until $x \approx 0.3$ as this increases the absorption of photons with energy below the band gap of the CdTe layer. On the other hand the diffusion of Te into the CdS layer is undesirable because it reduces the window layer bandgap, consequently increasing the window layer absorption of photons with energy below the band gap of CdS. Unfortunately during the preparation of CdS/CdTe the interdiffusion between CdS and CdTe is mutual.

There are many preparation parameters which effect the interdiffusion between the CdTe and CdS layer, and so modify the spectral response. Interdiffusion is increased by:

- $CdCl_2$ treatment;
- the thickness of $CdCl_2$ used in treatment;
- the annealing time;
- the substrate temperature used during deposition of the CdTe;

Treatment of the CdS layer with $CdCl_2$ prior to CdTe deposition, may also enhance the diffusion of Te into CdS during subsequent CdTe deposition. However, our result are not conclusive and this issue remains undecided. Reports in the literature are equally conflicting. Uda et al [7] have reported that the presence of residual amounts of Cl ions in the CdS film might be expected to enhance interdiffusion in the CdS/CdTe prepared by sequential screen printing and sintering steps. In contrast Jensen et al [28] reported that pre-treatment of CdS prior to deposition of CdTe limited the diffusion of Te into the window layer.

The spectral response at wavelengths below the CdS band edge decreased as the CdS layer thickness increased as expected.

6.9-References.

(1)- Kim W. Mitchell. "Evaluation of the CdS/CdTe Heterojunction Solar Cell". Garland Publishing, Inc., New York & London (1979).

(2)- K. Ohata, J. Saraie and T. Tanaka. "Optical Energy Gap of the Mixed Crystal CdS_xTe_{1-x}". Japan. J. Appl. Phys.12 (1973) 1641.

(3)- K. Ohata, J. Saraie and T. Tanaka." Phase Diagram of the CdS-CdTe Pseudobinary System". Japan. J. Appl. Phys.12 (1973) 1198.

(4)- S. A. Galloway, A. W. Brinkman, K. Durose, P. R. Wilshaw and A. J. Holland. "A Study of the Effects of Post-Deposition Treatment on CdS/CdTe Thin Film Solar Cells using High Resolution Optical Beam Induced Current". Appl. Phys. Lett, 68 (1996) 3725.

(5)- A. Niemegeers, M. Burgelman, H. Richter and D. Bonnet. "A Simple Model for the Effects of the $CdCl_2$ Treatment on the Performance of CdTe/CdS Solar Cells". 14th European Photovoltaic Solar Energy Conf., Barcelona Spain (1997).

(6)- D. Bonnet, B. Henrichs and H. Richter. "Some Phenomena in CdTe/CdS Thin Film Solar Cells Made by Close-Spaced Sublimation". Int. J. Solar Energy, 12 (1992) 133.

(7)- H. Uda, H. Sonomura and S. Ikegami. "Screen Printed CdS/CdTe Cells for Visible-Light-Radiation Sensor". Meas. Sci. Technol., 8 (1997) 86.

(8)- J. S. Lee, H. B. Im, " Effects of Junction Formation Condition on the Photovoltaic Properties of Sintered CdS/CdTe Solar Cells". Journal of Materials Science, 21 (1986) 980.

(9)- R. W. Birkmire, B. E. McCandless and S. S. Hegedus. "Effects of Processing on CdTe/CdS Materials and Devices". Int. J. Solar Energy, 12 (1992) 145.

(10)- S. A. Ringel, A.W. Smith, M. H. MacDougal and A.Rohatgi. "The Effects of $CdCl_2$ on the Electronic Properties of Molecular-Beam Epitaxally Grown CdTe/CdS Heterojunction Solar Cells". J. Appl. Phys. 70 (1991) 881.

(11)- T. L. Chu and S. S. Chu. "Thin Film II-VI Photovoltaics". J. Solid State Electronics, 38(1995) 533.

(12)- T. L. Chu, S. S. Chu, J. Britt, C. Ferekides, C. Wang, C. Q. Wu and H. S. Ullal. "14.6% Efficient Thin – Film Cadmium Telluride Heterojunction Solar Cells". IEEE Electron Device Let.,13 (1992) 303.

(13)- T. Toyama, T. Yammamoto and H. Okamoto. " Interfacial Mixed-Crystal Layer in CdS/CdTe Heterostructure Elucidated by Electroreflectance Spectroscopy". Solar Energy Mater. and Solar Cells 49 (1997) 213.

(14)- B. E. McCandless, L. V. Moulton and R. W. Brikmire. "Recrystallization and Sulphur Diffusion in $CdCl_2$-Treated CdTe/CdS Thin Film". Prog. Photovoltaic: Res. and Appl., 5 (1997) 149.

(15)- I. Clemminck, M. Burgelman, M. Casteleyn and B. Depuydt. "Screen Printed and Sintered CdTe-CdS Solar Cells ". Int. J. Solar Energy, 12 (1992) 67.

(16)- R. G. Dhere, D. S. Albin, D. H. Rose, S. E. Asher, K. M. Jones, M. M. Al-jassim, H. R. Moutinho, and P. Sheldon. "Intermixing at the CdS/CdTe Interface and its Effect on Device Performance". Mater. Res. Symp. Proc., 426 (1996) 361.

(17)- X. Li, D. Albin, S. Asher, H. Moutinho, B. Keyes, R. Matson, F. Hasoon, and P. Sheldon. "The Effect of Substrate Temperature on Material Properties and Device Performance of Close-Space Sublimation Deposited CdTe/CdS Devices". AIP Conf. Proc. 353, 1 (1996) 376.

(18)- C. S. Ferekides, B. Tetali, D. Marinskiy, S. Marinskaya, and D. Morel. "Effects of Processing Temperature on the Thickness of CdS and the Performance of CdTe Solar Cells". 14th Conf. NREl/SNL Photovoltaics Program Rev., (1996) 631.

(19)- K. Zweibel, H. S. Ullal, L. Mitchell, and R. Noufi. "The U.S. DOE/NREL Polycrystalline Thin Film Photovoltaic Project". 22nd IEEE Photovoltaic Specialists Conf., Las Vegas Nevada, (1991) 1057.

(20)- C. Ferekides, J. Britt, Y. Ma, and L. Killian. "High Efficiency CdTe Solar Cells by Close Space Sublimation". 23rd IEEE Photovoltaic Specialist Conf., (1993) 389.

(21)- J. E. Granata, J. R. Sites, G. Contreras-Puente, and A. D. Compaan. "Effect of CdS Thickness on CdS/CdTe Quantum Efficiency". 25th IEEE Photovoltaic Specialist Conf., Washington DC, (1996) 853.

(22)- C. S. Ferekides, K. Dugan, V. Ceekala, J. Killian, and D. Oman. "The Effect of CdS Processing and Glass Substrates on the Performance of the CdTe Solar Cells". 1st Word Conf. Photovoltaic Energy Conversion, Hawaii, 1 (1994) 99.

(23)- A. Rohatgi, "A Study of Efficiency Limiting Defects in Polycrystalline CdTe/CdS Solar Cell". Int. J. Solar Energy, 12 (1992) 37.

(24)- N. Nakayama, H. Matsumoto, A. Nakano, S. Ikegami, H. Uda, and T. Yamashita. "Screen Printed Thin Film CdS/CdTe Solar Cell". Japan. J. App. Phys., 19 (1980) 703.

(25)- R. Radojcic, A. E. Hill, and M. J. Hampshire. "Preparation and Properties of Mixed CdS_xTe_{1-x} Thin Films". Solar Cells, 4 (1981) 101.

(26)- R. Hill, and D. Richardson. " The Variation of Energy Gap with Composition in ZnS-Te Alloys". J. Phys. C: Solid State Phys., 6 (1973) L115.

(27)- R. Pal, J. Dutta, S. Chaudhuri, and A. K. Pal. "CdS_xTe_{1-x} Films: Preparation and Properties". J. Phys. D: Appl. Phys., 26 (1993) 704.

(28)- D. G. Jensen, B. E. McCandless, R. W. Birkmire. " Thin- Film Cadmium Sulfide/ Cadmium Alloys". Mat. Res. Soc. Symp. Proc. Vol.426, (1996) 325.

Chapter Seven:

Capacitance and Electroluminescence Measurements.

7.1- Introduction:

The effect of $CdCl_2$ treatment of CdS and CdTe on some of the properties of CdS/CdTe solar cells such as depletion width W_o, the acceptor concentration N_A and the built–in-junction potential V_b were investigated by measurements and analysis of C-V characteristics.

Some traps levels have been determined using photocapacitance measurements. The electroluminescence spectrum of CdS/CdTe solar cells at different temperatures has been compared with the corresponding bandgaps of CdS and CdTe.

7.2- Capacitance –Voltage Characteristics.

7.2.1-Room Temperature Measurements.

To investigate the effects of $CdCl_2$ treatment on the depletion layer width W_o and the ionised acceptor concentration N_A, capacitance-voltage characteristics of untreated CdS/untreated CdTe, untreated CdS/treated CdTe, and treated CdS/ treated CdTe cells were carried out in the dark at room temperature. A typical set of C^{-2} versus voltage plots of the three types of cell is illustrated in figure (7-1). The ionised acceptor concentration N_A, obtained from the slopes of linear section at low voltage bias, built–in-junction potential V_b, and the depletion layer width W_o (using a one side junction approximation, i.e. $[C/V]_{V=o} = \varepsilon_o \varepsilon_s / W_o$) are listed in table (7-1). The measurements were taken at 1MHz. The values of depletion width of treated CdTe and untreated cells are in good agreement with the values used for the simulation of the spectral response in chapter 6. The values of N_A and V_b of treated CdTe are close to values reported by Singth et al. [1] and Tang et al.[2].

The values V_b obtained from the conventional analysis of the C^{-2}-V curves in figure (7-1) are unrealistically large and suggest that the characteristics are dominated by interface states [3]. If this is the case the estimates for N_A may also be unreliable and this might explain their low magnitude. Closer inspection of the C^{-2}-V characteristics reveal that they are not completely straight lines as reported by other workers [4] [5], providing further confirmation of the presence of non-ideal junction. This may indicate the presence of interface states and /or inhomogeneous acceptor distribution [6]. Nevertheless, the C^{-2}-V curves provide a signature for the devices.

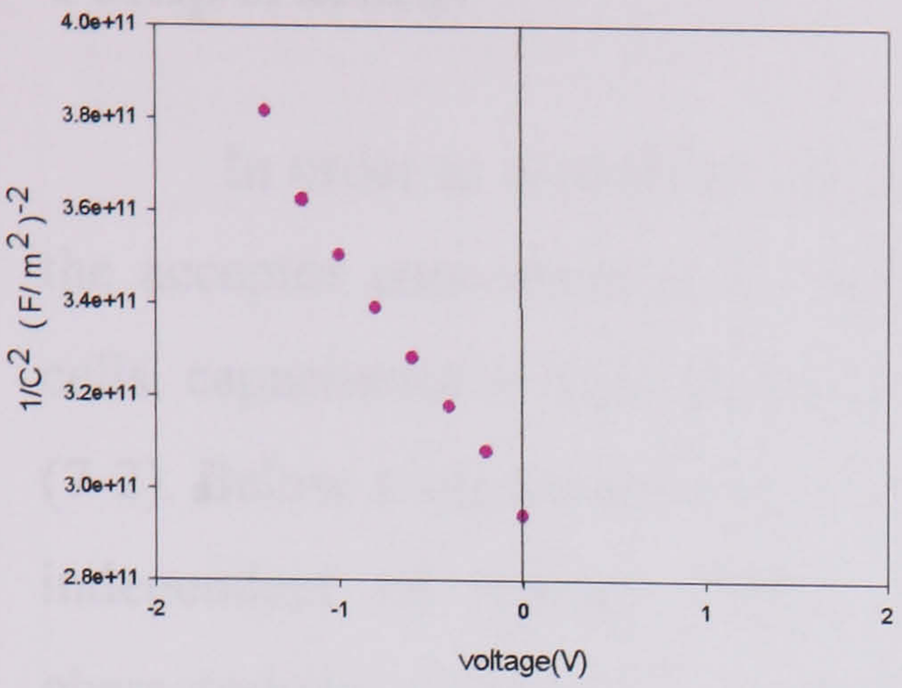

(A)

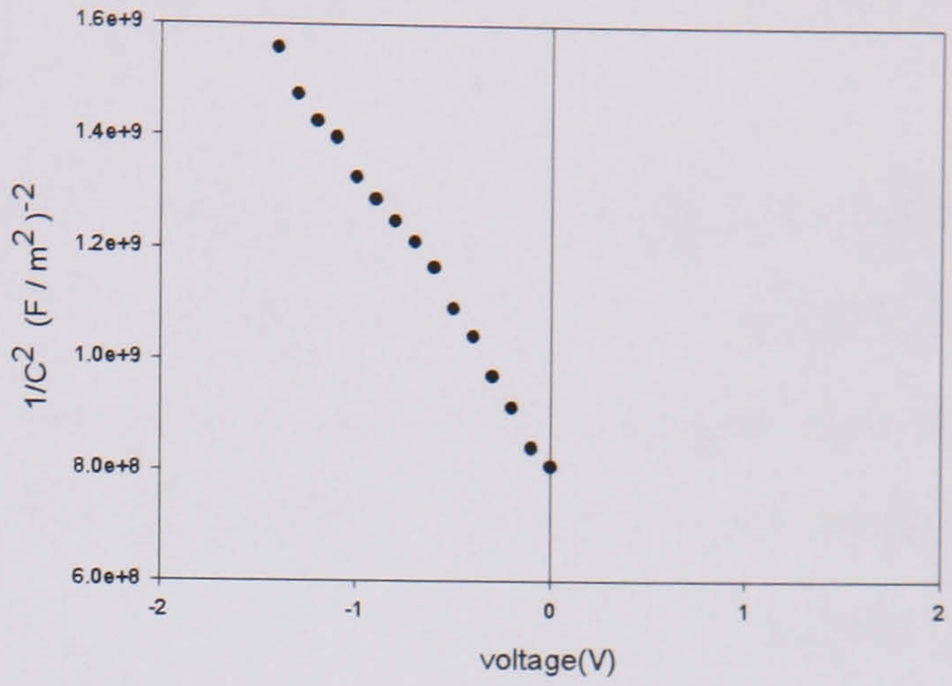

(B)

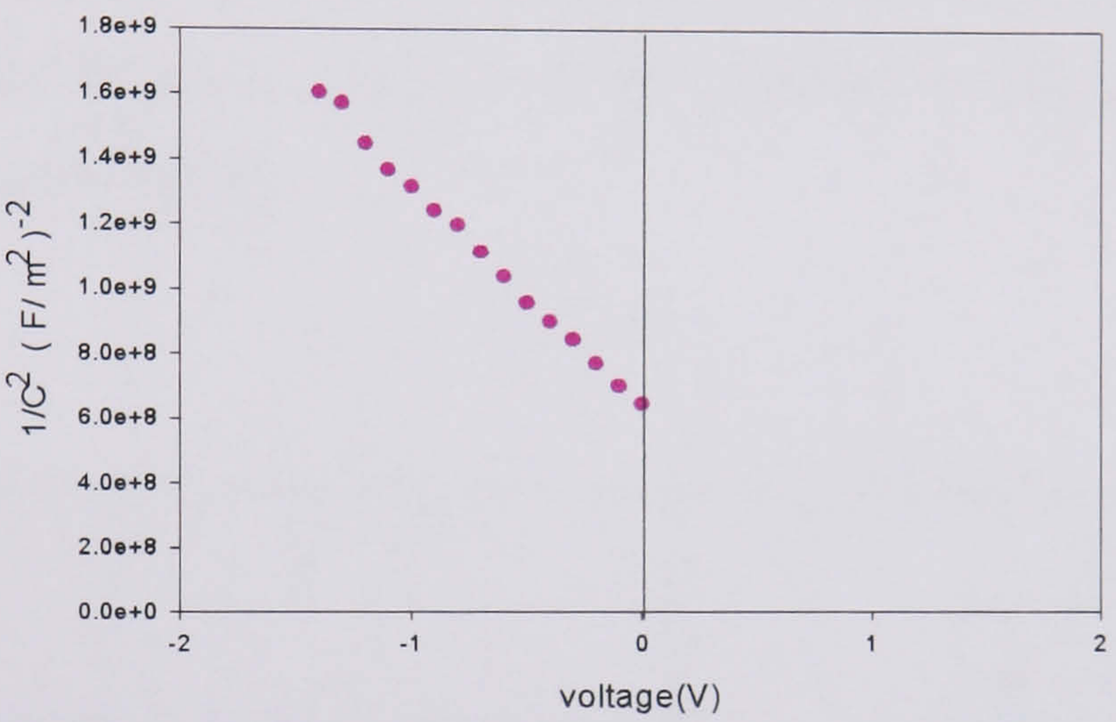

(C)

Figure (7-1)- C^{-2} vs. voltage of; (A) untreated cell, (B)- untreated CdS/treated CdTe, (C)-treated CdS/treated CdTe.

sample	N_A (cm^{-3})	V_b (V)	W_o (μm)
Untreated	2.2×10^{12}	5.3	0.525
Treated CdTe	2.19×10^{14}	1.3	2.6
Treated CdTe&CdS	2.1×10^{14}	0.95	2.3

Table (7-1)- Acceptor density N_A, built–in-junction potential V_b, depletion width W_o values of the three samples in figure (7-1).

7.2.2- Capacitance–Voltage Measurements as a Function of Temperature.

In order to investigate the variation with temperature of the depletion width W_o, the acceptor concentration N_A and the built–in-junction potential V_b of treated CdTe cells, capacitance-voltage characteristics were measured at several temperatures, figure (7-2). Below a temperature of ~190K, it was found that the capacitance was essentially independent of voltage and so only values of W_o, V_b and N_A deduced from characteristics measured at temperatures above 224K are listed in table (7-2). Ionised acceptor concentration would appear to have increased slightly with increasing temperature, whereas, W_o and V_b both decreased with increasing temperature. The decrease in W_o was expected because of the increase in the carrier density as the temperature was raised [7] [8].

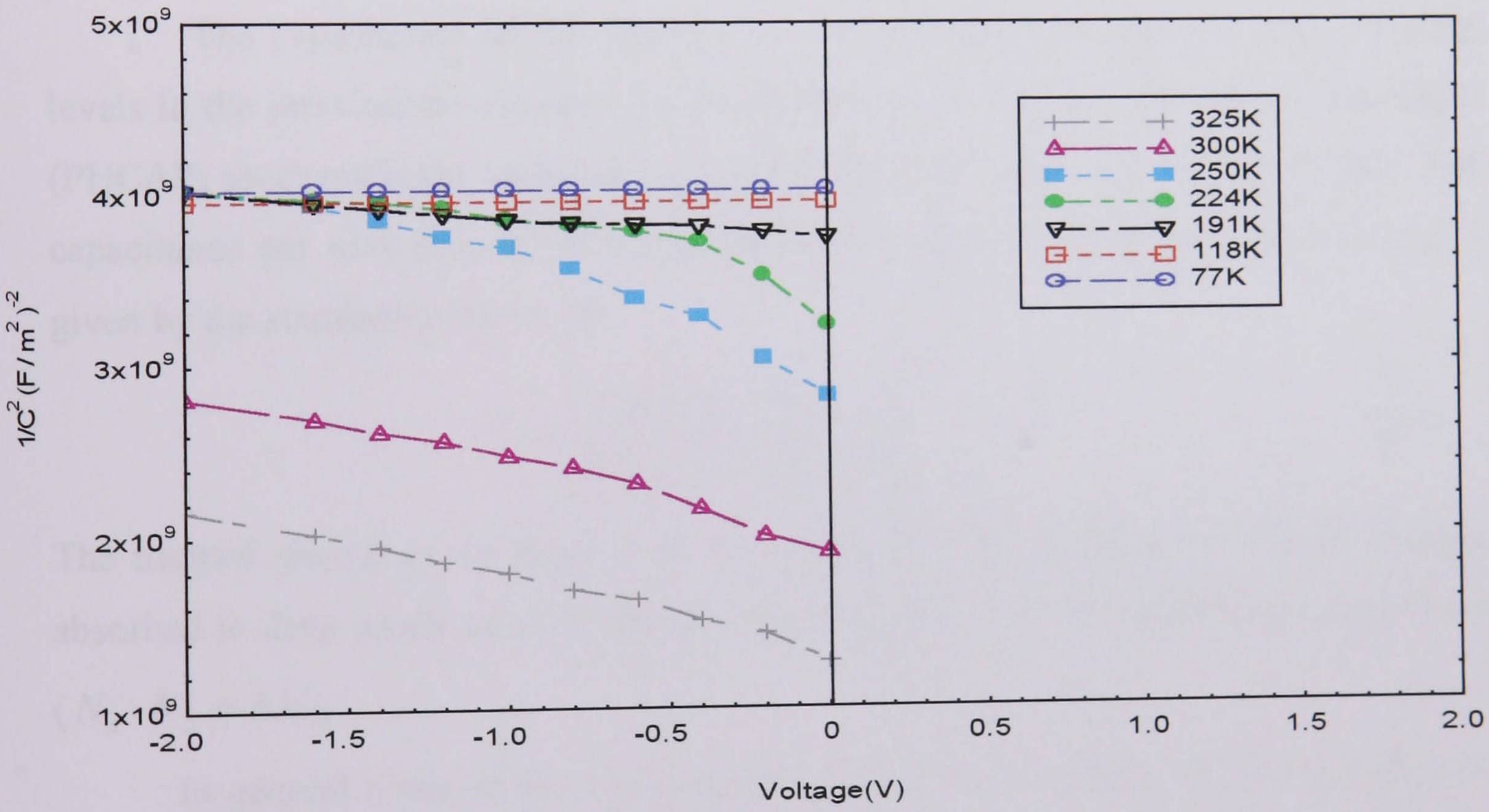

Figure (7-2)- $C^{-2} - V$ Characteristics for a treated CdTe cell at different temperatures.

Table (7-2) –The values of N_A, W_o and V_b of treated CdTe solar cell at different temperatures.

Temperature (K)	$N_A(cm^{-3})$	$W_o(\mu m)$	V_b (V)
77	-	5.8	-
118	-	5.7	-
191	-	5.6	-
224	1.1×10^{14}	5.2	2.5
250	2.6×10^{14}	4.8	2.4
300	3.6×10^{14}	3.9	2.3
325	3.3×10^{14}	3.2	2

7.3- The Photocapacitance Measurements:

The capacitance of the junction is changed when the charge states of deep levels in the junction are changed by the absorption of photons. The photocapacitance (PHCAP) spectrum is the variation in the junction capacitance with photon energy. The capacitance per unit area of the diode depletion region in a p-type semiconductor is given by the standard relation: [9]

$$C = \left[\frac{q\varepsilon_s (N_a^- - N_d^+)}{2(V_d + V_r - kT/q)} \right]^{1/2} \qquad (7.1)$$

The trapped charge in the deep level can also effect the capacitance because if light absorbed in deep levels gives a change in charge ΔN_t, thus the capacitance depend on $(N_a^- - N_d^+ \pm \Delta N_t)$.

In general a rise in the capacitance corresponds to the either the excitation of electrons from an electron trap to the conduction band [10] in an n-type semiconductor or to the emptying of hole traps in a p-type semiconductor, whereas a fall in capacitance corresponds to the capture of electrons by a trap (in an n-type material) or to the capture of holes by a holes trap from the valance band (in p-type).

The spectral response of the photocapacitance of a treated solar cell was carried out at 200K and at room temperature. The wavelengths of the light was scanned very

slowly from long, 2000nm, to short, 414nm, wavelengths. At temperatures lower than 200K, the capacitance was independent of the wavelength. Figure (7-3) and figure (7-4) show the photocapacitance of a treated solar cell at 200K and room temperature respectively.

Figure (7-3)- Photocapacitance of treated CdTe solar cell at 200K.

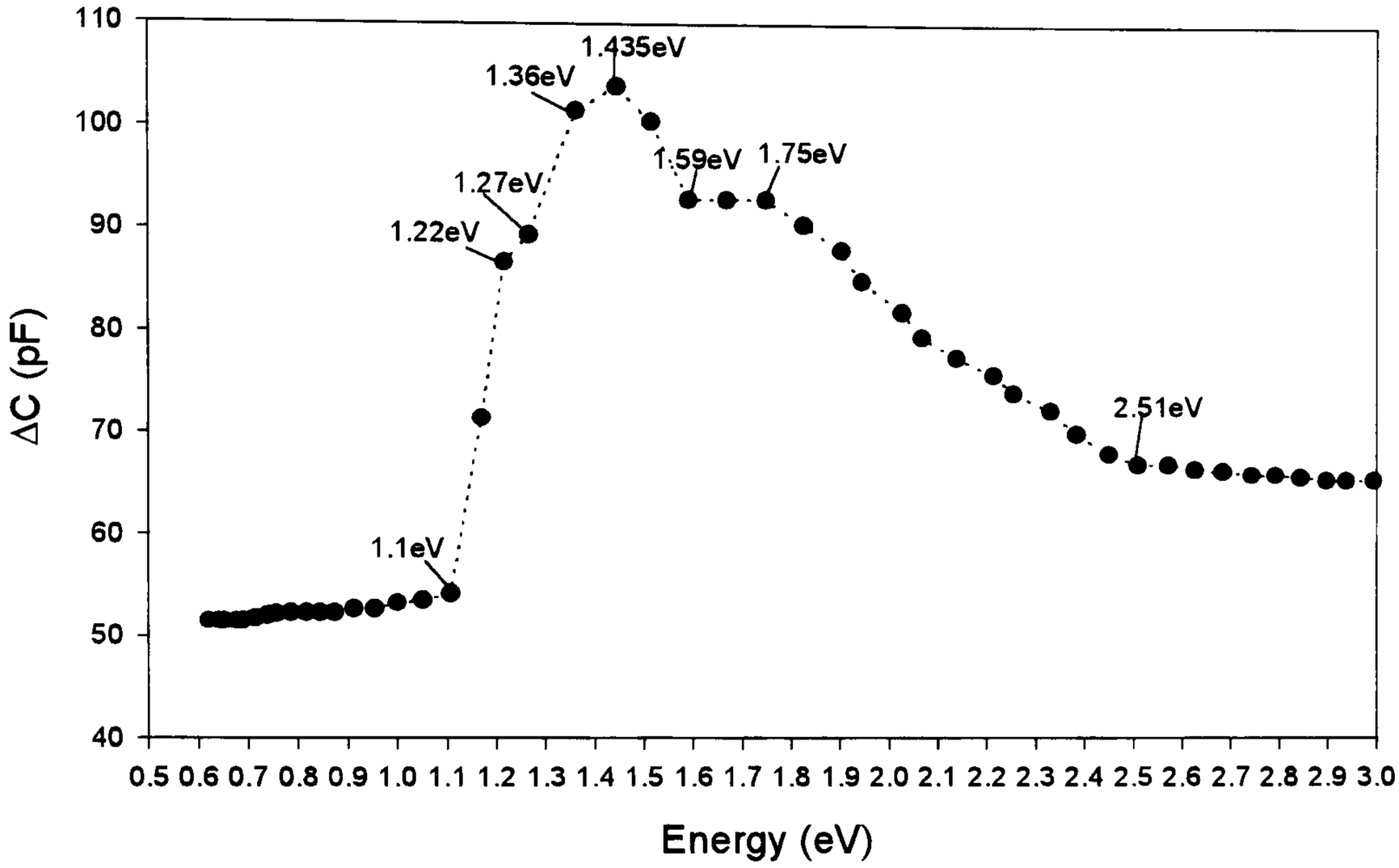

Figure (7-4) –Photocapacitance of treated CdTe solar cell at room temperature.

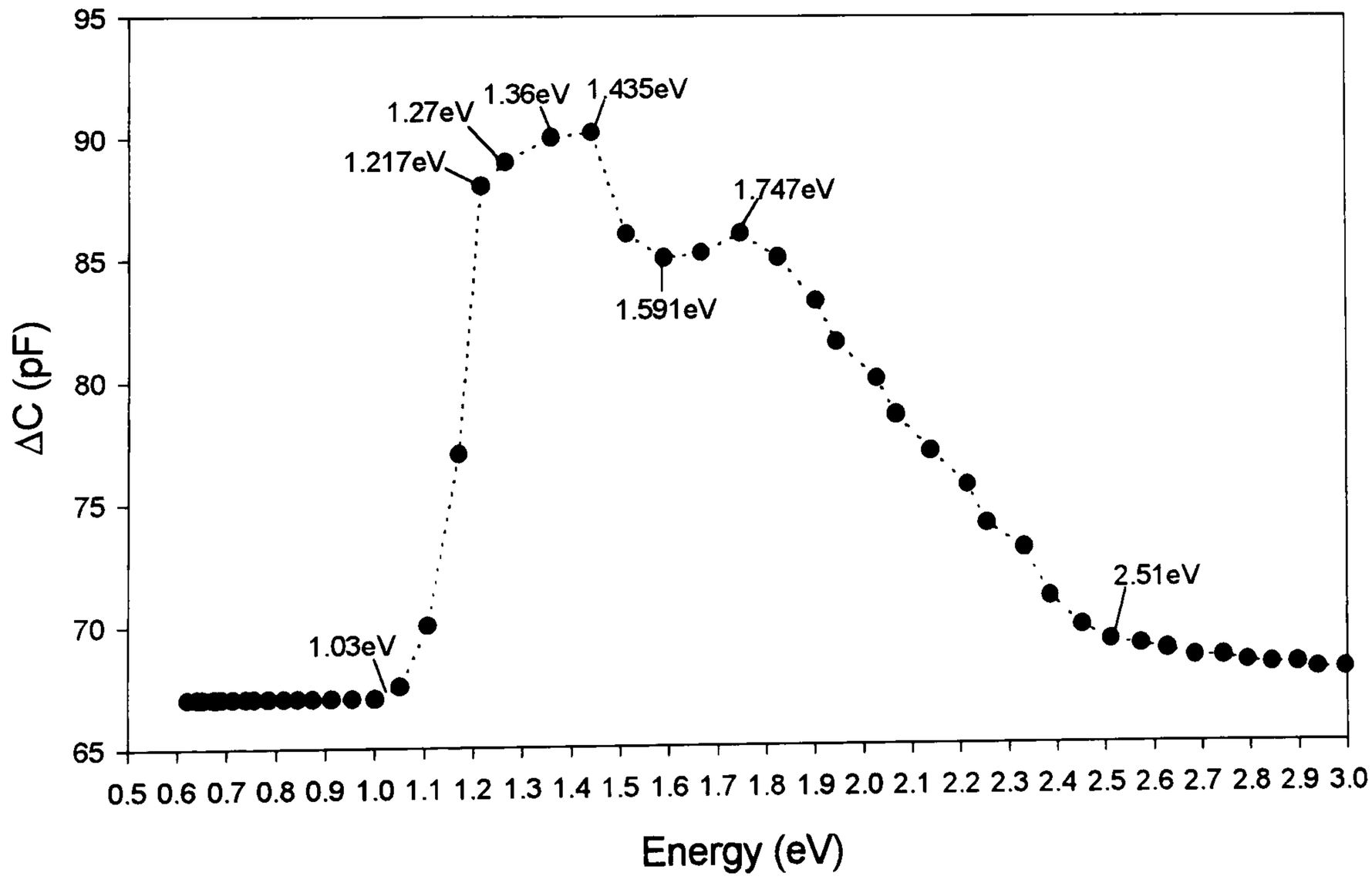

The photocapacitance measurements give essentially the same results at 200K and at room temperature with slight differences between 1.22eV and 1.435eV and a shift to lower energy of the first threshold. The threshold values occurred at 1.1, 1.22, 1.27, 1.36, 1.59 and 1.75 eV. The deep centres identified from the photocapacitance spectra are summarised in figure (7-5) in the form of band diagrams which show the transitions. Values in brackets correspond to the threshold energies at room temperature. Figure (7-5) shows that some levels below the conduction at ~ 0.4, 0.2 eV in p-CdTe and at 0.55eV in n-CdS, also some levels above the valance band at 0.24, 0.1 eV in p-CdTe and 0.71eV in n-CdS.

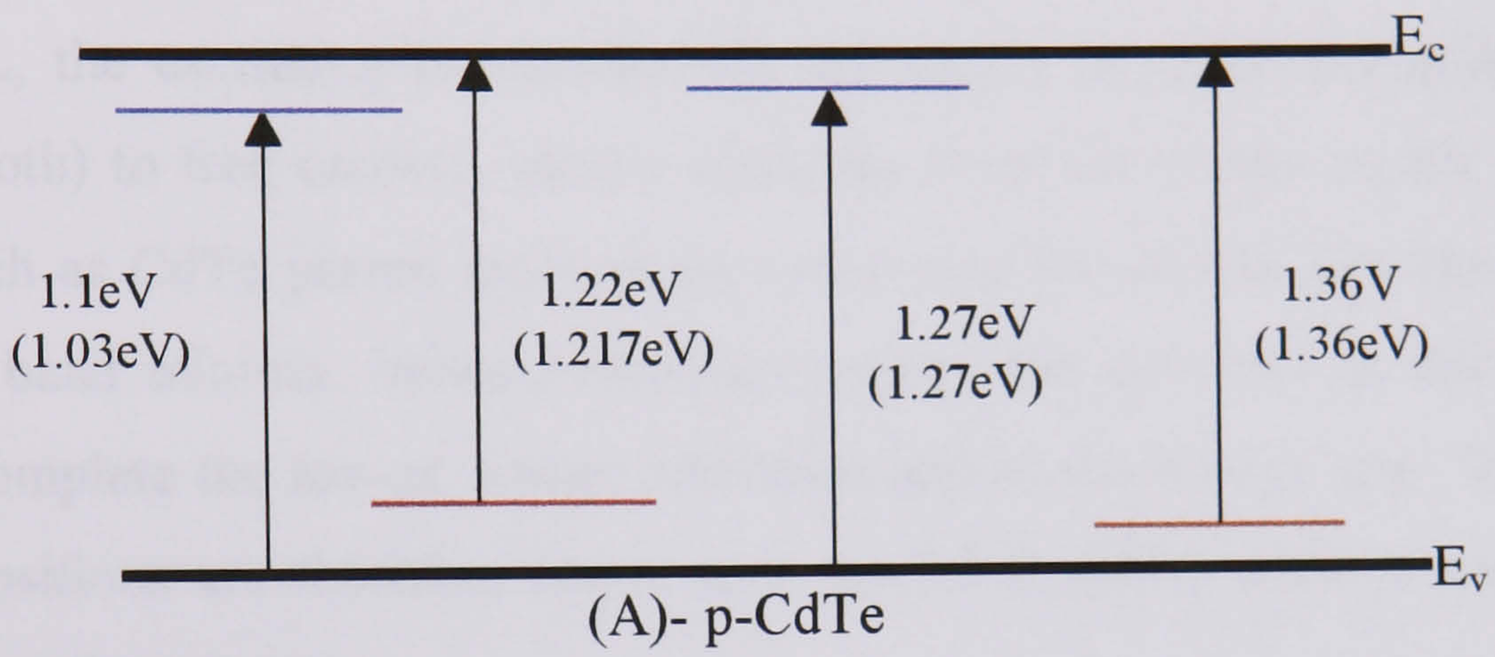

Figure (7-5)- Band diagrams show the transitions in CdTe (A) and CdS (B).

7.4-The Electroluminescence Measurements.

Electroluminescence (EL) is the direct conversion of electrical energy into light by electron-hole recombination as distinct from incandescence. Under forward bias minority carrier injection is increased dramatically (electrons from n-type to p-type regions and holes from p-type to n-type regions) because the net restraining field is reduced and the concentration of minority carriers on both sides of the junction increases very rapidly. As a result of carrier injection there is a region, centred on the depletion layer in which there is a high density of both electrons and holes; if these carriers can recombine radiatively then EL will result [11].

In EL, the excitation is provided by the supply of either potential or kinetic energy (or both) to free carriers, mostly electrons from the power supply. Direct gap materials such as CdTe permit momentum conserving transitions between conduction and valance band minima. Indirect materials require the emission or absorption of a phonon to complete the lowest energy transition across the energy gap. Band-to-band radiative transitions are therefore much more probable across a direct rather than an indirect gap semiconductor.

The Electroluminescence measurements of a treated CdTe cell were carried out at different temperatures of 10, 30, 50, 100 and 200K. The Electroluminescence emission spectrum was observed by pulsing currents of up to 15mA through the device for a period of approximately 10ms. Figure (7-6) shows the Electroluminescence at the different temperatures. The intensity peaks varied from 1.457 eV at 10K to 1.4597 eV at 200K. These variations are very small indicating that the peak intensity is temperature independent in this range of temperature. The bandgap of CdTe and CdS were calculated according to the following equations:[12] [13]

$$E_{CdTe}\,(eV) = -3.1\times10^{-4}\,T(K) + 1.523 \qquad (7.5)$$

$$E_{CdS}\,(eV) = -4.1\times10^{-4}\,T(K) + 2.378 \qquad (7.6)$$

The differences between the peak photon energy and the bandgap of CdTe and CdS are illustrated in figure (7-7) and figure (7-8) respectively. The differences between the CdTe bandgap and the peak reduces as the temperature increases because the peaks

were nearly constant with the temperature, whereas the CdTe bandgap decreases as the temperature increases according to equation (7.5). The peak of intensity at 200K is very close to the bandgap of CdTe (1.4597). Figure (7-8) shows the differences between the peak and the bandgap of CdS are higher compared to the CdTe bandgap which indicate that the detected Electroluminescence spectrum is probably due to the transition of excited electrons from the conduction band to the valance band in CdTe.

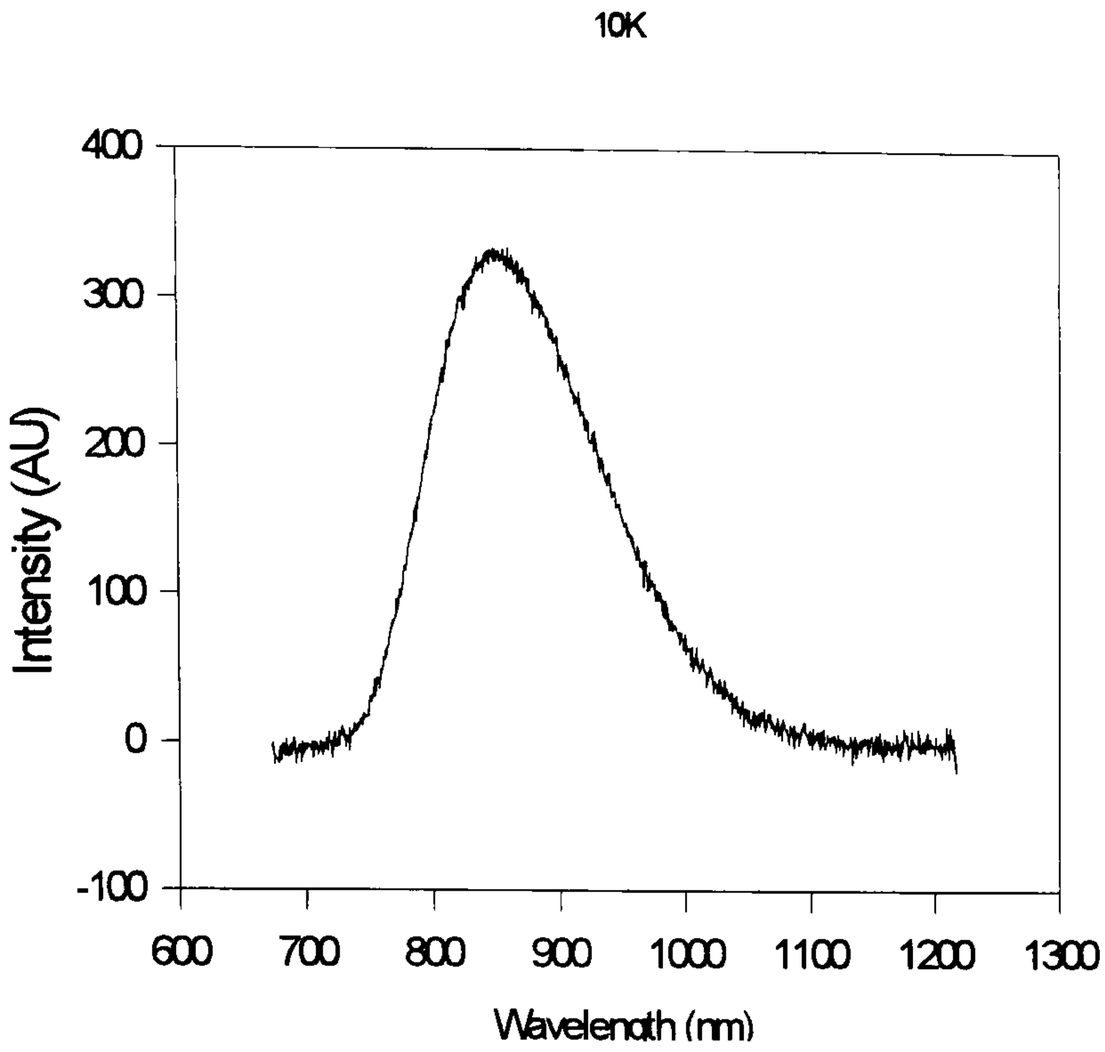

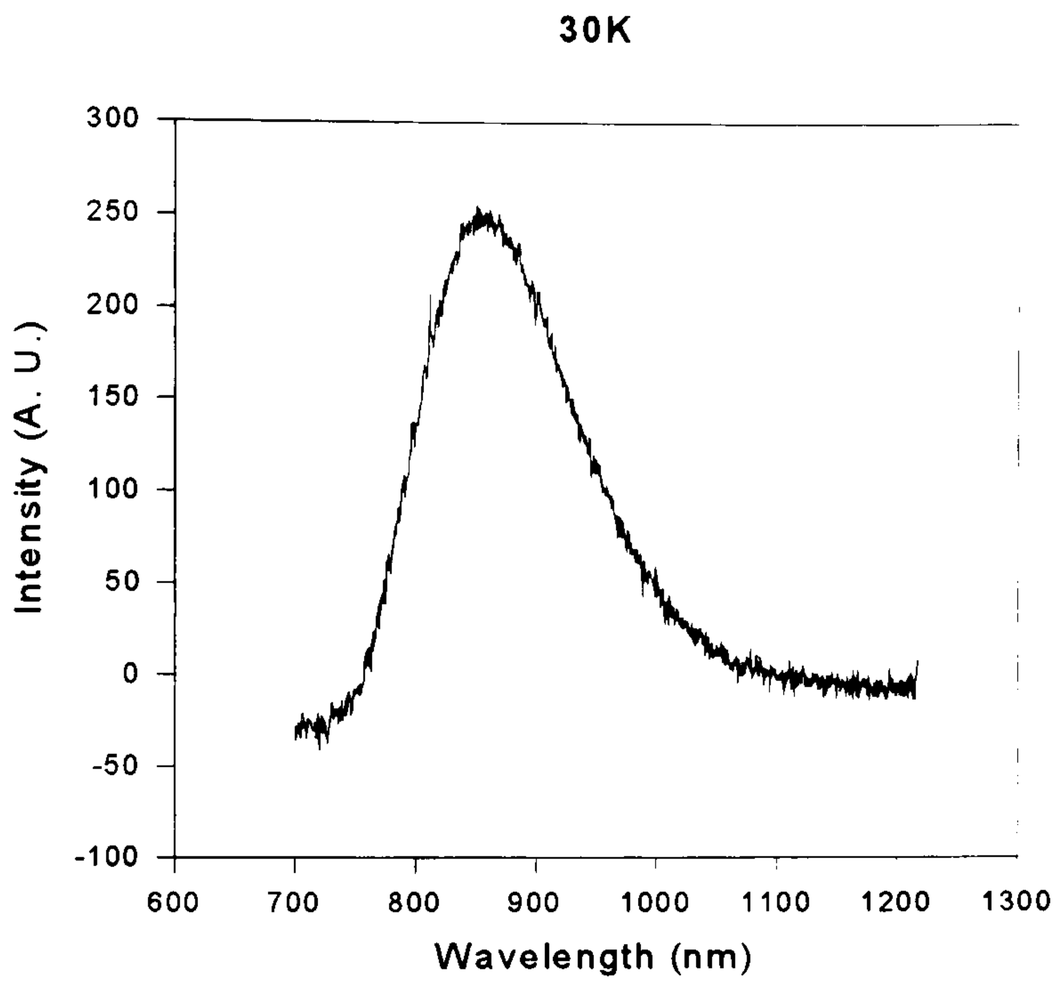

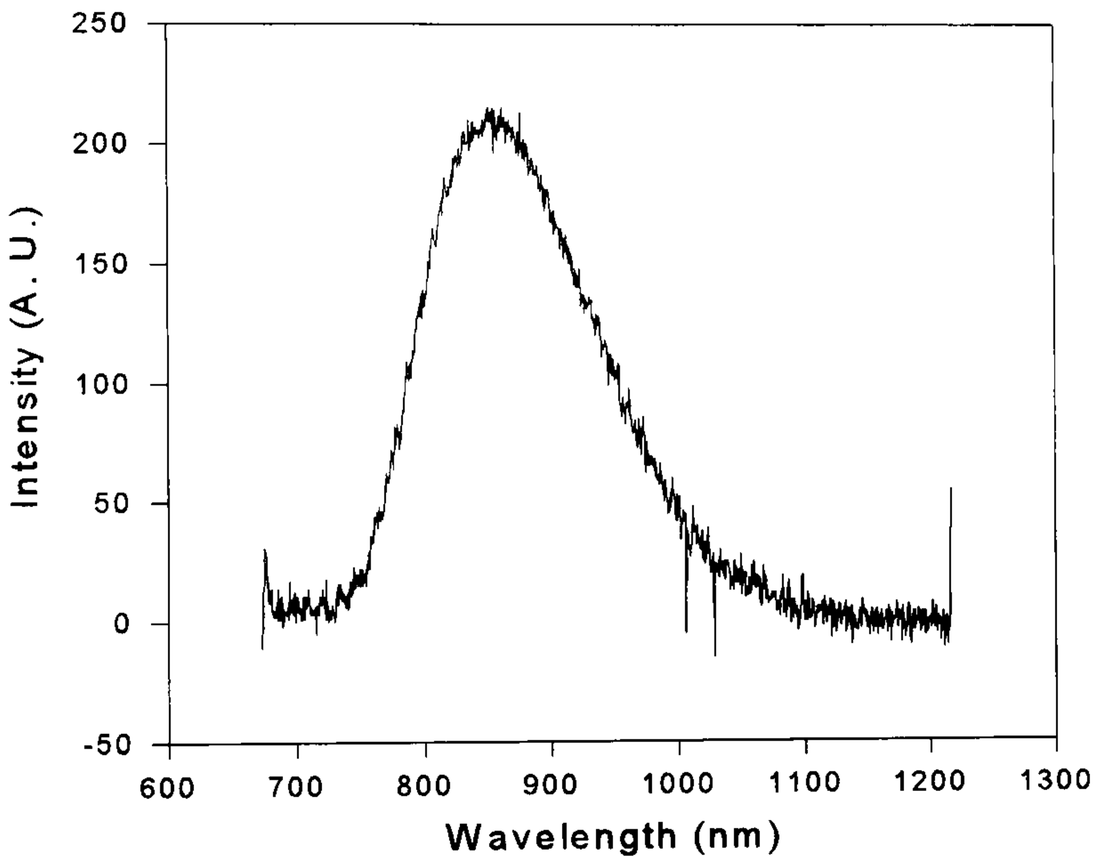

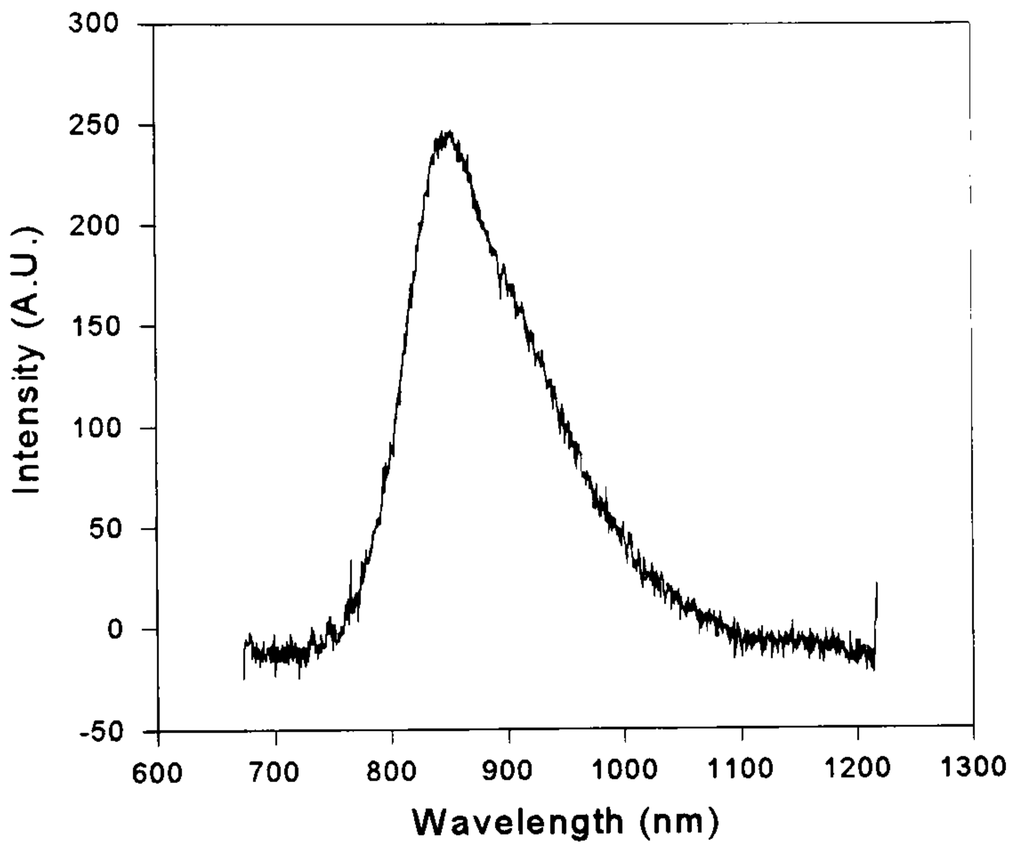

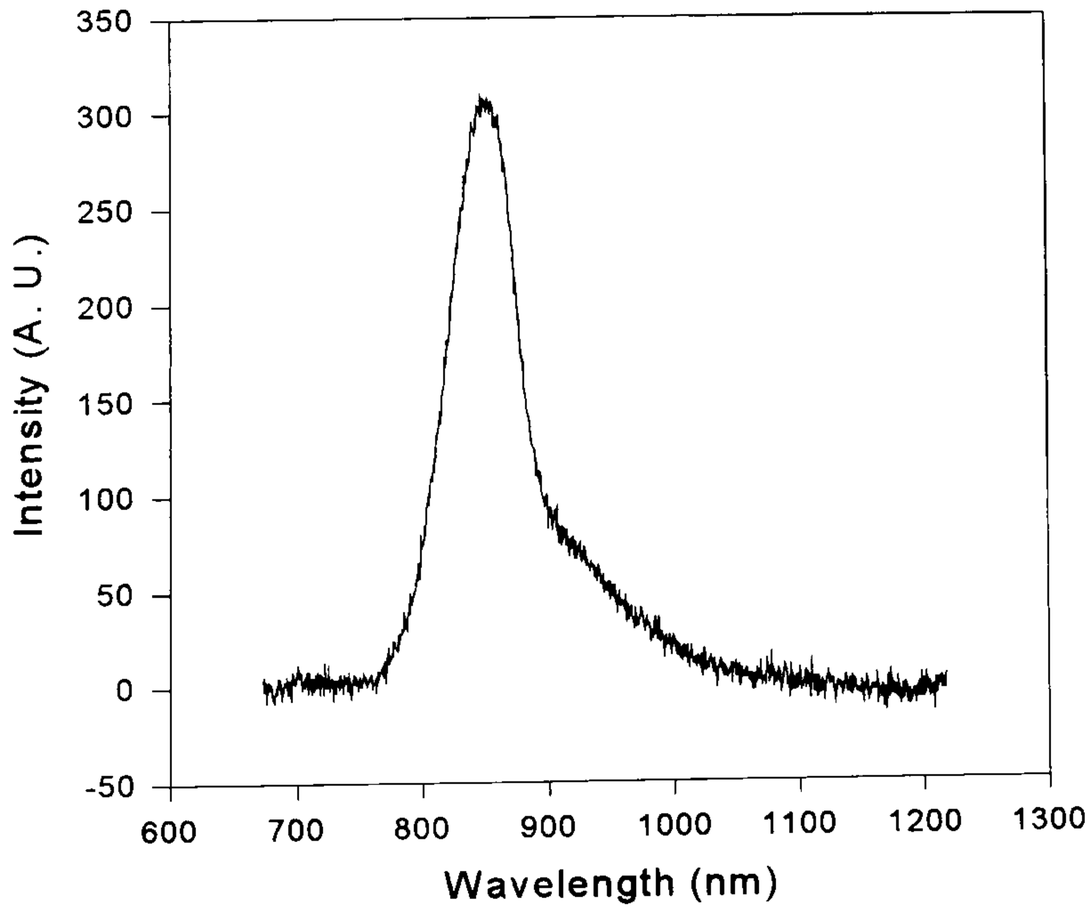

. Figure (7-6)- The El. emission spectra of treated CdTe cell at different temperatures.

Figure (7-7)- The differences between the CdTe bandgap and the peaks energy vs. temperature.

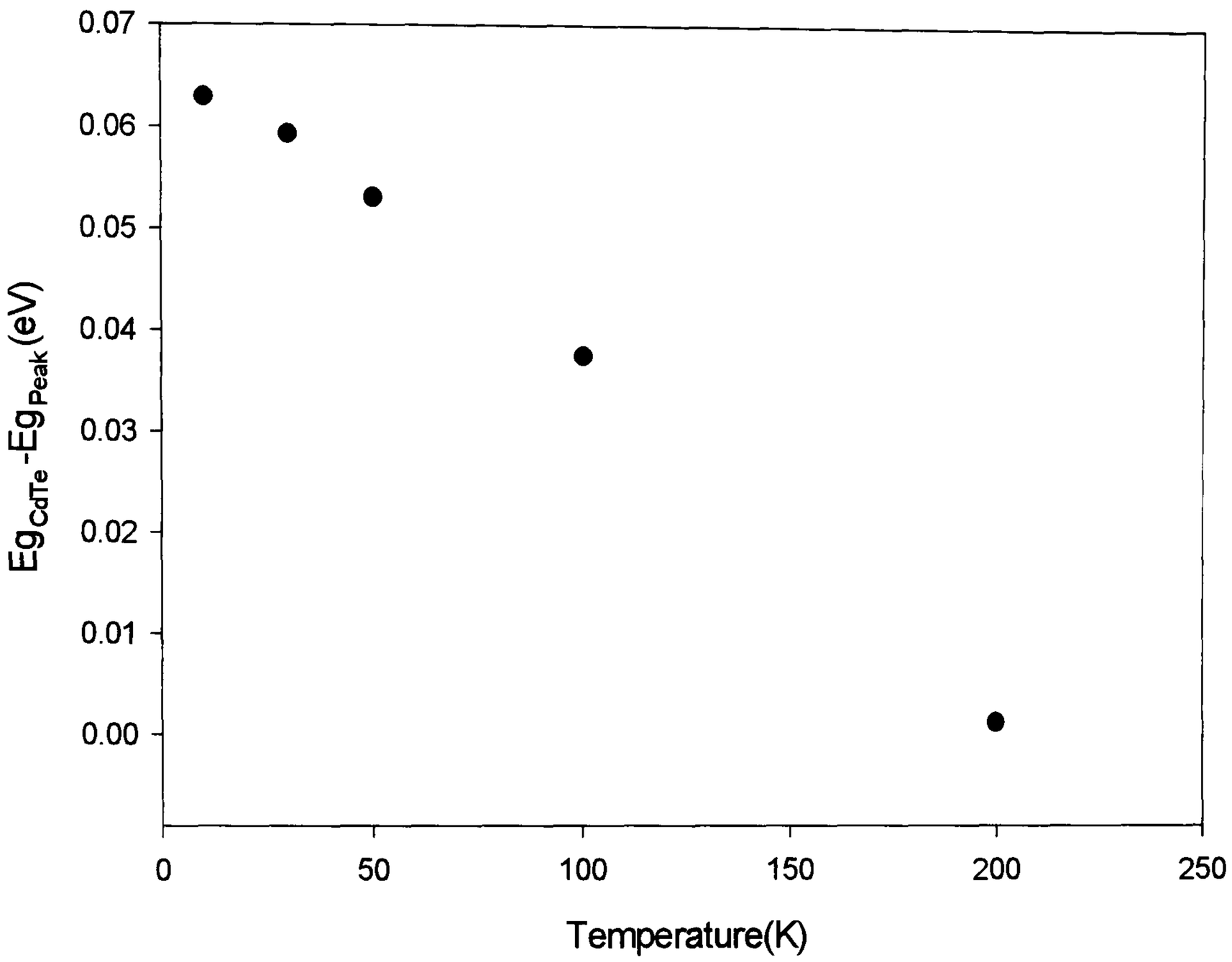

Figure (7-8)- The differences between the CdS bandgap and the peaks energy vs. temperature.

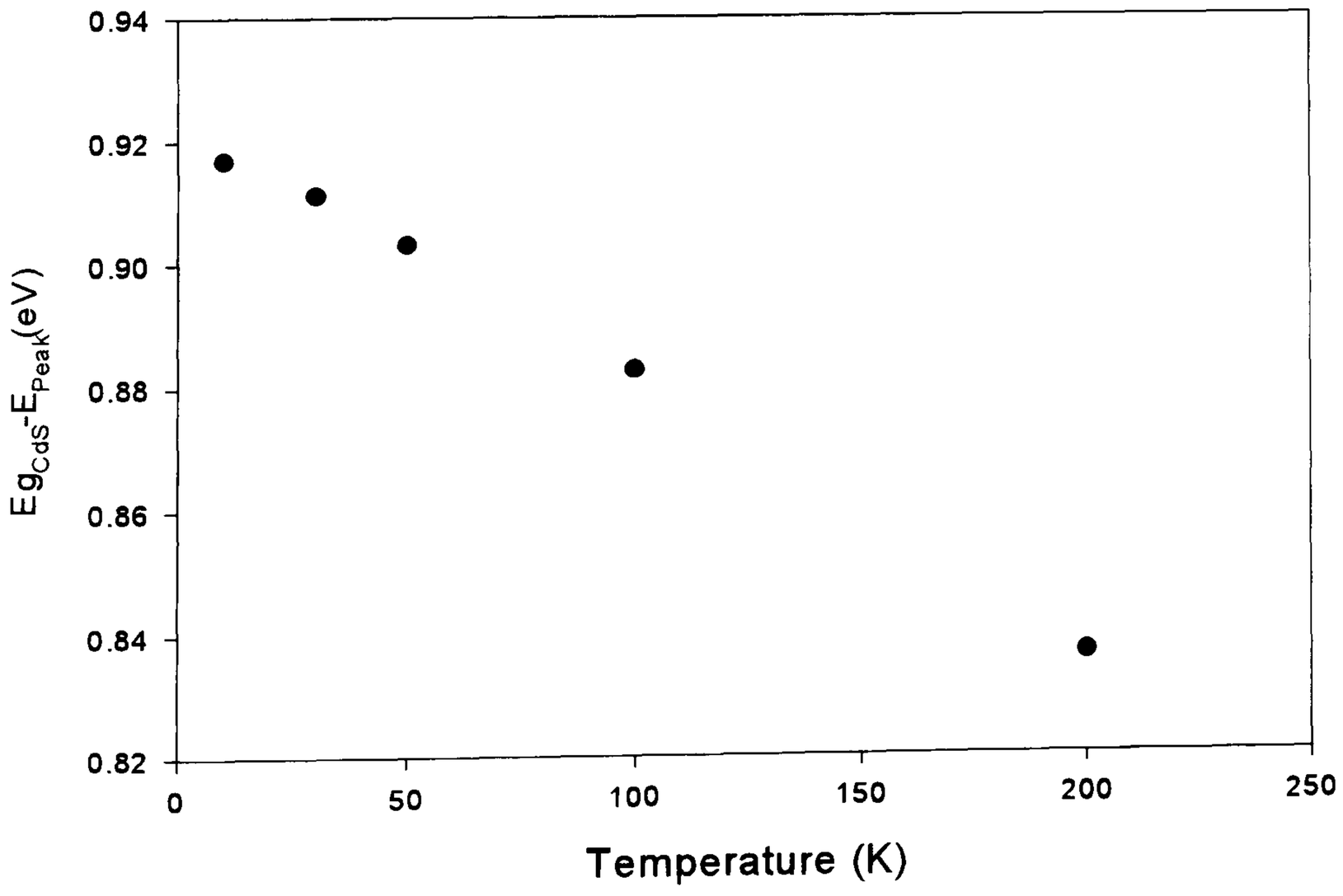

7.5- Conclusion:

The capacitance - voltage characteristics have been used to calculate the depletion width W_o, the acceptor concentration N_A and the built–in-junction potential V_b of n-CdS/p-CdTe thin film solar cells. The *C-V* measurements gave reasonable values of W_o and V_b for treated solar cells, whereas, the values of N_A are less than expected compared to other published values [14][15][16]. It is generally believed that in the CdTe, the acceptor centres are related to Cd vacancies [17]. The lower values of N_A obtained here probably suggest that the CdTe was either more stoichiomtric or that the material was compensated.

The photocapacitance measurements indicated the existence of some levels below the conduction at 0.4, 0.2 eV in p-CdTe and at 0.55eV in n-CdS, also some deep levels above the valance band at 0.24, 0.1 eV in p-CdTe and 0.71eV in n-CdS. Basol [18] reported that the level 0.2eV above the valance band in p-CdTe corresponds to a cadmium vacancy–complex. In general, most deep traps present in p-CdTe are thought to be due to Cd vacancies, Te inerstitials or structural defects [17].

The energy of the peak emission in the Electroluminescence spectrum at temperatures ≤ 200 K was around 1.45eV corresponding approximately with the bandgap of CdTe. This suggests that the Electroluminescence is the result of electron transition from conduction to valance band in CdTe .

7.6- References

(1)- V. P. Singth, H. Brafman, and J. Makwana. "Characterisation of Thin Film CdS-CdTe Solar Cells" Solar cells, 31(1991) 23.

(2)- J. Tang, L. Feng, D. Mao, W. Song, Y. Zhu and J. U. Trefny. "Study of ZnTe:Cu Back Contacts on CdTe/CdS Thin Film Solar Cells". Mater. Res. Soc. Symp. Proc. Vol. 426, (1996) 355.

(3)- Stephen J. Fonash. " Solar Cell Device Physics" Academic Press, London, 1981.

(4)- H. Bayhan and C. Ercelebi, "Electrical Characterisation of Vacuum-Deposited n-CdS/p-CdTe Heterojunction Devices" Semicond. Sci. Technol. 12(1997) 600.

(5)- B. E. McCandless, Y. Qu, and R. W. Brikmire, " A Treatment of Alloy Contacting CdTe with Different Conductors". First World Conf. on Photovoltaic Energy Conversion, Hawaii, 1(1994) 107.

(6)- J. Touskova, D. Kindl, and J. Tousek. "Photovoltaic Cells on CdS/CdTe Heterojunctions" Phys. Stat. Sol., 142 (1994) 539.

(7)- Abdalla A. A. Alnaajjar. "Single Crystal CdS/CdTe :P Solar Cells" Ph.D. Thesis, University of Durham, UK (1992).

(8)- H. Tavakolian and J. R. Sites. "Individual Losses in Thin-Film CdTe Solar Cells". 21st IEEE Photovoltaic Specialist Conf., 556,(1990).

(9)- B. L. Sharma. " Metal-Semiconductor Schottky Barrier Junctions and Their Applications" Academic Press, Plenum Press New York (1984).

(10)- Abdullah M. Al-Dhafiri, "CdS-Cu_xS Single Crystal and Thin Film Solar Cells". Ph.D. Thesis, University of Durham, UK (1988).

(11)- P. R. Thornton. "The Physics of Electroluminescent Devices". E.& F.N. Spon Limited, London, 1967.

(12)- Landolt-Börnstein. Numerical Data and Functional Relationships in Science and Technology, Group III Vol. 17(b), 3.12, (Springer -Verlag, 1982)

(13)- Landolt-Börnstein. Numerical Data and Functional Relationships in Science and Technology, Group III Vol. 17(b), 3.10, (Springer-Verlag, 1982)

(14)- H. M. Al-Allak, A. W. Brinkman, H. Richter, D. Bonnet. "Dependence of CdS/CdTe Thin Film Solar Cell Characteristics on the Processing Conditions". J. Crystal Growth, 159 (1996) 910.

(15)- T. L. Chu, Shirley S. Chu, and S. T. Ang. "Electrical Properties of CdS/CdTe Heterojunction" J. Appl. Phys. 64 (1988) 1233.

(16)- C. M. Fortmann, A. L. Fahrenbruch, and R. H. Bube. "Relative Carrier Density and Trap Effects on the Properties of CdS/CdTe". J. Appl. Phys. 61 (1987) 2038.

(17)- K. Zanio, "Semiconductors and Semimetals", vol. 13 Cadmium Telluride, Academic Press, London 1978.

(18)- B. M. Basol. "Electrodeposited CdTe and HgCdTe Solar Cells". Solar Cells, 23 (1988) 69.

Chapter Eight:

Conclusion.

The aim of the work described in this thesis has mainly been concerned with the characterisation of n-CdS/p-CdTe thin film solar cells where close space sublimation has been used to deposit the CdTe films. In particular to study the effects of preparation conditions on either the structure properties of the CdTe thin films such as grain size or preferred orientation, or the performance of the resulting devices such as the *I-V* and *C-V* characteristics and spectral response.

The deposition of CdTe by Close Space Sublimation is affected by several interrelated parameters; substrate and source temperature, the ambient gas pressure and the separation and temperature difference between the source and the substrate. These parameters effect the growth rate and also the texture of the films, and thus could influence the performance of CdS/CdTe solar cells. To obtain a given growth rate and film texture, the deposition conditions must clearly be optimised.

The equilibrium vapour pressure of Cd and Te_2 over solid CdTe are governed by the equilibrium constant for dissociation of the compound, $K_{CdTe,}$ This is strongly dependent on the temperature and increases exponentially with the reciprocal temperature, with a characteristic temperature of 8.4×10^3 K. Thus the vapour pressure of Cd and Te_2 over the substrate, and therefore the growth rate should follow a similar relationship. In fact, growth rate was found to vary exponentially on the reciprocal of the source temperature, but with a much larger characteristics temperature of 2.2×10^4 K, i.e. more strongly. The reason for this stronger dependence is not known but is presumably related to some temperature dependent aspects of the vapour transport.

For a given source temperature the growth rate was constant and independent of the substrate temperature, up to some breakpoint temperature, above which the rate decreased rapidly to zero. For a given supply rate (source temperature) the growth rate may be understood as the result of the competition between two process: compound formation and re-evaporation. The implication here is that at substrate temperatures above the breakpoint, re-evaporation is dominant and below this temperature compound formation is more likely. The latter will also be temperature dependent, but so long as the arrival rate is much less than the compound formation rate, then growth rate below the breakpoint temperature should be essentially constant.

The pressure of ambient gas defines the mechanism for the vapour transport involved in the CSS system. Free sublimation and transport is involved at low pressures such as 7.5×10^{-5} mbar because the mean free path is longer or equal to the space between the source and substrate. Diffusion limited transport was involved at pressures of 2, 6, and 10 mbar of N_2, because the mean free path is short compared to the space between substrate and the source and the Cd atoms and Te_2 molecules are likely to be scattered by collision with other gas molecules. Consequently, the transport rate is reduced resulting in lower growth rates. However, the higher gas pressures also restrict re-evaporation, allowing growth to continue to higher temperatures. Films grown at low pressures were observed to be pinhole free. Unlike those grown at higher temperature and pressures. The pinholes found in the high temperature films could have been the result of collisions between the Cd, Te_2 and N_2 molecules during the deposition.

To avoid "spitting" of particles of CdTe from the source on the substrate it was necessary to use a baffle. However, this had a significant effect on the uniformity of the film. When the substrate was too close to the baffle (less than 11mm) at high vacuum (7.5×10^{-5} mbar), those parts of the film which were directly above the holes, were thicker than the rest of the film. Since the growth rate increased as the separation between the source and the substrate decreased, this obviously meant there was a trade off between growth rate and uniformity.

The microstructure of the CdTe films was strongly affected by the substrate temperature, according to the Scanning Electron Microscopy (SEM) and X-ray diffraction observations. The grain size increased from <1μm at 335°C to more than 2.5μm above 445°C. The CdTe films grown at 335 °C showed a highly preferred (111) orientation. The intensity and the (111) texture coefficient reduced when the substrate temperature increased.

The thickness of the CdTe and CdS films should be a compromise between the requirements for complete absorption of the incident radiation and the need to keep series resistance low and shunt resistance high. The optimum thickness of CdTe and

CdS of CdS/CdTe solar cells deposited by Close Space Sublimation are 5μm and 0.2μm respectively.

The $CdCl_2$ treatment for the CdTe layer increased the efficiency of the solar cells from 2.8% to around 10% due to an improvement in all the photovoltaic parameters of the cells. The series resistance was reduced from ~ 34Ω.cm^2 to ~ 6 Ω.cm^2 and the shunt resistance increased from ~ 48Ω.cm^2 to ~ 196 Ω.cm^2. The reduction in R_s and the increase in R_{sh} increased the fill factor from 36.3 % to 54.4%, the open circuit voltage from 438mV to 684mV and short circuit current density from 17.6 to 27.3 mAcm^{-2}.

The reverse saturation current of the untreated cell varied exponentially with inverse temperature, while after the $CdCl_2$ treatment the variation became exponential with temperature. This suggests that the $CdCl_2$ treatment changed the current transport mechanism across the junction from emission/recombination with an activation energy of around 0.07eV to a tunnelling mechanism.

The Space Charge Limited Current measurements indicated that the CdTe layer in CdS/CdTe cells had a near uniform distribution of traps with energy above the valance band with a density around 3.7-6 $\times 10^{14}$ cm^{-3}eV^{-1} before $CdCl_2$ treatment, which reduced to 1.6-2.8 $\times$ 10^{14} cm^{-3}eV^{-1} after treatment. The position in energy of the Fermi level was calculated for untreated and treated CdTe to be 0.6 eV and 0.23eV respectively.

Solar cells fabricated with SnO_2 give higher efficiencies than cells fabricated with ITO. This was due to the interface between the ITO and CdS layer, which becomes rectifying after heating at 400°C in air. The change in the ITO/CdS interface from ohmic to Schottky behaviour after heating, suggests that some chemical interaction had taken place between the ITO and the CdS. The nature of this interaction is not clear.

Interdiffusion between the CdS and CdTe layers plays a crucial role in the performance of CdS/CdTe solar cells. It has a strong influence on the photogeneration of the cell at each wavelength, as shown in the spectral response measurements. The interdiffusion between CdS and CdTe layer in CdS/CdTe, which occurs during cell fabrication, result in a graded interface CdS_xTe_{1-x} layer, which is S-rich on the CdS side and Te-rich on the CdTe side. In effect this gives two different composition at the interface between CdTe and CdS.

The bandgap of $CdTe_{1-x}\ S_x$ is reduced below the bandgap of CdTe for $0.3 \geq x > 0$, i.e. for Te-rich compositions, explaining the shift to longer wavelengths of the spectral response. So the diffusion of S to CdTe is desirable until $x \cong 0.3$ as this increases the absorption of photons with energy below the band gap of the CdTe layer. On the other hand the diffusion of Te into the CdS layer is undesirable because it reduces the window layer bandgap, consequently increasing the window layer absorption of photons with energy below the band gap of CdS. Unfortunately during the preparation of CdS/CdTe the interdiffusion between CdS and CdTe is mutual.

There are many preparation parameters which affect the interdiffusion between the CdTe and CdS layers, and so modify the spectral response. In particular, it seems that the $CdCl_2$ treatment promotes the interdiffusion of CdS and CdTe. Why this appears to be the case, is not at present understood, but the results of this study suggest that the more intensive the treatment, the greater the degree of cross diffusion. The spectral response at wavelengths below the CdS band edge decreased as the CdS layer thickness increased as expected.

The capacitance- voltage characteristics were used to calculate the W_o, N_A and V_b of n-CdS/p-CdTe thin film solar cells. The C-V measurements gave reasonable values of W_o and V_b for treated solar cells, whereas, the values of N_A are less than expected, this could be due to the stoichiometry of the CdTe material.

The photocapacitance measurements indicated the existence of some levels below the conduction at 0.4, 0.2 eV in p-CdTe and at 0.55eV in n-CdS, also some deep levels above the valance band at 0.24, 0.1 eV in p-CdTe and 0.71eV in n-CdS.

The energy of the peak emission in the Electroluminescence spectrum at temperatures ≤ 200 K was around 1.45eV corresponding approximately with the bandgap of CdTe. This suggests that the Electroluminescence is the result of electron transition from conduction to valance bands in CdTe.